Theoretical Studies of Chemisorption Processes on Nickel Surfaces

Thesis by

Thomas Hallworth Upton

In Partial Fulfillment of the
Requirements for the Degree of
Doctor of Philosophy

California Institute of Technology
Pasadena, California

1980

(submitted April 14, 1980)

Acknowledgments

During my rather lengthy stay at Caltech, some good people have passed through my life, and it would be inappropriate for me not to acknowledge the influence of at least a few of them. I must thank Tim Surratt and Carl Melius for providing me with a few sage-like insights long ago that got me pointed in the right direction. Thanks must also go to Larry Greaves and Dan Murphy for allowing me the option of periodically escaping Caltech. But most of all I must acknowledge the friendship of Carl and Joan Koval who, from the beginning helped make life here much more of a pleasure.

It has been a particular pleasure to be able to work with my advisor Bill Goddard. His depth of knowledge and enthusiasm are well known, but I have especially appreciated his unwavering support of this somewhat unorthodox research. I hope that the results will prove to be worthy of his interest. I must also recognize members of the Goddard group, and in particular thank Ray Bair, Art Voter, and Marv Goodgame for sharing their interests in things non-scientific.

Finally, I must thank my parents for their constant encouragement and especially my wife Nancy. Her sacrifices and endlessly cheerful affection have contributed enormously to the completion of this work. It will be a pleasure to share with her the rewards.

Abstracts

Part I: Generalized Valence Bond and Configuration Interaction calculations are reported for the zero valent nickel complexes NiC_2H_2, NiC_2H_4, $Ni_2C_2H_4$, and $Ni_2C_2H_2$. It is found that the NiC_2H_2 and NiC_2H_4 a coordination complex is formed in which the ligand π orbital delocalizing into an empty Ni 4sp orbital. The $4s^1\,3d^9$ configuration of the Ni atom is stabilized. Bond energies of 16.7 and 14.2 kcal are found for the two complexes, respectively. In both complexes, the ligand is very weakly distorted, a result that is supported by complementary experimental data characterizing the IR and UV-visible spectral properties of NiC_2H_4 and the $Ni_2C_2H_4$ π-complex.

Acetylene is coordinated to Ni_2 in both di-σ and di-π bonded form, for which bond energies of 23 and 60 kcal (relative to C_2H_2 + 2Ni) are found, respectively.

Configuration interaction calculations are also reported characterizing all ligand valence ionization levels for the NiC_2H_2, NiC_2H_4 and $Ni_2C_2H_2$ complexes. Excellent agreement is found between the UPS results for chemisorbed ethylene and the NiC_2H_4 calculated spectrum. "Bonding shifts" are found to result from a differential screening effect.

Part II: Extensive generalized valence bond (GVB) and configuration interaction calculations (POL-CI) have been carried out for the lowest states of Ni_2 and Ni_2^+ for bond lengths from 1.6 to 4.0 Å. The six lowest states of Ni_2 are found to be essentially degenerate with an average equilibrium bond length r_e = 2.04 Å and D_e = 2.92 eV. A $^4\Sigma_g^-$ ground state is found for the ion with a bond length R_e = 1.96 Å and

dissociation energy D_e = 4.14 eV. The bonding of Ni is dominated by the interactions of the 4s orbital on each Ni with each Ni of Ni_2 corresponding to a $(4s)^1(3d)^9$ configuration. The lowest states lead to singly occupied δ orbitals on each center with other 3d occupations leading to 100 electronic states within about 1.0 eV of the ground state.

Hartree-Fock calculations are also reported, characterizing the low-lying states of an Ni_8 cluster. It is found that the $4s^1 3d^9$ valence configuration of the Ni atom is strongly stabilized, and that here too, the 3d orbitals remain localized and are of secondary importance in the bonding.

As a result of these findings, further first principles calculations have been carried out characterizing the "conduction band" properties of high and low symmetry clusters up to Ni_{87}. Macroscopic properties [ionization potential (IP), electron affinity (EA), bandwidth, and cohesive energies] are not sensitive to cluster geometry, and except for EA, show definite convergence towards the bulk limit by Ni_{87}. Even for Ni_{87}, the EA is over 2.5 eV smaller than the IP, and the origin of this effect is discussed.

Part III: First Principles Hartree-Fock and Generalized Valence Bond Calculations are reported for the bonding of atomic H, Cl, Na, O, and S on high symmetry sites of the Ni(100) face using an Ni_{20} cluster as a model. All of the adsorbates are found to prefer the fourfold site, with bond energies (D_e) of 3.04, 4.9, 1.3, 3.63, and 4.34 eV, respectively. Bond distances are 0.78, 1.38, 2.7, 0.88, and 1.24 Å above the surface, which are (except for Na) in excellent agreement with available

experimental data. Vibrational frequencies of 73, 17, 30, 46, and 37 meV are found for each adsorbate, respectively. Decreasing site coordination is found to uniformly increase vibrational frequencies, and bond distances while decreasing bond energies. The data are analyzed through the introduction of the concepts of site acidity and basicity, and it is found that site basicity increases with increasing coordination. This trend is responsible for the observed preference of each adsorbate for high coordinate sites, and it is expected that donor adsorbates (such as CO) would show a reverse trend. The data for Na are found to be in poor agreement with the analogous bulk data, confirming the prediction from Part II.C that small particles should behave differently from the bulk when bonded to highly electropositive species.

Part IV: A technique is presented for carrying out ab initio Hartree-Fock calculations on systems of infinite three-dimensional periodicity. The method represents an adaptation of standard molecular basis set expansion techniques and fully utilizes translational and point group symmetry to simplify the calculations. It is shown that the expression for total energy may be written as a sum of pairwise interactions between neutral charge units consisting of a nucleus and a localized compensating electronic charge. The resulting sums are rapidly convergent. The technique is illustrated with sample calculations on face-centered cubic lattices of hydrogen, lithium, and sodium. Generalization to systems of lower symmetry is discussed.

Table of Contents

Table of Contents (continued)

Part One

Very Small Metal Cluster Models for Chemisorption: Theoretical Studies of Small Hydrocarbon Complexes of Zero-Valent Ni and Ni_2.

A. The Ni-C_2H_2 π Complex

I. INTRODUCTION

In theoretical and experimental studies of chemisorption and catalysis, a great deal of discussion has focused on the validity of employing localized models for elucidating the surface bonding between adsorbate and adsorbent.[1] For this model, the chemisorptive bond is described as localized, involving only a limited number of neighboring surface atoms near the adsorbate. This idea receives some support from analogies with a number of organometallic complexes and the homogeneous reactions of these complexes.[2] However, until very recently, a serious shortcoming of the localized model has been the difficulty of experimentally generating realistic molecular systems for interconnecting the infinite surface molecular state and its finite-cluster localized-bonding counterpart.[2c,3] Homogeneous catalysts often possess ligands that have no counterpart in bulk systems, and the influence of these ligands on metal atom states and catalytic properties is difficult to measure. While the correspondence between the catalytic properties of organometallic complexes involving small metal clusters and their bulk analogues has been well documented, attempts to draw more detailed mechanistic and structural comparisons must be made with caution.

In this study we have addressed ourselves to the challenge of producing a more "ideal" localized bonding model for a particular surface interaction, namely that of acetylene chemisorbed onto bulk nickel. As a model "surface complex" we have chosen to theoretically characterize a nickel atom interacting with an acetylene molecule,

namely $Ni(C_2H_2)$. This system has been the subject of recent cryochemical syntheses and a comparison of the picture obtained here with observed spectroscopic properties should provide valuable information on the mode of bonding.

To date, attempts to determine the mode of bonding for acetylene on bulk nickel have produced conflicting results. The simplest picture arises from the uv photoemission spectra of adsorbed acetylene at low temperatures. These have been compared with gas phase spectra, suggesting that the only significant effect of chemisorption is to shift the energy of the π level. From this and related theoretical investigations,[5] Demuth and Eastman concluded that the acetylene-nickel chemisorptive bond involves predominantly π-d interactions without significant distortion of acetylene relative to its gas phase geometry. The assumption here is that acetylene forms a π-complex coordinating symmetrically to one or more surface atoms in a manner similar to that originally proposed for organometallic complexes.[6] Such an interpretation is not dissimilar to that arising from experimental studies of the zero-valent complexes,[3,7] and it is expected that the results presented here should have some bearing on this question as well.

Under high coverage conditions chemisorbed acetylene apparently suffers a significant structural alteration.[8-10] This adsorbed phase has been characterized using several different spectroscopic probes, including LEED,[8] HRELS,[9] and UPS.[10] Nevertheless, the experimental picture remains unclear. It is unlikely however, that the simple complex studied here is relevant as a model

for this structure, and we leave it as a topic for further more detailed study.

In the next section, we present a discussion of our generalized valence bond (GVB) and configuration interaction (CI) calculations on the $Ni(C_2H_2)$ system in which the qualitative aspects of the bonding will be emphasized. In Section III we will discuss these results in light of both the experimental information concerning the zero-valent complexes and the results of previous theoretical studies. A discussion of these results with reference to the low temperature chemisorbed phase of acetylene on nickel surfaces will be reserved for section I.C of this thesis.

II. The Nickel-Acetylene Complex

A. Qualitative Details

We first consider what happens when the acetylene molecule is brought towards the Ni atom. With a cylindrically symmetric pair of equivalent π orbitals, the acetylene molecule present a highly polarizable distribution of charge when it approaches an isolated nickel atom in a "side-on" manner. One of these π orbitals will experience an initial interaction with the Ni 4s orbital. The ground state (^3F) of the Ni atom[11] has a doubly-occupied 4s orbital that leads to repulsive interactions with the acetylene π orbital, making strong bonding unfavorable. The first excited state of the Ni atom (^3D) has a singly-occupied 4s orbital and is only 0.03 eV above the ^3F state. This singly-occupied orbital can more readily mix in 4p character,

hybridizing away from the Ni-acetylene bonding region and thus minimizing repulsive interactions with the π orbital. It is possible to form two such "sp hybird" orbitals: one directed away from the acetylene molecule as described ($4s-4p_z$) and one directed towards it ($4s + 4p_z$). Placing the single Ni electron in the ($4s-4p_z$) orbital leaves the remaining one empty, and the acetylene π orbital is able to delocalize slightly into this orbital space, producing a net bonding interaction. This situation is depicted in Fig. 1 where bonding orbitals for the system are shown.

The interaction of the $3d^9$ shell of ^3D Ni with the acetylene is more subtle. These orbitals are very contracted in comparison with the 4s orbital, and the acetylene is unable to move close enough to the Ni atom to interact strongly with them. The singly-occupied 3d orbital in the ground state configuration is found to be a $d\delta$ orbital due to the intraatomic coupling effect[11-13] which allows optimum hybridization of the 4s orbital. This orbital, and the remaining doubly-occupied 3d orbitals are all localized on the Ni atom. The interactions of these orbitals with the acetylene ligand are so weak in fact that the five states of $Ni(C_2H_2)$ formed by placing the single 3d electron in each of the five d orbitals span a range of only 0.5 ev above the $^3A_1$ ground state. In particular, there is almost no delocalization of the $3d\pi_{yz}$ orbital into the acetylene π^* orbital, a feature that is in direct contradiction with the standard Dewar-Chatt-Duncansen[6] model for metal-olefin bonds (see Fig. 1).

This description leads to a particularly simple model for the Ni-olefin bond. With the hybridization of the singly-occupied 4s

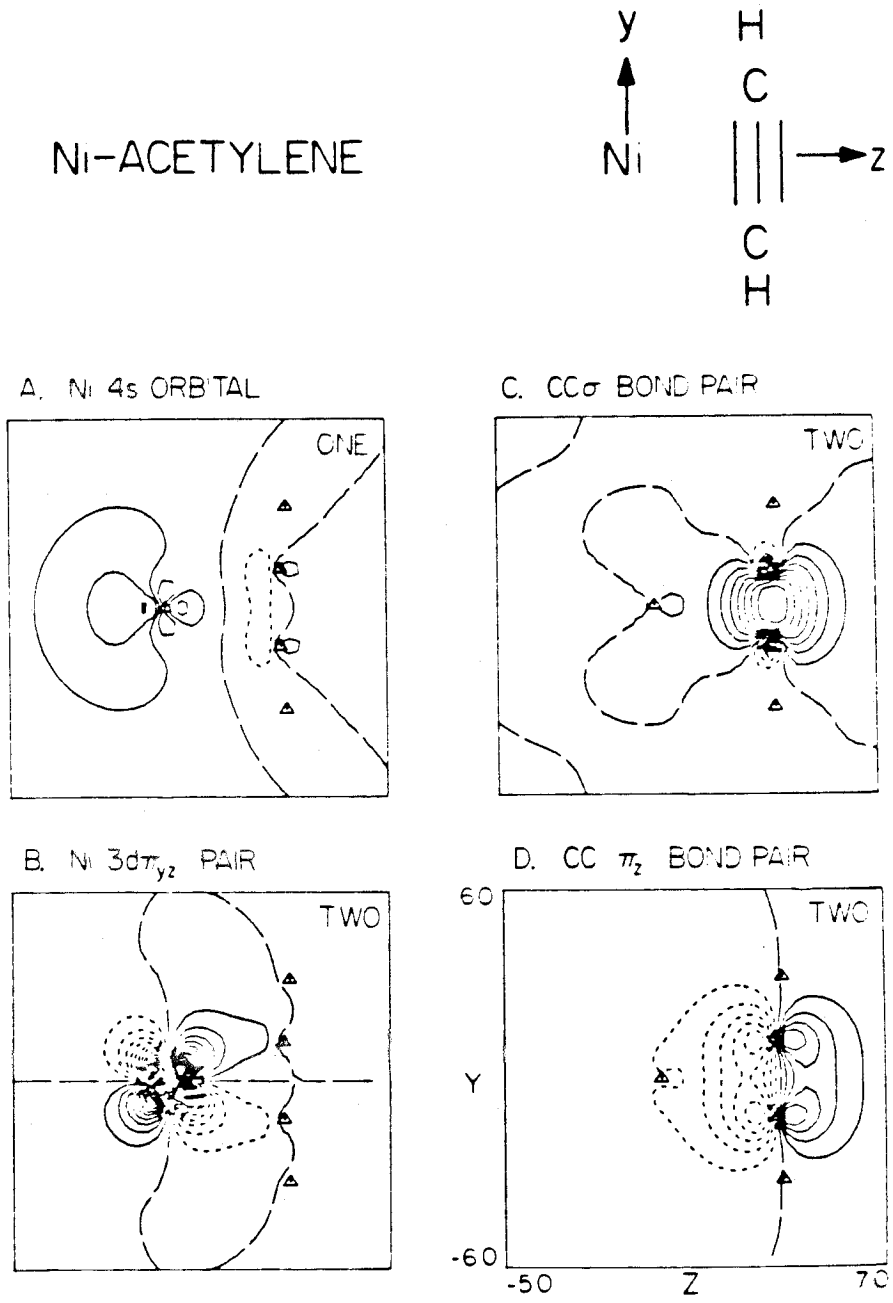

Figure 1: Bonding orbitals for the ground state of the $Ni-C_2H_2$ π-complex. Atom positions in plots are as indicated at upper right.

orbital away from the acetylene molecule, a $3d^9$ shell (largely unperturbed from atomic Ni) is left partially exposed. The acetylene π orbital, delocalizing into the remaining 4sp space is drawn towards this slightly electropositive center, its final distance (and binding energy) being limited by its repulsive interaction with the occupied 4s orbital.

With this type of model, little perturbation of the acetylene molecule would be expected. The CC bond distance (see Fig. 2) is found to increase by only 0.01 Å to 1.21 Å and the CH bonds bend back only 5° out of the acetylene molecule plane. The optimum Ni-C bond distances are found to be 2.01 Å. In comparison, these bonds are somewhat longer than Ni-C covalent bonds (1.78 for $NiCH_2$[14] and 1.87 for $NiCH_3$),[15] or sigma lone pair coordination bonds (1.90 for NiCO).[16] The slight CC bond elongation may be seen to be a result of the π orbital delocalization. Similarly, the distortion in the HCC bond angle is a result of the mixing between acetylene σ and π orbitals that is necessary to maximize this delocalization.

It should be emphasized here that the strength of the bonding interaction is strongly dependent upon the presence of the 4s orbital. For the zero-valent complex at the optimum geometry, a binding energy of only 16.7 kcal is obtained. Removal of the 4s electron to form an Ni(I) complex leads to significant changes. The repulsive 4s-C_2H_2 π interaction is eliminated, leading to an increase in the binding energy, at the same geometry, to almost 60 kcal. The delocalization of the π orbital onto the Ni becomes more complete,

FINAL GEOMETRY

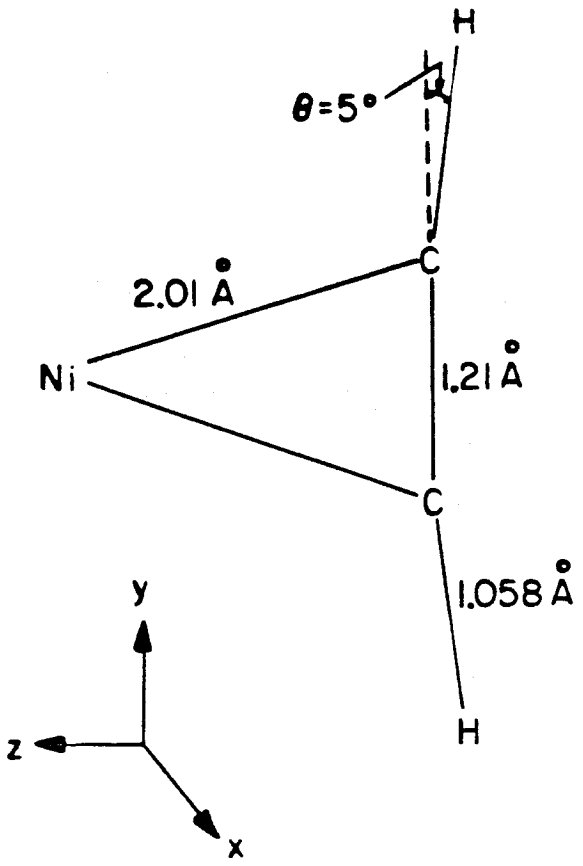

Ni–ACETYLENE

Figure 2: Optimum geometry for the π-complex. CH bond distances were not varied.

and it experiences a much stronger interaction with the positively charged Ni atom.

B. Calculational Details

In all calculations, the modified effective potential for Ni was used to eliminate the need for explicit treatment of the Ni core electrons[17] (see Appendix V.A). The Ni basis set was truncated to include three 4s and two 4p contracted gaussian functions, as well as Wachters[18] set of 3d gaussians, contracted DZ. For the carbon atoms, a full DZ set of contracted gaussians was used,[19] augmented with a set of d polarization functions (α = 0.6769). Hydrogen functions[19] were also contracted DZ.

The optimization of R(CC), (HCC), and R(NiC) parameters was carried out at the GVB-CI level. Correlation effects were included self-consistently in both π bonds as well as the CC σ bond. Sufficient configurations were included in the CI calculations to relax the perfect pairing and strong orthogonality constraints present in the GVB wavefunction.[20] In all calculations, R(CH) distances were fixed at the experimental gas phase distance.

III. Discussion

The simple bonding form found for this system finds some support in both experimental and theoretical studies. A species assigned as NiC_2H_2 has been observed in matrix isolation studies by Ozin and Power.[7a] They find IR bands at 3130, 1734 and 572 cm^{-1} which they attribute to ν_{CH}, ν_{CC} and ν_{NiC}. The ν_{CC} mode is redshifted by this assignment by about 240 cm^{-1} from the gas phase value (ν_{CC} = 1974 cm^{-1}), suggesting a modest amount of CC bond weakening. Similarly, a distortion of the HCC angle is implied by the value of ν_{CH}. Neither value approaches those levels associated with the corresponding ethylenic stretch frequencies, and the authors conclude that the acetylene is only weakly distorted.

Related information comes from recent ESR studies of $Cu(C_2H_2)_{1,2}$[7b,c] and $Cu(C_2H_4)_{1,2}$.[7b] Examination of the g and hyperfine coupling tensors for the mono- compounds leads to structures very similar to those predicted here. Specifically, for $Cu(C_2H_2)$ a large isotropic coupling tensor is found, with $A_{||}$ = 4111 Mhz and $A_{\perp}$ = 4053 Mhz, which is consistent with an unpaired spin in an orbital that is $\sim \frac{2}{3}$ 4s and $\frac{1}{3}$ 4p. Similar results are found for $Cu(C_2H_4)$ and both are extremely similar to our calculated Ni analogues.

It must be noted that an undistorted C_2H_2 ligand is a rarity among finite transition metal complexes. A wide variety of such systems have been isolated, and most show extensive bond elongations and HCC angle distortion.[1] However, all of the systems for which structural data are currently available employ di-substituted acetylenes where the sub-

stituents are typically quite large (alkyl or aryl groups). Neither the steric nor electronic effects of such changes on the coordination bond are known.

Nevertheless, the lack of structural data may be indicative of simply the instability of the π-coordinate form as it is described here. Neither the NiC_2H_2[7a] nor the NiC_2H_4[2c] complexes are stable beyond $\sim$ 50K in a matrix. Whether this is a reflection of the weakness of the bond or the coordinative unsaturation of the complex is not clear, but the existence of tris-ethylene nickel at temperatures as high as 0°C suggests that the latter may be of greater importance.[21] Highly stable complexes for which structural data are available typically achieved coordinative saturation through the binding of donor ligands such as triphenyl phosphines or carbonyls.[1] In such systems, the Ni atom is almost certainly stabilized in a $3d^{10}$ configuration, and a coordination bond with rather different properties becomes highly likely.

A coordination form similar to that in evidence here has been considered by Anderson[22] using a derivative of the extended huckel method. In studies of an Ni_4 C_2H_2 system, bond parameters very similar to our own have been determined. Only upon higher coordination is the acetylene found to distort seriously. Few details of the bonding are given, but the implication is that the interaction is largely a result of $3d\text{-}\pi^*$ backbonding.

IV. Conclusion

The results of this study may be summarized as follows:

1) The interaction between an Ni atom and acetylene has a very simple form: the highly polarizable acetylene π orbital delocalizes slightly into an empty 4s-p orbital on the Ni atom. This interaction produces a bond of 16.7 kcal. The acetylene ligand is very mildly distorted and there is little evidence of 3d-π^* backbonding.

2) The results compare favorably with the interpretation of IR bands found for a matrix isolated NiC_2H_2 species. Here too, there is little evidence for a highly distorted ligand. Both this experiment and the theoretical result contrast sharply with available X-ray structural data for stable transition metal acetylene complexes, where large distortions are typically observed.

3) The mode of bonding is in qualitative agreement with the results of ESR data that suggest a mode of bonding for CuC_2H_2 very similar to that found here.

References and Notes

1. For a recent review see E. Muetterties, T. Rhodin, E. Band, C. Brucker, and W. Pretzer, Chem. Rev. 79, 91 (1979).
2. (a) R. Ugo, Catal. Rev. 11, 225 (1975); (b) E. L. Muetterties, Bull. Soc. Chim. Beg. 84, 959 (1975); 85, 7 (1976); Science, 196, 839 (1977); (c) G. A. Ozin, Acc. Chem. Res. 10, 21 (1977), and references cited therein.
3. (a) G. A. Ozin and M. Moskovits in "Cryochemistry", G. A. Ozin and M. Moskovits, Ed., Wiley, New York, N.Y., 1976; (b) G. A. Ozin and W. J. Power, Inorg. Chem. 16, 212 (1977); (c) D. Mcintosh and G. A. Ozin, ibid. 16, 51 (1977); (d) D. McIntosh and G. A. Ozin, ibid. 16, 59 (1977); (e) H. Huber, W. J. Power, and G. A. Ozin, J. Am. Chem. Soc. 98, 6508 (1976); (f) J. E. Hulse and M. Moskovits, Surf. Sci. 57, 125 (1976), and references cited therein.
4. J. E. Demuth and D. E. Eastman, Phys. Rev. Lett. 32, 1123 (1974).
5. (a) J. E. Demuth and D. E. Eastman, Phys. Rev. B13, 1523 (1976); (b) J. E. Demuth, IBM J. Res. Develop. 22, 265 (1978); (c) This view is revised in J. E. Demuth, Surf. Sci. 84, 315 (1979).
6. J. Chatt and L. Duncanson, J. Chem. Soc. 2939 (1953).
7. (a) G. Ozin and W. Power, to be published; (b) P. Kasai, D. McLeod and T. Watanabe, J. Am. Chem. Soc. 102, 179 (1980); (c) P. Kasai and D. McLeod, J. Am. Chem. Soc. 100, 625 (1978).
8. J. C. Hemminger, E. L. Muetterties, G. A. Somorjai, J. Am. Chem. Soc. 101, 62 (1979).

References (continued)

9. J. E. Demuth and H. Ibach, Surf. Sci. 78, L238 (1978).

10. J. E. Demuth, Surf Sci. 69, 365 (1977).

11. C. E. Moore, NSRDS-NB5 35, Vol. II, 1971.

12. See Part II.A of this thesis.

13. S. P. Walch and W. A. Goddard III, J. Am. Chem. Soc. 98, 7908 (1976).

14. A. K. Rapp and W. A. Goddard III, J. Am. Chem. Soc. 99, 3966 (1977).

15. W. A. Goddard III, S. P. Walch, A. K. Rappé, and T. H. Upton, J. Vac. Sci. Technol. 14, 416 (1977).

16. S. P. Walch and W. A. Goddard III, Surf. Sci., submitted.

17. M. Sollenberger, M.S. Thesis, Calif. Inst. of Technology, 1977.

18. A. J. H. Wachters, J. Chem. Phys. 42, 1293 (1965).

19. T. H. Dunning and P. J. Hay in "Modern Theoretical Chemistry", Vol. 3, H. F. Schaefer III, Ed. (Plenum, New York, 1977) p. 1.

20. W. J. Hunt, T. H. Dunning Jr. and W. A. Goddard III, Chem. Phys. Lett. 3, 606 (1969).

21. See Section I.B of this thesis and refs. within.

22. A. Anderson, J. Am. Chem. Soc. 100, 1153 (1978).

B. Experimental and Theoretical Studies of $Ni_n(C_2H_4)_m$ for $n = 1, 2$ and $m = 1, 2, 3$

I. Introduction

The experimental and theoretical characterization of the $Ni_n(C_2H_4)_m$ complexes (N = 1, 2 and m = 1, 2, 3) provides an excellent opportunity to further characterize the nature of π-coordinate Ni-olefin bonds through comparison with similar theoretical studies of $Ni(C_2H_2)$[1] and $Ni_2(C_2H_2)$.[2] Here, we present a discussion of the infrared and UV-visible properties of the matrix isolated Ni_n-ethylene complexes. Trends in these results will be interpreted by comparing with the results of generalized valence bond (GVB) and configuration interaction (CI) calculations on the $Ni-C_2H_4$ and $Ni_2-C_2H_4$ π-complexes. In addition, in Section I.C of this thesis we will use these results in conjunction with data from HRELS,[3] UPS,[4] and other experimental studies[5] to provide some additional insights into the nature of the chemisorptive bonding of ethylene on bulk nickel.

II. Synthesis and Spectroscopic Characterization

A. Experimental

Monotomic Ni vapor was generated by directly heating a 0.020-in ribbon filament of the metal with ac in a furnace similar to that described previously.[6] The nickel (99.9%) was supplied by McKay, New York. Research grade C_2H_4 (99.9%) and Ar (99.9%) were supplied by Matheson of Canada. The rate of Ni atom deposition was continuously monitored using a quartz crystal micro balance.[7]

In the infrared experiments, matrices were deposited onto a CsI optical plate cooled to 15°K (optimum reaction temperature) by means

of an Air Products Displex, closed-cycle helium refrigerator. Infrared spectra were recorded on a Perkin-Elmer 180 spectrophotometer. Ultraviolet visible spectra were recorded on a standard Varian Techtron in the range 190-900 nm, the sample being deposited onto a NaCl optical window.

B. Results and Discussion

The existence of binary nickel olefin complexes of the form $Ni(ol)_n$ was first demonstrated by Fischer et al.[8] from the reaction of $Ni(1,5\ COD)_2$ and C_2H_4 at -196°C. Tris-ethylene nickel (0), $Ni(C_2H_4)_3$, could be crystallized from liquid ethylene and was found to decompose to metallic nickel and ethylene at 0°C.[8] Subsequently, the same compound was directly synthesized[9] by cocondensing atomic Ni with C_2H_4 in the temperature range 77 - 10° K and its infrared, Ozin and Powers,[10] and uv-visible spectra were recorded. By matrix dilution and warm-up techniques, isotopic ^{13}C and ^{2}H labeling, and metal concentration experiments, the reactive intermediates $Ni(C_2H_4)$ and $Ni(C_2H_4)_2$ were identified and their infrared and uv-visible spectral properties recorded.[11] All of these matrix experiments were conducted under extremely high dilution conditions with respect to the nickel, such that mononuclear complex formation predominated.[12] The relevant spectroscopic details for $Ni(C_2H_4)_n$ (where n = 1, 2, 3) are tabulated for reference purposes in Table 1.

1. Nickel Atom-Nickel Diatom Ultraviolet-Visible Experiments

That one is really manipulating atomic nickel in these crochemical $Ni/C_2H_4/Ar$ reactions can easily be demonstrated by recording the uv-

Table I. Relevant γ_{CC} and δ_{CH_2} Vibrational Modes of $Ni(C_2H_4)_n$ and $Ni_2(C_2H_4)_m$ Species (where n = 1, 2, 3; and m = 1, 2).

$Ni(C_2H_4)$[a]	$Ni(C_2H_4)_2$[a]	$Ni(C_2H_4)_3$[a]	$Ni_2(C_2H_4)$[b, d]	$Ni_2(C_2H_4)_2$[b, d]	Mode[c]
1499	1465	1514	1488	1504	$\nu C{=}C$
1160	1223	1246	1208	1232	δCH_2
			1180		

[a] A complete list of vibrational frequencies and assignments for these species are listed in Ref. 11.

[b] A species absorbing at 1508/1240 cm^{-1} could be a matrix split component of $Ni_2(C_2H_4)_2$. A structural isomer is also possible as is a higher stoichiometry species such as $Ni_2(C_2H_4)_3$ (see text).

[c] Frequencies in cm^{-1}.

[d] νCH_2 stretching modes at 2880 and 2908 cm^{-1} can be associated with these species, although their low intensities precludes a specific assignment. The persistence of the $\rho_w CH_2$ band at 910 cm^{-1} after warmup to 30-35 °K implies that part of the intensity of this band is attributable to $Ni_2(C_2H_4)_1$ or $_2$. Low frequency bands were also observed at 446, 416, 376 cm^{-1} (probably NiC modes) which, from their warmup behavior, appear to belong to three different species; the 376 cm^{-1} band seems to parallel the growth-decay properties of $Ni(C_2H_4)_{2,3}$ while those at 446/416 cm^{-1} follow the pattern of $Ni_2(C_2H_4)_2/Ni_2(C_2H_4)$, respectively.

visible spectrum of the corresponding Ni/Ar mixture under identical concentration and deposition conditions.[13] For example, using Ni/Ar $\simeq 1/10^4$ dilutions which minimize surface diffusion and metal aggregation processes, one observes at 10° K the optical spectrum shown in Figure 1A. Apart from the usual matrix induced frequency shifts and band splittings, the majority of the observed absorptions can be reasonably well correlated with the atomic resonance lines of gaseous nickel (see Gruen for details of atomic-matrix-correlation [AMCOR] techniques).[14] In particular, note that the region to energies lower than 330 nm is completely devoid of spectral lines.

On increasing the Ni/Ar matrix ratio by a factor of ten ($1/10^3$) and recording the optical spectrum at 10° K (Figure 1B) one observes three new absorptions in the regions of 350, 420 and 510 nm, besides those previously ascribed to atomic Ni. The 350 nm and 510 nm bands display associated vibrational fine structure with spacings of the order of 330 cm^{-1} and 360 cm^{-1}, respectively. This group of three new absorptions always appears with approximately the same relative intensities under a variety of deposition and warmup conditions. Of particular importance is the fact that they are the first observable spectral lines to develop on entering the nickel concentration regime, which favors appreciable surface diffusion and aggregation effects.[15] On the basis of a series of Ni/Ar concentration experiments in the range $1/10^4$ to $1/10^2$ and by comparison with the more complete analysis of Moskovits and Hulse,[16] we feel confident in ascribing the three absorptions at 350, 420 and 510 nm to diatomic nickel, Ni_2. The nature of these transitions may be understood by considering the

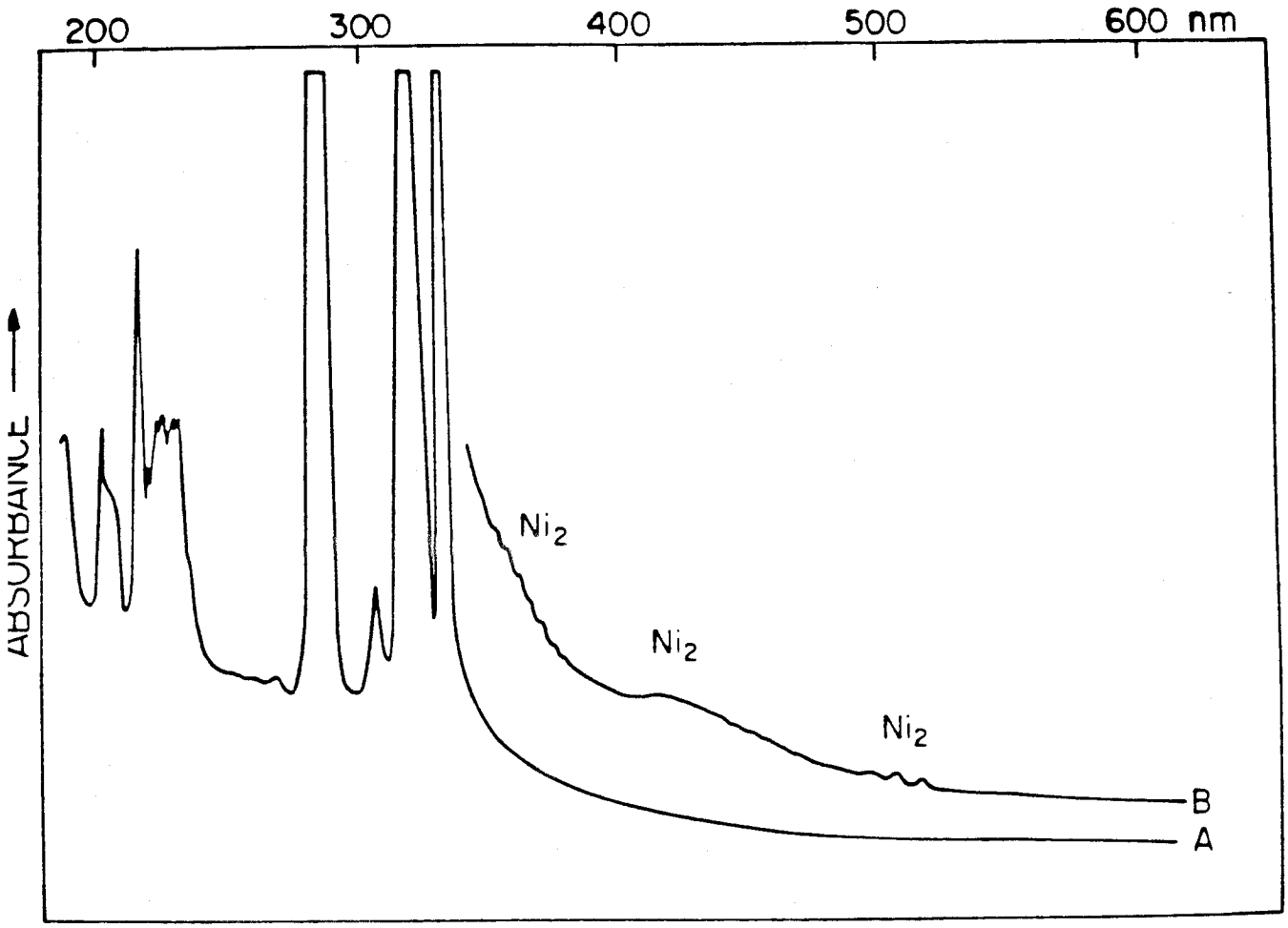

Figure 1. The uv-visible spectrum of Ni/Ar (A) $1/10^4$ and (B) $1/10^3$ matrices at 10° K showing the presence of isolated Ni atoms under high dilution conditions (A) and both Ni atoms and Ni_2 molecules under lower dilution conditions.

essential features of the Ni_2 bond.[17] The ground state of the dimer involves $^3D(4s^1\,3d^9)$ atoms coupled to produce primarily a 4s-4s bond (see Section III). Thus diatomic transitions should be of four general types: $3d \rightarrow 4p$, $3d \rightarrow 4s\sigma_u$, $4s\sigma_g \rightarrow 4p$, and $4s\sigma_g \rightarrow 4s\sigma_u$. The observed Ni_2 bands at 350 and 510 nm each exhibit vibrational structure very similar to the ground state.[17,18] and thus must correspond to transitions that do not strongly perturb the 4s-4s bond. Only $3d \rightarrow 4p$ transitions satisfy this requirement; for atomic Ni these transitions are observed in the regions of 270 to 320 nm and 350 to 390 nm (differing only in the coupling of the open-shell orbitals).[19] As such, each set of atomic transitions may be considered as the source of the observed features at 350 and 510 nm, respectively. The structureless band at 420 nm is more ambiguous. Disruption of the 4s-4s bond is suggested by the band shape; however, transitions from any of the four types listed could produce this effect, and none can presently be eliminated from consideration (preliminary matrix photochemical experiments of samples containing Ni and Ni_2 suggest that 420 nm radiation leads to dissociation of Ni_2 and regeneration of atomic nickel).[20]

2. Infrared Experiments. Having established the experimental conditions required to generate appreciable amounts of Ni_2 in Ar, we proceeded to perform a series of $Ni/C_2H_4/Ar$ concentration experiments in an effort to identify binuclear $Ni_2(C_2H_4)_n$ species in the presence of the previously indentified complexes of $Ni(C_2H_4)_n$. By operating in the $C_2H_4/Ar \simeq 1/50$ concentration range [which under $Ni/Ar \simeq 1/10^4$ conditions favors mononuclear $Ni(C_2H_4)_{1,2}$] we hoped

that by examining Ni/Ar $\simeq 1/10^3 - 1/10^2$ depositions we would be able to identify low stoichiometry binuclears, such as, $Ni_2(C_2H_4)_{1,2}$. In these experiments, the most intense and definitive vibrational modes for identifying new products turned out to be ν_{CC} stretching and δ_{CH_2} deformations. The results of a typical infrared experiment under mononuclear conditions are displayed in Figure 2A, whereas those under combined mononuclear/binuclear conditions are shown in Figure 2B. Besides the ν_{CC} and δ_{CH_2} of $Ni(C_2H_4)$ (1499/1160 cm^{-1}) and $Ni(C_2H_4)_2$ (1465/1223 cm^{-1}) labelled I and II, respectively, in Figure 2B, one notices the conspicuous appearance of a new ν_{CC} stretching mode at 1488 cm^{-1} and new δ_{CH_2} deformational modes at 1208/1180 cm^{-1}. These absorptions always appear with approximately the same intensities under a variety of deposition conditions (vide infra) and display parallel growth and decay behavior during matrix annealing. It is particularly noteworthy that this new species appears to dominate the spectrum on warming $C_2H_4/Ar \simeq 1/50$ mixtures to 35° K. Further warming to 40 - 45° K causes the ν_{CC} stretching mode of $Ni(C_2H_4)_2$ at 1465 cm^{-1} as well as the δCH_2 of $Ni(C_2H_4)$ at 1160 cm^{-1} to essentially decay to zero with the concomitant growth of the ν_{CC} of $Ni(C_2H_4)_3$ at 1514 cm^{-1} (Figure 3). The persistence of the bands around 1232 cm^{-1} and 1504 cm^{-1} [which cannot be associated with $Ni(C_2H_4)_2$ and $Ni(C_2H_4)$, respectively, at this stage of the experiment][11] suggests but does not prove the presence of a second new species (vide infra). Since the new species absorbing at 1488/1208/1180 cm^{-1} only appears under reaction conditions favoring binuclear complex formation and since there is a carbon-carbon stretching mode in the 1500 cm^{-1} region, we assign this

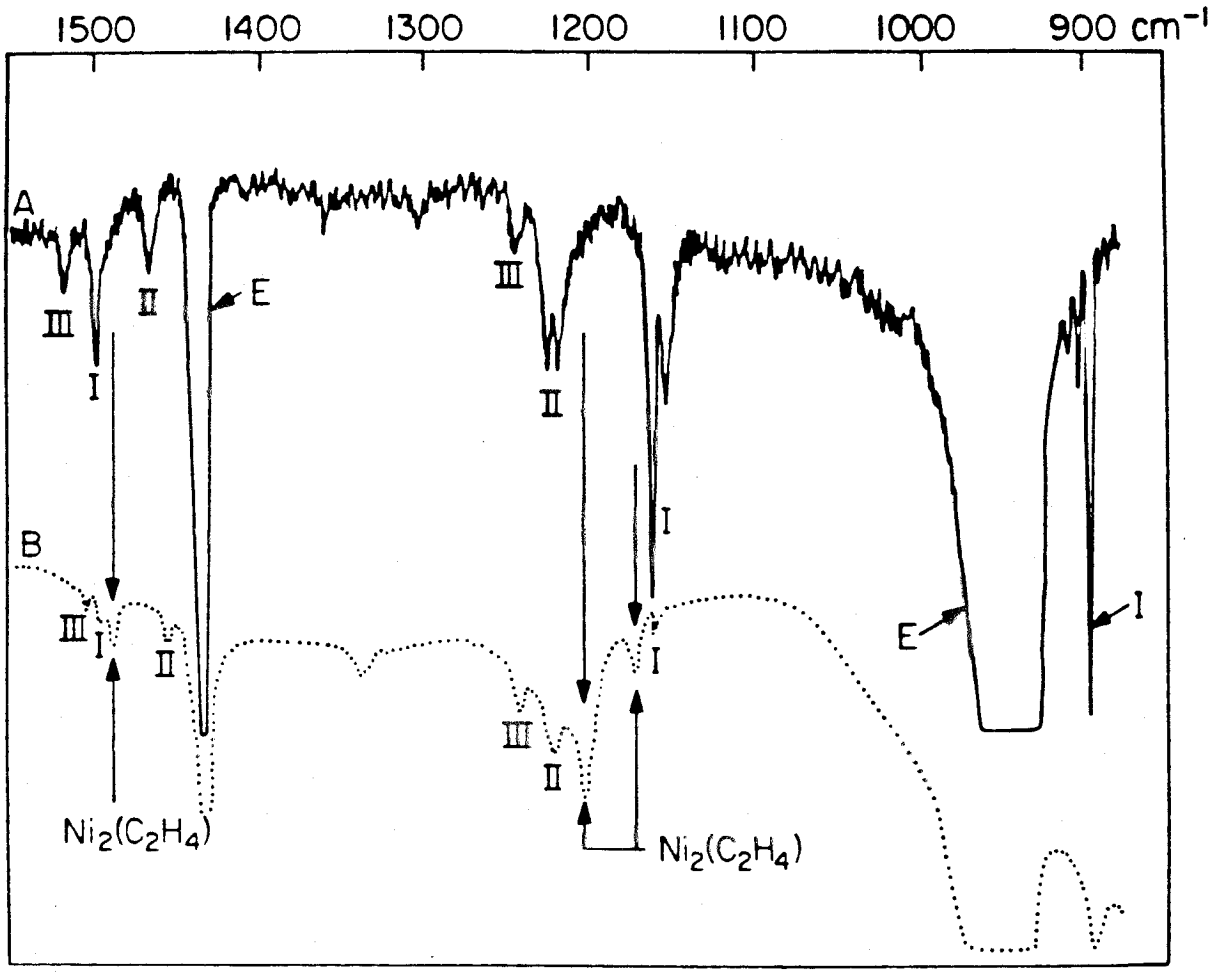

Figure 2. The matrix infrared spectrum observed on depositing Ni atoms with $C_2H_4/Ar \simeq 1/50$ mixtures at 15°K with (A) $Ni/Ar \simeq 1/10^4$ and (B) $Ni/Ar \simeq 1/10^3$ [absorptions associated with free ethylene in the matrix are labelled E and $Ni(C_2H_4)_n$ where n = 1, 2, 3 and labelled I, II, III, respectively], showing the formation of $Ni_2(C_2H_4)$.

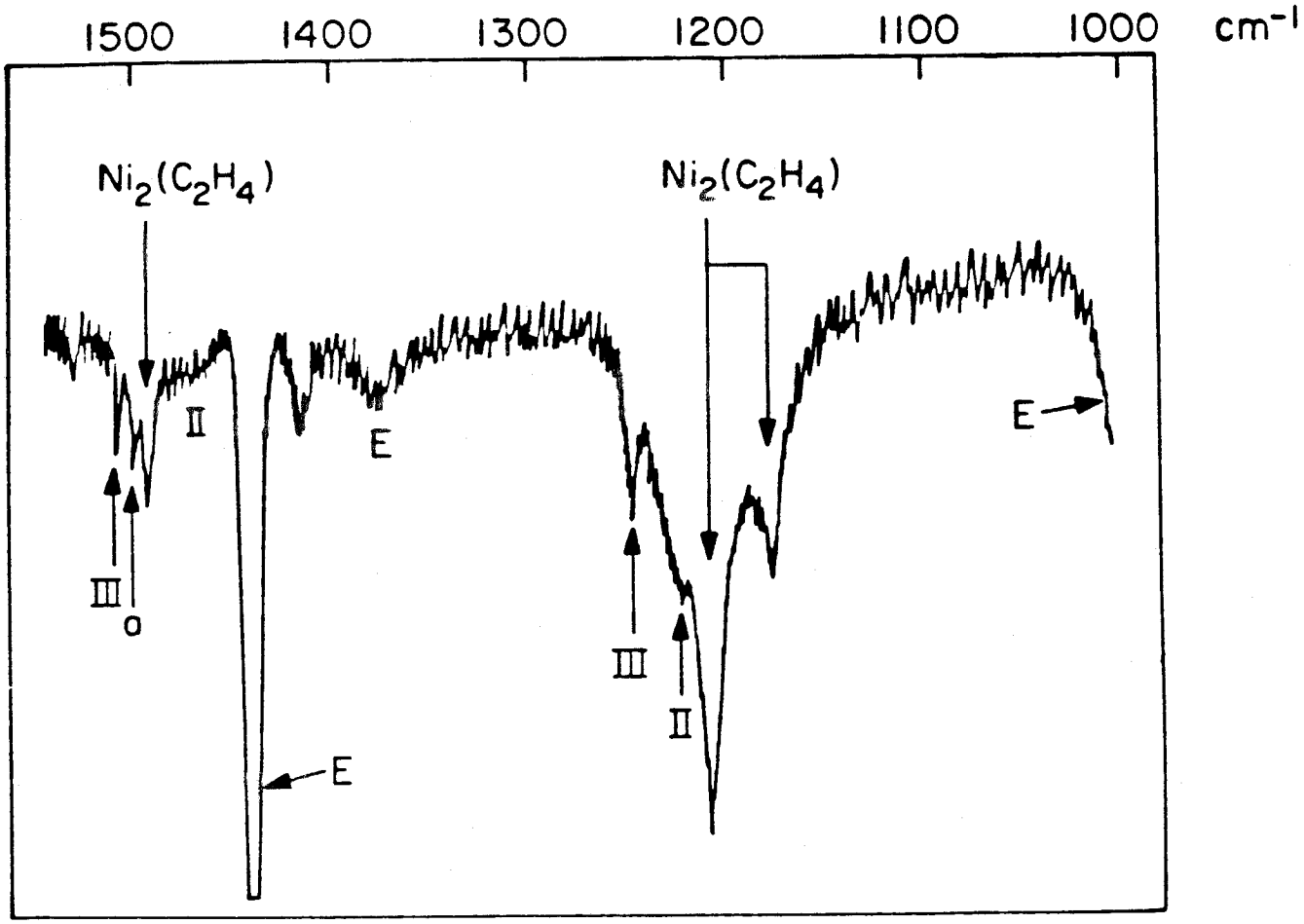

Figure 3. The same as Figure 2B except after matrix annealing to 40-45° K and recooling to 10° K ["a" represents either a trace of I or the new species $Ni_2(C_2H_4)_2$ (see text)].

species as $Ni_2(C_2H_4)$ containing a π-complexed form of ethylene.

Further evidence for the assignment of the lowest ethylene stoichiometry binuclear stems from experiments in $C_2H_4/Ar \simeq 1/10$ to 1/50 with $Ni/Ar \simeq 1/10^4$ to $1/10^2$. A typical infrared trace at $C_2H_4/Ar \simeq 1/10$ is shown in Figure 4A under Ni/Ar conditions which favor mononuclear complex formation, from which the characteristic absorptions of $Ni(C_2H_4)$ (1496/1158 cm^{-1}), $Ni(C_2H_4)_2$ (1465/1235/1224 cm^{-1}, and $Ni(C_2H_4)_3$ (1514/1246 cm^{-1}) are easily recognized. By moving to Ni/Ar conditions which favor mononuclear and binuclear complex formation and using $C_2H_4/Ar = 1/25$, we obtain infrared spectra of the type shown in Figure 4B. Note especially under these conditions the spectroscopic absence of $Ni(C_2H_4)$, which is best appreciated by the inability to detect the characteristic δ_{CH_2} mode at 1160 cm^{-1}. Of particular significance in Figure 4B is the appearance of two new ν_{CC} modes at 1488 and 1504 cm^{-1} which appear to go together with the new δ_{CH_2} modes at 1232 cm^{-1} and 1208/1180 cm^{-1}, respectively. This can be illustrated from a typical warmup experiment to 30° K and 35° K which shows the growth of the 1504/ 1232 cm^{-1} pair at essentially the same rate, concomitant with the decay of the 1488/1208/1180 cm^{-1} group of absorptions associated with the low stoichiometry fragment $Ni_2(C_2H_4)$ (Figure 5B). Therefore the results of high Ni concentration $C_2H_4/Ar \simeq 1/50 - 1/24$ experiments provide convincing evidence that two binuclear binary nickel ethylene complexes can be generated, most probably containing one and two π-complexed ethylene ligands, that is, $Ni_2(C_2H_4)$ and $Ni_2(C_2H_4)_2$, respectively. A small splitting observed on the ν_{CC} mode of

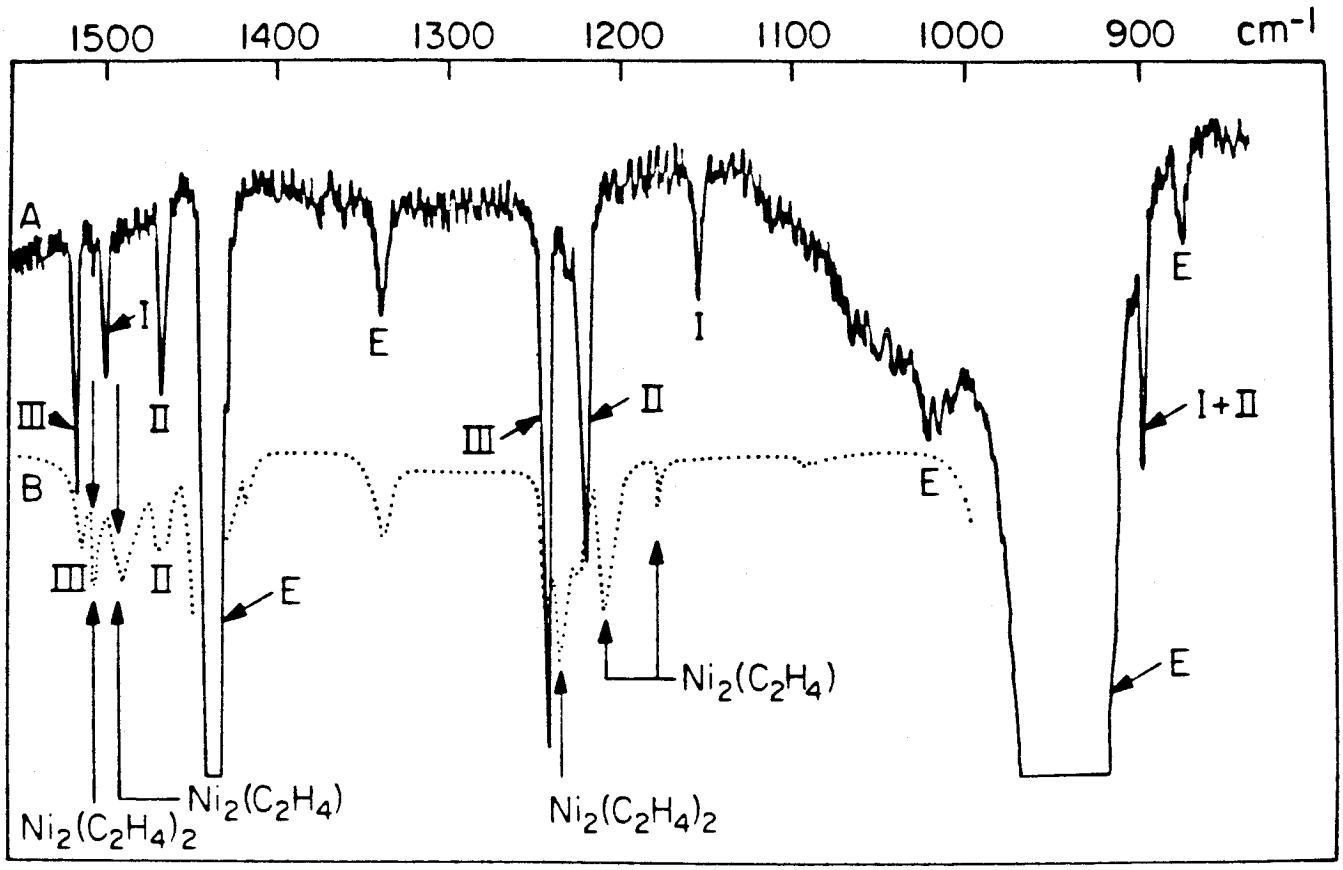

Figure 4. The matrix infrared spectrum observed on depositing Ni atoms with (A) $C_2H_4/Ar \simeq 1/10$ mixtures at 15° K with $Ni/Ar \simeq 1/10^4$ and (B) $C_2H_4Ar \simeq 1.25$ mixtures at 15° K with $Ni/Ar \simeq 1/10^3$ showing the formation of $Ni_2(C_2H_4)$ and $Ni_2(C_2H_4)_2$.

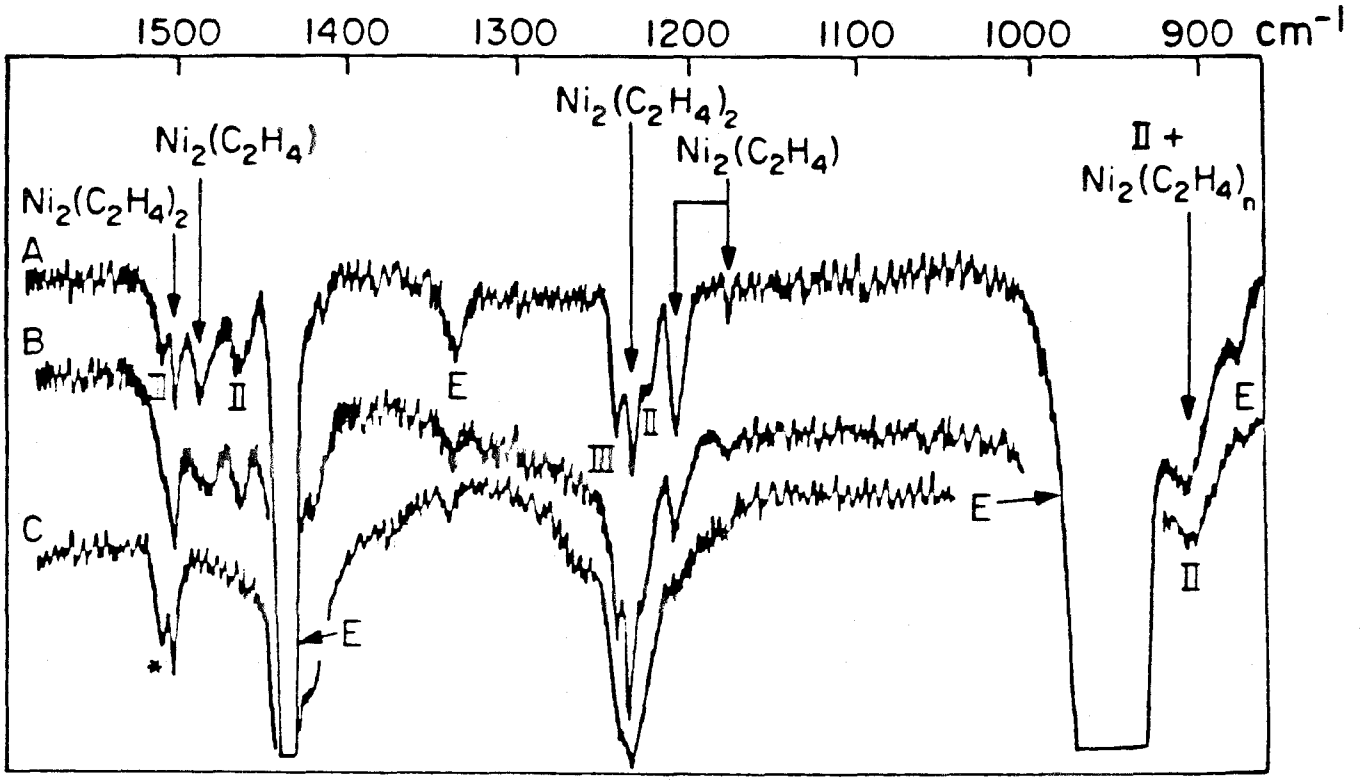

Figure 5. (A) The same as Figure 4B, (B-C) the effect of 30° K and 35° K annealing. The asterisk probably indicates a matrix site splitting of $Ni2(C_2H_4)_2$ rather than evidence for a higher stoichiometry binuclear $Ni_2(C_2H_4)_m$ where $m > 2$.

$Ni_2(C_2H_4)_2$ at 1508/1504 cm^{-1} probably represents a matrix site effect rather than evidence for a higher stoichiometry mononuclear (vide infra).

Similar experiments performed in $C_2H_4/Ar = 1/10$ matrices and $Ni/Ar \simeq 1/10^4$ to $1/10^2$ generally confirmed the above proposals. On deposition at 15° K, apart from the characteristic ν_{CC} and δ_{CH_2} modes of $Ni(C_2H_4)_2$ and $Ni(C_2H_4)_3$,[11] one observes only those lines ascribed earlier to $Ni_2(C_2H_4)$ and $Ni_2(C_2H_4)_2$ (Figure 6A). As seen in the 1/25 experiments, a small splitting is again observed on the ν_{CC} mode of $Ni_2(C_2H_4)_2$ at 1508/1504 cm^{-1} and is probably best ascribed to a matrix site effect rather than evidence for a higher stoichiometry binuclear (Figure 6).

Finally, it is worth commenting briefly on the effect of increasing the Ni/Ar ratio into the range $1/10^2$ - 1/10 and the deposition temperature from 15 to 25° K. From a uv-visible point of view the Ni/Ar spectrum "in the absence of C_2H_4" shows the growth of a new absorption centered at roughly 460 nm with vibrational fine structure and an average spacing of approximately 200 cm^{-1}. In accordance with the work of Moskovits and Hulse[16] we feel confident that this new absorption is probably best associated with the second stage of the nickel aggregation process, namely to tri-nickel, Ni_3. We refer the reader to Ref. 16 for details of the Ni_3 analysis and note in passing that an earlier Ni/Ar report by DeVore et al.[21] of a band at 460 nm with an average vibrational spacing of 192 cm^{-1} and a assignment to Ni_2 is probably incorrect. On the basis of our experiments and those of Moskovits and Hulse,[16] the 460 nm absorption is best assigned to Ni_3.

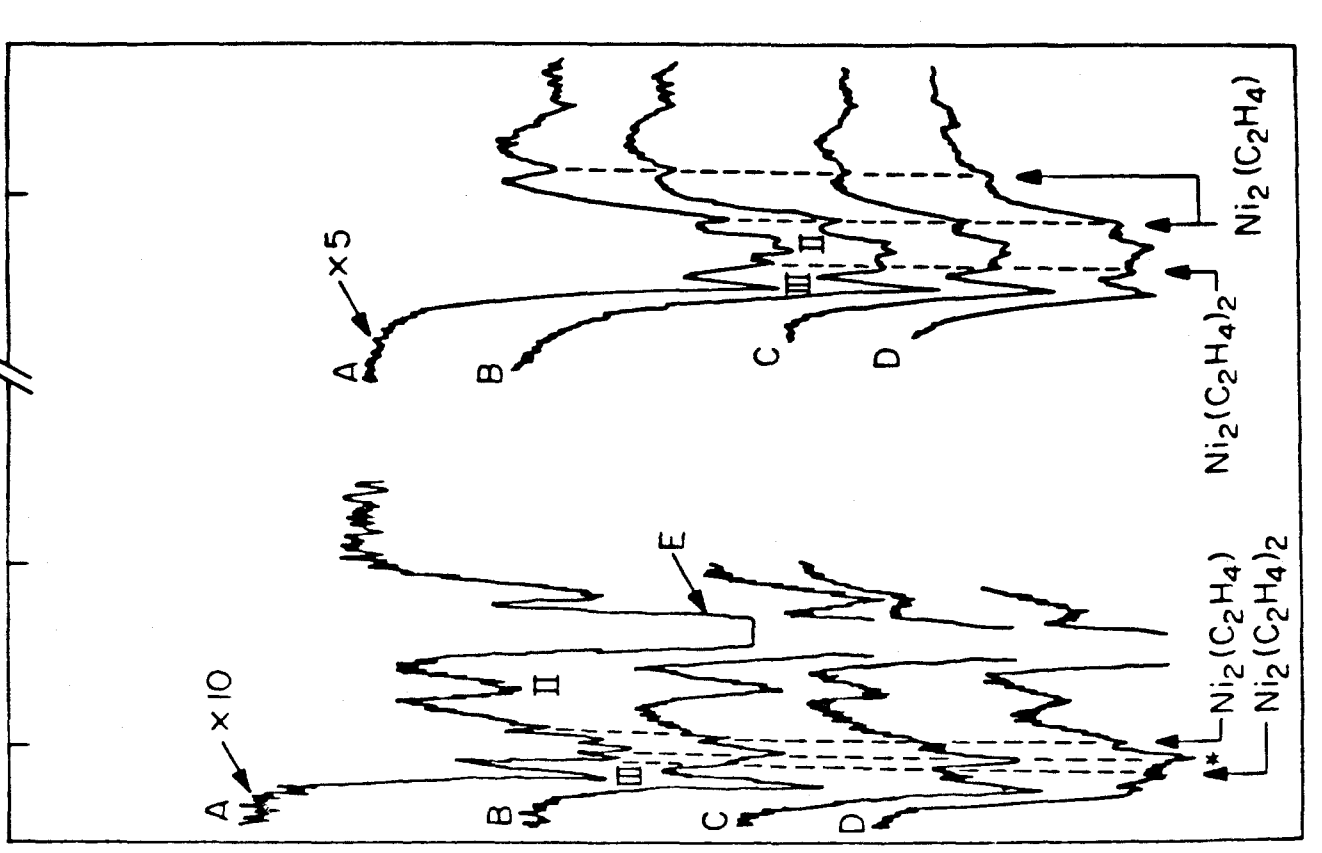

Figure 6. (A) The same as Figure 2B except that $C_2H_4/Ar \simeq 1/10$ mixtures were used. (B-D) represent a series of warmup experiments to 25, 30, and 35° K, respectively, and recooling to 10° K for spectral recording.

By experimenting with $Ni/C_2H_4/Ar$ cocondensations under conditions which favor the presence of some Ni_3, we observe a general broadening of the infrared ν_{CC} and δ_{CH_2} modes in the region of 1520 - 1450 cm^{-1} and 1250 - 1180 cm^{-1}, respectively (Figure 7). The breadth of the spectral absorbances and the generally ill-defined nature of the infrared spectra preclude a definitive assignment to a particular $Ni_3(C_2H_4)_p$ species. However, it is pertinent to note that on passing from $Ni(C_2H_4)_n$ to $Ni_2(C_2H_4)_m$ experimental conditions, a noticeable increase in the ν_{CC} and δ_{CH_2} bandwidths is experienced (Figure 7B) which becomes even more pronounced under conditions which favor $Ni_3(C_2H_4)_p$ and higher cluster species (Figure 7C). In fact the general crowding of infrared active ν_{CC} and δ_{CH_2} modes around the 1500/1220 cm^{-1} spectral regions closely extrapolates to the situation experienced for C_2H_4 chemisorbed on Group VIII supported metals.[22]

These observations, in conjunction with the presence of ν_{CC} stretching modes in the 1500 cm^{-1} region for $Ni_x(C_2H_4)_y$ (where x = 1, 2, 3) taken in combination with the general similarity of the vibrational spectra of these small nickel-ethylene cluster complexes, provide convincing support for a localized bonding description of ethylene chemisorbed on nickel and a π-nickel-ethylene interaction (see Section I.C of this thesis).

Ultraviolet-Visible Experiments. Recall that on depositing Ni atoms with $C_2H_4/Ar \simeq 1/50$ mixtures at 15° K, under metal concentration conditions favoring mononuclear complex formation ($Ni/Ar \simeq 1/10^4$), one observes an optical spectrum dominated by an intense

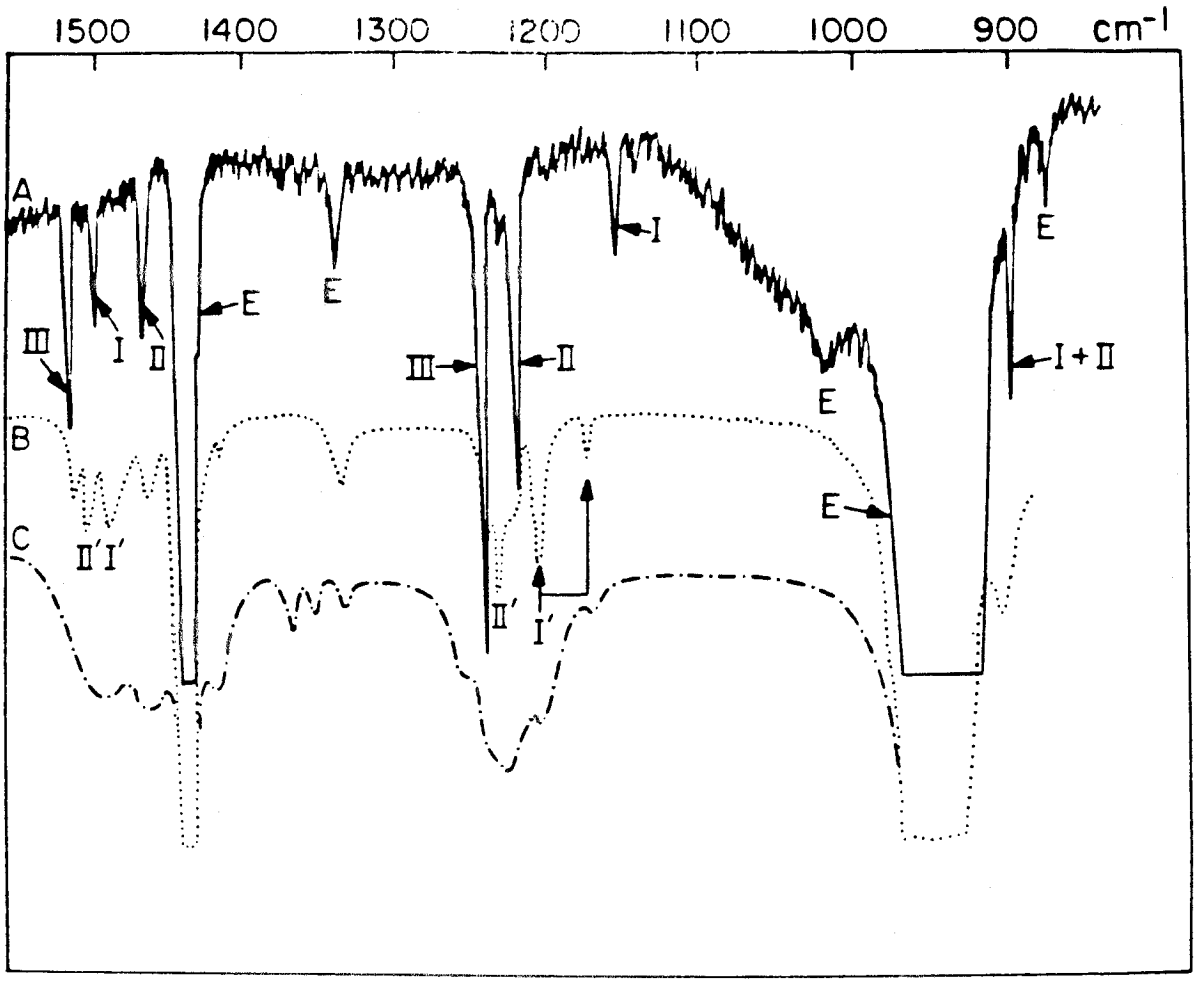

Figure 7. The matrix infrared spectrum observed on depositing Ni atoms (A) with $C_2H_4/Ar \simeq 1/10$ mixtures at 15°K with $Ni/Ar \simeq 1/10^4$, (B) with $C_2H_4/Ar \simeq 1/25$ mixtures at 15°K with $Ni/Ar \simeq 1/10^3$, and (C) $Ni/Ar \simeq 1/10^2$ showing the formation of $Ni_2(C_2H_4)$ [denoted as I'] and $Ni_2(C_2H_4)_2$ [denoted as II'] and the gradual progression from $Ni(C_2H_4)_n$ to $Ni_2(C_2H_4)_n$ to $Ni_x(C_2H_4)_n$ (where $x \simeq 3$).

uv-absorption centered at roughly 320 nm.[23] The corresponding infrared data imply that this uv band is associated with $Ni(C_2H_4)$.[11] A typical series of optical spectra for the mononuclear complexes $Ni(C_2H_4)_n$ [and for comparison $Ni(C_3H_6)_n$] obtained under these dilute conditions is shown in Figure 8. The spectra were recorded under constant concentration conditions for a variety of temperatures in the range 15° - 40° K and serve to illustrate the predominance of the mono-olefin species upon deposition and the subsequent conversion to the bis- and tris-olefin complexes on matrix annealing. Increasing the Ni concentration to the range $Ni/Ar \simeq 1/10^3$ while holding $C_2H_4/Ar \simeq 1/50$ enhances the formation of $Ni_2(C_2H_4)$, and we observe optical spectra of the type shown in Figure 9A, in which the 320 nm absorption of $Ni(C_2H_4)$ no longer dominates the spectrum. Instead, an intense uv-absorption peaking at roughly 243 nm with a noticeable shoulder at about 314 nm is the most prominent spectral feature, with the 280 nm band of $Ni(C_2H_4)_2$ appearing as a shoulder. On warming these matrices to 30 - 40° K, the 280 nm shoulder and the 320 band tend to decay (Figure 9B) which parallels the warm-up behavior observed for $Ni(C_2H_4)$ in the presence of $Ni_2(C_2H_4)$ (see Section II.B.2). On these grounds we feel reasonably confident in assigning the 243 nm absorption to $Ni_2(C_2H_4)$. Experiments performed at higher C_2H_4/Ar ratios and higher temperature depositions 20-25° K [designed to enhance the generation of $Ni_2(C_2H_4)_2$] produce a noticeable broad spectral feature in the region of 370 nm (Figure 10) which cannot be attributed to either $Ni(C_2H_4)_{1,2,3}$[11,23] or $Ni_2(C_2H_4)$. We tentatively assign this band to an electronic transition associated with the presence

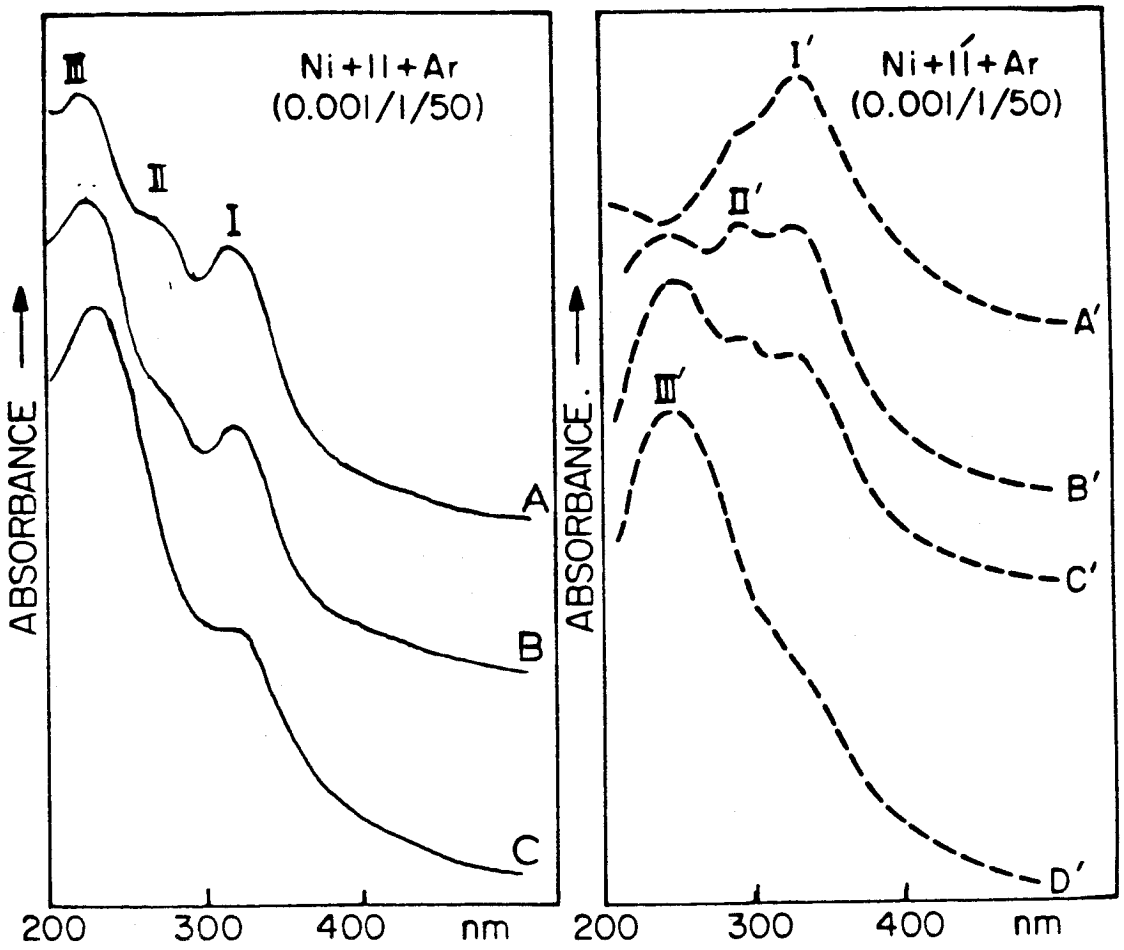

Figure 8. The uv-visible spectra obtained on depositing Ni atoms with (A) $C_2H_4/Ar \simeq 1/50$ and (A') $C_3H_6/Ar \simeq 1/50$ mixtures with $Ni/Ar \simeq 1/10^4$ at 15° K; (B-C) and (B'-D') the effects of warming these matrices in the range 20-35° K. showing the initial formation of $Ni(C_2H_4)$, (I) and $Ni(C_3H_6)$, (I') and the gradual conversion to $Ni(C_2H_4)_2$, (II), $Ni(C_3H_6)_2$, (II'), and $Ni(C_2H_4)_3$, (III), $Ni(C_3H_6)_3$, (III') where C_3H_6 is propylene.[23]

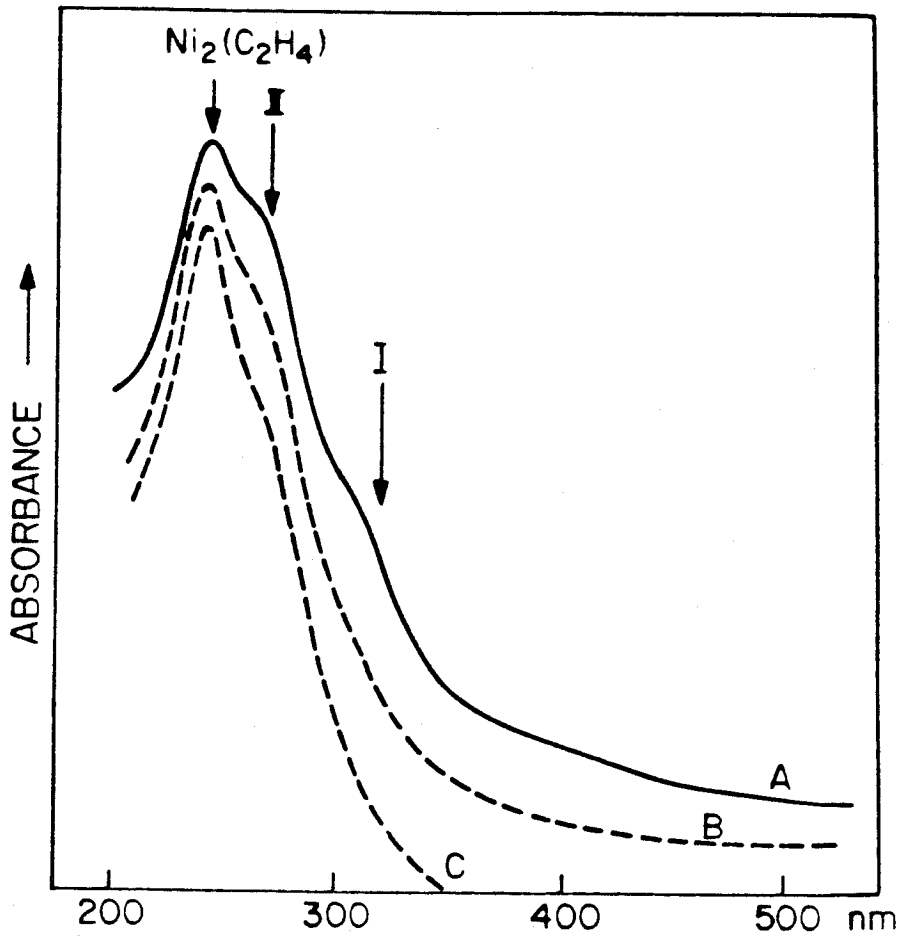

Figure 9. The matrix uv-visible spectrum observed (A) on depositing Ni atoms with a $C_2H_4/Ar \simeq 1/50$ mixture at 15° K with $Ni/Ar \simeq 1/10^3$ and (B-C) after warming the matrix to 30° K and 40° K, respectively, and recooling to 10° K for spectral recording purposes [I and II represent traces of $Ni(C_2H_4)$ and $Ni(C_2H_4)_2$, respectively].

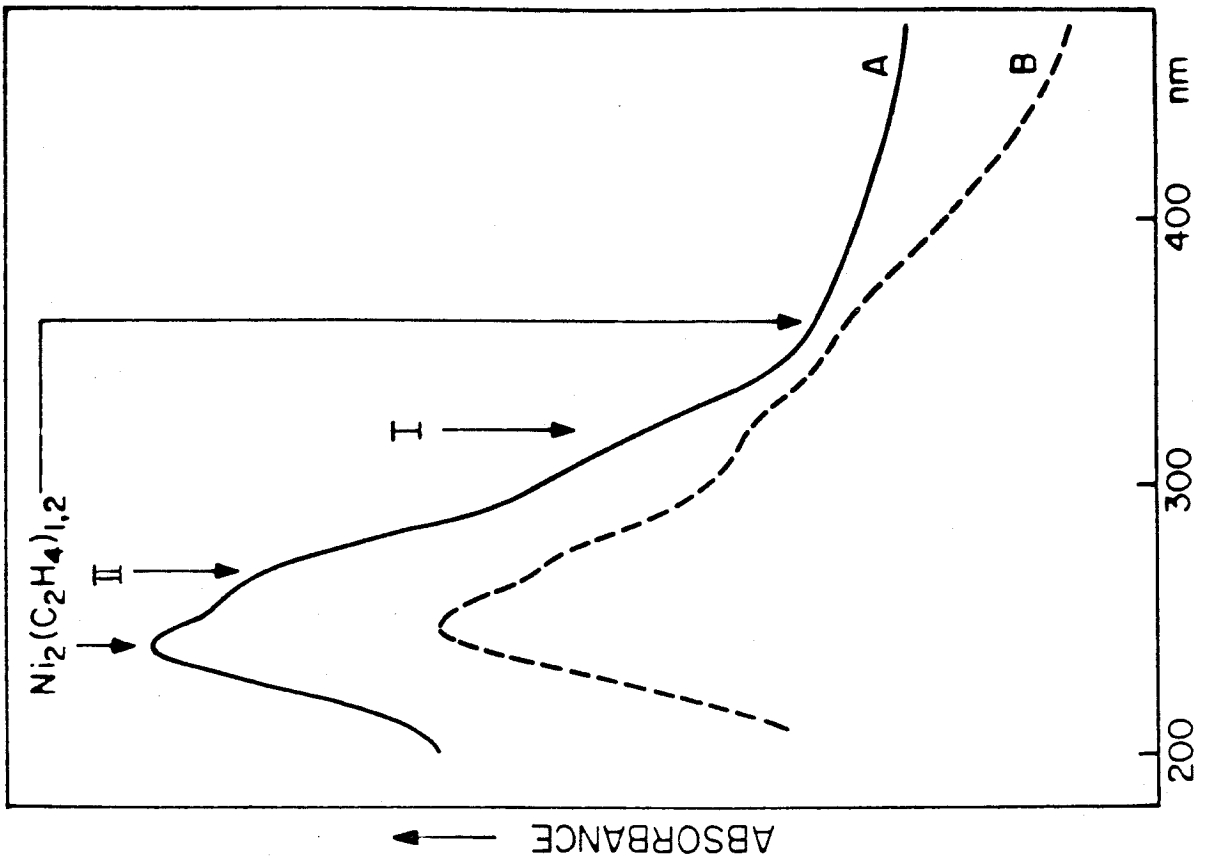

Figure 10. The same as Figure 9A and B showing the effect of increasing the Ni concentration (two-fold) and deposition temperature (25° K).

of the Ni-Ni bond in $Ni_2(C_2H_4)_2$ although one cannot be confident that band overlap in the 200-300 nm region has not obscured any other spectral characteristics of $Ni_2(C_2H_4)_2$.[24] The nature of these intense uv bands is difficult to determine, and we will defer discussion of them until the bonding in these finite clusters has been described.

III. The Generalized Valence Bond Description of $Ni_2(C_2H_4)$

Before discussing the bonding and spectral properties of the $Ni_2(C_2H_4)$ complex itself, we will first consider these same properties for the various molecular fragments from which $Ni_2(C_2H_4)$ may be considered to be derived. Specifically, we will consider first the bonding and low-lying states of the Ni_2[17] and $Ni(C_2H_4)$[25] molecules, noting the features common to both of them that make the formation of $Ni_2(C_2H_4)$ a logical next step in the sequence of nickel-ethylene cluster complexes.

A. $Ni(C_2H_4)$ π-Complex

The formation of an Ni-ethylene complex occurs in a manner that closely follows what was found for $Ni(C_2H_2)$.[1] The key to bond formation in each case is the presence of a polarizable π orbital on the ligand. Bringing up the C_2H_4 molecule to the Ni atom along an axis bisecting the CC bond and normal to the ethylene molecular plane causes this π orbital to interact initially with the Ni 4s orbital. This interaction is repulsive and, as for $Ni(C_2H_2)$,[1] causes a stabilization of the $^3D(4s^1\,3d^9)$ state of the Ni atom. The singly occupied 4s orbital mixes 4p character and polarizes away from the ligand. This allows

the ethylene π orbital to delocalize into the empty 4s-p orbital on the Ni. The 3d orbitals remain highly localized on the Ni atom, and there is little evidence for 3d-ethylene π^* backbonding. The lowest state results from placing the single 3d electron in a δ_{xy} orbital, but the four other possible 3d occupations produce states all within 0.5 eV of the ground state. The similarity between the ethylene and acetylene complexes is clearly illustrated in Figure 11 where bonding orbitals for the two π-complexes are compared. The bond energy for the ethylene complex, 14.2 kcal, is very close to that calculated for acetylene (16.7 kcal). The distortions of the ethylene ligand are very small, and serve to maximize the delocalization of π-orbital towards the Ni. The optimum geometry is illustrated in Fig. 12a, and the distortion in this system may be compared with those of $Ni(C_2H_2)$ shown in Fig. 12b.

To a large extent, the strength of the bond is determined by the degree to which the 4s and π orbitals are able to minimize repulsive interactions. If the 4s electron is removed via ionization, the bond strength increases dramatically, to about 60 kcal at the same geometry. The orbitals for this system are shown in Fig. 13, where it can be seen that the changes from the neutral are minor. Only the π-orbital changes noticeably, delocalizing more onto the Ni atom. The removal of the 4s electron increases the electrostatic attracting between the Ni atom and the olefin π bond, producing the increased binding energy.

B. Ni_2

A similar approach may be used to describe the bonding in the

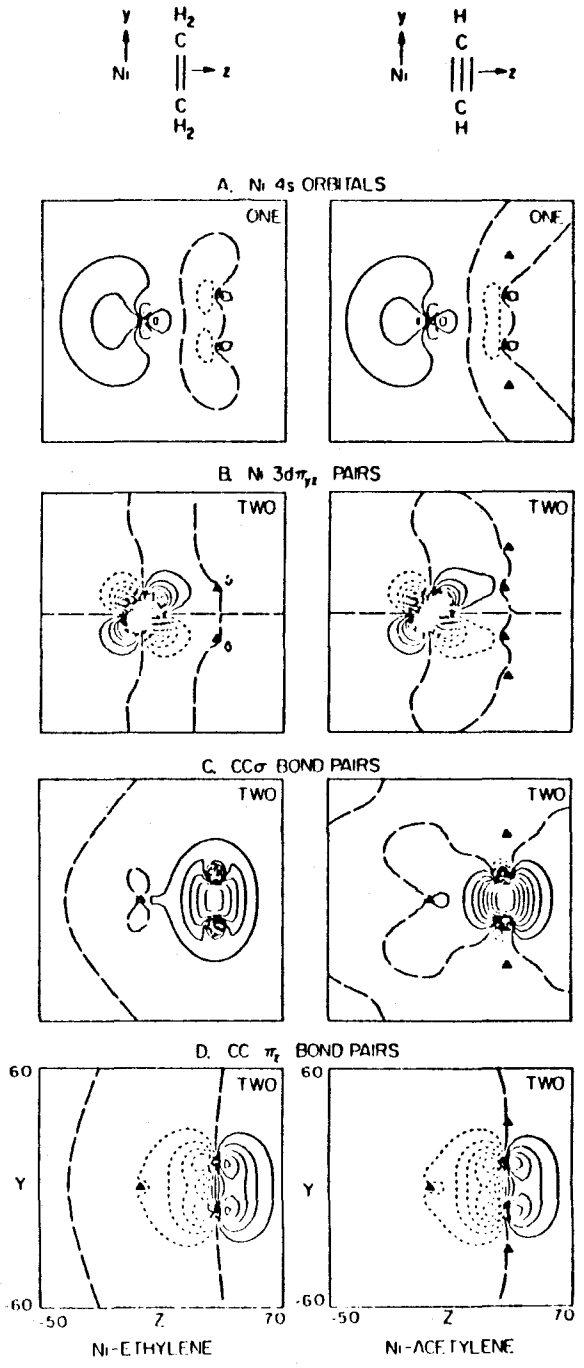

Figure 11. Contour plots of orbitals important in the bonding of Ni-ethylene and Ni-acetylene. Long dashes indicate nodal lines and all contours are uniformly spaced at 0.05 a.u.

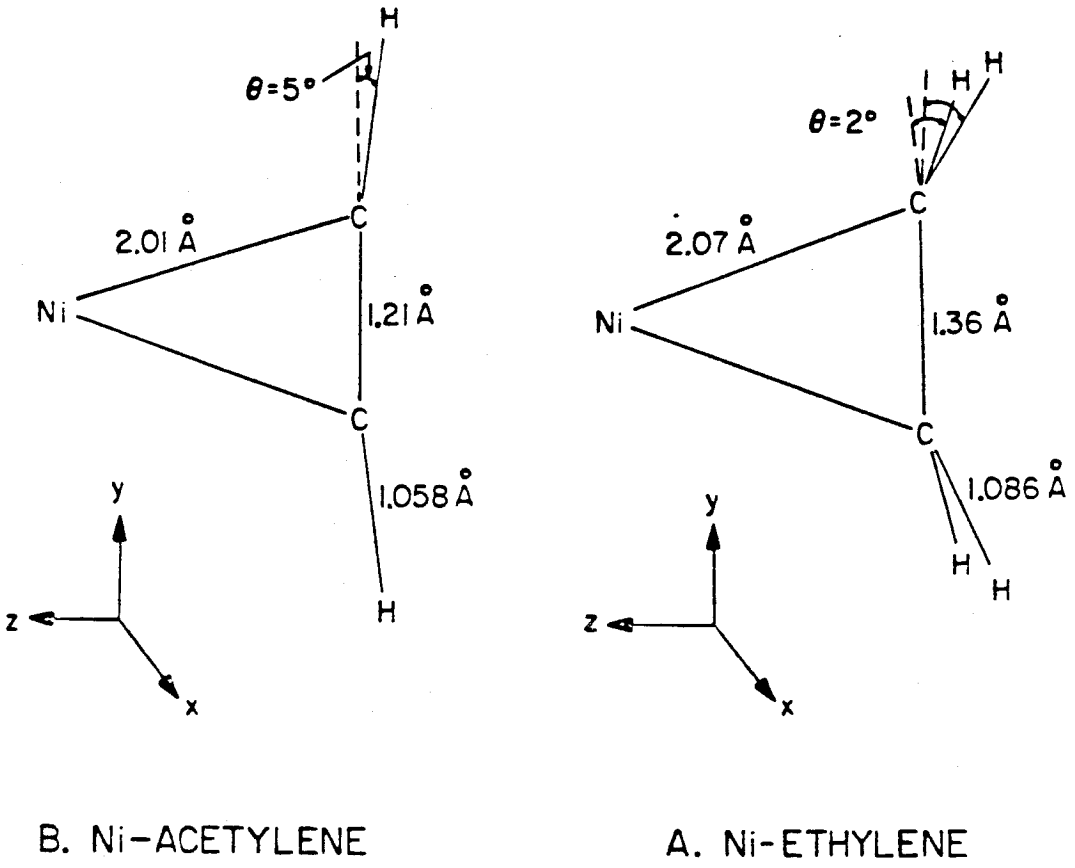

Figure 12. Results of geometry optimization from GVB-CI calculations. CH bond distances were fixed at free molecule values.

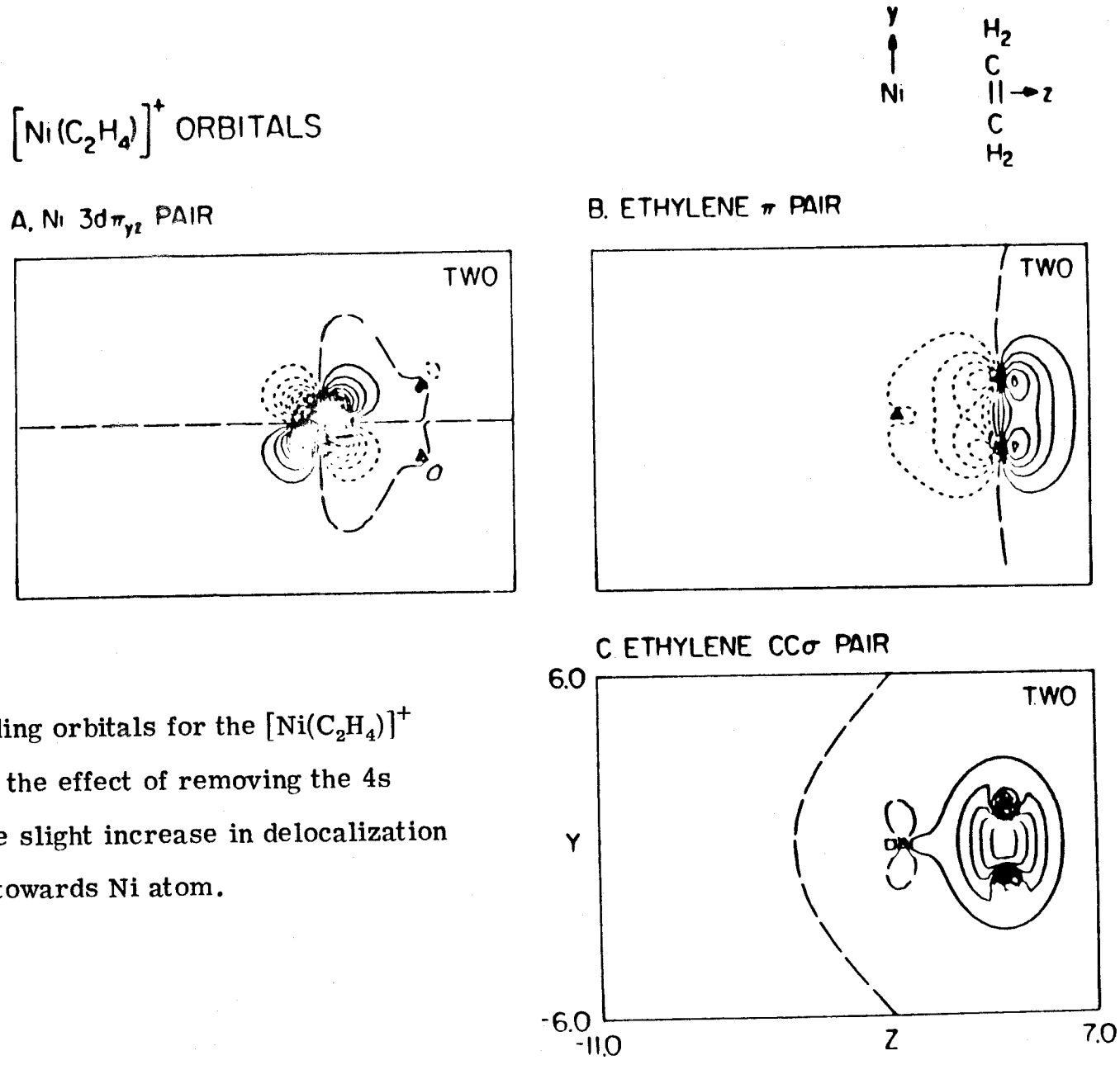

Figure 13. Bonding orbitals for the $[Ni(C_2H_4)]^+$ complex showing the effect of removing the 4s orbital. Note the slight increase in delocalization of the π orbital towards Ni atom.

nickel dimer and a complete discussion has appeared elsewhere.[17] Briefly, since the combination of two Ni atoms in their ^3F ground state configurations would lead to repulsive interactions between the doubly-occupied 4s orbitals, the lowest states of Ni_2 are formed by combining the Ni atoms in their $4s^1 3d^9$ (^3D) states. As a result, there are 50 low-lying states (25 singlets and 25 triplets) that arise from considering the different spin couplings and possible occupations of the singly-occupied 3d orbital on each center. The lowest of these involve singly-occupied δ orbitals on each center. As in the case of $Ni(C_2H_4)$, these 3d orbitals are fully localized on each center, leading to extremely low overlap between δ orbitals on opposite centers. As a result, the lowest triplet state ($^3\Sigma_g^-$) and the lowest singlet ($^1\Gamma_g$) state are essentially degenerate. At the optimum bond distance for Ni_2, the 3d orbitals interact very weakly, and the system is well described as a 4s-4s single-bonded molecule.

C. $\underline{Ni_2(C_2H_4)}$

The essential point to be gained from the above discussion, as it relates to $Ni_2(C_2H_4)$, is that the Ni atoms of both Ni_2 and $Ni(C_2H_4)$ have the same electronic configuration. In $Ni(C_2H_4)$ the singly- occupied 4s orbital is hybridized away from the C_2H_4 region and is triplet coupled to a singly-occupied 3dδ orbital. As described above, this is precisely the configuration most favorable for formation of an Ni-Ni bond. Thus it is expected that the most stable conformation for the $Ni_2(C_2H_4)$ system would involve an ethylene unit π-coordinated "end-on" to the Ni_2 dimer. In Figure 14 are shown the optimum geometries for the

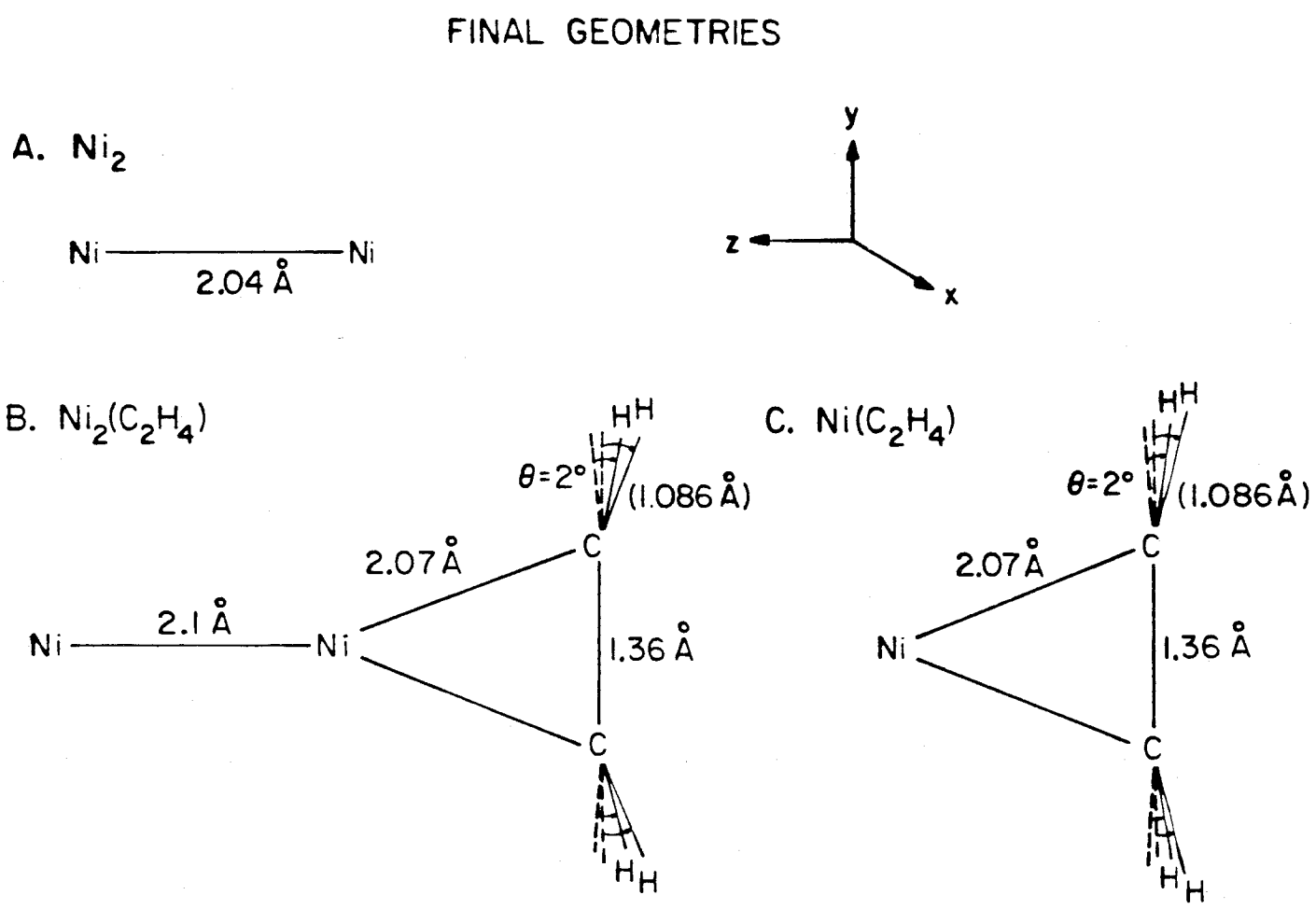

Figure 14. Final geometries for the complexes discussed here from GVB-CI calculations. No change was found in CC distance for $Ni_2(C_2H_4)$ relative to $Ni(C_2H_4)$, so no further optimization of HCC angles was attempted.

$Ni_2(^3\Sigma_g)$, $Ni(C_2H_4)\,^3A_1$, and $Ni_2(C_2H_4)\,^3A_2$ systems obtained from generalized valence bond calculations. In the case of $Ni_2(C_2H_4)$, both the Ni-Ni and CC bond distances were optimized. There was essentially no change (less than 0.01 Å) in the CC distance relative to $Ni(C_2H_4)$. The Ni-Ni distance increased by 0.1 Å relative to Ni_2 to a value of 2.10 Å. The reasons for this may be seen by examining Fig. 15 where orbitals for the $Ni_2(C_2H_4)$ system are shown. The 4s-4s bond of the Ni unit is polarized away from the ethylene molecule, just as for $Ni(C_2H_4)$. This polarization allows a slightly larger exposure of the $3d^9$ shell of the central Ni atom to the C_2H_4 as evidence by the slight increase in binding energy for $Ni_2(C_2H_4)$ to 16.8 kcal. It is this distortion of the 4s-4s bonding orbital that leads to the increase in Ni-Ni distance.

As implied by Fig. 15, there is little change in the nature of the Ni-olefin bond upon coordination of the second Ni atom. This is consistent with the results of the matrix infrared experiments described in Section II of this paper. The slight increase in exposure of the $3d^9$ shell of the Ni atom upon adding the second Ni atom produces opposing effects on ν_{CC} and δ_{CH_2}. The delocalization of the π orbital towards the Ni atom increases slightly, weakening the CC bond as is reflected in the decrease of ν_{CC} from 1499 to 1488 cm^{-1}. Similarly, the slightly bent CH bonds may relax toward the free molecule equilibrium due to the reduction in repulsive interactions with the 4s orbital. The value of δ_{CH_2} then should move towards the free matrix ethylen value of 1243 cm^{-1}; an increase from 1160 cm^{-1} to 1208 cm^{-1} is noted experimentally.

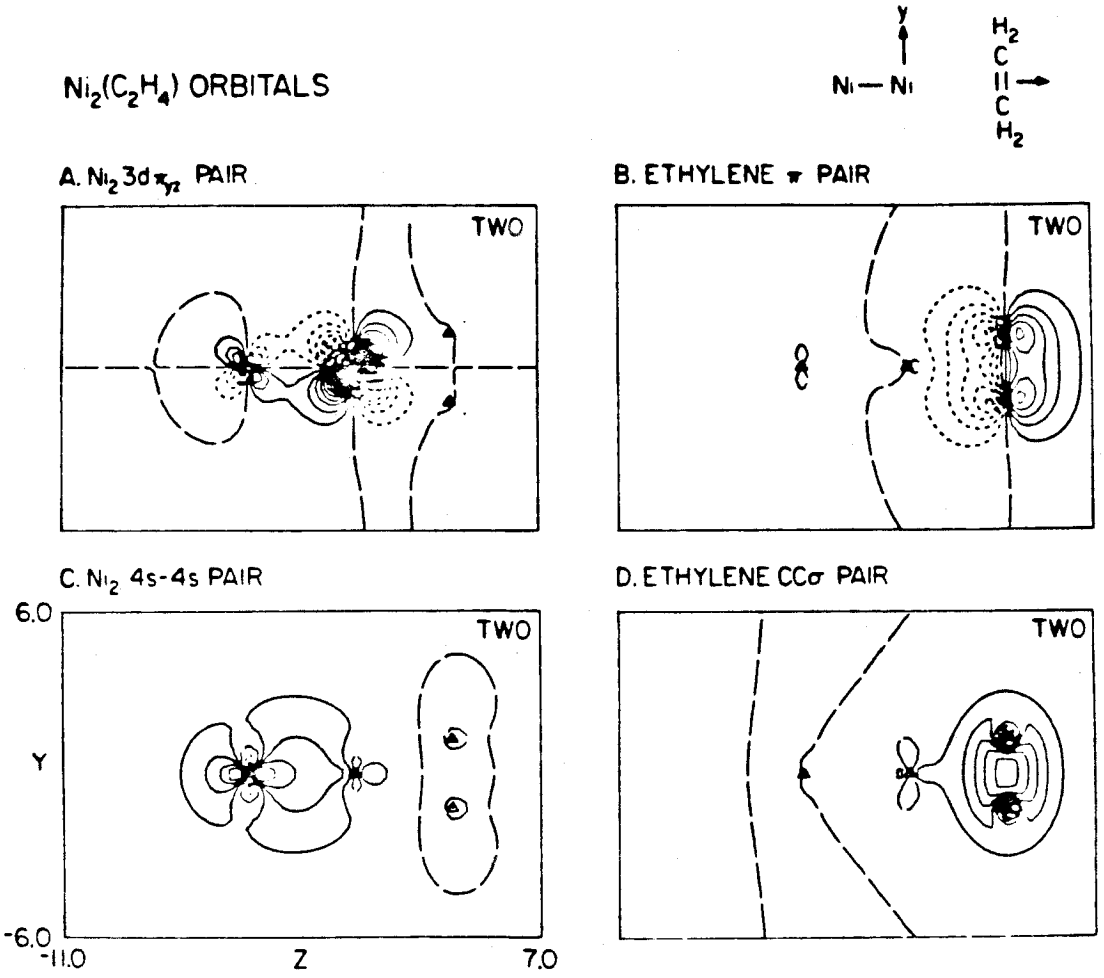

Figure 15. Bonding orbitals for the $Ni_2(\pi\text{-}C_2H_4)$ complex. Long dashes indicate nodal lines.

At this point, it is worthwhile to draw on the bonding description presented above and to attempt tentative assignment of the intense uv transitions noted earlier for $Ni(C_2H_4)$ and $Ni_2(C_2H_4)$. To aid in characterizing these bands, it is helpful to draw on further experimental information. In Table II we show the position of the dominant band for a variety of mononuclear complexes of alkyl-substituted olefins, listed by decreasing transition energy. Included in this table are the gas phase frequencies for the $^1(\pi \rightarrow \pi^*)$ transition of each olefin.[26] In almost all cases, the trend towards decreasing energy for the Ni-olefin bands is paralleled by decreasing $^1(\pi \rightarrow \pi^*)$ transition frequencies. A correlation is suggested between the position of the virtual π^* level of the free olefins and the corresponding transition energy of the complex. There are several transitions that could lead to such a correlation: (1) ligand $\pi \rightarrow \pi^*$, (2) M4s $\rightarrow$ ligand π^*, (3) M3d $\rightarrow$ ligand π^*, (4) M4s $\rightarrow 4p_y$, and (5) M3d $\rightarrow 4p_y$. The distinction between (2) and (4) [or (3) and (5)] is small; certainly a transition that may be classified as $3d \rightarrow 4p_y$ will possess some degree of delocalization of the $4p_y$ into the ethylene π^* (and hence its inclusion in the list above). In fact, certain of these may be eliminated as possibilities. A simple ligand, $\pi \rightarrow \pi^*$, occurring at 7.6 eV[27] for free ethylene, will be shifted to far lower energies in the $Ni(C_2H_4)$ complex. This transition leaves a singly-occupied π orbital which may bond to the singly-occupied Ni 4s orbital. The strength of such a bond may be estimated from consideration of $[Ni(C_2H_4)]^+$ where the ethylene is bound by ~ 60 kcal. Preliminary calculations place this $(\pi\pi^*)$ state at less than 2 eV above the $^3A_1$ ground state for $Ni(C_2H_4)$. In addition, it

Table II. Ultraviolet-Visible Spectroscopic Data for a Selection of Ni(olefin) Complexes in Argon Matrices[26]

Olefin	Ni-olefin band position (cm^{-1})	Relative Energy (cm^{-1})	Gas phase olefin $^1(\pi \rightarrow \pi^*)$ frequency (cm^{-1})	Relative Energy (cm^{-1})
C_2H_4	31250	0	61700	0
C_3H_6	30910	-340	58000	-3700
cis but-2-ene	30770	-480	57470	-4230
trans but-2-ene	30675	-575	57140	-4560
1-butene	30630	-620	57800	-3900
iso butene	30440	-810	54350	-7350

should be noted that the final state description for this ($\pi \rightarrow \pi^*$) state will be essentially identical to that expected of (2) [and thus (4)]. In each case, an occupation of $(\pi)^2(\pi^*)^1(3d)^9(4s)^0$ is expected for the upper state [where it is assumed that a ($4s - \pi$) bond is indistinguishable from a $(\pi)^2 4s^0$ occupation]. Thus the arguments leading to rejection of (1) apply to (2) and (4) as well. Only (3) and (5) above do not perturb the $(4s)^1(\pi)^2$ configuration of the ground state and will be expected at energies similar to the atomic Ni($3d \rightarrow 4p$) transitions.[19] Preliminary calculations place the $3d \rightarrow 4p_y$ transition for $Ni(C_2H_4)$ at 6.1 eV, reasonably close to the observed value of 3.8 eV. Delocalization into the ethylene π^* is extensive, allowing classification of this state as formally $3d \rightarrow \pi^*$ MLCT (metal-ligand charge transfer). Since $Ni(C_2H_4)$ has a triplet ground state, to maintain spin symmetry in this transition it is necessary to pair the π^* and Ni 4s orbitals into a net singlet (the $3d^8$ shell is left in a ^3F state), an unfavorable coupling. Such is not the case for $Cu(C_2H_4)$ which has a $^2A_1$ ground state. As a result, the $^2B_2$ excited state of $Cu(C_2H_4)$ requires no open-shell singlet coupling of orbitals and is stabilized relative to the analogous atomic $^2(3d \rightarrow 4py)$ state; consequently, the corresponding transition appears at 3.2 eV.[28] Similarly for $[Cu(C_2H_4)]^+$, the excited state is strongly bonding, reducing the atomic $^2(3D \rightarrow 4py)$ transition[19] by 2 eV to 5.6 eV.[28] For $Ni_2(C_2H_4)$, there should be transitions similar to those observed for Ni_2 ($3d \rightarrow 4p\pi$), producing a partial Ni_2 π bond in addition to the higher energy MLCT transition. Thus we tentatively assign the intense 243 nm band as a MLCT transition, which here is blue-shifted relative to $Ni(C_2H_4)$ as a result of the greater stabilization of the 3d levels in

$Ni_2(C_2H_4)$. The band positions for both species, along with their tentative assignments, are collected for comparison in Table III.

D. Calculational Details.

All calculations on $Ni(C_2H_4)$ and $Ni_2(C_2H_4)$ employed the effective potential of Melius et al.[29] as modified by Sollenberger et al.[30] to replace the argon core of the Ni atom. This allowed truncation of the Ni basis set to include only the four most diffuse s functions from Wachters[31] Ni basis set, contracted "double zeta". The 3d basis consisted of Wachters' five d functions contracted using atomic coefficients for the $^3D(4d^1\,3d^9)$ state to a single basis function of each type. A single 4p gaussian ($\alpha = 0.1$) was added to the Ni basis to allow hybridization of the 4s orbital. The potential and basis set are listed in Appendix V.A. The ethylene basis set was the 9s/5p basis of Huzinaga[32] contracted to 3s/2p by Dunning[33] and augmented with a single set of d polarization functions ($\alpha = 0.6769$) on each C. All calculations on $Ni(C_2H_4)$ utilized the GVB(1)-PP wavefunction[34] where correlation effects wereincluded in the ethylene π bond. For $Ni_2(C_2H_4)$, a GVB(2)-PP description was used with correlation effects included for both the ethylene π bond and Ni_2 σ bond. The orbitals obtained from these calculations were used as a basis for CI calculations in which all excitations were allowed between orbitals describing GVB pairs along with single and double excitations of the remaining Ni and Ni_2 orbitals (this is denoted as GVB-CI). A summary of energies from GVB and GVB-CI calculations for the complexes discussed here is listed in Table IV.

Table III. Ultraviolet-Visible Spectroscopic Data for $Ni(C_2H_4)$ and $Ni_2(C_2H_4)$ in Argon Matrices

$C_2H_4/Ar \simeq 1/50$ $Ni/Ar \simeq 1/10^4$ (nm)	$C_2H_4/Ar \simeq 1/50$[a] $Ni/Ar \simeq 2/10^3$ (nm)	Assignment
320[b] (s)	320[b] (w)	MLCT: $Ni(C_2H_4)$
280 (w)	280 (mwsh)	MLCT: $Ni(C_2H_4)_2$
	243 (s)	MLCT: $Ni_2(C_2H_4)$
230 (mw)		MLCT: $Ni(C_2H_4)_3$

[a]Depositions at higher Ni/Ar ratios and higher temperatures (20-25° K) show the growth of a band at roughly 370 nm concomitant with a general broadening of the spectra. This band and possible overlap in the region of 240 nm are tentatively ascribed to $Ni_2(C_2H_4)_2$ (see text).

[b]The band initially ascribed to $Ni(C_2H_4)$ at 280 nm[11] was subsequently found to be the MLCT of $Ni(C_2H_4)_2$. The 320 nm band had been obscured by the absorptions of unreacted Ni atoms. This will be more fully detailed in a forthcoming report on Ni/olefin cocondensations.[23]

Table IV.

Complex	State	GVB[a]	GVB-CI[a]
Ni_2 (R = 2.1 Å)	$^3\Sigma_g^-$	-81.0864[b]	-81.0867
$Ni(C_2H_4)$	$^3A_2$	-118.5820	-118.5822
$Ni_2(C_2H_4)$	$^3A_2$	-159.1800	-159.1801
Ni	^3D	-40.4943	-40.4943
C_2H_4	$^1A_1$	-78.0668	-78.0668

[a]All energies are in hartrees.

[b]All calculations where Ni atoms are present employ an effective potential[30] replacing the Ar core of each Ni atom. The energies given reflect the absence of core contributions to total energies.

IV. Discussion

Probably the most significant results to emerge from the infrared and uv-matrix experiments concern (i) the minimal perturbation of the coordinated ethylene vibrational spectrum on placing the second nickel atom on $Ni(C_2H_4)$ to form $Ni_2(C_2H_4)$ and (ii) the observation of a uv transition for $Ni(C_2H_4)$ at 320 nm which blue shifts to 243 nm on passing to $Ni_2(C_2H_4)$. In essence, one is observing the perturbation of the electronic structure of π-bonded C_2H_4 on a single nickel atom site by a neighboring Ni atom as shown below:

By analogy, with the electronic transitions for dinickel itself which occur in a similar energy range, the observation of an absorption at roughly 370 nm for $Ni_2(C_2H_4)_2$ can be considered to support the idea of a nickel-nickel bond in this binuclear complex. Presumably a corresponding band for $Ni_2(C_2H_4)$ is either too weak to be observed or is hidden by other spectral features. Furthermore, the relatively small frequency perturbation of the ν_{CC} and δ_{CH_2} (aside from drastic band broadening effects) on passing into the $Ni_n(C_2H_4)$ regime with $n \geq 2$ and the noticeable resemblence of these infrared spectra to those of chemisorbed C_2H_4 lend experimental credence to the proposal that cluster species like $Ni_2(C_2H_4)$ are valuable models for evaluating the properties of surface complexes, at least for the case of alkenes. However, our experiments do not allow us to dismiss the

possibility that π-$Ni_2(C_2H_4)$ is the kinetically stable form under the conditions of our matrix experiments (10 - 45° K) and that higher temperature matrix experiments could lead to conversion to a di-σ-$Ni_2(C_2H_4)$ complex. Therefore, we cannot eliminate the possible existence of di-σ-$Ni_2(C_2H_4)$ and, as previously noted,[35] the di-σ-surface complex may well play the role of a reaction intermediate for various surface reactions due to its weaker C-C bond. In this context we recall that Soma[22d] recently observed only the π-surface complex for C_2H_4 chemisorbed on Al_2O_3 supported Pd and Pt catalysts at -86° C. However, when the catalyst was allowed to gradually warm up, infrared bands, which he assigned to the di-σ bonded surface species, were observed to grow in at 2940/2880 and 1338 cm^{-1}. Similarly, Broden and Rhodin[36] have recently noted that the photoemission spectrum of ethylene chemisorbed on Ir(100) -(1×5) exhibits warmup behavior consistent with a transition from a simple π-bonded form to a stretched or even fragmented carbon-carbon bond species. For the finite complex being considered here, it is possible to consider directly the competing energetics of π- vs. di-σ bonded forms. Under the conditions of our experiment, it is necessary to consider the formation of $Ni_2(C_2H_4)$ as resulting from the interaction of ethylene with either Ni atoms or Ni_2. From similar calculations (GVB-CI) on the analogous di-σ $Ni_2(C_2H_2)$ species,[37] the strength of the NiC σ- bond may be estimated at 65 (±10) kcal for the olefinic system. With this information, the following comparisons may be made:

$$2Ni \rightarrow Ni_2 \qquad \Delta H = -65 \text{ kcal}^{17} \qquad (1)$$

$$Ni_2 + C_2H_4 \rightarrow Ni_2(C_2H_4)\text{di-}\sigma \qquad \Delta H \approx -5(\pm 20) \text{ kcal} \qquad (2)$$

$$Ni_2 + C_2H_4 \rightarrow Ni(C_2H_4)\pi \qquad \Delta H = -16 \text{ kcal} \qquad (3)$$

$$2Ni + C_2H_4 \rightarrow Ni_2(C_2H_4)\text{di-}\sigma \qquad \Delta H = -70(\pm 20) \text{ kcal} \qquad (4)$$

$$2Ni + C_2H_4 \rightarrow Ni_2(C_2H_4)\pi \qquad \Delta H = -81.5 \text{ kcal} \qquad (5)$$

Within the estimates of error given, the di-σ and π forms appear competitive. Formation of the di-σ form requires breakage of the π bond and, unlike the π complex, formation of this species will involve a significant (< 20 kcal) activation energy. For the finite complex, then, the di-σ form should be thermally inaccessible.

Within the context of this discussion, it is worthwhile to consider the importance of other possible geometries for the $Ni_2(C_2H_4)$ complex. Along with the di-σ form, the μ-bridging configuration, with the carbon-carbon bond oriented perpendicular to the Ni-Ni bond, is often suggested for chemisorbed species.[38] This form, well-known for finite-cluster metal-alkyne complexes,[39] is less favorable for the analogous olefinic systems. The reasons for this may be seen by examining the nature of the bonding involved. When in the μ-bridging configuration, acetylenic species may form two π-coordination bonds of the type described in this study, one to each metal atom.[39] The 4s orbitals on each Ni atom polarize away from the acetylene, reducing the Ni_2 bonding overlap.[37] There is no corresponding scheme for ethylene in this orientation. This may be understood by considering

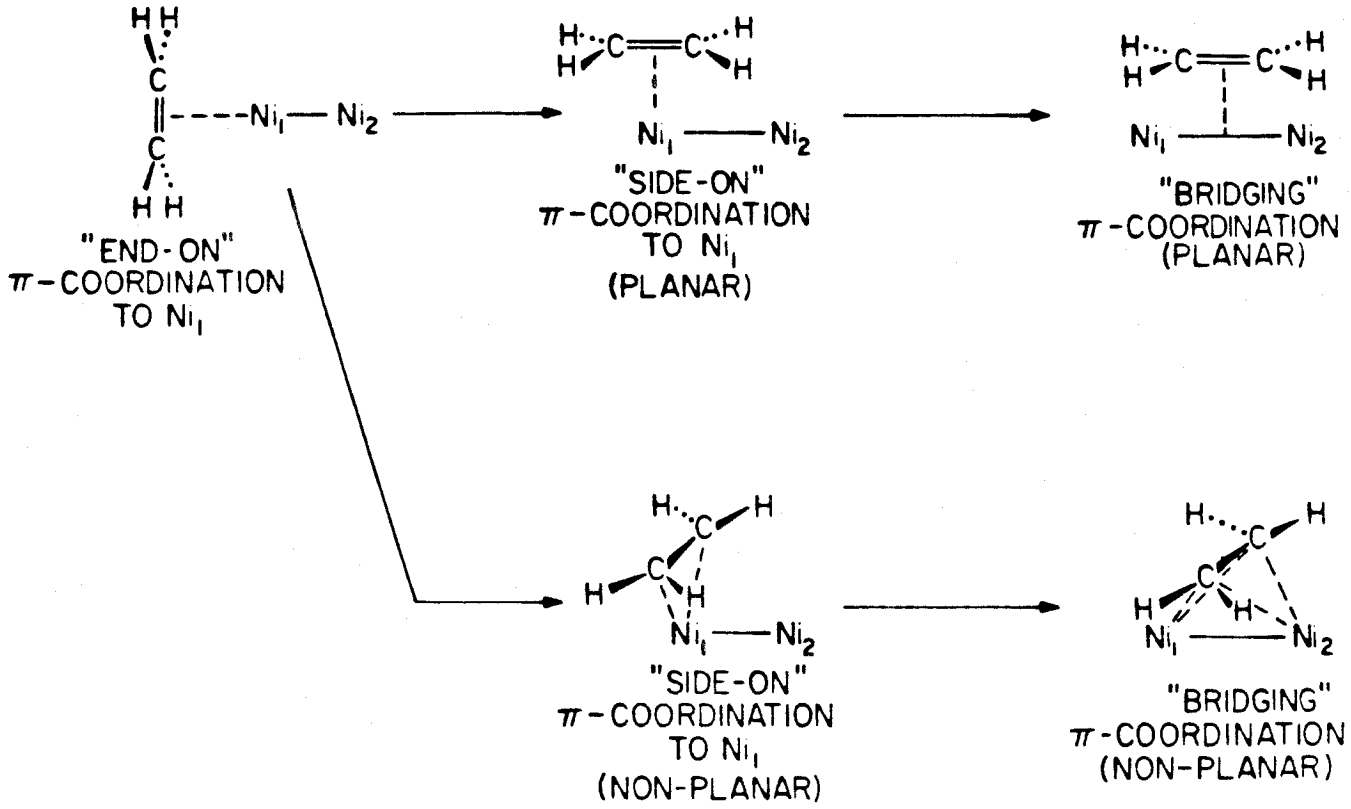

Figure 16. Other possible geometries for $Ni_2(C_2H_4)$ as they might be reached through ligand migration. Note that the initial movement of the ligand is different for the two indicated pathways.

the energy surface for the transformation from the π form to both the μ-bridging and planar forms shown in Fig. 16. The initial step, moving the ethylene in its π-coordinate form around to either of the two "side-on" configurations (with respect to the Ni_2 bond), should be endothermic. It is still possible to expose the electropositive $3d^9$ shell on the bonding Ni atom; however, to do so requires polarization of the 4s orbital associated with this atom in a direction away from the Ni bond. Continuing to move the ethylene to either final position (see Fig. 16) requires polarization of both 4s bonding orbitals away from the ethylene and their region of maximum overlap. Unlike acetylene, there is no compensation for this disruptive polarization to be had through formation of a second ($\sim$ 15 kcal) π bond.[2] Thus, we would expect this "ligand migration" to be endothermic with respect to the "end-on" π-configuration. It is important to reiterate at this point that these arguments for both di-σ and μ forms are specific to the finite cluster complex. The presence of neighboring Ni atoms at the metal surface is sufficient to obscure both the importance of 4s overlap between neighboring atoms and the related thermochemical arguments.

In addition to the coordination scheme presented here, there is also a "metallocyclopropyl" form[40] in which the Ni assumes a $^3F(s^2d^8)$ configuration and forms a σ bond to each C. (This state is quite distinct from that of an ethylene π bond to an s^1d^9 Ni.) Forming individual Ni-C σ-bonds between 4s electrons on the Ni and "sp^2" hybrid orbitals on the ethylene produces a ring compound more analogous to cyclopropane. Aside from the rather different spectral properties to be expected from such a form,[41] it is energetically

unfavorable to couple the Ni 4s electrons in this manner. (Attempts to calculate the orbitals for this form collapsed to the Ni-C_2H_4 π complex.) The Ni 4s orbitals are very diffuse (see Figure 11) and when coupled into separate σ-bonds favor a linear configuration to minimize overlap between bond pairs. Thus, a "ring strain" is expected to be an even greater problem for the metallocycle than its cycloalkane analogue.

Finally, we may consider the coordination of a second Ni atom to $Ni(C_2H_4)$ across the ethylene CC bond to form a second weak π bond and a planar $Ni(C_2H_4)Ni$ "di-π" complex:

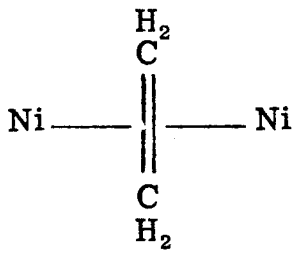

Such a system should exhibit spectral properties very similar to $Ni(C_2H_4)$ as little additional perturbation of the ethylene would be expected relative to $Ni(C_2H_4)$. However, coordination of the second Ni in this position is exothermic by only $\sim$15 kcal, while formation of the Ni_2 bond yields 65 kcal. Unless steric and/or kinetic effects in the matrix are particularly important, this structure should not be favored.

The $Ni(C_2H_4)$ and Ni2(C_2H_4) systems have been examined by other methods, notably Xα-SW[35,42] and EH.[43] Both of these methods use approximate Hamiltonians in their description of the molecules and at best should reproduce the Hartree-Fock (HF) description. The EH result favors the di-σ form by over 25 kcal, yielding a binding energy

of 68 kcal per bond.

The study presented here finds a direct parallel in the Xα-SW work. In two separate studies, the $Ni(C_2H_4)$[42] and $Ni_2(C_2H_4)$[35] complexes were considered, both in the π-coordinate orientation. In each case, a bonding description very similar to the Dewar-Chatt-Duncansen[44] model emerges, with significant interaction of the Ni $3d\pi_{yz}$ and ethylene π* orbitals, although the authors appear to disagree on the assignment of these two orbitals. This interaction is balanced by donation from the ethylene π orbital into a Ni σ-orbital. This result is similar to that obtained from HF calculations, and the strong interactions between 3d and ethylene π-orbitals may be attributed to the overestimation of ionic character inherent in the HF description. The di-σ form is also considered in this study, and although no energetic comparisons may be made, the π-coordinate geometry was favored by its better correspondence with known ethylene chemisorption data.

References and Notes

1. See section I.A of this thesis.
2. See Appendix I.A of this thesis.
3. J. E. Demuth, H. Ibach, S. Lehwald, Phys. Rev. Lett., 40, 1044 (1978).
4. (a) J. E. Demuth and D. E. Eastman, 32, 1123 (1974); (b) K. Horn, A. Bradshaw and K. Jacobi, J. Vac. Sci. Technol. 15, 575 (1978); (c) J. E. Demuth, Phys. Rev. Lett. 40, 409 (1978).
5. R. Zuhr and J. B. Hudson, Surf. Sci. 66, 405 (1977).
6. E. P. Kündig, M. Moskovits, and G. A. Ozin, J. Mol. Struct., 14, 137 (1972).
7. M. Moskovitz and G. A. Ozin, Appl. Spectrosc., 26, 487 (1972).
8. K. Fischer, K. Jonas, and G. Wilke, Angew. Chem., 85, 629 (1973); idem, Angew. Chem. Int. Ed. Engl., 12, 565 (1973).
9. (a) First communicated at the Merck Symposium on Metal Atoms in Chemical Synthesis, Darmstadt, Germany, May 1974; (b) P. L. Timms, communicated in a paper given at the C.I.C. Meeting on Chemistry Under Extreme Conditions, Toronto, Canada, June, 1975; (c) R. M. Atkins, R. McKenzie, P. L. Timms, and T. W. Turney, J. Chem. Soc. Chem. Commun., 764 (1975).
10. G. A. Ozin and W. J. Power, manuscript in preparation.
11. H. Huber, W. J. Power and G. A. Ozin, J. Am. Chem. Soc., 98, 6508 (1976).

References (continued)

12. E. P. Kündig, M. Moskovits, and G. A. Ozin, Angew. Chem. Int. Ed. Engl., 14, 292 (1975).

13. W. Koltzbücher and G. A. Ozin, Inorg. Chem., 15, 292 (1976).

14. See D. M. Gruen in "Cryochemistry", G. A. Ozin and M. Moskovits, Eds., John Wiley, New York, 1976.

15. (a) R. Busby, W. Klotzbücher, and G. A. Ozin, J. Am. Chem. Soc., 98, 4013 (1976); (b) A. Ford, H. Huber, W. Klotzbücher, E. P. Kündig, M. Moskovits, and G. A. Ozin, J. Chem. Phys., 66, 524 (1977).

16. J. E. Hulse and M. Moskovits, J. Chem. Phys., 66, 3988 (1977).

17. T. H. Upton and W. A. Goddard III, J. Am. Chem. Soc., 100, 5659 (1978).

18. A. Kant, J. Chem. Phys., 41, 3806 (1964).

19. C. E. Moore, "Atomic Energy Levels," NBS Circular No. 467, Vol. II, U. S. Government Printing Office, Washington, D.C., 1949.

20. H. Huber, H. Gray, G. A. Ozin, D. Tyler, and W. Trogler, unpublished results.

21. T. C. Devore, A. Ewing, H. F. Franzen, and V. Calder, Chem. Phys. Lett., 35, 78 (1975).

22. (a) B. A. Morrow and N. Sheppard, J. Phys. Chem., 70, 2406 (1966); idem, Proc. Roy Soc., Ser. A, 311, 391 (1969); (b) J. Erkelens and Th. Liefkens, J. Catal., 8, 36 (1967); (c) J. D. Prentice, A. Lesiunas, and N. Sheppard, J. Chem. Soc. Chem. Commun., 76 (1976); (d) Y. Soma, ibid., 1004 (1976);

References (continued)

(e) G. Blyholder, D. Shihabi, W. V. Wyatt, and R. Bartlett, J. Catal., 43, 122 (1976).

23. W. J. Power and G. A. Ozin, Inorg. Chem., 17, 2836 (1978).

24. (a) R. G. Denning, F. R. Hartley, and L. M. Venanzi, J. Chem. Soc., A, 1322 (1967); (b) D. J. Trecker, J. P. Henry, and J. E. McKean, J. Am. Chem. Soc., 87, 3261 (1965);

25. T. H. Upton and W. A. Goddard III, J. Am. Chem. Soc., 100, 321 (1978).

26. M. B. Robin, "Higher Excited States of Polyatomic Molecules," Vol. II, Academic Press, New York, 1974, p. 24.

27. P. G. Wilkinson and R. S. Mulliken, J. Chem. Phys., 23, 1895 (1955).

28. H. Huber, D. McIntosh, and G. A. Ozin, Inorg. Chem., to be published.

29. C. F. Melius, B. D. Olafson, and W. A. Goddard III, Chem. Phys. Lett., 28, 457 (1974).

30. M. Sollenberger, C. F. Melius, and W. A. Goddard III, manuscript in preparation. See also M. Sollenberger, M.S. Thesis, California Institute of Technology, Pasadena, California, 1976.

31. A. J. H. Wachters, J. Chem. Phys., 52, 1033 (1970).

32. S. Huzinaga, J. Chem. Phys., 42, 1293 (1965).

33. T. H. Dunning, Jr., and P. J. Hay, "Modern Theoretical Chemistry: Methods of Electronic Structure Theory," Vol. 3,

References (continued)

H. F. Schaefer III, Ed., Plenum Press, New York, 1977, pp.1-17.

34. P. J. Hay, W. J. Hunt, and W. A. Goddard III, Chem. Phys. Lett., 13, 30 (1972).

35. N. Rösch and T. N. Rhodin, Faraday Disc. Chem. Soc., 58, 28 (1975).

36. G. Broden and T. Rhodin, Chem. Phys. Lett., 40, 247 (1976).

37. See Appendix I.A of this thesis.

38. L. L. Kesmodel, P. C. Stair, R. C. Baetzold, and G. A. Somorjai, Phys. Rev. Lett., 36, 1316 (1976).

39. V. W. Day, S. S. Abdel-Meguid, S. Dabestani, M. G. Thomas, W. R. Pretzer, and E. L. Muetterties, J. A. Chem. Soc., 98, 8289 (1976).

40. P. W. Jolly and G. Wilke, "The Organic Chemistry of Nickel," Vol. I, Academic Press, New York, 1974.

41. C. R. Noller, "Chemistry of Organic Compounds," W. B. Saunders Co., Philadelphia, 1965.

42. R. P. Mesomer in "The Physical Basis for Heterogeneous Catalysis," E. Dragulis and R. I. Jaffee, Eds., Plenum Press, New York and London, 1975.

43. A. Anderson, J. Am. Chem. Soc., 99, 696 (1977).

44. J. Chatt and L. A. Duncanson, J. Chem. Soc., 2939 (1953); M. J. S. Dewar, Bull. Soc. Chim. Fr., 18, C71 (1971).

C. Ionization Properties of Zero-Valent Nickel Complexes and their Relevance to the Photoemission Properties of Adsorbed Hydrocarbons

I. Introduction

The technique of ultraviolet photoemission spectroscopy (UPS) has proven to be invaluable as a source of information concerning the bonding in chemisorbed species.[1-6] However, just as for UPS studies on gas phase systems,[7] the data obtained in surface photoemission studies do not lead to unambigous qualitative interpretation. High quality theoretical studies have played an important role in the interpretation of gas phase UPS spectra,[7] but to date, few theoretical studies have been carried out to address the more complex problem of understanding the photoemission properties of molecules bound to a metal surface.[8-10] As has been well documented in the literature, certain chemisorbed molecules (such as CO[1], C_2H_2 and C_2H_4[2]) produce UPS spectra that are similar, but not identical to those obtained for their gas phase counterparts. Levels observed for the chemisorbed species are sometimes shifted by several eV (the so-called "bonding" and "relaxation" shifts[2]) relative to gas phase spectra and the origin of these shifts is not well understood. When such shifts are present, assignments based on qualitative similarities between the spectra of gas phase and adsorbed species may be current.

More serious are those cases where the observed photoemission of the adsorbed species bears little resemblance to that of the corresponding gas phase species. Methanol,[6] ethylene,[2-4] and acetylene[2-4] all produce such spectra under more extreme conditions and the structures leading to these spectra are still the subject of controversy.

Thus, an adequate theoretical study of ionizations in chemisorbed species must consider two additional problems not present in a gas phase study. First, it is not possible in most cases to assume a particular structure for the chemisorbed species and thus geometry searches must be considered. Second, as the effect of the chemisorptive bond on the ionization properties is not well understood, it is necessary not only to explicitly include metal atoms in the study, but to provide some means in which to gauge directly their effect on the spectrum.

In this study we consider the photoemission properties of the low coverage, low temperature phases of ethylene and acetylene on Ni(III). It is under these conditions that both molecules produce spectra reminiscient of the respective gas phase species,[2] and it was primarily this feature that led Demuth and Eastman[2] to interpret the spectra as indicative of π-bonded species. In light of recent high resolution electron loss (HRELS) data for C_2H_2 on Pt[11] and Ni,[12,13] this assignment has been challenged. In both studies, it has been found that observed frequencies for ν_{CH} and ν_{CC} are not in agreement with what would be expected of a weakly bound metal-alkyne system. In this paper we evaluate the ionization properties of a number of small nickel-acetylene, and nickel-ethylene complexes, as models for the bulk system. Specifically, we consider Ni-C_2H_4[14] and Ni-C_2H_4[14-15] complexes in which the hydrocarbon is coordinated to the Ni atom through a single π bond. In addition, we consider Ni_2-C_2H_2 complexes in which the acetylene is coordinated to the Ni_2 unit through both π bonds (di-π bonding) and through individual σ bonds formed to each Ni atom after breaking one of the

acetylene π bonds (di-σ bonding).[16] In Section II, we discuss briefly the important effects requiring explicit consideration in the calculation of ionization potentials. Based on this discussion, Section III presents an overview of the methods used here as well as a qualitative discussion of the final results. Detailed discussion of the method and comments on the experimental data are reserved for Sections IV and V, respectively.

II. Fundamental Considerations in Calculating Ionization Potentials

The theoretical evaluation of an ionization potential necessarily involves a comparison of the energies of both neutral and ion state wavefunctions for a given system. There are a variety of techniques by which this comparison may be made, and it is useful in choosing the technique to first consider the dominant effects that lead to changes in the ion wavefunction relative to the neutral.

To begin, consider a ground state wavefunction for acetylene in which localized orbitals for each of the bonds have been optimized, but correlation effects have not been considered. If we remove an electron from each of the bond pairs without allowing any changes in the wavefunction, the ionization spectrum would appear qualitatively as shown in Figure 1a. The smallest I.P. is obtained for the doubly degenerate π orbitals. The next two levels, denoted $3\sigma_g$ and $2\sigma_u$, correspond to ionization of CH bonding levels. The $3\sigma_g$ level, a symmetric combination of CH bonds shows a larger I.P. than the corresponding antisymmetric $2\sigma_u$ combination in this description. The deepest level is the CC bonding $2\sigma_g$ level.

Upon moving to Figure 1b, the ion states have been allowed to interact. The $2\sigma_g$ and $3\sigma_g$ orbitals are not orthogonal in the description of Figure 1a. The CCσ bonding orbital ($2\sigma_g$) delocalizes somewhat into the CH region (to become 35% CHσ) and the $3\sigma_g$ level, to become orthogonal to the lower $2\sigma_g$ orbital builds in a negative (de-stabilizing) component of CCσ bonding character. This causes the $3\sigma_g$ orbital to

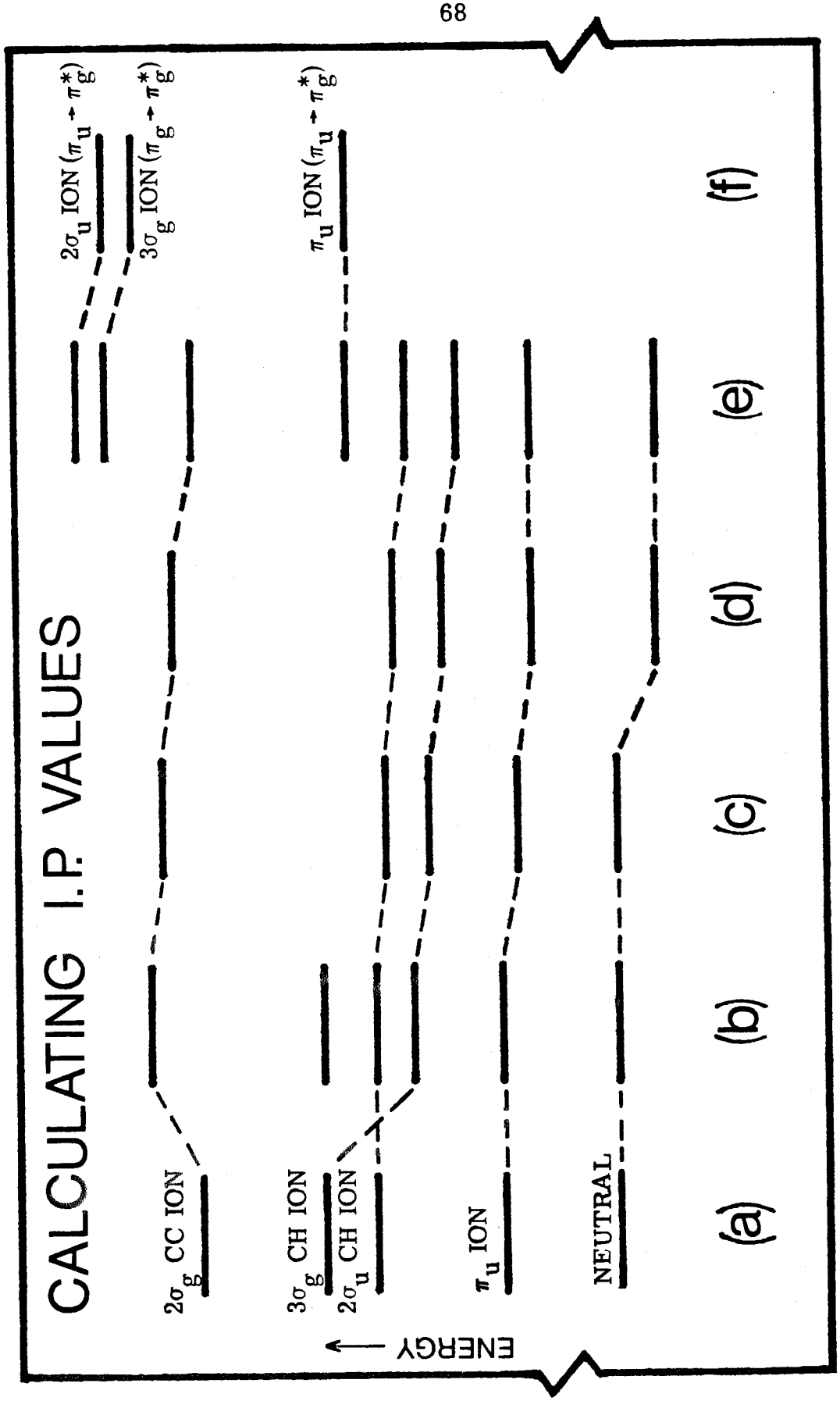

Figure 1: Energetic contributions that determine the final position of neutral and ion states, using acetylene as an example.

be shifted above the $2\sigma_u$ in energy, resulting in the (counterintuitive) ordering shown.

The readjustments described above do not involve relaxation contraction of the orbitals due to decreased shielding in the ion, but rather a simple remixing of the neutral orbitals in a manner more optimum for the (n-1) electron system. If we now allow the orbitals of the ions to contract about the nuclei, the result in Figure 1c is obtained. Allowing this contraction amounts to improving the wave-functions for these ion states and thus lowers their energies. This produces smaller I. P. 's for each of the levels.

The changes considered thus far over the zero order description (Figure 1a) have each affected only the ion states. If we now consider electron-electron correlation, a significant improvement in ground state energy is obtained as well, as noted in Figure 1d. For the N electron system, there will be N(N+1)/2 unique electron-electron interactions, while for the N-1 electron ions this number is reduced to N(N-1)/2. In general then, the N additional interactions in the neutral result in greater total correlation error for the ground state than for any of the ions. The relative separation between ions and neutral (I. P.) increases in going to this description.

Finally, in Figure 1f we note that there are additional ion states that require consideration These so-called "shake-up" states result from electronic excitation occurring simultaneously with ionization. The lowest such states involve $\pi_u - \pi_g^*$ excitations, as would be expected since the lowest electronic excitations in the neutral are of this type.

As may be seen in the figure, these shake-up states may be of the same symmetry as some of the direct ion states. Allowing them to mix produces the result shown in Figure 1e. Each of the σ levels is stabilized significantly by this interaction, while the π level is left unaffected.

The various levels of approximation defined by Figure 1 encompass several different techniques for calculating I. P. 's. The simplest and most commonly used of these is the Koopmans Theorem (KT) approximation, which incorporates the effects only through Figure 1b. The utility of this approximation rests upon a cancellation of the effect of ion state stabilization due to orbital relaxation (Figure 1c), by the (relative) neutral state stabilization resulting from correlation corrections (Figure 1d). At best this cancellation is approximate, and the approach totally ignores ion state mixing (Figure 1F), leading to errors usually of the order of 1 eV or more. For the most part, studies published to date considering ionizations in chemisorbed systems have used this KT level of approximation.[8,10]

The best results are obtained by performing separate calculations on ion and neutral states, including in both the effect of electron correlation. The remaining important effect, interaction with shake up states, is included in CI calculations. The difficulty with the CI method lies in the excessive computation needed to obtain such accurate wavefunctions, especially in systems where transition metal atoms are present. In general, this approach is only practical for obtaining the lowest I. P. 's.[17]

III. Qualitative Discussion

A. Method. As mentioned above, the calculation of ionization potentials by including all significant correlations and relaxations is extremely cumbersome if a full spectrum of ionizations is needed. However, any less extensive method must, to some extent, rely on the cancellation of error between differential electron correlation (biased towards the ion) and orbital relaxation (biased towards the neutral) as described in Section II for Koopman's Theorem. If the dominant electron correlation effects are included in both neutral and ion state calculations, and the dominant ion orbital relaxations are described as well, then the cancellation of error required to obtain adequate results is minimized and the results are expected to be less erratic than those of Koopmen's Theorem. If, in addition, interactions with shake-up states are also included, results with an acceptable level of accuracy (± 0.5 eV in most cases) are attainable for the entire I. P. spectrum of the molecule.

In practice, the method described above is carried out predominantly within the framework of CI calculations. An orbital basis optimized for the ground state, including electron correlation, is first obtained. This basis is then augmented with additional orbitals capable of describing the more tightly bound ion state orbitals. Limited CI calculations ($\sim$ 200-400 terms) are then carried out on both neutral and ion states using this basis, including those configurations necessary to describe higher shake-up states (henceforth denoted as an IP-CI).

Using this method, both the free molecule and the corresponding nickel complex(es) were examined in each case. Examining the free molecule was important for several reasons. First, it allowed an evaluation of the accuracy of the method for each particular molecule so that reliable estimates of the error present could be made when the corresponding complex was examined. In addition, it allowed a quantitative evaluation of the importance of various CI effects (correlation, shake-up mixing, etc.) with and without the metal present. As will be described below, program restrictions necessitated the exclusion of certain spatial configurations in the metal complex calculations, and prior examination of the free molecule allowed monitoring of the importance of this restriction.

B. Acetylene and Acetylene Complexes

1. Free Acetylene. The essential qualitative features of the acetylene ionization spectrum were described in the previous section. In the valence region, two CH bonding levels ($3\sigma_g$ and $2\sigma_u$), the CCσ bonding level ($2\sigma_g$) and the π bonding levels are expected. In Figure 2, we compare results obtained using Koopman's Theorem (KT) and extensive IP-CI calculations with the experimental vertical ionization spectrum.[7,18] The KT values show a trend towards increasing error with increasing ionization potential, producing an error in excess of 4 eV for the deep CCσ bonding level. Both CI calculations show results within 0.4 eV of the experimental results for all levels except the π level. While a considerable amount of this improvement may be traced

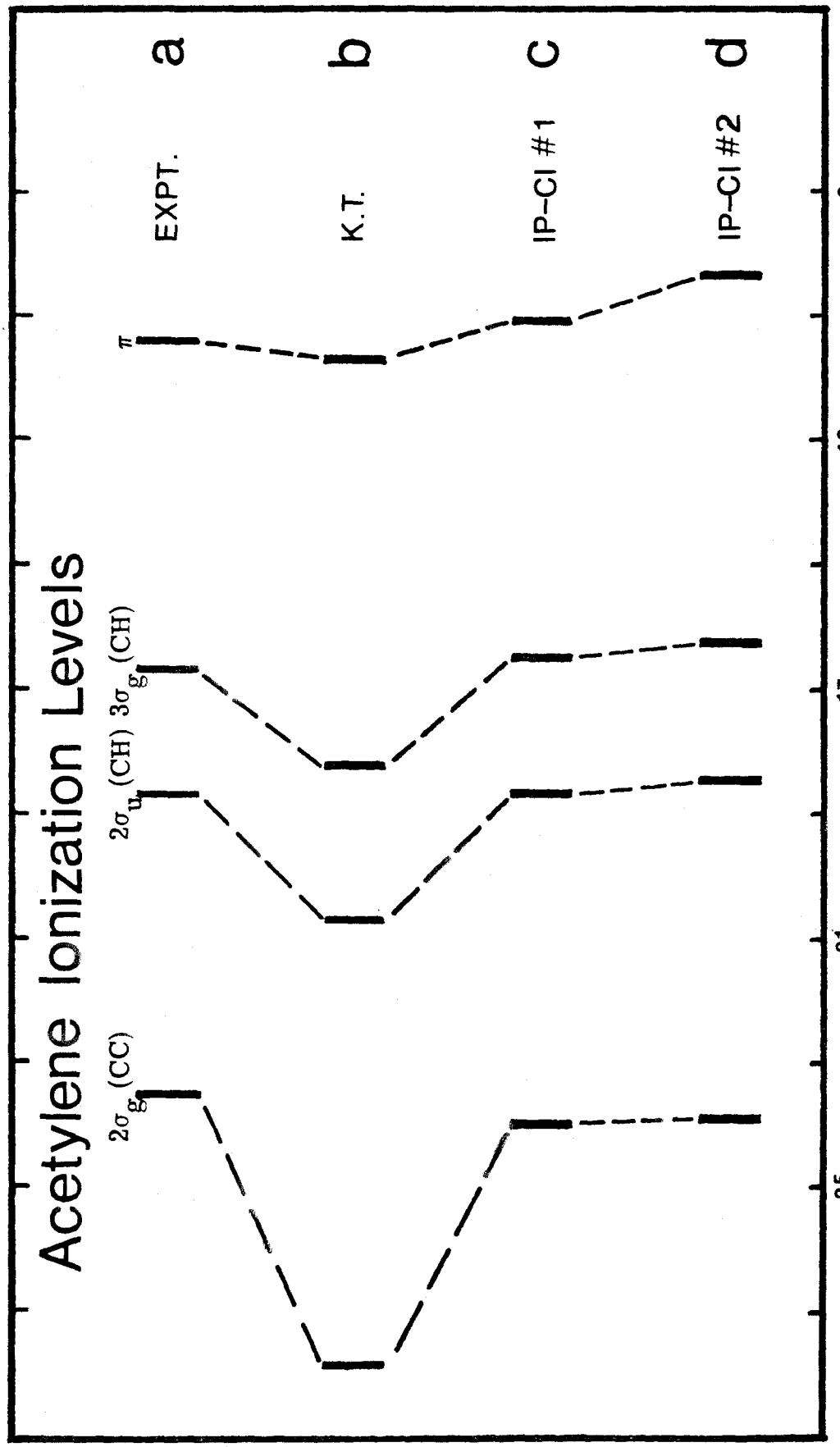

Figure 2: Comparison of calculated IP values for free acetylene.

directly to the reduced dependence upon error cancellation, it is important to note that the majority of the improvement may be traced to the interaction of these direct ionization states with shake-up states of the molecule. In Figure 3 are shown KT values for the direct ion states (Figure 3a) as well as a series of shake-up states resulting from either singlet or triplet $\pi \rightarrow \pi^*$ excitation occuring simultaneously with ionization (Figure 3c). When these states are allowed to interact, the shifts indicated are produced (Figure 3b). The predominant interactions are those between states represented in the Figure by heavy lines of the same symbol, the effect on the direct ionization increases with increasing IP, bringing each level into better agreement with the experimental spectrum.

The IP-CI result of Figure 26 is obtained upon using the method as outlined in Section III A above, and the agreement is excellent. The presence of the metal atoms in the final complex introduces some restrictions in the level of calculation attainable. The results in Figure 2d, which serve as a reference for the metal complex calculations, were obtained after excluding inter-electron pair correlation effects. The most notable effect is on the position of the π level, where important π-π inter-pair effects have been excluded. This problem will be discussed in more detail below.

2. The Ni-C_2H_2 π-Complex. The bonding in this system has been described in more detail elsewhere,[14] and only the essential points will will be repeated here. Upon bringing up the Ni atom, the $4s^1\,3d^9$ valence configuration of the atom is stabilized, and the 4s orbital

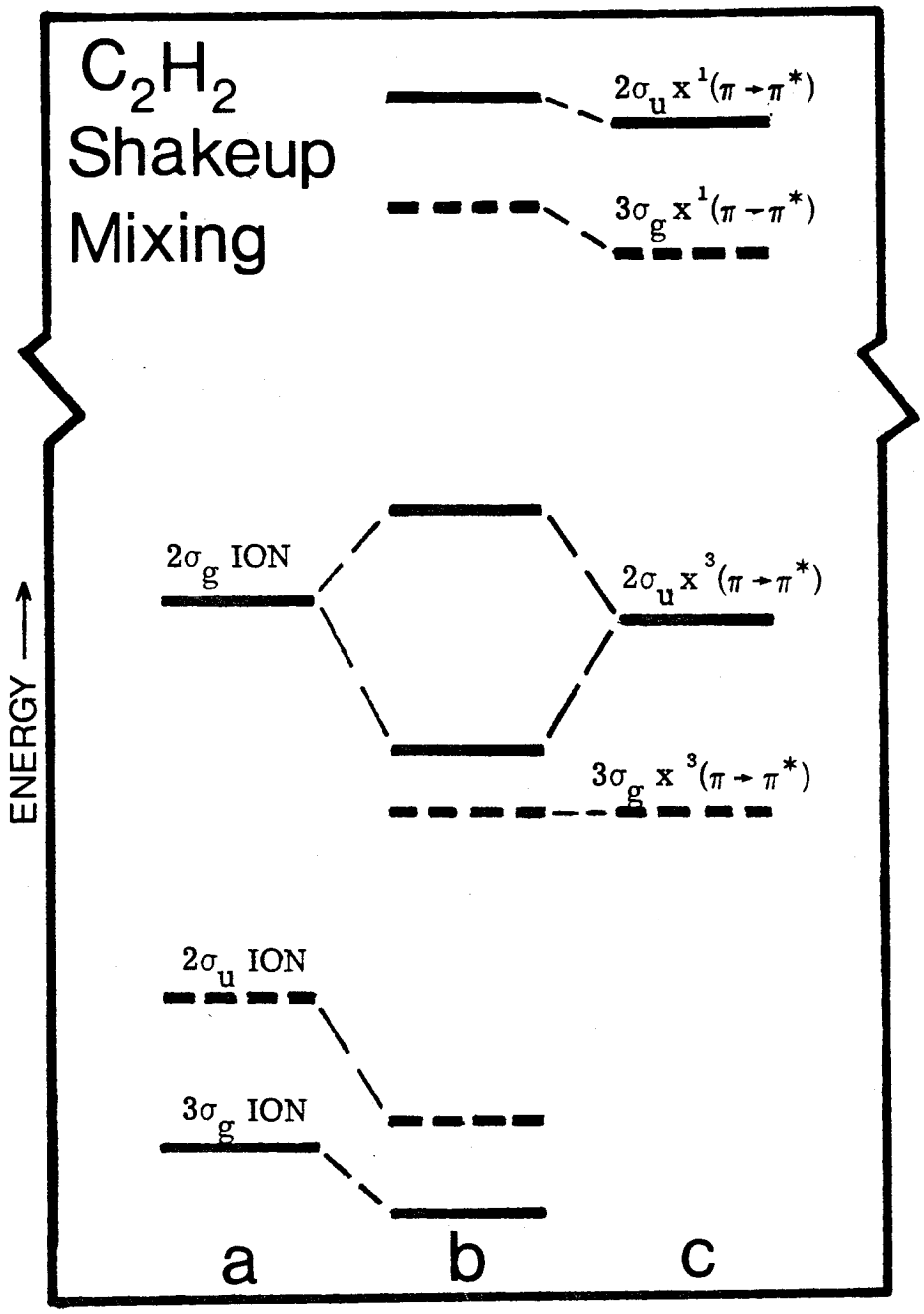

Figure 3: The effect of shake-up states on the acetylene ion spectrum: (a) zero order direct ion states; (b) final positions of all levels after perturbation; (c) zero order shake-up states. Dashed lines are states of $^2\Sigma_u^+$ symmetry, solid lines are $^2\Sigma_g^+$.

polarizes strongly away from the ligand π_y orbital. Bonding in this system (~ 17 kcal) is a result of the electrostatic interaction that occurs between the π_y electrons and the partially exposed 3d core of the Ni atom. The 3d orbitals and the π_y orbital remain essentially localized in their unperturbed positions and there is no evidence of "back bonding" as in the Dewar-Chatt-Duncansen model.[19] The lowest state of the complex is a triplet, in which the 4s orbital is coupled with the singly-occupied 3d orbital.

The same electrostatic interaction that is responsible for the bond also has a significant effect on ionization potentials for the complex. The attractive coulomb interaction between each of the doubly-occupied acetylene orbitals and the Ni core is halved upon ionization of the orbital (neglecting orbital readjustment). The effect of this reduction may be seen in Figure 4b, where IP-CI results for the Ni-C_2H_2 complex (at the optimum geometry) are shown. A comparison of the free acetylene results reproduced in Figure 4a shows that the difference between coulomb interactions for the neutral and each of the ions produces a 1.5 to 3.0 eV increase in the ionization potentials.

In ionizing the triplet ground state of the complex, both doublet and quartet ion states are possible, and are each indicated in the Figure. Only those doublets retaining triplet coupling of the 4s and 3d orbitals are spin allowed final states and only these are indicated in the Figure. In some cases such an assignment was not possible, and both doublets are shown. In addition, certain of the low-lying acetylene ion states mix with Ni 3d ionizations to such an extent that clear assignment is not possible. These are indicated by dotted lines in the Figure.

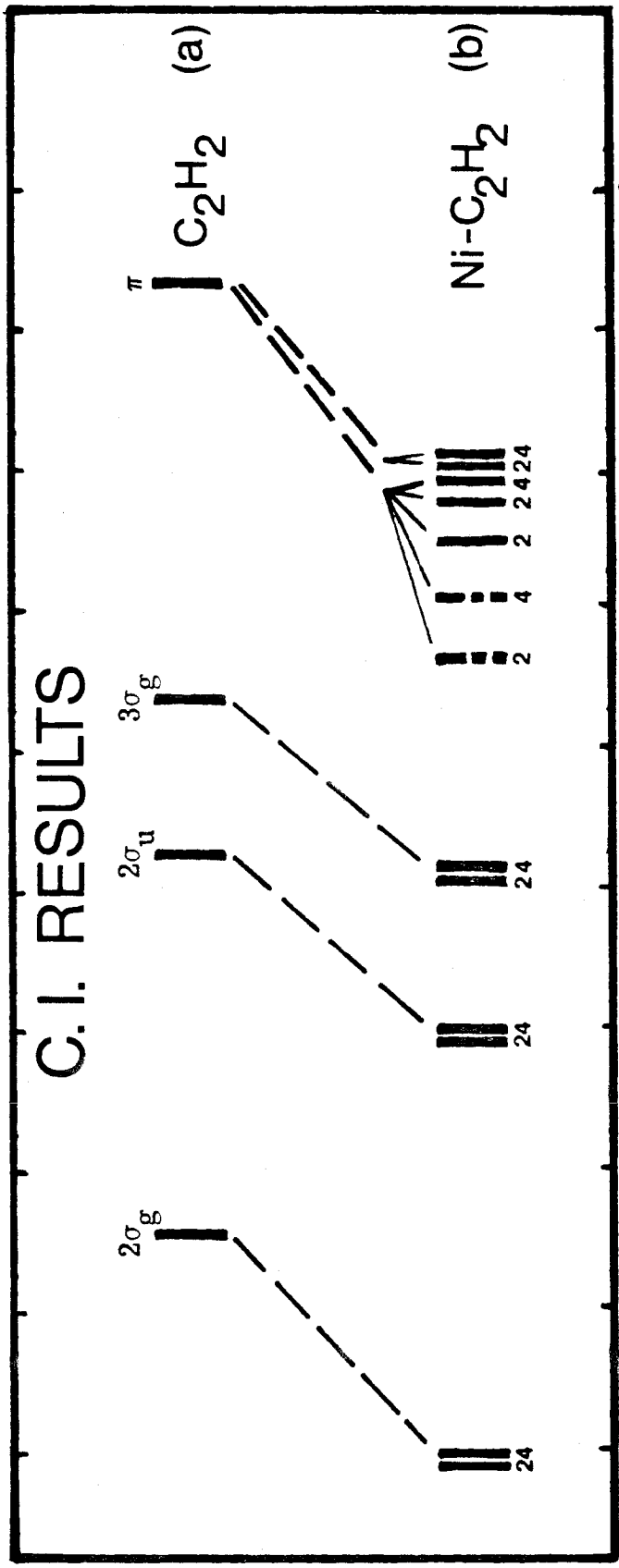

Figure 4: Comparison of IP-CI results for free and π-complexed acetylene.

Qualitatively, then the net result is that there is a broadening of the spectrum, with the CCσ level shifting to deeper energies by a larger amount than the other levels due to its increased interaction with the 3d core. The degeneracy in the π level is split by this same interaction and by the shape change that occurs in the π_y orbital upon bonding. The splitting is still very small, however. The 4s level, also shown, occurs at 5.8 eV and thus is destabilized considerably from the free Ni value of 7.63 eV.[23]

3. The Ni_2-C_2H_2 di-π Complex. The form of the bonding found for the Ni-C_2H_2 π-complex suggests that a larger Ni_2-C_2H_2 complex could be formed where each π orbital is bound to an individual Ni atom. In the complex studied here, the two Ni atoms were fixed at the bulk separation of 2.49 Å and the acetylene molecule was oriented such that the CC bond axis was above and perpendicular to the Ni-Ni bond. This allowed each π orbital to be directed towards one of the Ni atoms (the angle to the Ni atoms subtended at the CC axis is 75°). Only the perpendicular distance was optimized for this complex, as the ligand was fixed in the geometry found to be optimal for the Ni-C_2H_2 π complex.[14]

In this configuration, the lowest state is one in which the 4s orbital on each Ni atom is directed away from the acetylene π orbitals. The bond is very similar in origin to that found for the mono-π complex and at 24 kcal,[16] is not quite twice as strong. The 3d orbitals, once again, are atomic in shape and are coupled to produce a triplet. For the purpose of calculating the ionization spectrum, the 4s orbitals are singlet coupled.

Figure 5 shows IP-CI results for the di-π complex at two different values for the ligand to metal distance. The most prominent difference from Fig. 4b is the continuation of the general trends towards larger IP's for each level. This trend is observable to a lesser extent between Figures 5a and 5b where the acetylene is brought closer to the metal. Thus, the CCσ bonding level splits further away from the CH levels as a result of its larger interaction with the unshielded metal cores. Similarly, the splitting between π and CH levels is reduced. Qualitatively, however, the total spectrum retains its acetylene character in this configuration.

4. The Ni_2-C_2H_2 di-σ Complex. The remaining acetylene complex differs significantly from the two described above. In this system the acetylene π_z bond is broken, allowing each carbon atom to form a σ bond with an individual Ni atom. The resulting configuration is reminiscent of a 1,2-di-substituted ethylene as the CH bonds are found to bend away from the Ni-C bonds. To maintain the surface analogy, the Ni-Ni separation was fixed at either the nearest neighbor (2.49 Å) distance[20] or the second nearest neighbor separation (3.52 Å). The C-C and Ni-C bond distances were optimized as well as the HCC angle. The CC distance increased significantly from an acetylene value of 1.21 Å to 1.35 Å (close to the value of 1.339 for ethylene).[21] The Ni-C σ bonds were found to be 1.86 Å, similar to values found for Ni-C distances in other finite complexes (1.87 Å for $NiCH_3$, 1.91 Å for Ni_2CH_2).[22] In this configuration the acetylene is bound by 60 kcal to second nearest neighbor Ni_2 and by slightly less (56 kcal) to nearest neighbor nickel atoms.[16]

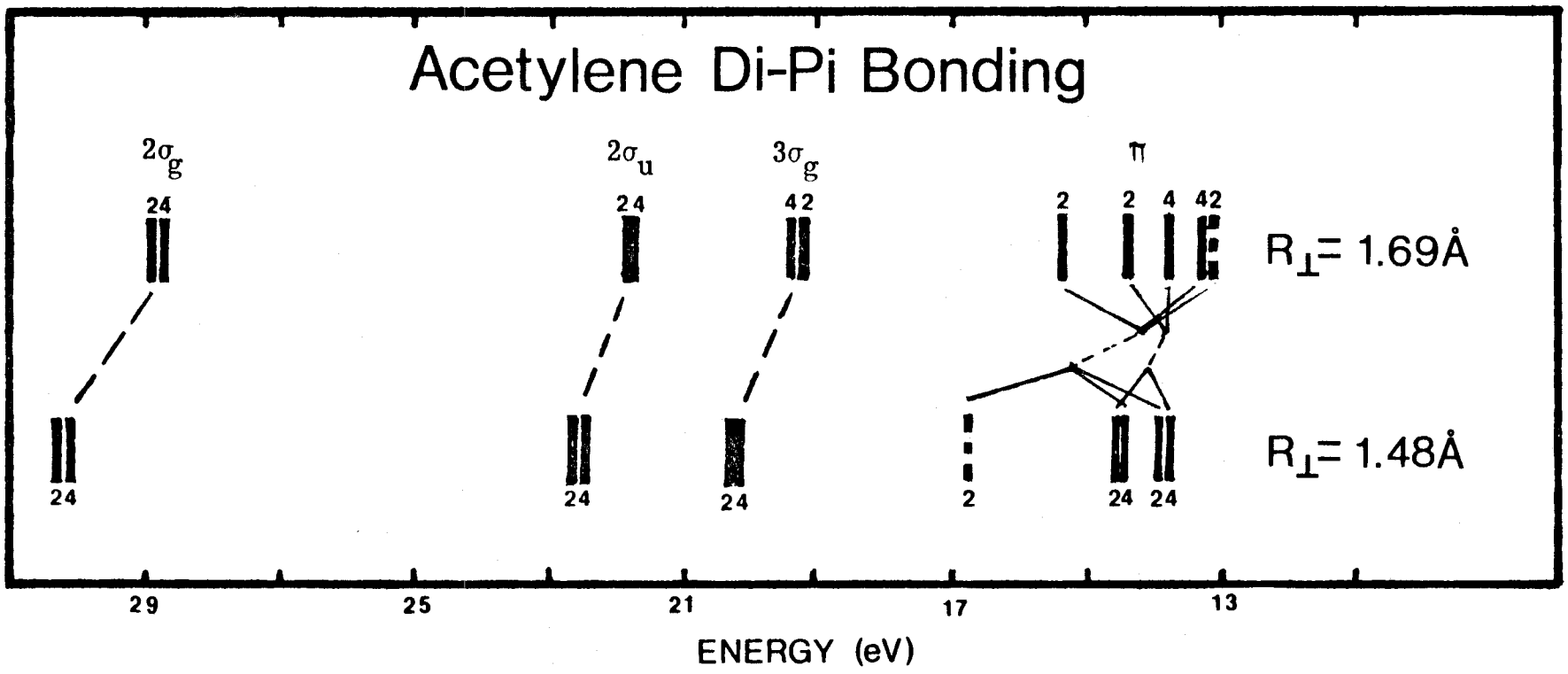

Figure 5: Effect of R(⊥) and higher Ni coordination on IP levels: $Ni_2C_2H_2$ di-π complex.

The Ni-C bonds are both diffuse (due to 4s orbital participation), and polar with about 0.2 electrons transferred to the carbon atom. As a result of the greater σ denotation on each C, the remaining π orbital is more shielded from the nucleus, leading to some destabilization of this orbital to causing it to become more diffuse (and less tightly bound) than in either acetylene or ethylene. Once again, the Ni 3d orbitals are localized and the single-occupied orbitals are triplet coupled.

The effect on the ionization spectrum of this bonding is significant as may be seen in Figures 6. The shifts of the σ levels to deeper energies are eliminated, as the electrostatic interaction is no longer present. In addition, there is very little similarity between this spectrum and what might be expected for an ethylenic species. The incorporation of 4s character into the NiC σ bonds moves them to much smaller IP. A comparison of the IP of the Ni atom at 7.63 eV[23] (or bulk Ni at 5.2 eV)[24] and the H atom at 13.6 eV,[23] suggests the source of this shift. Thus, for both Ni_2 distances, the σ bonding region of the di-σ spectrum retains significant similarity to the free acetylene spectrum. As a result of the diffuse character of the π bond, the π level shows a shift to smaller IP in this complex.

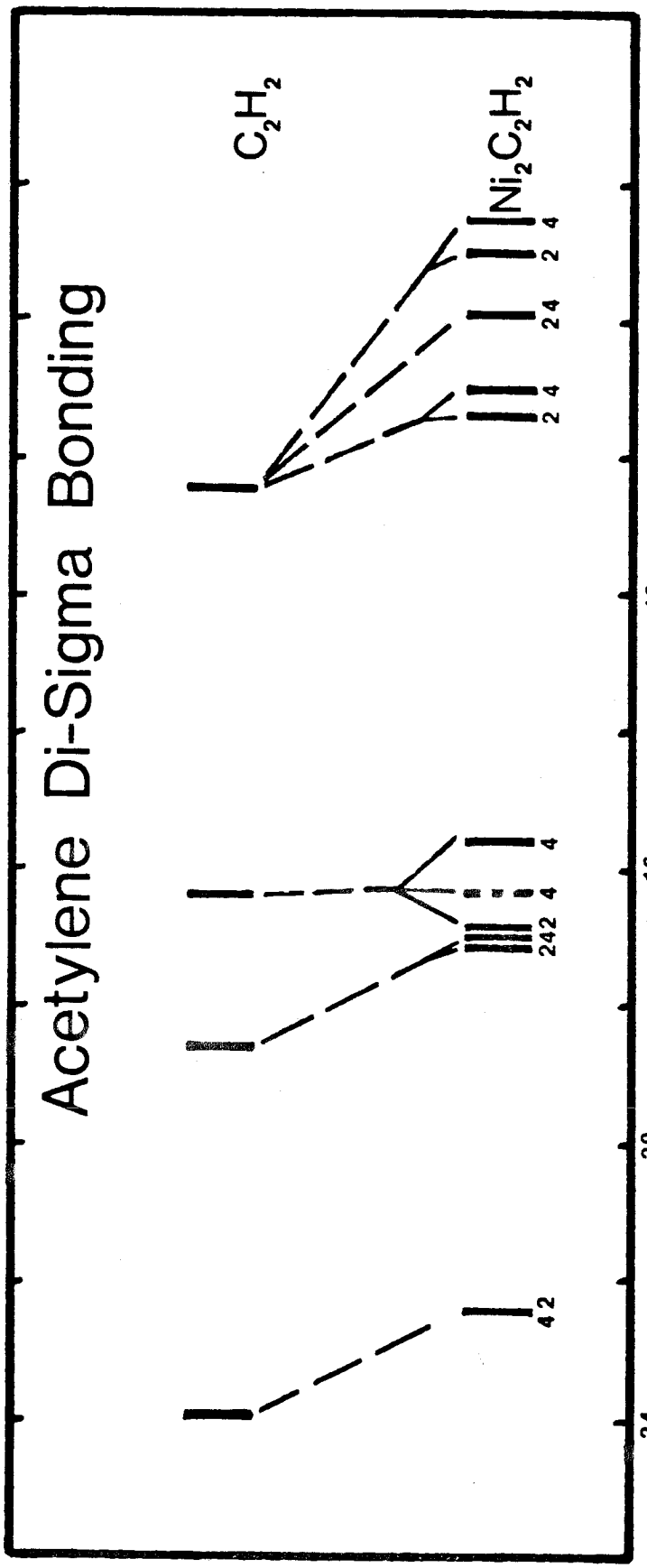

Figure 6: Comparison of IP-CI results for free acetylene and the $Ni_2C_2H_2$ di-σ complex.

5. Free Ethylene. There are six valence levels for the gas phase ethylene molecule: the π_z level, four CH levels, and a deep CC_σ bonding level. The experimental vertical spectrum[7] is shown in Fig. 7a, and it should be noted that there is a non-intuitive ordering of the CH levels there, as was found for acetylene. The $3a_1$ "nodeless" (totally symmetric) combination of CC bonding orbitals would be expected to be the deepest of the CH levels, but to zero order it is not orthogonal to the CC_σ level. Thus, the $3a_1$ must mix in an antibonding component of CC_σ character and it moves to smaller IP. This feature has led some investigators[3-4] to describe the $3a_1$ orbital as a CC_σ bonding level, an assignment that produces some confusion in the analysis of ethylene photoemission properties.

The KT results for ethylene are shown in Fig. 7b, where large shifts to deeper energies are observed for all but the π level. Carrying out both IP-CI calculations, in which shake-up effects are included, produces the improvements shown in Figs. 7c and 7d. As for acetylene, the results in Fig. 7d are from calculations carried out at a level appropriate for the corresponding Ni-complex, and they exclude some inter-pair correlation effects. This restriction was of major importance for acetylene where π_y-π_z inter-pair effects were left out, but for ethylene there is no corresponding restriction and the effect is smaller.

6. Ni-C_2H_4 π-complex. Since the dominant bonding features of the Ni-C_2H_4 complex are identical to those of the Ni-C_2H_2 π-complex it is not surprising that the ionization spectrum of the ethylene complex shows many of the properties as that of the acetylene complex. Here

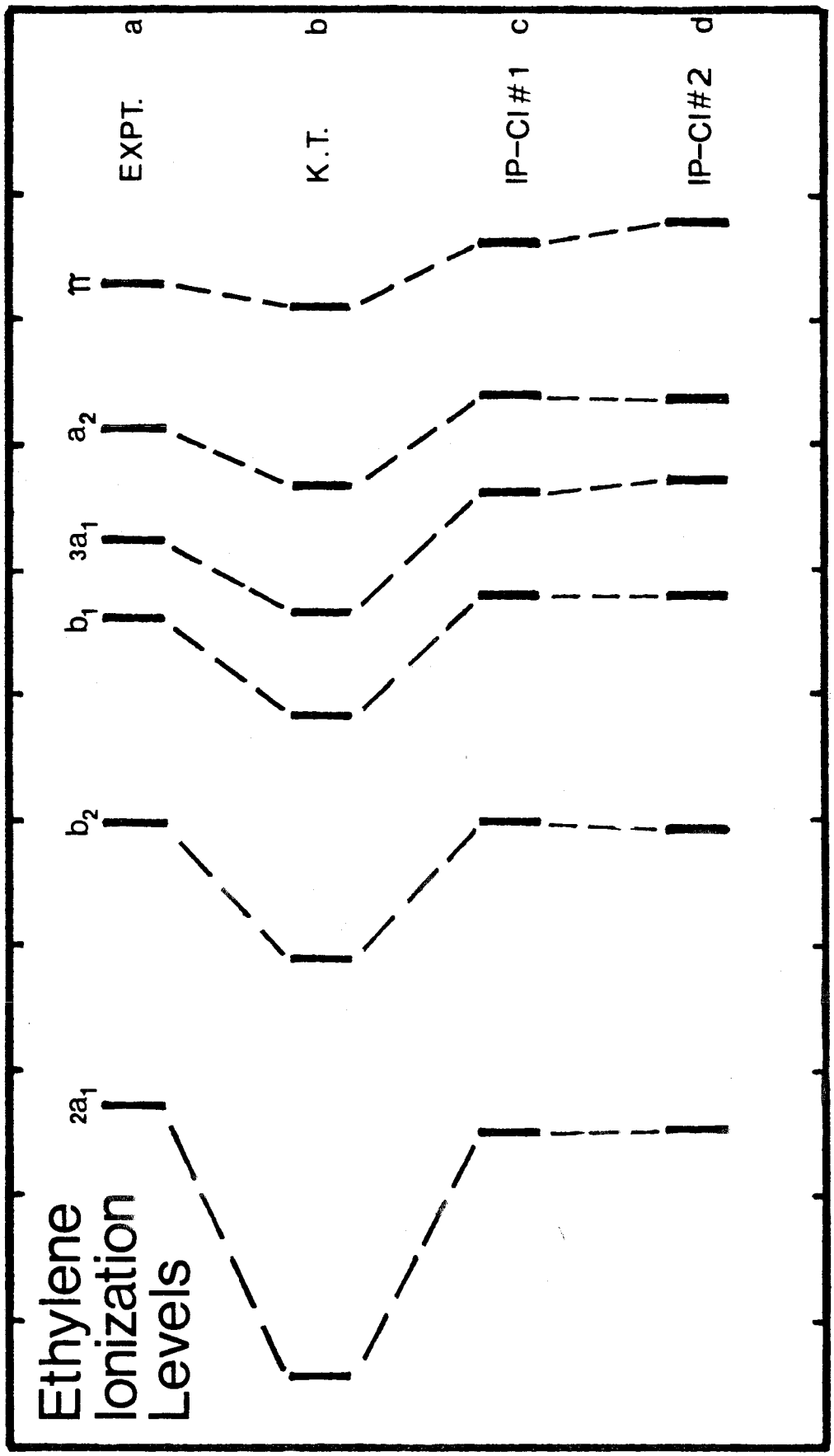

Figure 7: Comparison of calculated ionization levels with the experimental vertical spectrum.

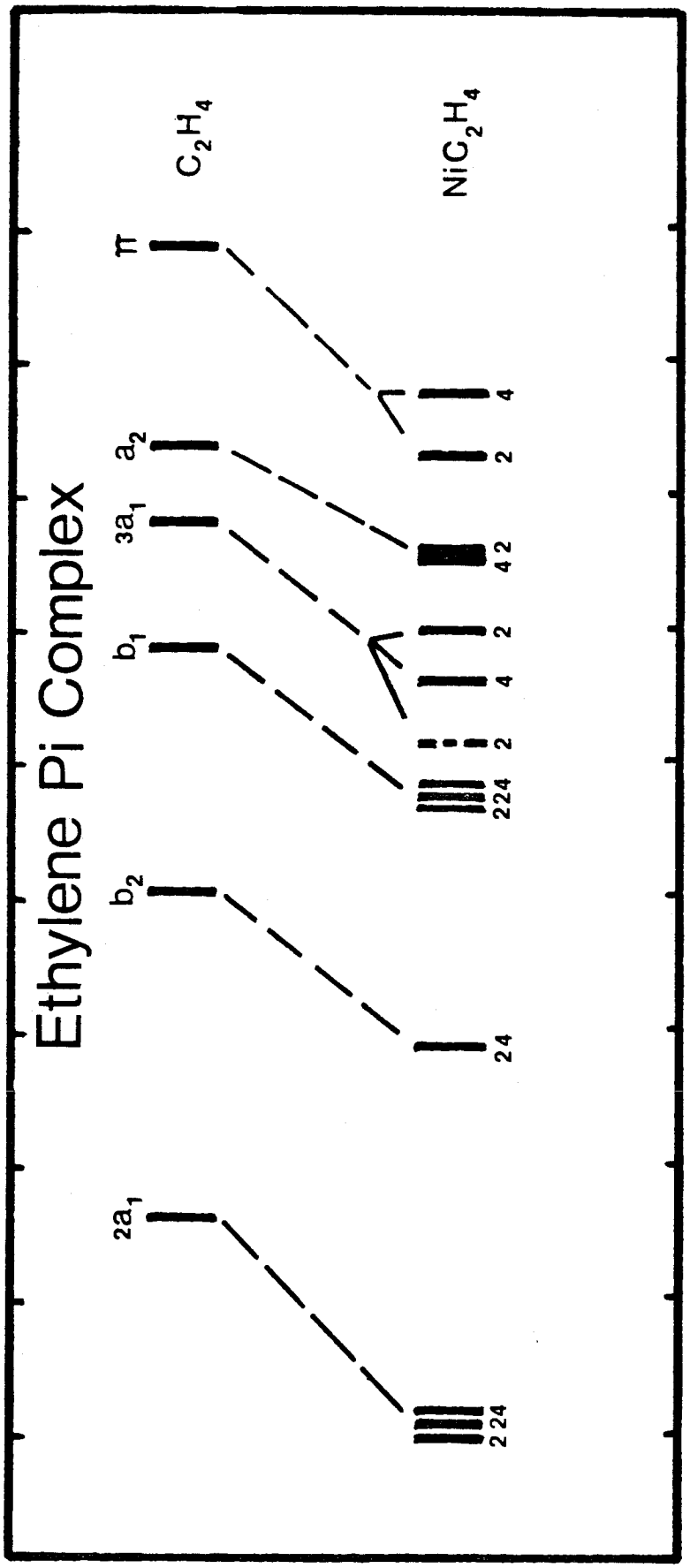

Figure 8: Comparison of IP-CI results for free and π-complexed ethylene.

again, the attractive interaction experienced by each of the doubly occupied ethylene orbitals is reduced by half upon ionization, leading to a net increase in the IP values for these orbitals. This is illustrated in Fig. 8 where IP-CI results for free ethylene are compared to the analogous complex IP-CI results.

There are small differences in the Ni complex spectra that reveal an important point however. As was mentioned elsewhere for both Ni-C_2H_2 and Ni-C_2H_4, the lowest ion states resulting from the removal of the single 4s electron are bound by ~ 60 kcal as compared with the ~ 15 kcal bond found for each of the neutral species.[14] An almost identical state results from ionizing the π_z orbital of either ligand. Here, the now singly occupied π_z orbital may couple with the 4s orbital to produce a strong bond. We find one level, of predominantly 4s character at 5.8 and 5.5 eV in the acetylene and ethylene complex spectra, respectively. This is considerably less than the Ni atom 4s value of 7.63 eV and reflects the final state character described above. But the second π_z ion state mentioned is not orthogonal to the 4s level. In producing the final spectrum, the 4s and π_z ions will interact and "repel" one another in energy (much as the $2\sigma_g$ and $3\sigma_g$ levels discussed in section II). As a crude approximation, the size of this interaction may be related to the splitting between the zero order (non-interacting) level positions. This splitting is smaller for ethylene than acetylene [IP($C_2H_2\pi$) = 11.4 and IP($C_2H_4\pi$) = 10.5 eV] and thus the final 4s IP is less for Ni-C_2H_4 than for Ni-C_2H_2.

IV. Calculational Details

A. Free Molecule Calculations

1. The Orbital Basis. In attempting to isolate the dominant correlation effects, the criterion was not so much to determine which orbitals showed large effects, but rather which orbitals might show a large change in electron correlation effects on going from the netural ground state to various ions. Although the intra-pair correlation of two electrons in a π-bond is large, this was not sufficient reason to demand inclusion of π-intra-pair correlation in both neutral and ion species. It was necessary to also examine inter-pair effects, that is the tendency of one electron pair to correlate its motion with that of another pair as the wavefunction minimizes the electron-electron repulsion between various doubly occupied orbitals. For systems that involve several orbitals localized in the same region of space, such as the π and CCσ orbitals of acetylene, these effects may be large. Removal of an electron effect on the magnitude of this interaction produces a distinct differential contribution to the energies of neutral and ion wavefunctions. The CH bonds of such molecules are in general more spatially separated and this inter-pair effect is less significant. Thus, for each of the molecules in this study, correlation effects were explicitly considered for π bonds as well as CCσ bonds. Limitations created by the nickel complex CI's (vide infra) in many cases necessitated the exclusion of some inter-pair effects in both free molecule and complex CI's. In each case, however, the importance of such a restriction was first examined explicitly for the free molecule, as discussed below.

The π orbitals used in the CI calculations were obtained from GVB calculations in which correlation effects were included only in the π orbitals as:

$$\Psi = a\{\Phi_\sigma(\pi_u^2 - \lambda^2\pi_g^2)(\chi)\} \quad (1)$$

$$= a\{\Phi_\sigma(\pi_e\pi_r + \pi_r\pi_e)(\chi)\} \quad (2)$$

where Φ_σ represents occupied σ orbitals and χ represents the appropriate spin function. The natural orbitals (1) obtained in this manner were adequate to describe intra-pair effects as in (2) as well as the inter-pair effects described above.

The method for obtaining σ orbitals was not as straightforward. As implied by Figure 1 and the discussion of Section II, the Hartree-Fock orbitals for the ground state are mixed in a manner to allow optimum description of the ionic states without allowing the orbitals to relax. For a system with a closed shell ground state, (e.g., acetylene or ethylene) such a mixing of orbitals has no effect on the neutral energy (as indicated in Figure 1b). For simplicity, it is advantageous to retain this feature of the HF orbital in the CI calculations. This creates a problem if correlation effects in σ orbitals are to be considered. Using the acetylene example, a GVB calculation designed to include correlation in the CCσ bond "unmixes" the $2\sigma_g$(CC) and $3\sigma_g$(CH) orbitals. When performing CI calculations with these orbitals to describe ion states, configurations must be included that effectively "remix" the $2\sigma_g$ and $3\sigma_g$ orbitals in a manner optimum for the ion.

To avoid this expansion of the configuration list, the HF $2\sigma_g$ and $3\sigma_g$ orbitals were used in the CI basis. A separate GVB calculation was performed using the wavefunction:

$$\Psi_{C_2H_2} = a\{\Phi_{\sigma^1}\Phi_{\pi}(\sigma^2_{CC} - \lambda^2\sigma^{*2}_{CC})(\varphi)\}$$

from which only the σ^*_{CC} natural orbital was retained for use in the CI. In this way, an appropriate selection of configurations allowed inclusion of correlation (vide infra) without disturbing the shape of the dominant orbitals.

The above discussion defines the dominant σ and π orbitals in the CI along with those virtual orbitals needed to describe correlation. This virtual list was further expanded to include orbitals capable of describing the dominant shape adjustments expected to occur upon ionization. Thus, for each bonding orbital from which ionization was to be considered a second (more contracted) orbital of similar bonding character was included. These orbitals were obtained by the Improved Virtual Orbital (IVO) method.[25] Here all of the occupied orbitals except one are frozen in their ground state (neutral) configuration. The remaining orbital is single-occupied to describe ionization and allowed to contract within the field defined by the remaining frozen orbitals. Singly-occupied orbitals obtained in this manner are orthogonal to the remaining dominant orbitals and represent the main relaxation effects not described by the ground state orbital.

2. Configuration Interaction Calculations. For this study it was of utmost importance that the results of the free molecule calculations be directly comparable to the corresponding Ni-complex calculations. The CI calculations of the free molecule were designed in such a manner that exactly the same treatment could be applied to the molecule when it served as a ligand in the metal complex. Since the Ni-complex calculations were significantly larger than those of the free molecule (due to the presence of the Ni atom), restrictions on the size of the free molecule CI's were, to a large extent, dictated by the CI required in the corresponding complex. These restrictions were of four basic types: 1) For all of the molecules considered, the addition of the Ni atom to the system resulted in a lowering of the usable symmetry. Thus C_2H_4, with D_{2h} symmetry, was reduced to C_{2V} upon formation of the Ni π-complex resulting in a significantly larger set of symmetry allowed configurations. The CI calculations were designed in such a manner as to eliminate this discrepancy and preserve compatability.

2) Since the Ni atom bound in the complex contains two open shells, there were always two additional open shells in each spatial configuration of the complex than in the analogous configuration for the free molecule. This necessarily leads to a significant increase in the number of linearly independent spin eigenfunctions. For example, a single excitation from closed shell with that of the free molecule leads to a single spin eigenfunction. However, in the metal-molecule complex (triplet state) the same excitation produces a spatial configuration with four open shell orbitals for which there are two linearly independent spin-functions. The result is a far larger CI matrix from the metal-complex than from the free molecule.

3) The CI programs used are restricted to a maximum of six open shells for any given spatial configuration and thereby induce a restriction on the maximum member of open shell orbitals allowed in the ligand. For the metal complex, the ion requires one open shell in addition to that involved in the neutral due to the presence of a single electron in the ionized orbital. Because of the two open shell Ni orbitals, this leaves a maximum of three open shells available for relaxation and correlation excitations within the ligand (and molecular) orbital space.

4) To obtain a full spectrum of valence ionization states in the molecule requires extracting from the CI matrix all roots down to the most tightly bound valence orbital. Thus, in addition to ligand ion states, numerous higher-lying Ni ions as well as "shake-up" states had to be extracted before the lowest ligand ion root could be obtained. The CI matrices were of an order of up to 500 by 500 and hence direct diagonalization was impractical; instead, each root was obtained by an iterative root extraction technique. To facilitate this process, it was of utmost importance to keep the CI matrix of the metal complex (and thus the CI matrix of the free molecule) as small as possible.

Within the framework provided by this rather extensive list of restrictions, the spatial configurations for the CI calculations on both the neutral and ionic states of the free molecule were generated in two stages. For the neutral an initial set of basic configurations was generated that included (in addition to the ground state configuration) all spatial configurations resulting from a single excitation of a dominant orbital into its correlating orbital (when present). Table Ia lists the

ORBITAL BASIS	$2\sigma_g$	$3\sigma_u$	$2\sigma_g'$	$3\sigma_g$	$3\sigma_g'$	$2\sigma_u$	$2\sigma_u'$	π_{uz}	π_{gz}	π_{uz}'	π_{ux}	π_{gx}	π_{ux}'
ORBITAL SYMMETRY	A_1	B_2	A_1	A_1	A_1	B_2	B_2	A_1	B_2	A_1	B_1	A_2	B_1
a-Neutral State Generating Configurations	2	0	0	2	0	2	0	2	0	0	2	0	0
	1	1	0	2	0	2	0	2	0	0	2	0	0
	2	1	0	1	0	2	0	2	0	0	2	0	0
	2	0	0	2	0	2	0	1	1	0	2	0	0
	2	0	0	2	0	2	0	2	0	0	1	1	0
b-Ion State Generating Configurations	1	0	0	2	0	2	0	2	0	0	2	0	0
	2	0	0	2	0	2	0	2	0	0	2	0	0
	2	0	0	2	0	1	0	2	0	0	2	0	0
	2	0	0	2	0	2	0	1	0	0	2	0	0
	2	0	0	2	0	2	0	2	0	0	1	0	0
	1	0	0	2	0	2	0	1	1	0	2	0	0
	1	0	0	2	0	2	0	2	0	0	1	1	0
	1	1	0	1	0	2	0	2	0	0	2	0	0
	2	0	0	1	0	2	0	2	0	0	1	1	0
	2	0	0	1	0	2	0	1	1	0	2	0	0
	1	1	0	2	0	1	0	2	0	0	2	0	0
	2	0	0	2	0	1	0	1	1	0	2	0	0
	2	0	0	2	0	1	0	2	0	0	1	1	0
	2	1	0	1	0	1	0	2	0	0	2	0	0
	1	1	0	2	0	2	0	1	0	0	2	0	0
	2	0	0	2	0	2	0	1	0	0	1	1	0
	2	1	0	1	0	2	0	1	0	0	2	0	0
	1	1	0	2	0	2	0	2	0	0	1	0	0
	2	0	0	2	0	2	0	1	1	0	1	0	0
	2	1	0	1	0	2	0	2	0	0	1	0	0
Orbital Grouping	Group 1			Group 2		Group 3		Group 4			Group 5		

orbitals from GVB calculations in which correlation effects were included only in the π orbitals (providing, thereby, also π^* correlating orbitals). As in the case of the molecular calculations, the CCσ^* or COσ^* correlating orbitals were obtained from separate GVB(1) calculations in which σ correlation alone was considered. The virtuals used to describe relaxation were obtained using the NO technique as described above.

In all cases, the nickel orbitals were obtained from the first GVB calculations described above. As highly accurate values for Ni ion states were of only secondary importance, the Ni orbitals were treated at a minimum basis level, that is no IVO orbitals were included to describe relaxation in the size of the metal orbitals upon relaxation. As these orbitals were highly localized, the effect of this restriction on ligand states was presumed to be minimal.

2. The CI calculations. As mentioned previously, care was taken to ensure that the treatment of the ligand in the CI calculations for the metal complex was identical to that of the CI calculations for the free molecule. Thus, for each complex, configurations describing ligand neutral and ion states were generated from the same set of basic configurations listed in Table I. For each of these configurations the NI atom(s) was frozen in its ground state occupation. This list was then expanded to include configurations describing Ni ion states. This ion set was generated by removing a single electron from the Ni orbitals while allowing simultaneous excitations (through doubles) from dominant ligand orbitals into appropriate correlating orbitals. No excitations describing ligand relaxation due to Ni ionization were allowed.

C. Basis Sets and Effective Potential

In all of the calculations described here an effective potential was used to replace the argon core of the Ni atom. This potential was a modification[26] of the ab initio potential of Melius et al.[27] designed to correctly describe the ordering of states of the Ni atom.

For all but the acetylene complexes, the basis sets used for the ligand atoms (C and O) were the Dunning (3s/2p) contractions of a (9s/5p) basis.[28] These basis sets were augmented by a single set of 3d gaussians (α = 0.6769 for carbon and α = 0.8853 for oxygen). The H basis set was the Dunning DZ contractions of a (4s) basis[28] scaled by a factor of 1.2. For the acetylene complexes the Dunning (4s/2p) contraction of the (9s/5p) basis was used to allow comparison with the acetylene studies of Yaffe and Goddard.[29] Here, a single set of 3d gaussians (α = 0.6384) was used to augment the basis. The H atom basis was the same as above, but not scaled.

For the NiC_2H_2 complex a full double zeta (2d) contraction of Wachter's (5d) basis of d gaussians[30] was used for the Ni atom. For each of the remaining complexes a (1d) contraction (minimal basis set) of the (5d) set was obtained using the orbitals from the atom $Ni\ ^3D\ (s^1 d^9)$ state. This use of the effective potential allowed truncation of the Ni s basis to only the four most diffuse functions of Wachter's, contracted to double zeta (2s). A single set of 4p gaussian with α = 0.1 was used in all cases to augment this basis.

V. Relevance to C_2H_2 and C_2H_4 Chemisorption on Nickel

A. Ethylene

The simple, relatively weak bond found for Ni-ethylene suggests that these should be a highly mobile phase of chemisorbed ethylene on the low index faces of nickel. There are several pieces of experimental evidence that support this prediction:

i) Angle integrated photoemission spectra exist for C_2H_4 on Ni(111)[2,3] and angle resolved UPS data has appeared for the Ni(100) surface.[4] Each of these is reproduced in Fig. 9. The (111) and (100) data are very similar, and are in substantial agreement with our calculated spectrum (shown in Fig. 9a). In the figure, each of the calculated levels has been corrected as follows:

$$\text{I.P.}(\text{Ni-}C_2H_4\ \text{corr.}) = \text{I.P.}(\text{Ni-}C_2H_2\ \text{calc.}) + [\text{I.P.}(C_2H_2\ \text{expt.}) - \text{I.P.}(C_2H_2\ \text{calc})]$$

The assumption here is that the errors found in the free ethylene calculations should also be present in the Ni-ethylene calculations. This view finds support in the weak distortion of the ethylene that results upon complexation with the Ni atom. In creating the figure, the $3a_1$ orbital was aligned with the experimental peaks at ~ 8 eV, and thus it is relative rather than absolute peak positions that are probed. This choice of alignment is consistent with the results of the ARUPS studies which show, for each feature (except $1a_2$), the expected angular dependence.

The calculation correctly reproduce several shifts that have been the subject of some interest in the literature.[1-3] The (filtered) 40.8 eV spectrum shows a $2a_1$ peak that is shifted relative to the $3a_1$ peak by

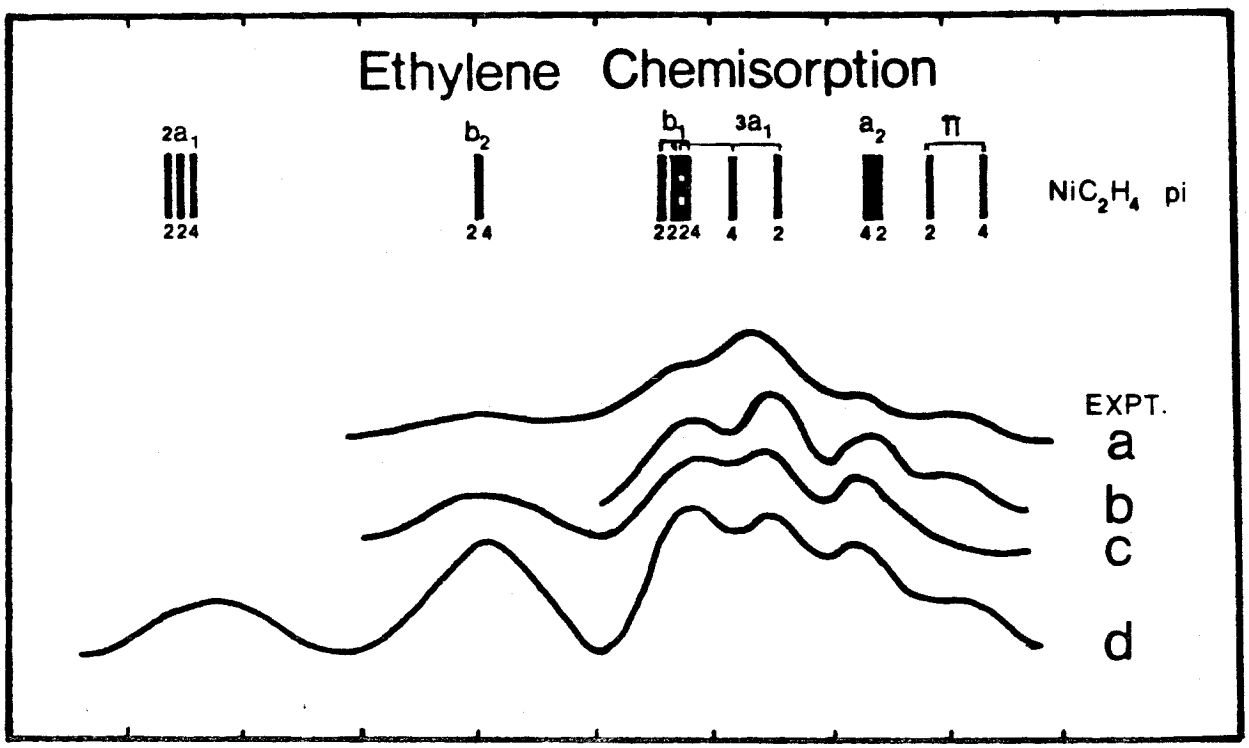

Figure 9: Comparison of IP-CI results for the Ni-C_2H_2 complex with experimental UPS spectra of C_2H_4: (a) Ni(100) at 80 K ARUPS (60° angle shown), 21.2 eV spectrum (ref. 4); (b) Ni(111) at 100 K, 21.2 eV spectrum (ref. 39); (c) Ni(111) at 80 K, 40.8 eV spectrum (ref. 8b); (d) Ni(111) at 100 K, filtered 40.8 eV spectrum (ref. 3).

about 1 eV. Similarly, there is a smaller shift of the b_2 level to deeper energies. These larger relative shifts show up plainly in Fig. 8, and are the result of the differential "electrostatic" interactions experienced by each C_2H_4 orbital. The only other orbital expected to exhibit such a relative shift is the π level and this has been observed. Thus, the so-called "relaxation" or "bonding-shifts" have a very simple and intuitive explanation using the model presented here.

ii) Modulated C_2H_4 molecular beam experiments have been carried out by Zuhr and Hudson[31] in which ethylene molecules were scattered from the Ni(110) surface. At room temperature, it was observed that take-up was more rapid than predicted by Langmuir kinetics (assumes non-interacting, immobile adsorbates). By measuring the scattered intensity as a function of temperature (and correcting for change in background with temperature) an Arrhenius plot was obtained with $A = 1 \times 10^{10}$ and $\Delta H = 11.9$ kcal/mol. This result is in very good agreement with our calculated π-coordination energy for ethylene of 14 kcal. The experimental value predicts a lifetime on the surface of only ~ 0.05 sec at room temperature, but at 80 K (the temperature used in the UPS studies[2-4]) essentially infinite lifetime is expected. These observations are also in agreement with those of Horn et al.,[4] who observe only a gradual loss of intensity in the Ni(100)-ethylene ARUPS spectrum upon heating to $T > 200$ K, and interpret this as evidence for desorption.

iii) The polarization of the Ni 4s orbital necessary to produce the coordination bond creates a net dipole between the Ni core and the 4s

orbital necessary to produce the coordination bond creates a net dipole between the Ni core and the 4s orbital. Evaluating this Ni dipole separately (i.e., without the ethylenic contribution to the total complex dipole) yields a value of 1.12 D. It is the interaction of the ethylene orbitals with this dipole that produces the shifts discussed in i) above, but it should also produce a change in the work function observed for the bulk chemisorption system. Using the simple expression:[32]

$$\Delta\phi = \mu_S n_S/\epsilon_0$$

where n_S [for p(2×2) C_2H_4 on Ni(111) is $\sim 4.75\times10^{14}/cm^2$ and $\Delta\phi$ = -1.2 eV at 80K[2], gives μ_S = 0.6 D. This formula makes no allowance for depolarization of adjacent dipoles however, an effect which could be large for ethylene. A formula due to Topping incorporates this effect as:[32]

$$\Delta\phi = \frac{\mu_S n_S}{\epsilon_0(1 + 9\alpha n_S^{\frac{3}{2}})}$$

where α is the adsorbate polarizability (4.26 $\mathring{A}^3$ for C_2H_4[38]). Using this expression yields μ_S = 0.94 D, in better agreement with our result.

It should be noted that elevating the temperature of the bulk chemisorption system (230 K on Ni(111);[2] $\sim$300K on Ni(110)[31]) produces drastic changes in the adsorbed phase. While the exact nature of the high temperature phase is not known, there is evidence that dehydrogenation to acetylenic or graphitic surface species occurs rather than desorption of the weakly bound phase.

B. Acetylene.

The experimental details surrounding the low temperature chemisorption of acetylene on nickel surfaces are more complicated than for ethylene. Beginning with UPS data, we compare in Fig. 10 our calculated spectra for both the π coordinate complexes (corrected as for ethylene above) and the di-σ model, with currently available experimental results. It is evident that there is a good match between the calculated positions of σ levels in the π complexes and the experimental peaks below 8 eV. Alignment of the π peaks with the low-lying UPS spectral feature is less satisfactory. As drawn here, the relative positions of the di-σ levels are in poor agreement with the experimental features. Two comments are appropriate here: 1) the positions of the di-σ levels have not been corrected to account for "systematic" errors in the IP-CI, since no free molecule analogue was available to provide reliable estimates of their magnitude. For the π complexes these corrections moved the π levels deeper in energy, and the $2\sigma_g$ level to smaller IP; 2) the strength of the π coordination bond found for ethylene suggests that low temperature adsorption of C_2H_2 on Ni(111) in a di-σ form might result in its coordination to a third Ni atom through the π bond. This would produce relative shifts in both the π and the $2\sigma_g$ levels to deeper energy. In this context, ARUPS results for C_2H_2 on Ni(100) deserve mention.[4] Here π coordination of the di-σ species cannot proceed so readily, and the position of the low-lying feature is shifted up to only 3.9 eV from the 4.9-5.5 eV found for Ni(111).

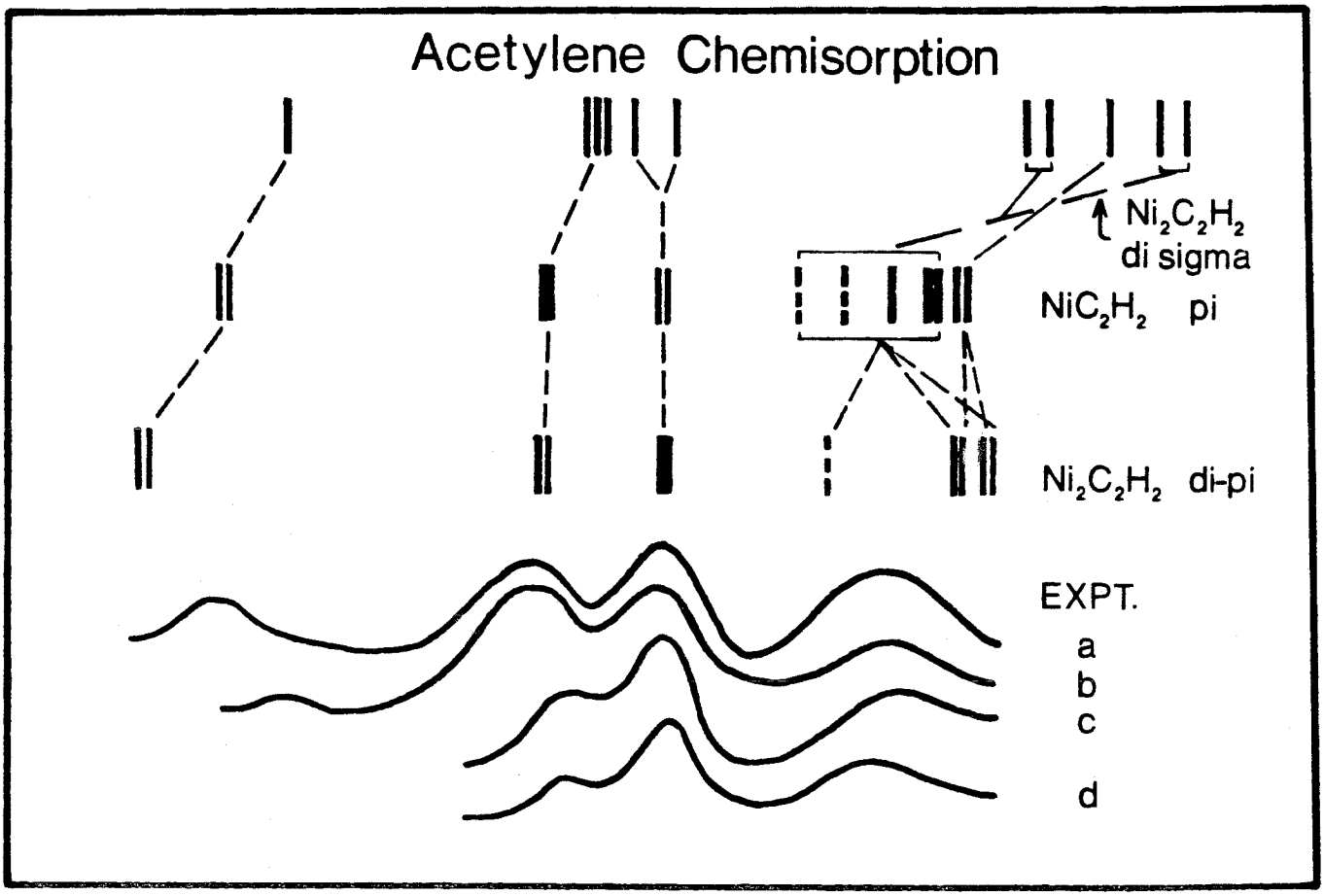

Figure 10: Comparison of IP-CI results for the three acetylene complexes with UPS spectra for C_2H_2 on Ni(111) at 80-100 K: a) filtered 40.8 eV spectrum (ref. 3); b) 40.8 eV spectrum (ref. 36); c) 21.2 eV spectrum (ref. 37); d) 21.2 eV spectrum (ref. 2).

In spite of the above qualifications, comparison of spectral features would suggest that π-coordination best describes the relative spacings observed experimentally. This conclusion is supported by the work function change ($\Delta\phi$ = -1.2 eV on Ni(111) at 80 K),[2] the results of IR-reflectance studies of C_2H_2 on Ni films,[33] and experimental studies of the Ni-C_2H_2 analogue.[34] It is supported by the HF (STO 4-31G) studies of Demuth,[8b] where KT IP values of distorted C_2H_2 and C_2H_2-Be_n are compared to the UPS spectra.

Unfortunately, there is considerable evidence against such a species being present at these (or higher) temperatures. This evidence comes chiefly in the form of HRELS data for C_2H_2 on Ni(111) at temperatures as low as 140 K.[12-13] Almost none of the features in this spectrum correspond to what might be expected of a weakly distorted acetylene, nor are they comparable to what has been observed for Ni-C_2H_2. They are suggestive of a strongly distorted di-σ species, although even here the analysis is less than convincing. Very unusual behavior of some of the vibrational features has been observed: the intensity of the 1200 cm^{-1} (1190 cm^{-1} for C_2D_2 leading to its assignment as ν_{CC}) feature is reduced by a factor of 4 upon coadsorption of hydrogen (factor of 2 for C_2D_2) and the line width of the 2910 cm^{-1} vibration is reduced noticeably under these same conditions (coadsorption). No evidence for H-D exchange or addition is found however. Similarly, too many modes are observed in the ELS experiment to allow any sort of simple bonding scheme in which the acetylene is symmetrically bonded to the surface. In support of this view, there are theoretical studies available that suggest a "tilted" di-σ species is favorable.[8a, 9]

Clearly, no simple resolution of this confusing situation may be expected. Our theoretical results are not unambiguous: thermodynamic estimates suggest that a di-σ or some other σ bonded form should be favored, yet the photoemission spectrum is well described by a π-coordinate form. There are experiments that could be carried out that would aid in the resolution of this confusion however, and our theoretical results would be valuable in this regard. If in fact the results of the HRELS experiments at $T \geq 140$ K are correct, then one must wonder what conditions are required to produce a π-coordinate species on the Ni surface. There is ample evidence drawn from finite complex studies to suggest that such a bonding form is favorable.[35] One must assume then that at temperatures used in current studies, the π-coordinate species is unstable with respect to π or σ bond cleavage and subsequent formation of a more strongly bound species. Performing UPS and HRELS experiments at low temperatures (4-10 K) would be exceedingly useful in that one could presumably trap such a π coordinate species and observe its modification with increasing temperature. While there is some concern that the sticking probability might vanish at low temperatures, we note that Ozin and Power[34] have formed the cryogenic complex NiC_2H_2 at 10 K. Indeed, this finite π complex is stable to only 50 K, a result lending support to this discussion. Presumably, the results of a low temperature HRELS study would show vibrations near the 3130 and 1734 cm^{-1} frequencies found to be characteristic of the NiC_2H_2 π-complex. Frequencies in this regime have already been observed in reflectance IR studies (3150 cm^{-1} and 1800 cm^{-1}) of C_2H_2 on Ni films at 300 K.[33] It is possible that the

low coordination sites present in the films stabilize the π-coordinate form, but the high coverage conditions used (30L) make these results suspect.

VI. Summary

Calculations have been carried out to accurately determine the ionization levels of model Ni-ethylene and Ni-acetylene complexes. The results may be summarized as follows:

1) The use of Koopmans' Theorem to estimate IP values is inappropriate for π bonded molecules. The position of $\pi \rightarrow \pi^*$ shake-up states has a strong effect on the appearance of the direct ion spectrum.

2) The inclusion of metal atoms in the modelling of UPS spectra for chemisorbed species has a major effect on the calculated levels, in contrast to what has been assumed elsewhere.[8] "Screening" effects vary greatly depending on the explicit details of the bonding and can lead to large shifts (1-4 eV) in the position of ionization levels.

3) Ionization levels calculated here for Ni-C_2H_4 are in very good agreement with those observed experimentally for low temperature chemisorbed ethylene. The predicted bond energy and work function changes are also in agreement with the bulk system.

4) Calculated UPS spectra for π-coordinate model complexes are in agreement with the observed level spacings, and a work function change in the right direction is suggested. Conflicting HRELS data preclude a firm assignment, however.

References and Notes

1. D. E. Eastman and J. K. Cashion, Phys. Rev. Lett., 27, 1520 (1971).
2. J. E. Demuth and D. E. Eastman, Phys. Rev. Lett., 32, 1123 (1974).
3. J. E. Demuth, Phys. Rev. Lett., 40, 409 (1978).
4. K. Horn, A. M. Bradshaw, and K. Jacobi, J. Vac. Sci. Technol., 15, 575 (1978).
5. J. E. Demuth and D. E. Eastman, J. Vac. Sci. Technol., 13, 283 (1976).
6. G. W. Rubloff and J. E. Demuth, J. Vac. Sci. Technol., 14, 419 (1977).
7. D. W. Turner, C. Baker, A. D. Baker, and C. R. Brundle, "Molecular Photoelectron Spectroscopy", (Wiley-Interscience, New York, N.Y.), 1970.
8. a) J. E. Demuth, Surf. Sci., 84, 315 (1979); (b) J. E. Demuth, IBM Journal of Res. and Development, 22, 265 (1978).
9. A. B. Anderson, J. Am. Chem. Soc., 100, 1153 (1978).
10. R. P. Messmer, in: "The Physical Basis for Heterogeneous Catalysis," Eds. E. Drauglis and R. I. Jaffe (Plenum, New York, 1975), p. 261.
11. H. Ibach and S. Lehwald, J. Vac. Sci. Technol., 15, 407 (1978).
12. J. E. Demuth and H. Ibach, Surf. Sci., 85, 365 (1978).
13. J. E. Demuth, H. Ibach, and S. Lehwald, Phys. Rev. Lett., 40, 1044 (1978).

References (continued)

14. T. H. Upton and W. A. Goddard III, J. Am. Chem. Soc., 100, 321 (1978); see also Part I.A of this thesis.

15. G. A. Ozin, W. J. Power, T. H. Upton and W. A. Goddard III, J. Am. Chem. Soc., 100, 4750 (1978); see also Part I.B of this thesis.

16. See Appendix I.A of this thesis.

17. G. T. Surratt and W. A. Goddard III, Chem. Phys., 23, 39 (1977).

18. D. G. Streets and A. W. Potts, J. Chem. Faraday Soc. Trans II, 70, 1505 (1974).

19. a) J. Chatt and L. A. Duncanson, J. Chem. Soc., 2939 (1953); b) M. J. S. Dewar, Bull. Soc. Chim. Fr., 18, C71 (1971).

20. W. P. Pearson, "Handbook of Lattice Spacings and Structures of Metals and Alloys," (Pergamon, New York, 1958).

21. M. D. Harmony, V. W. Laurie, R. L. Kuczkowski, R. H. Schwendeman, D. A. Ramsey, F. J. Lovas, W. J. Lafferty, A. G. Maki, J. Phys. Chem. Ref. Data, 8, 619 (1979).

22. W. A. Goddard III, S. P. Walch, A. K. Rappé, and T. H. Upton, J. Vac. Sci. Technol., 14, 416 (1977).

23. C. Moore, Natl. Bur. Stand. (U.S.) 35, Vol. II, 1971.

24. A. A. Holscher, Surf. Sci., 4, 89 (1966).

25. W. J. Hunt and W. A. Goddard III, Chem. Phys. Lett., 3, 414 (1969).

26. M. Sollenberger, M.S. Thesis, Calif. Inst. of Technology, 1977.

27. C. F. Melius, B. D. Olafson, and W. A. Goddard III, Chem. Phys. Lett., 28, 457 (1974).

References (continued)

28. T. H. Dunning and P. J. Hay in "Modern Theoretical Chemistry", Vol. 3, H. F. Schafer III, Ed. (Plenum, New York, 1977), p. 1.

29. L. G. Yaffe and W. A. Goddard III, unpublished results.

30. A. J. H. Wachters, J. Chem. Phys., 42, 1293 (1965).

31. R. A. Zuhr and J. B. Hudson, Surf. Sci., 66, 405 (1977).

32. G. Ertl and J. Kuppers, "Low Energy Electrons and Surface Chemistry," (Verlag-Chemie, Weinheim, Germany, 1974), p. 124.

33. M. Ito and W. Soetaka, Proc. 7th Intl. Vac. Congr. and 3rd Intl. Congr. Solid Surfaces, Vienna, 1977, p. 1043.

34. G. A. Ozin and W. J. Power, to be published.

35. E. L. Muetterties, T. N. Rhodin, E. Band, C. F. Brucker, W. R. Pretzer, Chem. Rev., 79, 91 (1979).

36. J. E. Demuth, Chem. Phys. Lett., 45, 12 (1977).

37. J. E. Demuth, Surf. Sci., 69, 365 (1977).

38. G. S. Somorjai, "Principles of Surface Chemistry", (Prentice-Hall, New Jersey, 1972), p. 192.

39. J. E. Demuth and D. E. Eastman, Phys. Rev. B13, 1523 (1976).

Appendix I.A: A Brief Discussion of the Bonding in $Ni_2(C_2H_2)$ di-π and di-σ Complexes

I. INTRODUCTION

Previously, we have reported the results of a theoretical study of a simple $Ni(C_2H_2)$ complex that suggested a very simple interaction was operational in the formation of the π-coordination bond.[1] The study of this system was made particularly relevant by the existence of experimental data characterizing such π-complexes of nickel[2] and other group VIII[3] and noble metals.[4] However, for the broader purpose of gaining insight into acetylene (and related hydrocarbon) chemisorption on nickel it is worthwhile to consider the bonding properties of other simple model complexes. The results of the previous study raise two questions in particular concerning acetylene chemisorption: 1) given the simple bonding picture found for $Ni(C_2H_2)$, is it possible to form two such bonds to the surface using both acetylene π orbitals; 2) are species involving C-Ni σ bonds energetically favorable relative to such a di-π bonded species.

As a first step in answering such questions we have considered the formation of two model $Ni_2(C_2H_2)$ complexes. The first, illustrated in Fig. 1a, has the acetylene bonding axis oriented above and perpendicular to the Ni_2 axis. In this configuration, the energetic importance of a di-π bonded acetylene moiety may be considered. In Figure 1b, a di-σ bonded complex is illustrated. Here, one of the acetylene π orbitals is broken, allowing the formation of sigma bonds to the individual Ni atoms. In this case, some estimate of Ni-C σ bond strengths may be made, allowing a crude comparison to be made between different possible isomeric chemisorbed acetylene structures.

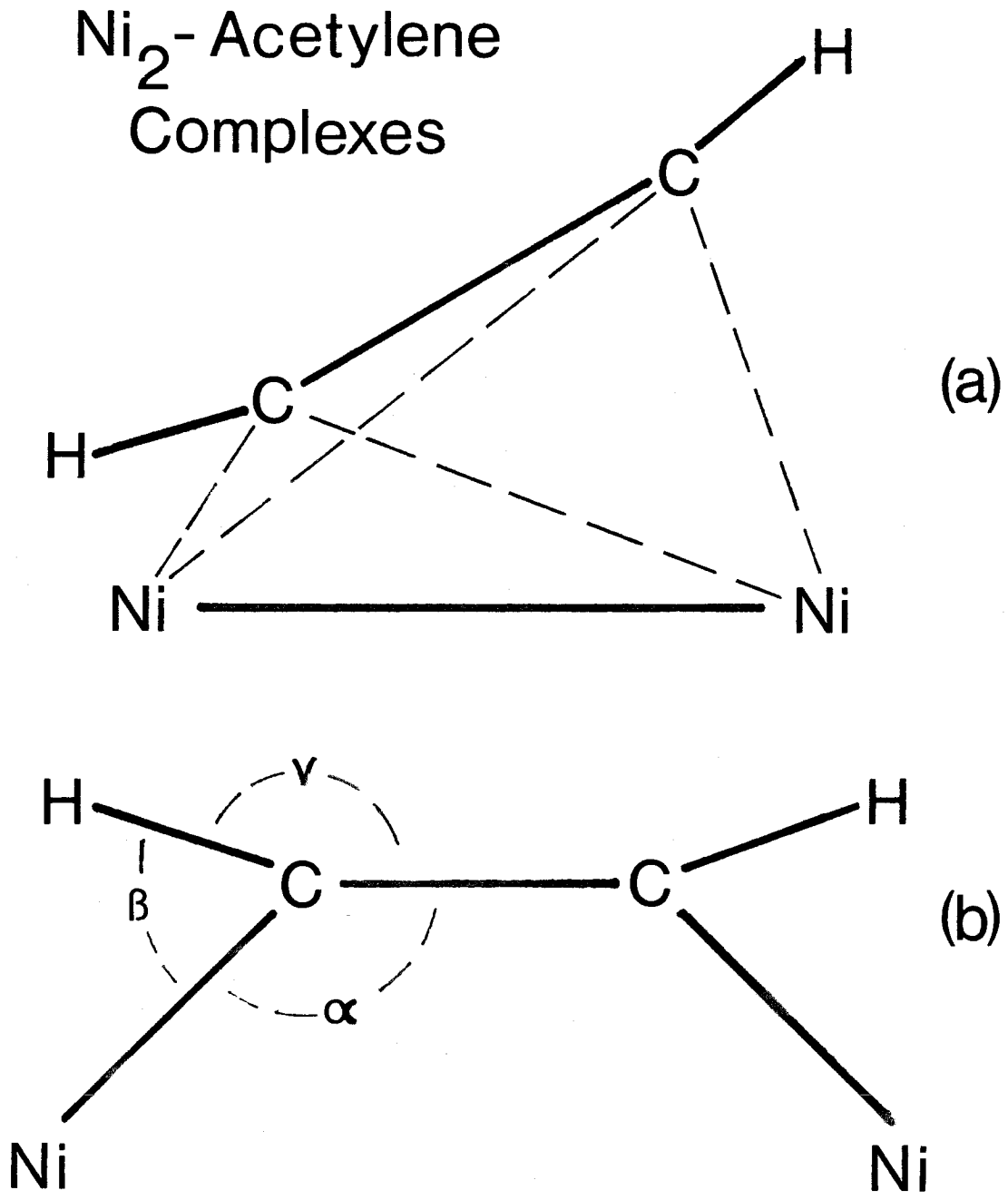

Figure 1: a) di-π complex; b) di-σ complex.

In this Appendix we present a brief discussion of the qualitative and quantitative aspects of the bonding in these complexes. A detailed discussion of their relevance as models for acetylene chemisorption on bulk nickel surfaces is presented in Section I.C of this thesis.

II. Qualitative Discussion

A. The $Ni_2(C_2H_2)$ di-π Complex

The attractiveness of π coordination as the predicted form of bonding for acetylene on a transition metal surface, lies in the fact that relatively strong bonds might be formed without activation energy. No bonds must be broken, rather the strength of the bonds depends on charge polarizability. Formally, the mode of bonding might be described as physisorption, were the possibility of strong bond formation (>15 kcal) less significant.

While the $Ni(C_2H_2)$ complex allows a single π-coordination bond (of ~ 17 kcal),[1] there is nothing inherent in the form of the bonding that would preclude the formation of two such bonds to adjacent atoms on a low index bulk nickel surface. To consider this possibility, the Ni atoms in Fig. 1a were fixed at the bulk nearest neighbor separation of 2.487 Å.[5] The acetylene molecule, for simplicity, was constrained to retain the minimally distorted geometry found to be optimum for the $Ni(C_2H_2)$ π-complex.[1] The distance between the Ni_2 and CC axes, was optimized in the calculation.

In this configuration, the lowest state is one in which the 4s orbital on each Ni atom is directed away from the acetylene π orbital directed towards it. Each individual π bond is very similar to that

found for $Ni(C_2H_2)$: the polarization of the 4s orbital allows each π bond to delocalize slightly onto the nearest Ni atom, into the empty 4s orbital. The 3d orbitals are atomic in shape and there is little evidence of interaction between the 3d and π^* orbitals. The 3d orbitals were triplet coupled in all calculations.

To determine a bond energy, it becomes necessary to consider the spin coupling of the 4s orbitals. For the purposes of determining the strengths of the π coordination bonds in this situation, we take as a reference, the limit,

$$Ni_2(C_2H_2)\ \text{di-}\pi \rightarrow C_2H_2 + 2Ni \qquad (1)$$

that is, we wish to avoid including the effect of Ni-Ni bonding (or anti-bonding) in the π bond strengths. To do this, both singlet (net triplet molecule) and triplet (net quintet) couplings of the 4s orbitals were considered, producing the total energies shown in Table I. Adequate GVB-CI calculations were not possible for the quintet states (due to a six open shell restriction in the program used) and thus the GVB total energies were used to determine optimum geometries and to calculate total energies. Comparison of the GVB and GVB-CI total energies for the singlet 4s states indicates that this was not a serious restriction.

To exclude the effect of Ni-Ni interactions we make use of the simple expression:

$$\frac{\text{BOND ENERGY (SINGLET)}}{\text{REPULSION (TRIPLET)}} \approx \frac{1 - S^2}{1 + S^2}$$

Table I: Geometry Optimization for di-π $Ni_2C_2H_2$

R(⊥) Å	R(NiC) Å	4s Coupling	Total energies (a.u.)[b] GVB	GVB-RCI	GVB(corr.)[a]	bond energy (kcal)
1.48	2.03	triplet	-157.8809	-	-157.8869	20.1
1.69	2.18	"	-157.8830	-	-157.8911	22.7
1.90	2.35	"	-157.8773	-	-157.8888	21.3
1.48	2.03	singlet	-157.8909	-157.9124	-157.8869	20.1
1.69	2.18	"	-157.8965	-157.9192	-157.8911	22.7
1.90	2.35	"	-157.8964	-157.9198	-157.8888	21.3
			Optimum Values			
1.72	2.21	decoupled	-	-	-157.8912	22.8

[a] see text.

where S is the overlap between 4s orbitals. Using an average value for the three geometries of S = 0.45, leads to a singlet state that is $\frac{2}{3}$ as bonding as the triplet state is antibonding. With an average splitting of 0.4 eV between singlet and triplet states, this suggest that the total Ni-Ni bond energy (singlet couplnig) is $\sim$ 0.16 eV in this configuration, while the Ni-Ni repulsion in the triplet state is only 0.24 eV. Correcting each of the GVB energies to exclude these quantities leads to the bond energies shown in the Table. A bond energy of $\sim$ 11.5 kcal per bond is predicted. While very crude, this prediction is qualitatively in keeping with the fact that repulsions between the Ni-4s orbitals and the acetylene orbitals are sufficient to prevent the system from attaining the geometry that would be expected to produce the strongest acetylene π-coordination bonds (α = 90°, R(NiC) $\approx$ 2.01 Å). In any event, this simple model suggests that an acetylene molecule bound to a nickel surface through such an unactivated process would seek a multiply coordinated site. Migration across the surface should occur thermally (assuming the system is stable with respect to introduction of $\sim$ 0.02 eV thermal energy).

B. The $Ni_2(C_2H_2)$ di-σ Complex

Scission of the acetylene π bond required in forming a species such as that in Fig. 1b is presumably a process that involves some activation energy (typically $\geq$ 20 kcal for gas phase systems). Whether this factor is of real concern in assessing the importance of such bond-cleavage structures as possible intermediate or final states in acetylene chemisorption is presently unknown. Surprisingly small

activation energies have been noted for a number of bond breaking processes (e.g., CO(ads) → C(ads) + O(ads) at 400 K on Ni(100)),[6] suggesting that these concerns may be much less important on a metal surface.

For this complex, both nearest neighbor ($R(Ni_2)$ = 2.487 Å)[5] and second nearest neighbor (R = 3.517 Å) nickel atom separations were considered. In the second nearest neighbor calculations, the CC bond distance was first optimized using R(NiC) = 2.84 Å).[1] Choice of R(NiC) and R(CC) effectively determines angle α in Fig. 1b. The remaining angles β and γ were determined by beginning with values appropriate for ethylene ($\beta = 117.6^\circ$ and $\gamma = 121.2^\circ$)[7] and reducing them equally as required by each new α. The distance R(NiC) was subsequently optimized in the same manner. The geometric parameters and total energies for this series of calculations are reported Table II. These optimum R(NiC) and R(CC) values were used in calculations employing R(NiNi) = 2.487 Å. Since this Ni-Ni separation leads to significant bond angle distortions, the angle β was optimized here separately with results as shown in Table III.

In these calculations, the same limit (1) was chosen as a reference. This led directly to the bond energies listed in Tables II and III. Using a value of 71 kcal as an estimate of the π bond strength[8] in acetylene leads to estimates for the Ni-C bond strength of 65.4 kcal for the second neighbor $Ni_2(C_2H_2)$ complex (Table II) and 63.3 kcal for the strained nearest neighbor complex. These values may be compared with 60 kcal found for the σ bond in $NiCH_3$[9] or 65 kcal for $NiCH_2$[9] where a weak π bonding interaction is also present.

Table II: Geometry Optimization for $Ni_2C_2H_2$ di-σ with $R(Ni_2) = 3.52$ Å

R(CC) Å	R(NiC) Å	α°	β°	γ°	Total energies (a.u.) GVB (3/6)	GVB-RCI[a]	bond energy (kcal)
1.29	1.84	127.3	114.5	118.2	-157.9522	-157.9617	56.1
1.34	1.84	126.3	115.0	118.7	-157.9575	-157.9668	59.3
1.39	1.84	125.3	115.5	119.2	-157.9564	-157.9656	58.5
1.35	1.87	125.3	115.5	119.2	-157.9580	-157.9675	59.8
1.35	1.90	124.7	115.9	119.4	-157.9573	-157.9668	59.3
			Optimum Values				
1.35	1.87	125.3	115.5	119.2	-	-157.9676	59.8

[a] $E(2Ni + C_2H_2(GVB(2)4)RCI)) = -157.8722$ a.u.

Table III: Geometry Optimization for $Ni_2C_2H_2$ di-σ with R(Ni_2) = 2.49 Å

R(CC)	R(NiC)	α°	β°	γ°	Total energies (a.u.) GVB(3/6)	GVB-RCI	bond energy (kcal)
1.35	1.87	107.7	152.3	100°	-157.9090	-157.9219	31.1
1.35	1.87	107.7	132.2	120°	-157.9471	-157.9598	54.9
1.35	1.87	107.7	112.3	140°	-157.9319	-157.9442	45.1
				Optimum values			
1.35	1.87	107.7	128.1	124.2	-	-157.9610	55.6

The bonding description that arises for this system is relatively simple. As expected, most of the acetylene orbitals retain their molecular character. The NiC σ orbitals are highly diffuse, and polarized towards the carbon atoms (Mulliken populations indicate a "charge" on each carbon of -0.4). The most noticeable effect of this charge distribution is on the remaining π orbital which becomes considerably more diffuse than the analogous ethylene orbital. Each of the Ni 3d orbitals remains highly localized and participates to only a minor extent in both σ and π bonding.

III. Summary

Results of GVB and GVB-CI calculations are presented that indicate:

1) acetylene is capable of forming two π coordination bonds to adjacent Ni atoms on the metal surface. For the simple $Ni_2(C_2H_2)$ complex considered each bond has a strength of ~ 11.5 kcal, less than the ~ 17 kcal found for one such bond in $Ni(C_2H_2)$.

2) in breaking one π bond, sigma bonds may be formed to adjacent surface Ni atoms (nearest neighbor or second neighbor) with a strength of ~ 65 kcal. These bond energies compare favorably with those found previously for other model Ni complexes.

References and Notes

1. T. H. Upton and W. A. Goddard III, J. Am. Chem. Soc., 100, 321 (1978); see also Part I.A of this thesis.
2. G. A. Ozin and W. Power, to be published.
3. H. Huber, G. Ozin, W. Power, J. Am. Chem. Soc., 98, 6508 (1976).
4. a) P. Kasai, D. McLeod Jr., and T. Watanabe, J. Am. Chem. Soc., 102, 179 (1980); b) P. Kasai and D. McLeod Jr., J. Am. Chem. Soc., 100, 625 (1978); c) H. Huber, D. McIntosh and G. Ozin, J. Organomet. Chem., 112, C50 (1976).
5. W. P. Pearson, "Handbook of Lattice Spacings and Structures of Metals and Alloys," (Pergamon, New York, 1958).
6. M. Araki and V. Ponec, J. Catal., 44, 439 (1976).
7. M. Harmony, V. Laurie, R. Kuczkowski, R. Schwendeman, D. Ramsey, F. Lovas, W. Lafferty, A. Maki, J. Phys. Chem. Ref. Data, 8, 619 (1979).
8. S. Benson, "Thermochemical Kinetics" (John-Wiley, New York, 1976).
9. W. A. Goddard III, S. P. Walch, A. K. Rappé, and T. H. Upton, J. Vac. Sci. Technol., 14, 416 (1977).

Part Two

Electronic Properties of Large Nickel Clusters and Their Relevance as Models for the Bulk Metal

A. The Nickel Dimer

I. Introduction

The diatomic molecules formed of the first row-transition metal elements represent a potential source of information relevant to the study of organometallic complexes, surface chemistry and solid-state physics. As they represent the smallest complexes for which metal-metal interactions may be studied, they are an appropriate starting point for a detailed study of metal cluster properties and their relationship to the bulk material.

Unfortunately, isolation of the dimers is quite difficult in a ligand-free environment. Experimental characterization to date has not been without ambiguities and has been primarily a result of high temperature mass spectroscopy,[1,2] and matrix isolation studies.[3]

Until recently, high quality theoretical studies of these molecules were not feasible. With the development of sound effective potential techniques the size of the problem has been greatly reduced. As a first step towards calculations on larger clusters of Ni atoms, we have carried out a study of the bonding in Ni_2 and Ni_2^+. In this paper we report the results of extensive generalized valence bond (GVB) and configuration interaction (CI) calculations on the lower states of these two molecules. In Section II we present a basic qualitative description of the bonding of Ni_2 followed by a more thorough discussion of the details. In Section III a similar treatment is given for Ni_2^+. Section IV describes the methods used, and in the final section (V) we relate our results to the known experimental data and discuss the implications on studies of larger clusters.

II. The Ni_2 Molecule

A. Qualitative Description. In this section we will develop a qualitative description of the states of Ni_2 by starting with the separated Ni atoms. The ground state of the Ni atom is $^3F_4$ corresponding to a configuration [4]

$$[Ar]\, 4s^2 3d^8 ,$$

while the first excited state (0.03 eV above $^3F_4$) is the $^3D_3$ corresponding to a configuration of

$$[Ar]\, 4s^1 3d^9 .$$

On the other hand, averaging the J components of each state (corresponding approximately to ignoring spin-orbit coupling), the ground state is $^3D(s^1 d^9)$ while the $^3F(s^2 d^8)$ state is only 0.03 eV higher.

Consider now bringing together two Ni atoms in the $s^2 d^8 (^3F)$ state. The size of a 4s orbital is about twice that of a 3d orbital. This indicates that the interactions of two Ni atoms will be dominated by the 4s orbitals on each center. As a result, two $s^2 d^8$ atoms will interact in a repulsive manner as they approach one another (analogous to He_2 or Be_2). Two $s^1 d^9$ (^3D) atoms, however, each have half filled 4s orbitals and can interact in a bonding manner as the orbitals begin to overlap (much as in H_2). Similarly, an $s^2 d^8$ Ni atom coupled with an $s^1 d^9$ Ni will lead to a total of three electrons in the 4s shell and would not be expected to bond as strongly as in the $s^1 d^9 - s^1 d^9$ case. The basic picture then for the lower Ni_2 states will be of a single 4s bond, analogous to the alkali metals on H_2. This leaves a single uncoupled 3d electron on each center, leading to a possibility of $(5 \times 2 \times 5 \times 2) = 100$ states, depending on their spin coupling (75 triplets and 25 singlets) and orbital

occupation. We will use a particle-hole notation in referring to the various states, where $\delta\delta$, $\pi\pi$, $\delta\pi$, etc., define the specific holes in the 3d shell of each atom. In all cases for Ni_2, a 4s-4s σ bond is understood.

The spectrum of states that results for Ni_2 is shown qualitatively in Figure 1. The states may be grouped, as shown, by their hole designations. In terms of the coupling of two Ni atoms, the trends shown here imply that a δ hole is energetically most favorable, with π and σ holes significantly less so. This contradicts the ordering that is obtained by the application of simple ligand field or crystal field arguments (i.e., the splitting resulting from overlapping filled ligand orbitals). As discussed in Appendix II.A.1, the origin for this ordering of states may be found in the configuration mixing that occurs upon hybridizing the 4sσ bond. In hybridizing this orbital to form the bond, each $4s^13d^9$ Ni mixes a component of $4s^23d^8$ Ni. The 3d occupation on the s^1d^9 Ni determines which components of s^2d^8 will be used. A ^3D Ni with a δ hole will mix in a low-lying s^2d^8 configuration with $\delta\sigma$ holes. A π hole in the ^3D atom forces the mixing of a higher $\pi\sigma$ hole s^2d^8 atom, while a σ hole in the ^3D forces mixing of very high-lying $\sigma\sigma$ hole s^2d^8 components. As a first approximation, these interactions are responsible for the ordering shown in Figure 1. The σ bond pairs for the $\sigma\sigma$, $\delta\delta$, and $\pi\pi$ states of Ni_2 are shown in Figure 2 (along with a 4s atomic orbital for reference). The $\delta\delta$ hole state may be seen to have much greater $3d_{z^2}$ character in its 4s pair than either the $\pi\pi$ or $\sigma\sigma$ states. This mixing is the only essential difference between these states and seems to be responsible for the slightly stronger bond in the $\delta\delta$ hole states. We will consider each of the possible hole combinations more carefully below.

B. Detailed Discussion of d-d Interactions.

1. Sigma-Sigma States. The sigma-sigma states have a singly-occupied d_σ orbital on each Ni. These can be coupled into singlet and triplet states,

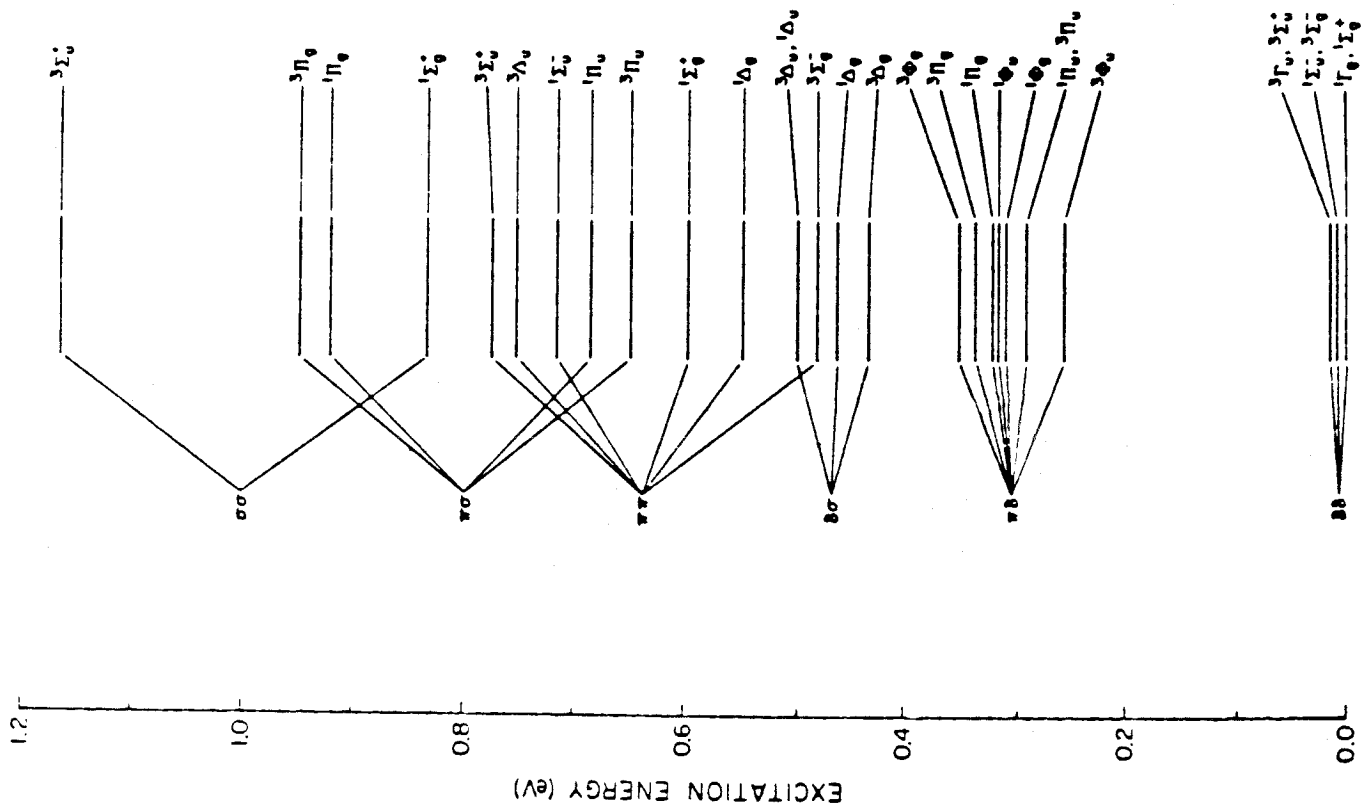

Figure 1. States of Ni_2 arising from possible occupations allowing a 3d hole on each center. 4s-4s bond exists for all states.

$^1\Sigma_g^+$ and $^3\Sigma_u^+$. Ignoring the 4s-4s bond (which is common to both states), $^1\Sigma_g^+$ can be considered as having a 3dσ-3dσ bond while $^3\Sigma_u^+$ has a 3dσ-3dσ antibond. Thus these states are analogous to the corresponding 1s-1s states of H_2. The difference is that at R_e for H_2 the 1s-1s overlap is ~0.8 leading to a $^3\Sigma_u^+$-$^1\Sigma_g^+$ separation of 10 eV, while for Ni_2 the dσ-dσ overlap is ~0.07 leading to a $^3\Sigma_u^+$-$^1\Sigma_g^+$ separation of 0.33 eV (at 3.8 a_0). Thus, although the $^1\Sigma_g^+$ state of Ni_2 can be formally represented as

$$Ni{=}Ni$$

with 4s-4s and 3dσ-3dσ bonds, the 3dσ-3dσ overlap is too small for a real bond. The $3d_{z^2}$ and 4s overlaps for the $^1\Sigma_g^+$ state are plotted as a function of bond length in Figure 3. For comparison, the overlaps of atomic orbitals are shown as well.

2. Delta-Delta States. States of this type will have doubly-occupied $3d_\sigma$ orbitals on each Ni. An examination of Figure 4, where potential curves for δδ and σσ states are shown, indicates that the effect of these extra electrons is to increase slightly the bond length as well as to increase the harmonic force constant for the δδ ($^1\Sigma_g^+$) state. These changes are a result of the fact that any overlap of the $3d_{z^2}$ orbitals now leads to repulsive interactions between the two centers. Unlike the σσ hole states, there is a number of states arising from δδ holes, differing only in the manner that the singly-occupied δ orbitals are coupled. Looking only at the δ orbitals, a single Ni atom will be depicted as

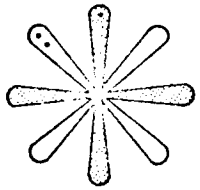

(1)

where the set of shaded lobes represent one of the deltas (δ_1 or $\delta_{x^2-y^2}$) and

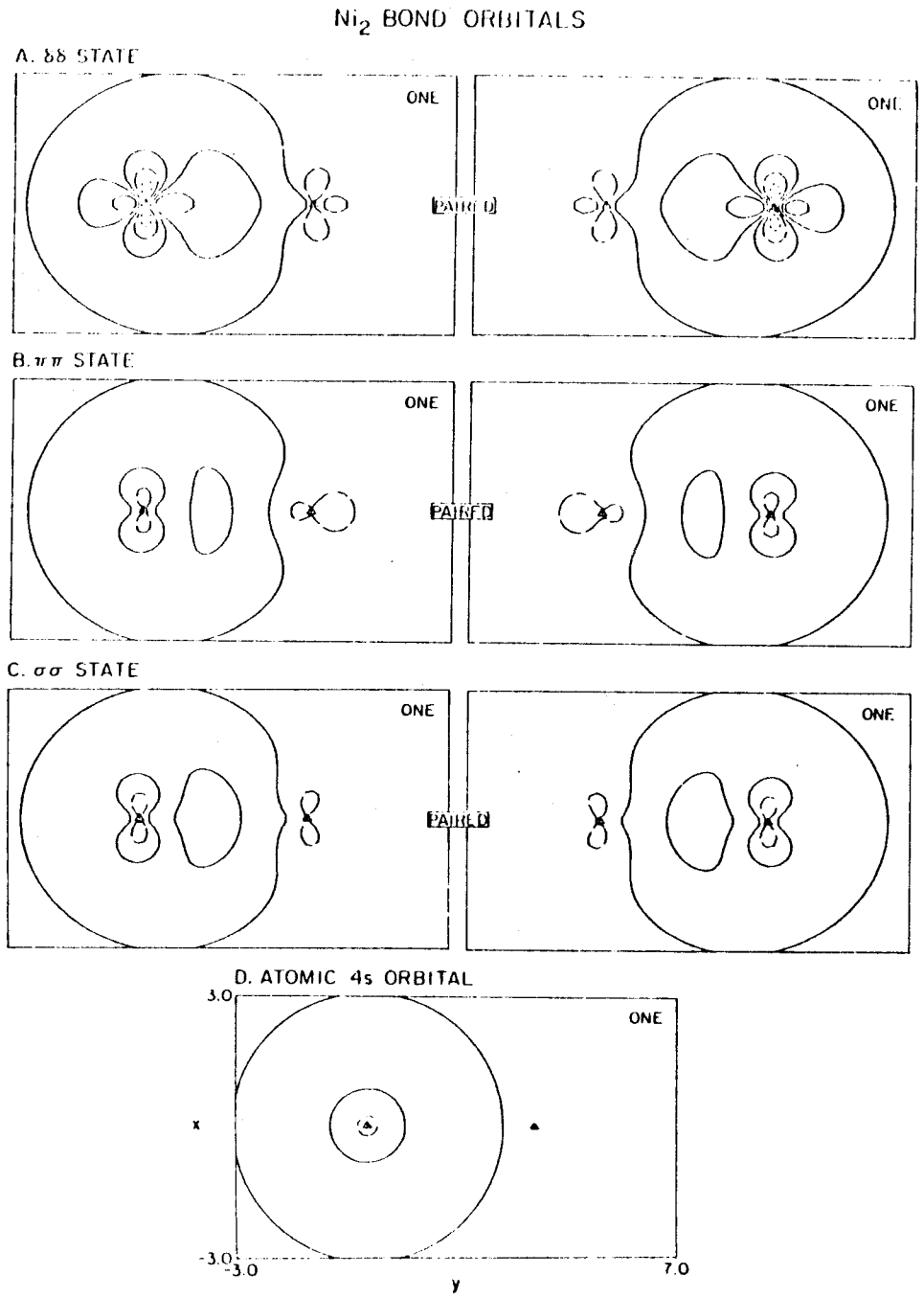

Figure 2. The bond orbitals for several states of Ni_2. Note the hybridization and polarization of the orbital for the δδ state. The atomic 4s orbital is shown for reference.

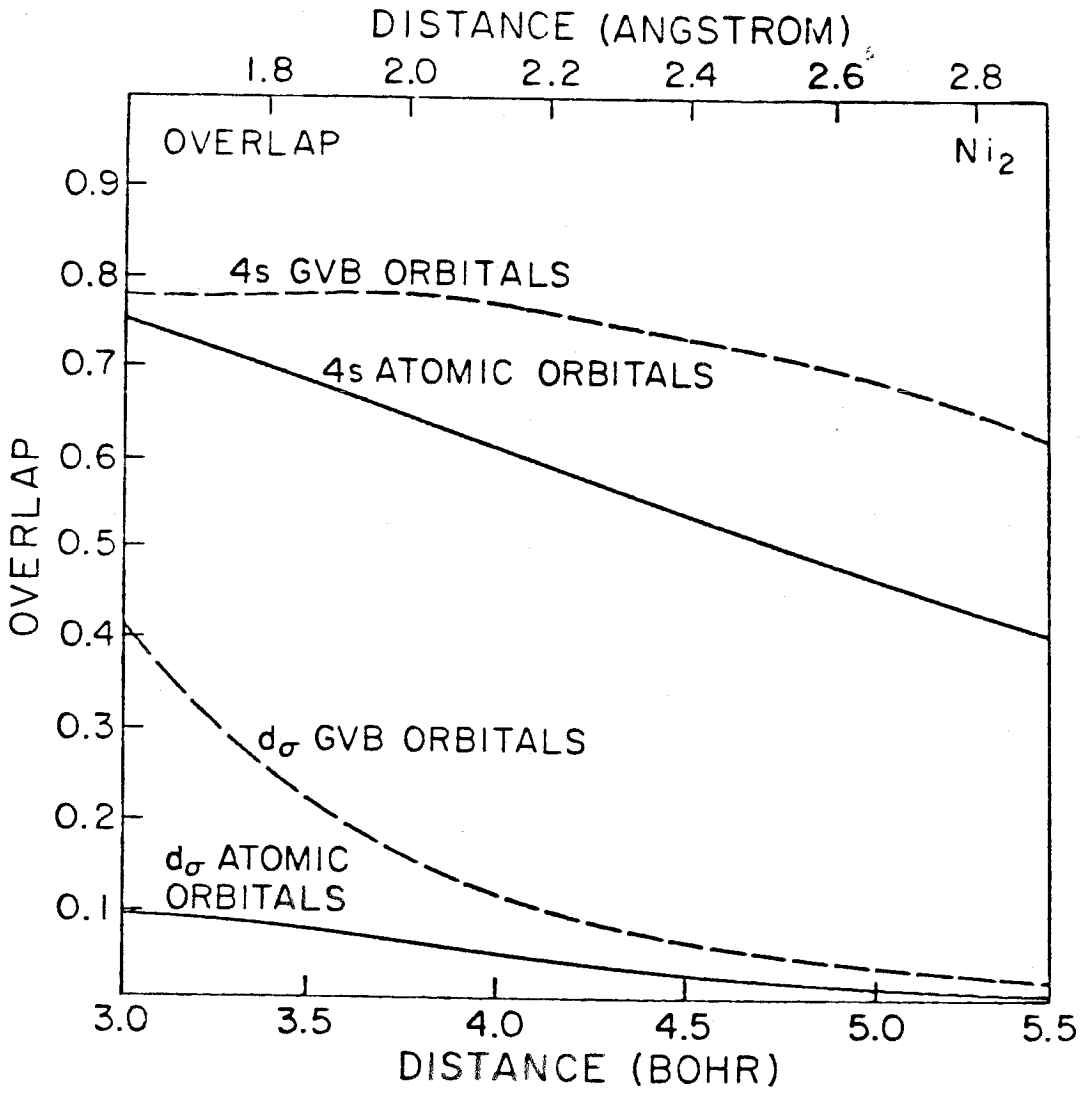

Figure 3. Overlap of 4s and $3d_{z^2}$ atomic orbitals as a function of R. Also shown are the overlaps from GVB calculations on the $^1\Sigma_g^+$ state.

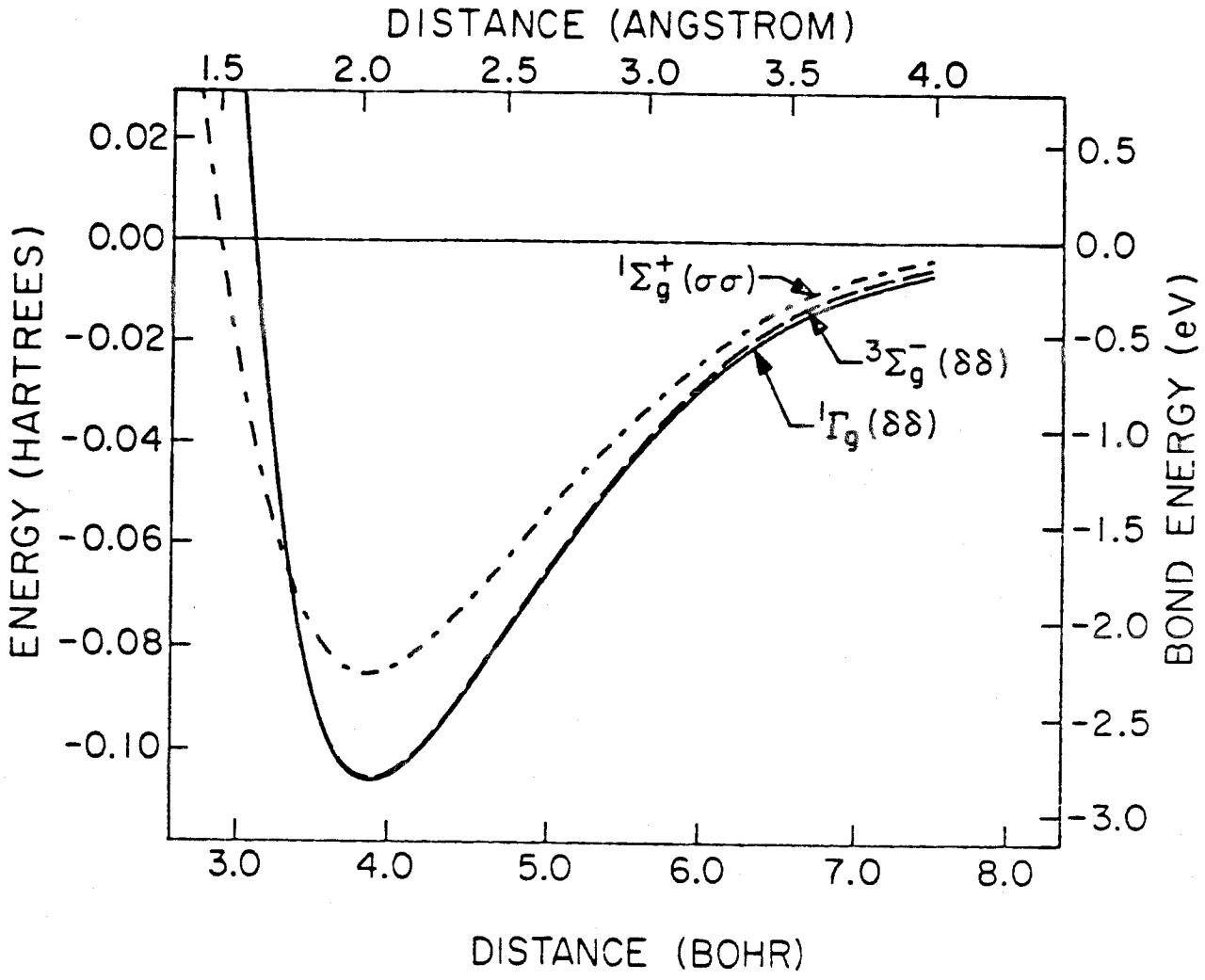

Figure 4. Potential curves for several states of Ni_2 (from POL-CI calculations).

the unshaded lobes the other delta (δ_2 or δ_{xy}). Thus defined, the possible ways in which two Ni atoms may be coupled are shown below where the dots indicate how many electrons are in each orbital:

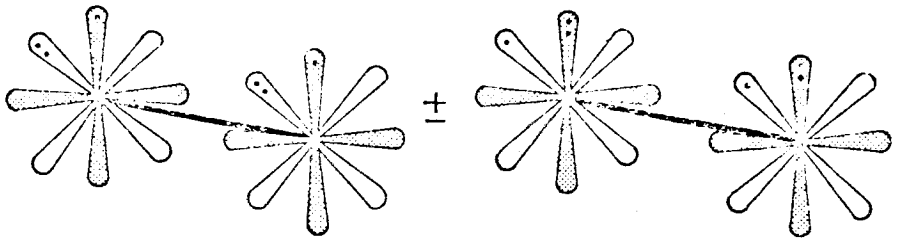

(2a)

(2b)

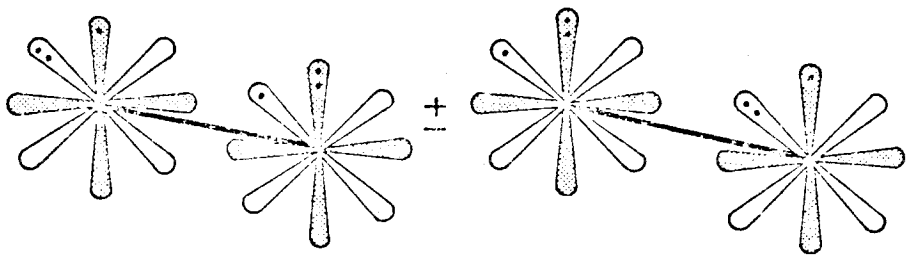

(3a)

(3b)

The four δδ configurations have been grouped so as to indicate the resonant and anti-resonant combinations. The symmetries resulting from these combinations are:

$^3\Sigma_u^+$, $^1\Sigma_g^+$	(+ sign)	(2a)
$^3\Gamma_u^+$, $^1\Gamma_g^+$	(-sign)	(2b)
$^3\Sigma_g^-$, $^1\Gamma_g^-$	(+ sign)	(3a)
$^3\Gamma_u^-$, $^1\Sigma_u^-$	(- sign)	(3b)

For (2a) and (2b), two singly-occupied orbitals can singlet couple to form a weak delta bond, the singlet necessarily lower than the triplet. For (3a) and (3b) the singly-occupied orbitals are orthogonal. With either configuration alone, the triplet would be expected to be lower by twice the exchange integral:

$$(\delta_{1\ell}\,\delta_{2r}|\delta_{2r}\,\delta_{1\ell})\,.$$

For the bond lengths of interest in Ni_2, this exchange integral is very small, ranging from 6.6×10^{-5} h at 3.0 bohr to 3×10^{-6} h at 7.5 bohr. For such a small exchange integral, the two spin states are expected to be essentially degenerate throughout the bonding region of the potential curve. When varying the bond length through distances ranging from R_e to very large R, as has been done here, it is not adequate to consider only one spin coupling. The correct wavefunction for the ground state must possess the capability of going to the separated atom limit to produce two ^{3}D Ni atoms, each with the 4s electron high-spin coupled to the $3d_\delta$ orbital. The overlap between the two δ orbitals is small enough that the coupling of the two triplets is determined almost completely by the 4s orbitals. At larger R this necessarily leads to the singlet being lower.

In order to compare (2) with (3), it is necessary to consider the doubly-occupied delta orbitals. For the configurations shown in (2), a weak δ_1 bond is formed, but there are doubly-occupied δ_2 orbitals on each center that lead to repulsive interactions. For the configurations in (3) a doubly-occupied orbital interacts with a singly-occupied orbital, allowing the doubly-occupied orbital to delocalize slightly on to the other center. The singly-occupied orbital must become orthogonal and takes on anti-bonding character. Orbitals optimized to describe one of the configurations in (3) with singlet-coupled delta orbitals are shown in Figure 5. [Only the $\delta_{x^2-y^2}$ orbitals are shown, the δ_{xy} orbitals being equivalent to these.] Here it can be seen that the delocalization of the doubly-occupied delta is so slight that the only indication of its occurrence is the node built in by the singly-occupied orbital for orthogonality. The net bonding interaction here, however small, should

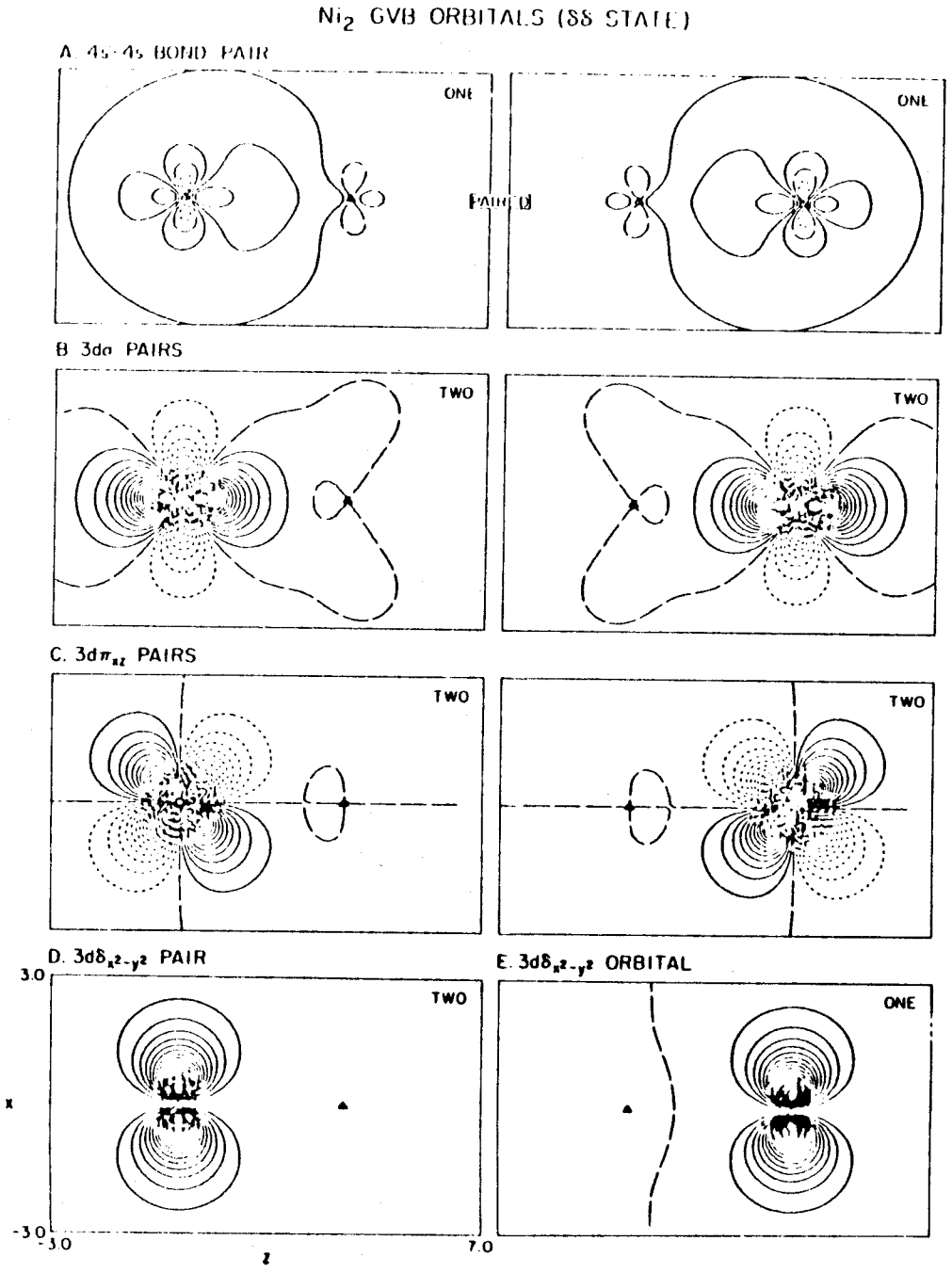

Figure 5. Contour plots of Ni_2 orbitals obtained from GVB calculations corresponding to one of the configurations in (3). The $3d\pi_{yz}$ and $3d\delta_{xy}$ orbitals are omitted.

be more important than bonding occurring in (2), leading to (3) being slightly lower than (2). It is unlikely that these effects will be large. As a result, the splitting of states similar to (2) and (3) remains very small, with singlets in each case being slightly lower than the triplets. Resonance stabilization of (2) or (3) is virtually nonexistent.

B. Intermediate States. A similar type of analysis may be applied to those states occurring intermediate in energy to the $\delta\delta$ and $\sigma\sigma$ states. As in the $\delta\delta$ case, all of the states in this region may be taken as resonant and anti-resonant combinations of equivalent VB configurations (which themselves do not possess full molecular symmetry).

There are eight states with $\pi\pi$ holes that are completely analogous to (2) and (3). Here again, a doubly-occupied $3d_\pi$ orbital may overlap a singly-occupied orbital on the opposite center as in (3) for the $\delta\delta$ case, and this type of state is expected to be the lowest in energy. Using the notation of (2) and (3), where now the orbitals are $3d_\pi$ (but with the same resonance combinations), the resulting states are

$$^3\Sigma_u^+ \quad , \quad ^1\Sigma_g^+ \qquad (+ \text{ sign}) \qquad (2a')$$

$$^3\Delta_u^+ \quad , \quad ^1\Delta_g^+ \qquad (- \text{ sign}) \qquad (2b')$$

$$^3\Sigma_g^- \quad , \quad ^1\Delta_g^- \qquad (+ \text{ sign}) \qquad (3a')$$

$$^3\Delta_u^- \quad , \quad ^1\Sigma_u^- \qquad (- \text{ sign}) \; . \qquad (3b')$$

The overlap of the π orbitals on each center is not as small as in the $\delta\delta$ case. This leads to a noticeable resonance stabilization energy whose effect may be seen by examining Figure 1. There is a much greater separation between $\pi\pi$ resonant and anti-resonant states (e.g., $^1\Delta_g$ and $^1\Sigma_u^-$ or $^1\Delta_g$ and $^1\Sigma_g^+$) than there is between analogous $\delta\delta$ hole states. The exchange integral

$$(\pi_{xz\ell}\pi_{yzr}|\pi_{yzr}\pi_{xz\ell})$$

is no longer insignificant (it is 0.002 h = 0.05 eV) at R_e, causing $^3\Sigma_g^-$ to drop below the $^1\Delta_g$, in opposition to what occurs for the $\delta\delta$ hole states.

The $\pi\delta$ states present a slightly different problem. Here there are eight equivalent VB configurations which may be denoted as (singly occupied orbitals only)

$$\delta_{1\ell}\pi_{xzr},\ \delta_{1\ell}\pi_{yzr},\ \delta_{2\ell}\pi_{xzr},\ \delta_{2\ell}\pi_{yzr}$$

$$\delta_{1r}\pi_{xz\ell},\ \delta_{1r}\pi_{yz\ell},\ \delta_{2r}\pi_{xz\ell},\ \delta_{2r}\pi_{yz\ell}\ ,$$

where subscripts ℓ and r refer to left and right, and each term represents an antisymmetrized pair. Due to the equivalence of π_{xz} and π_{yz} holes, as well as δ_1 and δ_2 holes, proper resonance is obtained only upon combination of four of these configurations as follows:[6]

$$\mathcal{A}[(\delta_{1\ell}\pi_{xzr}+\delta_{1r}\pi_{xz\ell})\pm(\delta_{2\ell}\pi_{yzr}+\delta_{2r}\pi_{yz\ell})] \quad \begin{cases} {}^{3,1}\Pi_g^+ \text{ (+ sign)} & (4a) \\ {}^{3,1}\Phi_g^+ \text{ (- sign)} & (4b) \end{cases}$$

$$\mathcal{A}[(\delta_{1\ell}\pi_{xzr}-\delta_{1r}\pi_{xz\ell})\pm(\delta_{2\ell}\pi_{yzr}-\delta_{2r}\pi_{yz\ell})] \quad \begin{cases} {}^{3,1}\Pi_u^+ \text{ (+ sign)} & (5a) \\ {}^{3,1}\Phi_u^+ \text{ (- sign)} & (5b) \end{cases}$$

$$\mathcal{A}[(\delta_{1\ell}\pi_{yzr}+\delta_{1r}\pi_{yz\ell})\pm(\delta_{2\ell}\pi_{xzr}+\delta_{2r}\pi_{xz\ell})] \quad \begin{cases} {}^{3,1}\Phi_g^- \text{ (+ sign)} & (6a) \\ {}^{3,1}\Pi_g^- \text{ (- sign)} & (6b) \end{cases}$$

$$\mathcal{A}[(\delta_{1\ell}\pi_{yzr}-\delta_{1r}\pi_{yz\ell})\pm(\delta_{2\ell}\pi_{xzr}-\delta_{2r}\pi_{xz\ell})] \quad \begin{cases} {}^{3,1}\Phi_u^- \text{ (+ sign)} & (7a) \\ {}^{3,1}\Pi_u^- \text{ (- sign)} \ . & (7b) \end{cases}$$

This leads to eight covalent states for singlet and triplet, which may be viewed as having two types of resonance occurring simultaneously. For

both singlets and triplets, the stabilization resulting from left-right resonance (terms in parentheses, e.g., $\delta_{1\ell}\pi_{xzr} \pm \delta_{1r}\pi_{xz\ell}$) is more important than resonance between orbitals on the same centers (between pairs of parentheses, e.g., $\delta_{1\ell}\pi_{xzr} \pm \delta_{2\ell}\pi_{yzr}$). This can be seen by examination of Figure 1.

Finally, there are $\delta\sigma$ and $\pi\sigma$ hole states. As expected, all of the $\delta\sigma$ states lie beneath the $\pi\sigma$ states in energy. There are four covalent Δ states with $\delta\sigma$ holes that separate in energy roughly into two pairs. These pairs consist of resonant ($^{1,3}\Delta_g$) and anti-resonant ($^{1,3}\Delta_u$) combinations of form

$$\mathcal{A}(\delta_\ell \sigma_r \pm \sigma_\ell \delta_r) \ . \tag{8}$$

The splitting energy is about 0.05 eV and is due to the overlap of σ orbitals in the resonance configurations. Similar states are obtained for $\pi\sigma$ holes. The overlap between π orbitals is that of the delta orbitals at R_e; thus the split between resonant ($^{1,3}\Pi_u$) and antiresonant ($^{1,3}\Pi_g$) states is about 0.25 eV here.

III. The Ni_2^+ Ion

A. Qualitative Description. As in the case of neutral Ni_2, we will begin by first examining the possible couplings at very long R. The ground state for the ion is ^2D with configuration $4s^0\ 3d^9$ which lies 7.62 eV above the ground state of Ni.[4] The first excited state for Ni^+ is ^4F which is 1.08 eV above the ^2D state and has the configuration $4s^1\ 3d^8$. The separated atom limit for Ni_2^+ is expected to be one of the following couplings (Ni - Ni^+)

^3D-^2D	^3F-^2D	^3D-^4F	^3F-^4F
(s^1d^9-s^0d^9)	(s^2d^8-s^0d^9)	(s^1d^9-s^1d^8)	(s^2d^8-s^1d^9)
0.0 eV	0.03 eV	1.08 eV	1.11 eV
($s^1d\sigma^4$)	($s^2d\sigma^3$)	($s^2d\sigma^3$)	($s^3d\sigma^2$) ,

where the sigma shell occupation is given in parentheses below the energy value (ionization is assumed to occur from the sigma shell[7]). The importance of a strong 4s bond in the lower states of Ni_2 has been demonstrated and the same reasoning should apply here. As is the case for Ni_2, s^2d^8-s^1d^9 coupling involving three 4s electrons should be less advantageous. The s^1d^9-s^0d^9 coupling leads to a one-electron 4s bond and is reasonably strong.

For example, the positive ion formed from each of the diatomic alkali metals involves essentially a one-electron ns bond, and each is more tightly bound than the corresponding neutral.[8] A similar ordering (bond energy ion > bond energy neutral) has been observed for each of the first-row transition metal diatomics.[2] This coupling, as well as the $s^2d\sigma^3$ couplings (which are found to lead to the ground state) will be examined in more detail.

B. Detailed Description of Bonding. In Figure 6, the spectrum of states for Ni_2^+ is shown for a bond length of 3.8 Bohr. Two sets of states are shown, corresponding to those having an $s^2d\sigma^n$ sigma shell (Figure 6a) and those that have an $s^1d\sigma^{n+1}$ sigma shell (Figure 6b). The preference for particular types of holes is exhibited in a similar manner as for Ni_2. The situation is somewhat complicated now as it is possible for the s^1 and s^2 states of the same symmetry to mix, leading to stabilized and destabilized mixtures. As an example we will consider the $\delta\delta$ hole states. For Ni_2 both $^3\Sigma_g^-$ and $^1\Sigma_u^-$ $\delta\delta$ states occur low in energy. Removing a 3d electron from the $^3\Sigma_g^-$ leads to possible $^{4,2}\Sigma_u^-$ s^2 states. Removing a 4s electron from the $^1\Sigma_u^-$ state produces a $^2\Sigma_u^-$ s^1 state. These $^2\Sigma_u^-$ states will mix, leading to the low-lying $\delta\delta$ state of this symmetry shown in Figure 6b. This mixing occurs very strongly in the Ni_2^+ states making it difficult in some cases to unambiguously assign them as s^1 or s^2. These

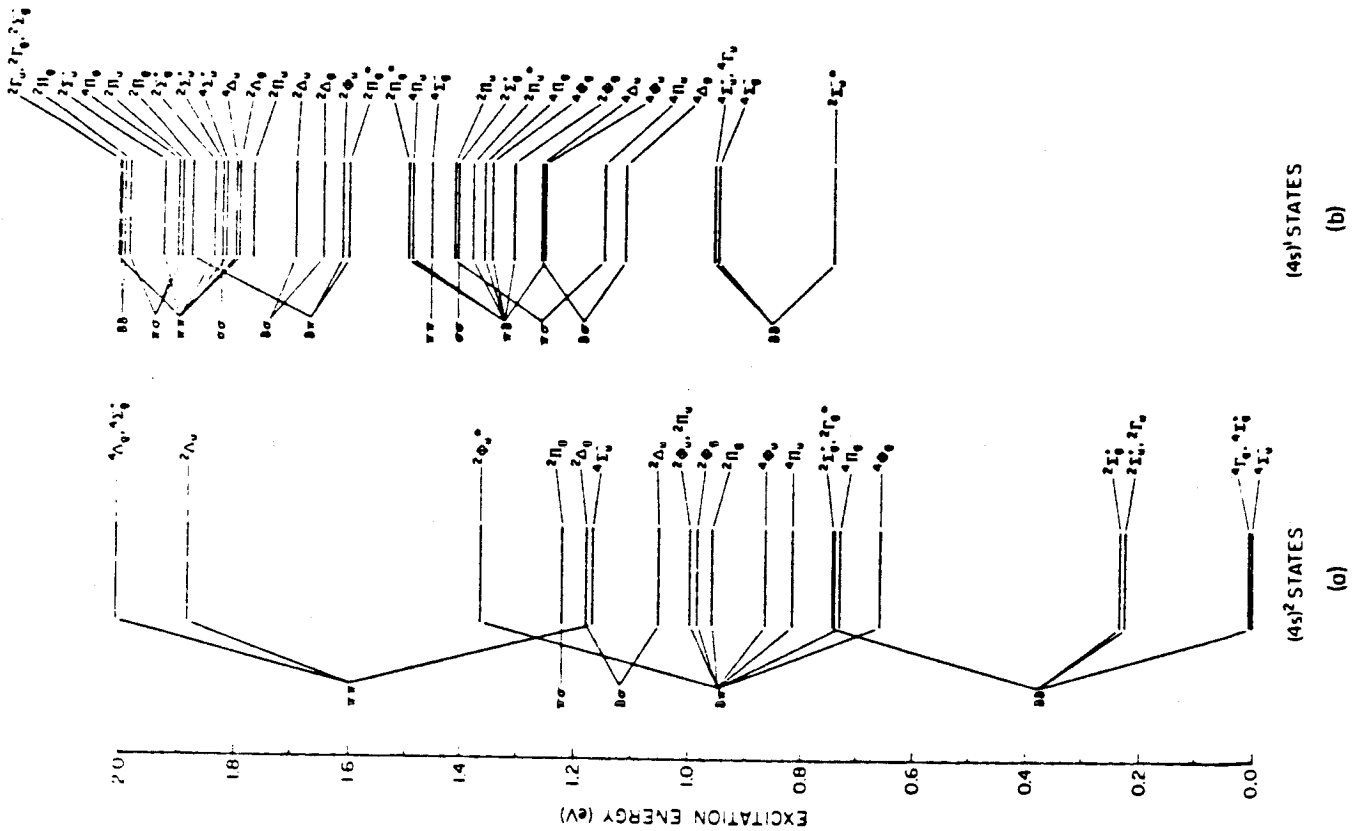

Figure 6. States of Ni_2^+ arising from possible location of 3d holes on each center. Ionization from 4s ($4s^1$) or 3dσ ($4s^2$) orbitals was allowed, giving rise to the two sets of states shown. Not all assignments are unambiguous; those shown with an asterisk are questionable.

states are marked with an asterisk in Figure 6. In still other cases it was not possible to assign even the occupation character, and these have been left unassigned in the figure.

A more notable difference that appears between Ni_2 and Ni_2^+ is that the low-spin coupling of the $\delta\delta$ holes does not lead to the ground state. The explanation for this lies in the two-electron energy terms. Evaluating the two-electron energy for the three-electron, three open-shell quartet (ignoring closed shells)

$$\varphi_1 = \mathcal{A}\{\delta_{1\ell}\,\delta_{2r}\,\sigma_\ell\,(\alpha\alpha\alpha)\} \tag{9}$$

leads to the two-electron terms

$$E_{\varphi_1} = J_{\delta_{1\ell}\delta_{2r}} - K_{\delta_{1\ell}\delta_{2r}} + J_{\delta_{1\ell}\sigma_\ell} - K_{\delta_{1\ell}\sigma_\ell} + J_{\delta_{2r}\sigma_\ell} - K_{\delta_{2r}\sigma_\ell},$$

where

$$J_{ij} = (ii|jj) \geq 0$$

$$K_{ij} = (ij|ij) \geq 0.$$

There are two doublets possible given by

$$\varphi_2 = \mathcal{A}\{\delta_{1\ell}\,\delta_{2r}\,\sigma_\ell\,(\alpha\beta - \beta\alpha)\alpha\} \tag{10}$$

$$\varphi_3 = \mathcal{A}\{\delta_{1\ell}\,\delta_{2r}\,\sigma_\ell\,(2\alpha\alpha\beta - \alpha\beta\alpha - \beta\alpha\alpha)\}\ . \tag{11}$$

These lead to the two-electron energies

$$E_{\varphi_2} = J_{\delta_{1\ell}\delta_{2r}} + K_{\delta_{1\ell}\delta_{2r}} + J_{\delta_{1\ell}\sigma_\ell} + J_{\delta_{2r}\sigma_\ell} - \tfrac{1}{2}(K_{\delta_{1\ell}\sigma_\ell} + K_{\delta_{2r}\sigma_\ell})$$

$$E_{\varphi_3} = J_{\delta_{1\ell}\delta_{2r}} - K_{\delta_{1\ell}\delta_{2r}} + J_{\delta_{1\ell}\sigma_\ell} + J_{\delta_{2r}\sigma_\ell} + \tfrac{1}{2}(K_{\delta_{1\ell}\sigma_\ell} + K_{\delta_{2r}\sigma_\ell}).$$

Combining,

$$E_{\varphi_1} - E_{\varphi_2} = -2K_{\delta_{1\ell}\delta_{2r}} - \tfrac{1}{2}(K_{\delta_{1\ell}\sigma_\ell} + K_{\delta_{2r}\sigma_\ell})$$

$$E_{\varphi_1} - E_{\varphi_3} = -\tfrac{3}{2}(K_{\delta_{1\ell}\sigma_\ell} + K_{\delta_{2r}\sigma_\ell}) .$$

It has been shown previously that $K_{\delta_{1\ell}\delta_{2r}}$ is very small; however, the remaining exchange integrals are not, and they are responsible for the observed preference for the high-spin coupling. The other effects observed, which lead to splittings of the various states (e.g., resonance, electron-electron repulsion, etc.) in Ni_2, apply identically to Ni_2^+.

From Figure 6, it can be seen that the preference for the $s^2 d\sigma^3$ sigma shell over the $s^1 d\sigma^4$ is not great; at R = 3.8 a.u., the $\delta\delta$ states resulting from each are separated by less than 1 eV. As is explained in more detail in Appendix I.A.2, the relative importance of either of these couplings is a function of bond length and is given by the approximate terms:

$$E_2^X = \frac{2S\tau}{1 + S^2} \qquad\qquad E_1^X = \frac{\tau}{1 + S} ,$$

where E_2^X and E_1^X represent the exchange effects responsible for bonding

in the two- and one-electron bonds, respectively. The quantity τ is the one-electron contribution

$$\tau = h_{\ell r} - \tfrac{1}{2} S(h_{\ell\ell} + h_{rr}) .$$

The point of such a partitioning of the energy terms is to make clear the dependence of the bonding energy on the degree of overlap between centers. When S is small, $E_1^X \ll E_2^X$, leading to $s^1 d\sigma^4$ states being lower than analogous $s^2 d\sigma^3$ states. However, as S increases with decreasing R, a crossing point is reached and the two-electron bond may become lower. These points may be seen more clearly by examining Figure 7. The $^2\Sigma_g^+$ and $^4\Sigma_g^-$ states shown are $s^1 d\sigma^2$ and $s^1 d\sigma^4$ states, respectively. The crossing occurs in the region of 5 bohr, and for all larger R, the $s^1 d\sigma^{n+1}$ states are lower in energy. For the same reasons, the minima for both $^2\Sigma_g^+$ and $^4\Sigma_g^-$ occur at longer bond lengths than the $^4\Sigma_u^-$ state.

There are other factors which may lead to an ever greater preference for the s^2d^3 states than is indicated above. There are two separate couplings of Ni and Ni^+, both of which lead to sigma occupation. By the non-crossing rule, the ground state must dissociate into the lowest of these, a s^2d^8 (^{3}F) Ni and a s^0d^9 (^{2}D) Ni^+. In Figure 8 the orbitals for a quartet $\delta\delta$ hole state are shown. Qualitatively, the shapes of the π and δ orbitals are very similar to those shown for the $\delta\delta$ singlet coupled state of Ni_2. The sigma shell has altered greatly due to the loss of the $3d_{z^2}$ electron. The doubly-occupied $3d_{z^2}$ has delocalized slightly onto the other center forcing the $3d_{z^2}$ orbital there to take on antibonding character to remain orthogonal. The 4s orbital on the left has shifted away from the doubly-occupied orbital. For the orbitals shown here, there is a net charge on the left of -0.34. Clearly this

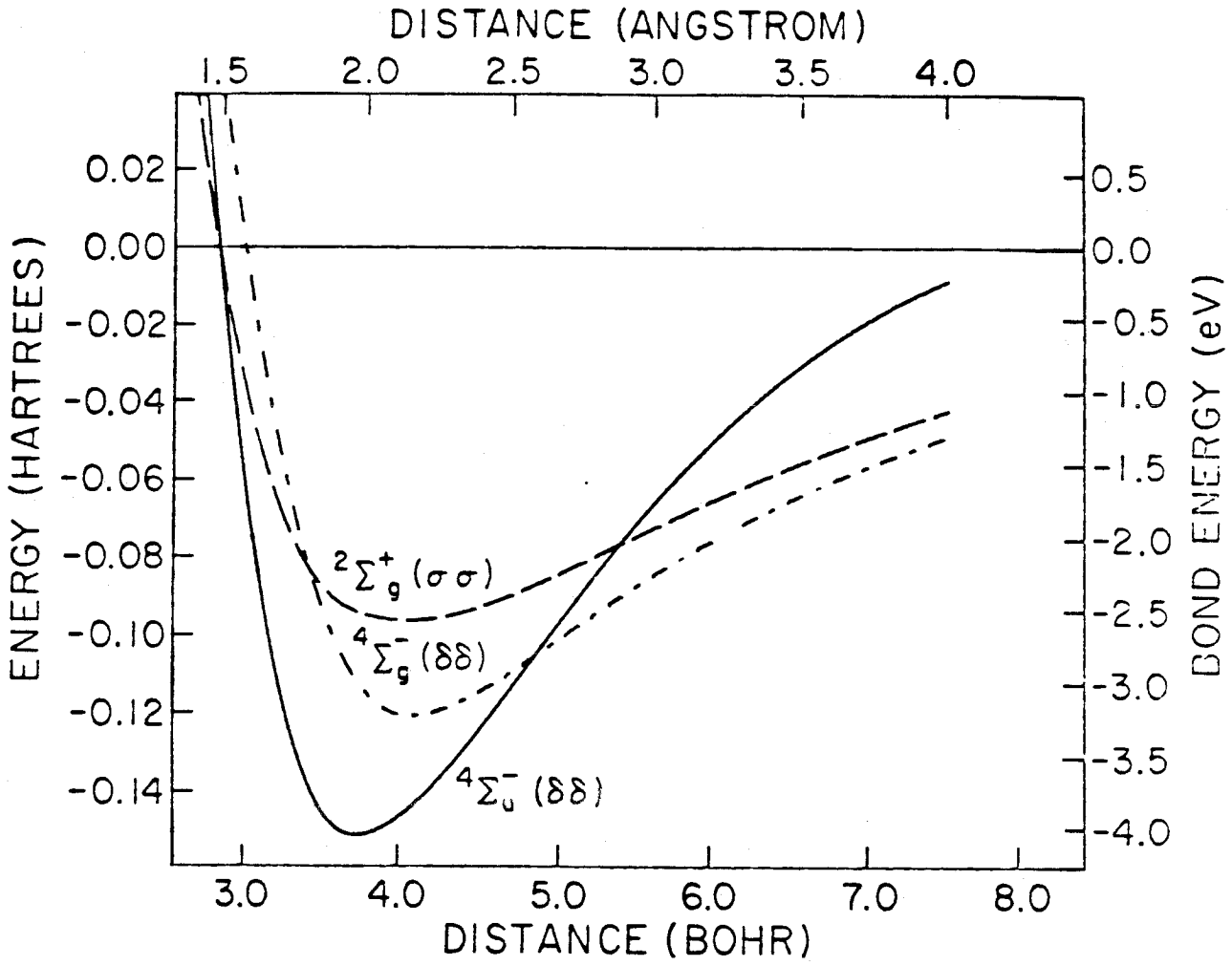

Figure 7. Potential energy curves for several low-lying states of Ni_2^+ (from POL-CI calculations). The two upper states have a $(4s)^1$ bond, while the lowest state has a $(4s)^2$ occupation.

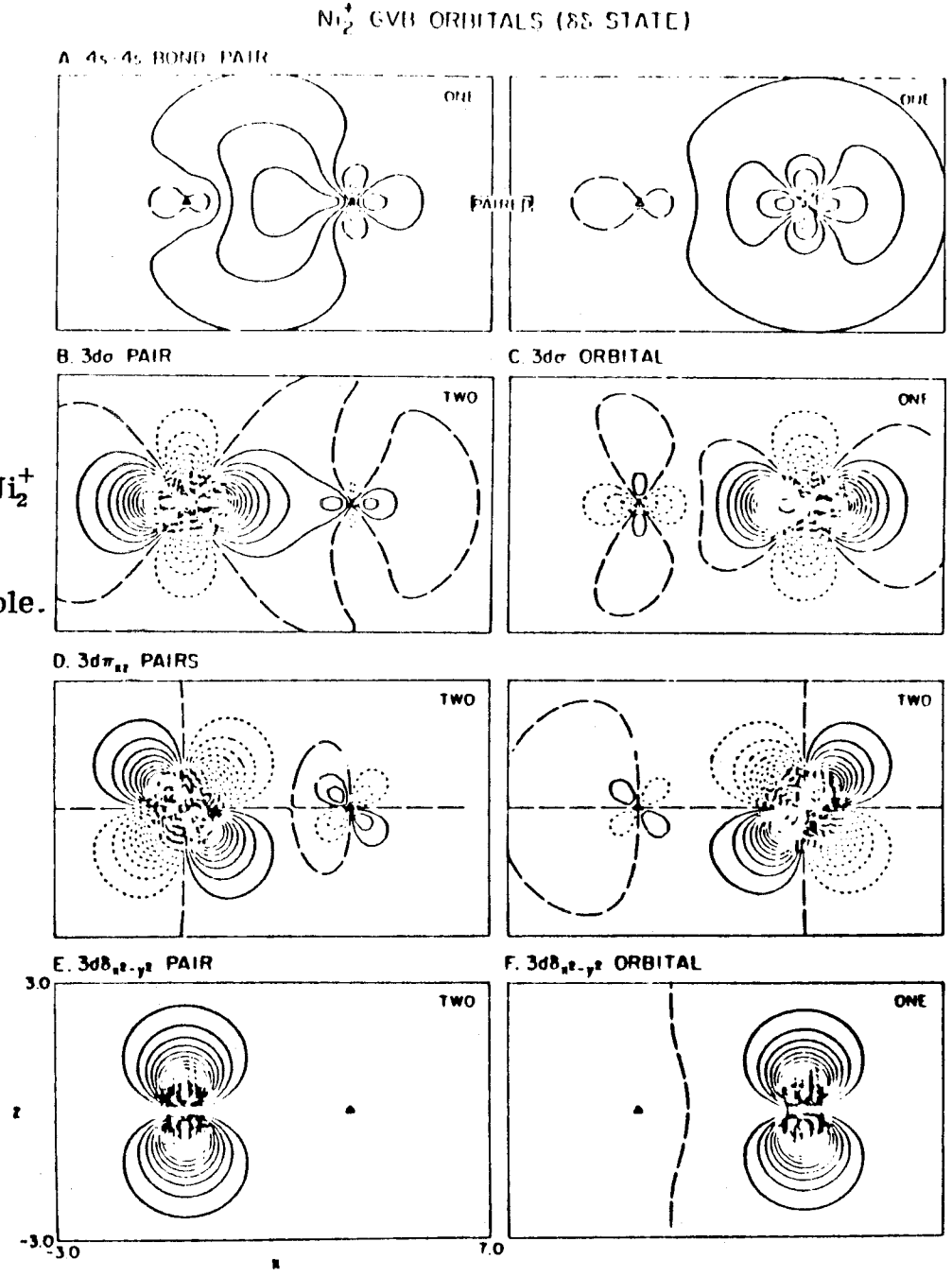

Figure 8. Contour plots of orbitals for Ni_2^+ obtained from GVB calculations for δ orbital occupation as in (3), and a 3dσ hole.

does not possess proper symmetry, and a rather complicated set of equivalent δ, $3d_\sigma$ and 4s resonance configurations are required in the actual wavefunction. There will be two ways to describe the sigma resonance corresponding to the $s^2d^8\,(^3F)$ - $s^0d^9\,(^2D)$ coupling (12) of Ni-Ni^+,

$$\mathcal{A}\{(\sigma^2_{\ell s} \pm \sigma^2_{rs})\,(\alpha\beta - \beta\alpha)\,(\sigma^2_{\ell d}\,\sigma_{rd} \pm \sigma^2_{rd}\,\sigma_\ell)\,(\alpha\beta - \beta\alpha)\,\alpha\}\,, \qquad (12)$$

or the $s^1d^9\,(^3D)$ - $s^1d^8\,(^4F)$ coupling of (13) Ni-Ni^+,

$$\mathcal{A}\{(\sigma_{\ell s}\,\sigma_{rs} + \sigma_{rs}\,\sigma_{\ell s})\,(\alpha\beta - \beta\alpha)\,(\sigma^2_{\ell d}\,\sigma_{rd} \pm \sigma^2_{rd}\,\sigma_{\ell d})\,(\alpha\beta - \beta\alpha)\,\alpha\}\,. \qquad (13)$$

The splitting in (12) will be large due to the 4s-4s overlap; however, (13) shows no 4s resonance and should not have such widely separated resonant and anti-resonant states. Careful examination of the 4s orbitals shown in Figure 8 indicates that the resonance there is not describable by either (12) or (13) above taken separately. The ground state wavefunction is a stabilized mixture of both of these wavefunctions. This favorable mixing, along with the loss of a $3d_\sigma$ electron, is probably the reason that $^4\Sigma_u^-$ Ni_2^+ is more strongly bound at a shorter R_e than $^4\Sigma_g^-$ Ni_2^+ or $^1\Gamma_g$ ($^3\Sigma_u^+$) Ni_2.

IV. Calculational Details

A. Effective Potential and Basis Set. In all of the calculations reported here, we make use of the fact that the argon core for the first row transition elements is essentially non-interacting and thus replaceable by an effective potential. This reduces the SCF problem to one of optimizing only the valence orbitals. We first used the potential of Melius, Olafson and Goddard[9] which was fit to an ab initio description of the Ni atom. This potential was modified by Sollenberger, Goddard, and Melius[10] to incorporate intraatomic electron correlation effects in an approximate sense, leading to the modified effective potential (MEP) used in all calculations reported here.

The basis set consisted of a (4s, 4p, 5d) set of gaussians on each center. Of the five d functions from Wachters,[11] the inner four were contracted together using the atomic coefficients. By using the effective potential, it was only necessary to use the four most diffuse s functions from Wachters' set (the inner two were contracted together using coefficients from the ^3D atomic state). The p functions used were obtained by Sollenberger; the inner three were contracted together using coefficients from the atomic state. This scheme results in a (3s, 2p, 2d) set of contracted gaussians on each center.

B. Wavefunctions. The primary goals in these calculations were to obtain not only good binding energies but also a clear physical description of the orbital interactions as a function of bond length. Almost all of the lower states of Ni_2 and Ni_2^+ involve weakly overlapping singly-occupied 3d orbitals. Thus, even at R_e, where the Hartree-Fock description is usually acceptable, many of the states cannot be properly described by this type of wavefunction. The GVB wavefunction, allowing each electron in a bonding pair to occupy its own orbital, accounts for the major correlation effects, leading to a qualitatively useful description. The separated atoms each possess at least four doubly-occupied valence orbitals, allowing us to choose as a minimal description for the molecule a GVB wavefunction that includes eight doubly-occupied orbitals and four singly-occupied orbitals. We find that the two 4s orbitals are always coupled into a singlet GVB pair for Ni_2. The remaining two singly-occupied orbitals have 3d character and allow the generation of all low-lying states. From these GVB calculations we obtain a set of spatially optimized orbitals (see Figures 5 and 8) from which we can obtain a good description of the bonding.

The GVB wavefunction accounts for the important electron correlation effects, but does not possess $D_{\infty h}$ symmetry. Using these orbitals, however,

we can perform small CI calculations that will build in resonance effects and provide the proper symmetry.

To make use of the full diatomic symmetry in these CI calculations, it is convenient to project the localized GVB orbitals into a set of symmetry orbitals. For a CI wavefunction, which includes resonance terms, the use of such functions is not a restriction. The equivalence of the localized and delocalized descriptions for this type of wavefunction is demonstrated for $\delta\delta$ hole cases in Table I. In making the transformation from localized to delocalized orbitals we have used the simple relations

$$\phi_g = (\phi_\ell + \phi_r)\frac{1}{\sqrt{2(1+S)}} \quad \phi_u = (\phi_k - \phi_r)\frac{1}{\sqrt{2(1-S)}} \quad .$$

A similar analysis may be performed for each of the other combinations of holes.

For Ni_2, to obtain a basis for the CI, we begin with the set of 12 localized GVB orbitals corresponding to a triplet-coupled $\delta\delta$ hole state with occupation as in one of the configurations of (3a) or (3b). We form the symmetric and antisymmetric projections, then orthogonalize to obtain 12 valence and 12 virtual symmetry orbitals. The process of orthogonalization changes the character of the valence orbitals somewhat but use of the virtuals allows this to be corrected in the CI. For the states of Ni_2^+ an analogous procedure was followed. The GVB orbital set used as a basis was that shown in part in Figure 8.

C. GVB-CI. The spectrum of states for Ni_2 and Ni_2^+ shown qualitatively in Figures 1 and 6 was obtained from a small restricted CI designed to characterize the ordering of states. In doing such a small CI, the configurations necessary to describe different occupations of the same

Table I. Equivalence of Configurations Based on Localized or Atomic Orbitals and Configurations Based on Delocalized Symmetry Functions

Orbital	Localized $\delta_{x^2-y^2}$ δ_{xy}	$\delta_{x^2-y^2}$ δ_{xy}	Delocalized $\delta_{x^2-y^2}$ δ_{xy}	$\delta_{x^2-y^2}$ δ_{xy}	
Function Type	L R L R	L R L R	G U G U	G U G U	eq
Configurations[a]	(2 1 1 2) + (1 2 2 1)		(2 1 2 1) - (1 2 1 2)		(3a)
	(2 1 1 2) - (1 2 2 1)		(1 2 2 1) - (2 1 1 2)		(3b)
	(2 2 1 1) + (1 1 2 2)		(2 2 1 1) + (1 1 2 2)		(2a)
	(2 2 1 1) - (1 1 2 2)		(2 2 1 1) - (1 1 2 2)		(2b)

[a] For example, (2 1 1 2) indicates configuration $\delta^2_{x^2-y^2a}\delta^1_{x^2-y^2b}\delta^1_{xya}\delta^2_{xyb}$.

symmetry (e.g., $^3\Sigma_g^-$ which arises from $\delta\delta$ and $\pi\pi$ hole states) could be allowed to interact within a single calculation and many more states could be obtained inexpensively. It was found that such interactions were not important and that the states could be clearly assigned in most cases according to the scheme presented in Sections II and III.

The method used to generate the configurations for the GVB-CI was straightforward. No excitations were allowed into the virtual orbitals. All $\sigma \rightarrow \sigma$, $\pi \rightarrow \pi$, $\delta \rightarrow \delta$ excitations were allowed but no excitations to shells of different ℓ values were allowed. The resulting set of configurations could be separated into symmetry types under D_{2h} and each type solved for separately.

The basis used for these calculations involved valence σ and δ orbitals obtained from a triplet-coupled $\delta\delta$ hole GVB calculation. The π basis was from an analogous $\pi\pi$ hole state. To avoid bias due to the different spatial character of singly- and doubly-occupied orbitals, the π and δ orbitals were averaged after projecting into symmetric and antisymmetric combinations.

D. POL-CI. This larger CI is designed to allow changes of orbital shape to occur when the full resonance is included in the wavefunction. Thus, in addition to excitations important for the GVB-CI, we allow single excitations into a set of virtual orbitals to allow "polarization" of the occupied orbitals. It was of obvious interest to fully examine the $^1\Gamma_g(\delta\delta)$ and $^3\Sigma_g^-(\delta\delta)$ states as they are nearly degenerate candidates for the ground state. We also chose to further examine the $^1\Sigma_g^+(\sigma\sigma)$ state since it initially seemed a clear choice for the ground state. More importantly, as a $\sigma\sigma$ hole state, it allows us to gauge the distance between the highest and lowest of the $4s^2$ states of Ni_2 as a function of bond length. For Ni_2^+ there were three states of primary interest. Aside from the $^4\Sigma_u^-$ ($s^2d\sigma^3$) ground

state, it was of interest to carefully determine the applicability of the one-electron bond ideas to Ni_2^+; thus the $^4\Sigma_g^-$ ($s^1d\sigma^4$) state was considered. In the same manner as for Ni_2, it was of interest to examine the $^2\Sigma_g^+$ ($\sigma\sigma$) state (also a $4s^1$ state) to determine the full range of 3d occupation effects as a function of bond length.

The manner in which the configurations were obtained for this state may best be seen by examining a particular occupation, for example, triplet-coupled $\delta\delta$ holes analogous to (3). The GVB wavefunction replaces the product

$$\mathcal{A}\{\varphi_{4s}\,\varphi_{4s}\,(\alpha\beta - \beta\alpha)\}$$

with the pair correlation function

$$\mathcal{A}\{(\phi_{4s\ell}\,\phi_{4sr} + \phi_{4sr}\,\phi_{4s\ell})\,\chi\}\ ,$$

where $\phi_{4s\ell}$ and ϕ_{4sr} are allowed to be completely general. In terms of symmetry orbitals, this becomes

$$\mathcal{A}\{(\phi_{4sg}^2 - \lambda^2\,\phi_{4su}^2)\,\chi\}\ . \tag{14}$$

This leads to two configurations describing the correlation in the 4s orbital; combining these with the four resonance configurations described by Table I leads to eight of the configurations shown in Table II(a). [The remaining four involve the $4sg^14su^1$ occupation.] For the triplet-coupled $\delta\delta$ hole states of (2), the configurations are shown in Table II(b). From this basic set, all singles into the virtual orbitals were considered under the restriction that only $\sigma_{val} - \sigma_{virt}$, $\pi_{val} - \pi_{virt}$, and $\delta_{val} - \delta_{virt}$ be allowed. The results of these POL-CI calculations for the lowest states of Ni_2 and Ni_2^+ are listed in Table III. In Table IV we compare the total energies for these states as obtained from each level of calculation reported here for a fixed bond distance of 2.01 Å.

Table II. Configuration Basis for the POL-CI Calculations

	$4s_g$	$4s_u$	$3d\sigma_g$	$3d\sigma_u$	π_{xzg}	π_{xzu}	π_{yzg}	π_{yzu}	$\delta_{x^2-y^2g}$	$\delta_{x^2-y^2u}$	δ_{xyg}	δ_{xyu}
a)	2	0	2	2	2	2	2	2	2	1	2	1
	2	0	2	2	2	2	2	2	1	2	1	2
	2	0	2	2	2	2	2	2	2	1	1	2
	2	0	2	2	2	2	2	2	1	2	2	1
	0	2	2	2	2	2	2	2	2	1	2	1
	0	2	2	2	2	2	2	2	1	2	1	2
	0	2	2	2	2	2	2	2	2	1	1	2
	0	2	2	2	2	2	2	2	1	2	2	1
	1	1	2	2	2	2	2	2	2	1	2	1
	1	1	2	2	2	2	2	2	1	2	1	2
	1	1	2	2	2	2	2	2	2	1	1	2
	1	1	2	2	2	2	2	2	1	2	2	1
b)	2	0	2	2	2	2	2	2	2	2	1	1
	2	0	2	2	2	2	2	2	1	1	2	2
	0	2	2	2	2	2	2	2	2	2	1	1
	0	2	2	2	2	2	2	2	1	1	2	2
	1	1	2	2	2	2	2	2	2	2	1	1
	1	1	2	2	2	2	2	2	1	1	2	2

Table III. POL-CI Results for Ni_2 and Ni_2^+.

	State	R_e (Å)	ω_e (cm^{-1})	D_e (eV)
Ni_2	$^1\Sigma_g^+(\sigma\sigma)$	2.03	308.6	2.36
	$^3\Gamma_u(\delta\delta)$	2.05	346.5	2.91
	$^3\Sigma_u^+(\delta\delta)$	2.05	349.3	2.92
	$^1\Sigma_u^-(\delta\delta)$	2.04	347.1	2.92
	$^3\Sigma_g^-(\delta\delta)$	2.04	342.5	2.92
	$^1\Sigma_g^+(\delta\delta)$	2.04	344.8	2.93
	$^1\Gamma_g(\delta\delta)$	2.04	344.2	2.93
	Exp't.[a]	--	---	2.4
Ni_2^+	$^2\Sigma_g^+(\sigma\sigma)$	2.15	178.7	2.64
	$^4\Sigma_g^-(\delta\delta)$	2.16	303.0	3.31
	$^4\Sigma_u^-(\delta\delta)$	1.97	390.0	4.14
	Exp't.[a]	--	--	3.8

[a] A. Kant, ref 1. In obtaining D_e values, Kant used estimates of R_e = 2.30 Å and ω_e = 325 cm^{-1}.

Table IV. Total Energies[a] for Some of the Low-Lying States of Ni_2 and Ni_2^+ from GVB-CI and POL-CI Calculations at R = 2.01 Å (Energies in Hartrees)

State	Ni_2				Ni_2^+	
	$^1\Gamma_g$ ($\delta\delta$)	$^3\Sigma_g^-$ ($\delta\delta$)	$^3\Gamma_u$ ($\delta\delta$)	$^1\Sigma_g^+$ ($\sigma\sigma$)	$^4\Sigma_u^-$ ($\delta\delta$)	$^2\Sigma_g^+$ ($\sigma\sigma$)
GVB-CI	-81.0870	-81.0867	-81.0864	-81.0563	-80.7729	-80.7211
POL-CI	-81.0960	-81.0956	-81.0943	-81.0721	-80.8595	-80.8037

[a] Using the effective potential, atomic energies are Ni (^{3}D) = -40.4943 h and Ni^+ (^{2}D) = -40.2150 h.

V. Discussion

A. The Bond Length. The Ni-Ni bond length in the bulk metal is 2.49 Å,[12] as compared with our value for Ni_2 of 2.04 Å. Such short metal-metal distances are quite unusual, even for those binuclear complexes with metal-metal bonds.[13] This short distance finds some support, however, in the recent work of Efremov et al.[14] Their rotational analysis of a band characteristic of the Cr_2 dimer[15] indicates a bond length of 1.71 Å, which is consistent with the result reported here. Melius, Upton, and Goddard[16] have examined a cluster of 13 Ni atoms consisting of a central Ni and 12 neighbors as in the free metal. An optimization of the bond length for this cluster yielded an Ni-Ni distance of 2.41 Å, quite close to the value of 2.49 Å for Ni metal. Wheras two Ni atoms may interact strongly with one another, the implication here is that the presence of other neighboring atoms (or ligands in finite complexes) leads to additional repulsive interactions between nonbonded electron pairs forcing the larger bond length. Thus the large difference between the atomic radii for the bulk metal and the (calculated) bond length of the dimer appears to be real.

B. The δδ Ground State. The calculation of a δδ hole ground state finds support in similar calculations that have been carried out on the NiH molecule. Here the hydrogen atom bonds directly to the singly-occupied Ni 4s orbital, leaving a single 3d hole on the Ni atom. It is found that the lowest state of this system is the $^2\Delta$ state which has a $3d_\delta$ hole.[10] In this case, experimental results clearly show a $^2\Delta_{5/2}$ ground state.[17]

C. The MO Description. It is important to note that a similar treatment of Ni_2 using molecular orbitals would lead to very different results. The difficulty is a result of the extremely small overlap ($S < 0.01$) that exists between

dδ orbitals on different centers. Just as the MO wavefunction is far more successful at describing the lowest triplet state of H_2 than the lowest (ground state) singlet state at large separation, here a bias towards high-spin states is introduced in the MO description of Ni_2. In Section IV.D and Table I we have demonstrated the equivalence of the MO and VB in describing δδ hole triplet states. There is no corresponding set of resonance configurations that may be used for singlet δδ hole states. Electron correlation error, a problem for H_2 only at large separation, seriously affects Ni_2 singlet wavefunctions at equilibrium separation. Thus the $^1\Sigma_g^+$ (δδ) state and $^1\Gamma_g^+$ component of the $^1\Gamma_g$ (δδ) state are both found to be almost 10 eV higher in the MO description. Clearly, a vast expansion of Figure 4 would be required to include the same spectrum of states described by MO wavefunctions. Only those singlet states resulting from the open-shell coupling of singly-occupied orbitals [such as $^1\Sigma_u^-$ (δδ)] would be properly described.

D. Comparison with Observed Spectra. The states discussed in this study all occur in a region of energy that has not, to date, been examined experimentally for Ni_2. It is possible, however, to use information obtained here concerning the ground state to comment on recently observed ultraviolet-visible spectra for the dimer. The two most complete studies, those of Ozin[18] and Hulse and Moskovits,[19] were both obtained with Ni deposited in argon matrices and show good agreement in the observed bands. Both studies show well-resolved bands at approximately 2.4 and 3.5 eV with vibrational spacings of about 330 cm^{-1} (Ozin reports 360 cm^{-1} for the 2.4 eV band). A third structureless band is noted in both studies at around 2.9 eV.

An important feature in the well-resolved bands is that the measured vibrational frequencies are very close to the value of 344 cm^{-1} obtained here for the ground state. Electronic transitions of the form $\sigma_{4s} - \pi_{4p}$ or $\sigma_{4s} - \sigma^*_{4s}$

that would be expected to carry oscillator strength should also lead to significant changes in vibrational frequency and thus do not represent reasonable assignments for these transitions. Similar arguments apply to allowed $3d - \sigma^*_{4s}$ transitions (since this produces a more weakly bound $4s^3$ bonding configuration). On the other hand, transitions of the form $3d - \pi_{4p}$ should have little effect upon the vibrational frequency and represent the most likely assignments for these transitions. In the separate atom, the analogous 3d – 4p transitions occur in the range from about 3.2 to 5.8 eV.[4] Upon formation of Ni_2, the 3d levels are only weakly perturbed, whereas the $4p\pi$ level is stabilized through formation of the partial π bond. As a result, the molecular $3d - \pi_{4p}$ transition energy should be reduced somewhat (~ 0.5 eV) relative to the atomic analogue, which is consistent with the observed bands.

Hulse and Moskovits,[19] through comparison with published Xα and Extended Hückel treatments of Ni_2, reach similar conclusions regarding the origin of the two structured bands. The third band, due to its structureless nature, apparently involves significant geometry change and thus weakening of the Ni_2 bond. For these reasons, Hulse and Moskovits assign this band to the $\sigma_{4s} \rightarrow \sigma^*_{4s}$ transition, expected to be strong. Though we cannot rule out such an assignment, simple overlap arguments suggest that this transition should occur at much higher energy. For clarity, we will consider the forbidden $\sigma_{4s} \rightarrow \sigma^*_{4s}$ singlet-triplet transition which must, by Hund's rule, occur at lower energies than the allowed singlet-singlet transition. Ignoring all but the 4s electrons, this leads to an excited state wavefunction of

$$\phi^*_{4s} = \mathcal{A}\{(\sigma_{4s_g}\sigma_{4s_g} - \sigma_{4s_u}\sigma_{4s_u})(\alpha\alpha)\} = \mathcal{A}\{(\ell r - r\ell)(\alpha\alpha)\},$$

where the equivalent valence bond wavefunction is also shown. Evaluating the energy for this wavefunction using the approach shown in Appendix I leads to

an expression

$$E^*_{4s} = E_{c\ell} - \frac{2S\tau_1}{1-S^2} \quad ,$$

which is very similar (the reason for choosing the triplet state) in form to that given in the Appendix for the ground state,

$$E_{g.s.} = E_{c\ell} + \frac{2S\tau_1}{1+S^2} \quad .$$

For bond lengths near the minimum $S \approx 0.7$ leading to

$$E^*_{4s} = E_{c\ell} - 2.75\ \tau_1$$

$$E_{g.s.} = E_{c\ell} + 0.94\ \tau_1 \ .$$

For all values of R, τ_1 is negative and dominates $E_{c\ell}$. Thus, near the minimum where the ground state is bound by 2.9 eV, the excited triplet state should be almost 8 eV higher by this simple approach (assuming $|\tau_1| \gg E_{c\ell}$). Using this value as a lower bound for the allowed singlet-singlet transition suggests that the 2.9 eV observed band must have a different source. The most reasonable transition still consistent with the changes implied by the spectra is a $\sigma_{4s} - \pi_{4p}$. Analogous atomic transitions occur in the region of 3.5-3.7 eV,[4] which is more consistent with the observed band position. Clearly these bands require further study, and a more quantitative analysis will be presented from this laboratory at a later date.

E. Bond Energies. Beyond these spectroscopic studies, there is little detailed experimental information regarding Ni_2. Bond energies have been estimated by Kant[1] using mass spectroscopic data. Assuming values for bond length, vibrational frequency, and degeneracy, he obtains $D_e(Ni_2) = 2.4 \pm 0.2$ eV and $D_e(Ni_2^+) = 3.8 \pm 0.2$ eV. This compares with $D_e(Ni_2) = 2.9$ eV and $D_e(Ni_2^+) = 4.1$ eV from our calculations. The experimental estimate changes very little (~ 0.1 eV) upon incorporating our calculated molecular constants into the formula used by Kant.

F. Spin-Orbit Coupling. As the spectrum of states found in this study spans a very narrow energy range, the possible influence of spin-orbit coupling on the ordering of states merits some consideration. A very simple assessment of the importance of this effect is made possible by the fact that each of the states involves highly localized singly-occupied 3d orbitals. Our approach was as follows. We considered the 100 lowest states $\{\psi_i; = 1, 2, \ldots, 100\}$ corresponding qualitatively to a d^9 configuration on each of the two Ni atoms. The eigenvalues $\{E_i^o; i = 1, 2, \ldots, 100\}$ illustrated in Figure 1 correspond to diagonalizing the usual nonrelativistic Hamiltonian over these 100 states. Considering the simplified spin-orbital Hamiltonians

$$\mathcal{H}_{SO} = \Sigma_j \zeta_j (r_j) \hat{\ell}_j \cdot \hat{s}_j ,$$

we evaluated this 100 x 100 matrix

$$\langle 4_i | (\mathcal{H}_o + \mathcal{H}_{SO}) | \psi_j \rangle = E_i^o \delta_{ij} + \langle \psi_i | \mathcal{H}_{SO} | \psi_j \rangle$$

and diagonalized this matrix to allow opponent spin-orbital eigenstates. In the process of evaluating $\langle \psi_i | \mathcal{H}_{SO} | \psi_j \rangle$ we made the additional simplifications of (i) ignoring the very slight contamination of $p\pi$ character into the $d\pi$ orbitals, (ii) the slight mixing of $p\sigma$ and s character with the $d\sigma$ orbitals, (iii) including only the one center contributions to H_{SO}, and (iv) ignoring the overlap of d orbital on different centers (the actual overlaps ranged from 0.006 a.v. for $d\delta$ to 0.04 and 0.06 for $d\pi$ and $d\sigma$ respectively. In addition we set the radial integrals $\langle \phi_d | \zeta (r) | \phi_d \rangle$ to -0.0756 eV, obtained from a fit to to the spin orbit splittings observed for the ^3D state of the Ni atom.[4]

The resulting ordering of the eigenstates including spin-orbit coupling differs very little from the scheme presented in Figure 1. Table V shows the energies with and without spin-orbital coupling for the lower states. The preference for δ holes rather than π or σ in the lowest states is not disturbed. Since the $\zeta(r)$ prefactor in each of the one-electron matrix elements is negative, the greatest stabilization due to spin orbit effects occurs for spin orbitals of maximum total angular momentum about the axis, Ω. Thus the ${}^3\Gamma_{u_5}$ state which appears, using complex orbitals, as

$$ {}^3\Gamma_{u_5} = \mathcal{A}\{\delta_\ell^{2+}\delta_r^{2+}\alpha\alpha\} $$

shows the strongest stabilization. Similarly, the ${}^3\Gamma_{u_3}$ state

$$ {}^3\Gamma_{u_3} = \mathcal{A}\{\delta_\ell^{2+}\delta_r^{2+}\beta\beta\} $$

experiences the strongest destabilization. The lowest state, including spin orbit coupling is

$$ {}^1\Sigma_g^+(\delta\delta) + {}^3\Sigma_g^-(\delta\delta) $$

with the state

$$ {}^1\Sigma_u^-(\delta\delta) + {}^3\Sigma_u^+(\delta\delta) , $$

only 0.007 eV higher. The ${}^3\Gamma_{u_5}$ state lies 0.012 eV above the ground state. Such small splittings among the lowest states could be perturbed by other weak interactions.

Table V. Effects of Spin-Orbit Coupling on Lowest Ni_2 States

State	Ω [a]	$\hat{H}_o$(eV) [b]	$\hat{H}_o+\hat{H}_{SO}$ [c]	Dominant Admixture Due to Spin-Orbit Coupling	
$^1\Sigma_g^+(\delta\,\delta)$	0	0.00	-0.147	$^3\Sigma_g^-(\delta\,\delta)$	(50%)
$^1\Gamma_g(\delta\,\delta)$	4	0.001	-0.030	$^3\Phi_{u_4}(\pi\,\delta)$	(10%)
$^1\Sigma_u^-(\delta\,\delta)$	0	0.006	-0.140	$^3\Sigma_u^-(\delta\,\delta)$	(50%)
$^1\Pi_g^-(\delta\,\delta)$	1	0.009	-0.020	--	
	0	0.009	-0.098	$^1\Sigma_g^+(\delta\,\delta)$	(50%)
$^3\Sigma_u^+(\delta\,\delta)$	1	0.016	-0.009	--	
	0	0.016	0.115	$^1\Sigma_u^-(\delta\,\delta)$	(50%)
$^3\Gamma_u(\delta\,\delta)$	5	0.016	-0.135	--	
	4	0.016	-0.008	--	
	3	0.016	+0.135	--	

[a] Total angular momentum about axis. [b] From GVB-CI calculations.

[c] Rediagonalized from 100 x 100 matrix.

Appendix II.A.1

The s^1d^9 and s^2d^8 states of the Ni atom will not have overall spherical symmetry. The location of the hole for the isolated s^1d^9 atom has no effect on the energy, each configuration is degenerate. When bringing up another atom however, a molecular axis is immediately defined. The configurations are no longer degenerate, the five original occupations splitting into the three types shown below:

4s	$3d_\sigma$	$3d_\pi$	$3d_\delta$	
1	2	4	3	(1a)
1	2	3	4	(1b)
1	1	4	4	(1c)

In the formation of a sigma bond the 4s orbital will mix in virtual 4p character to delocalize towards the other center. In addition, the 4s and $3d_\sigma$ orbitals, being of the same symmetry, will mix.

This mixing results from the interaction of configurations (1a-c) with s^2d^8 and d^{10} configurations:

4s	$3d_\sigma$	$3d_\pi$	$3d_\delta$	
2	1	4	3	(2a)
2	1	3	4	(2b)
2	0	4	4	(2c)
0	2	4	4	(2d)

obtained by carrying out $3d_\sigma \rightarrow 4s$ (or $4s \rightarrow 3d_\sigma$) single excitations from (1a-c). The result is a set of orbitals that may be described as

hybrids by (for example):

$$\varphi_{\sigma} = (1a) + \lambda(2a) .$$

The degree to which the orbitals may mix (i.e., the size of λ) depends on the energy of the configurations (2) shown above that will mix. If they are high in energy, mixing will be unfavorable leading to a weakly hybridized bond.

Upon analysis of the angular momentum eigenfunctions involved it is found that the hybridization scheme becomes:

$$\begin{aligned}
\delta \text{ holes:} \quad \varphi &= (1a) + \lambda(2a) \\
&= {}^3D + \lambda[{}^3F] \\
\pi \text{ holes:} \quad \varphi &= (1b) + \lambda(2b) \\
&= {}^3D + \lambda[.4({}^3P) + .6({}^3F)] \\
\sigma \text{ holes:} \quad \varphi &= (1c) + \lambda(2c + 2c') \\
&= {}^3D + \lambda[.59({}^1S) + .30({}^1D) + .11({}^1G)]
\end{aligned}$$

where, since (2b-c') do not represent pure states, the actual composition of the configurations are shown. It may be seen that with a δ hole present, hybridization introduces only low-lying ${}^3F$ character. On the other hand, for π and σ holes the hybridizing configurations are mixtures of high-lying s^2d^8 Ni states. They are not expected to mix favorably, leading to a preference for δ holes in a bonding situation.

Appendix II.A.2

Through the use of valence bond wavefunctions it is possible to make a direct comparison between the energy expressions arising from one- and two-electron bonds. For the one-electron bond, a simple wavefunction may be assumed,

$$\varphi_1 = \{(\ell + r)\alpha\} \quad , \tag{A-1}$$

and for the two-electron bond,

$$\varphi_2 = \mathcal{A}\{(\ell r + r\ell)(\alpha\beta - \beta\alpha)\}. \tag{A-2}$$

These give rise to the energy expressions

$$\begin{aligned} E_1 &= \frac{\langle \varphi_1 | \mathcal{H} | \varphi_1 \rangle}{\langle \varphi_1 | \varphi_1 \rangle} = \frac{h_{\ell\ell} + h_{\ell r}}{1 + S} + \frac{1}{R} \\ E_2 &= \frac{\langle \varphi_2 | \mathcal{H} | \varphi_2 \rangle}{\langle \varphi_2 | \varphi_2 \rangle} = \frac{2h_{\ell\ell} + 2Sh_{\ell r} + J_{\ell r} + K_{\ell r}}{1 + S^2} + \frac{1}{R} \quad , \end{aligned} \tag{A-3}$$

where the terms have their usual meaning.

Partitioning the energy expression into classical terms[20] [arising from ℓ in (A-1) or ℓr in (A-2)] and the exchange terms [arising from the superposition of terms in (A-1) or (A-2)] leads to

$$E_1 = E_1^{c\ell} + E_1^{x} \qquad E_2 = E_2^{c\ell} + E_2^{x} \quad , \tag{A-4}$$

where

$$E_1^{c\ell} = \tfrac{1}{2}(h_{\ell\ell} + h_{rr}) + 1/R$$

$$E_2^{c\ell} = h_{\ell\ell} + h_{rr} + J_{\ell r} + 1/R \quad ,$$

$$E_1^X = \frac{\epsilon_1 - SE_1^{C\ell}}{1 + S} = \frac{\tau_1}{1 + S}$$

and

$$E_2^X = \frac{\epsilon_2 - S^2E_2^{C\ell}}{1 + S^2} = \frac{2S\tau_1 + \tau_2}{1 + S^2} ,$$

where

$$\tau_1 \equiv h_{\ell r} - Sh_{\ell\ell} \qquad \text{and} \qquad \tau_2 \equiv K_{\ell r} - S^2J_{\ell r} ,$$

and where the exchange terms dominate the bonding. The term τ_2 is positive but dominated by τ_1 which is negative. Neglecting τ_2 we can write

$$E_1^X = \frac{\tau_1}{1 + S} ,$$

and

$$E_2^X = \frac{2S\tau_1}{1 + S^2} .$$

Thus the relative strengths of the one- and two-electron bonds depend upon the overlap. The exchange terms are equal for S = 0.42. Thus for this value of the atomic orbital overlap, the one- and two-electron bonds will be almost equal in strength. For smaller overlap (longer bond length), the one-electron bond will be stronger.

References and Notes

(1) A. Kant, J. Chem. Phys., 41, 1872 (1964).

(2) (a) A. Kant, J. Chem. Phys., 41, 3806 (1964); (b) P. Schissel, J. Chem. Phys., 26, 1276 (1957); (c) K. A. Gingerich, J. Crystal Growth, 9, 31 (1971); (d) R. Busby, W. Klotzbücher, and G. A. Ozin, J. Am. Chem. Soc., 98, 4013 (1976).

(3) T. C. DeVore, A. Ewing, H. F. Franzen, and V. Calder, Chem. Phys. Lett., 35, 78 (1975).

(4) C. E. Moore, "Atomic Energy Levels", National Bureau of Standards, 1949, Vol. II.

(5) A similar ordering has been observed for the low-lying states of NiCO: S. P. Walch and W. A. Goddard III, J. Am. Chem. Soc., 98, 7908 (1976).

(6) δ_1 refers to $\delta_{x^2-y^2}$ and δ_2 to δ_{xy}.

(7) This assumption is based on arguments given in Section II.A regarding hybridization of the 4s orbital in Ni_2. With ionization from the σ shell, hybridization requires mixing of low-lying s^0d^9 configurations of Ni^+. Removing a $3d_\pi$ or $3d_\delta$ electron necessitates mixing of very high-lying s^2d^7 configurations to hybridize the 4s orbital. Alternatively, an examination of orbital energies for Ni_2 shows the $3d_\sigma$ combination electrons to be least bound.

(8) See, for example, L. R. Kahn and W. A. Goddard III, J. Chem. Phys., 56, 2685 (1972).

(9) C. F. Melius, B. D. Olafson, and W. A. Goddard III, Chem. Phys. Lett., 28, 457 (1974).

(10) M. Sollenberger, C. F. Melius, and W. A. Goddard III, to be published; see also M. Sollenberger, M.S. Thesis, California Institute of Technology, 1976. The effective potential and basis set are summarized in Appendix V.A.

(11) A. J. H. Wachters, J. Chem. Phys., 52, 1033 (1970).

(12) W. B. Pearson, "A Handbook of Lattice Spacings and Structures of Metals and Alloys", Pergamon Press, New York, N.Y., 1958.

(13) F. A. Cotton and O. Wilkinson, "Advanced Inorganic Chemistry", Interscience, New York, N.Y., 1972.

(14) Yu. M. Efremov, A. N. Samoilova, and L. V. Gurvich, Opt. Spektrosk., 36, 381 (1974).

(15) E. P. Kundig, M. Moskovits, and G. A. Ozin, Nature, 254, 503 (1975).

(16) Section I.C of this thesis.

(17) G. Herzberg, "Spectra of Diatomic Molecules", Van Nostrand-Reinhold Co., New York, N. Y., 1950.

(18) G. A. Ozin, private communication.

(19) M. Moskovits and J. E. Hulse, J. Chem. Phys., 66, 3988 (1977) and references cited therein.

(20) C. W. Wilson, Jr., and W. A. Goddard III, Theor. Chim. Acta, 26, 195 (1972).

B. The Localization of 3d Orbitals: Ni_8

I. Introduction

In a previous investigation of the nickel dimer[1] it was found that the metal-metal bonding was dominated by interactions between the diffuse 4s orbitals present on each nickel atom. The tightly bound 3d orbitals are considerably smaller than these 4s orbitals and were found not to participate strongly in the bonding, even at relatively small internuclear separations. This finding is consistent with the results of ultraviolet photoemission[2] and soft X-ray[3] studies of bulk nickel which show a very narrow (~ 3.5 eV) 3d band in emission, indicative of weak 3d-3d interactions. It is in sharp contrast to the results of band calculations for bulk nickel,[4,5] as well as studies of finite particles[6] using similar approximate hamiltonians. Here, the metal-metal bonds are found to contain a large component of 3d character.

In this paper, we report results of first principles calculations on an eight-atom cluster of nickel atoms that suggest a bonding description in agreement with our dimer results. We will demonstrate that the highly localized character of the 3d orbitals allows a computational simplification that should make possible the similar, but more approximate study of much larger clusters (80-100 atoms).

II. Geometry, Basis Sets and Effective Potentials

In the Ni_8 cluster, the atoms were arranged at the vertices of a cube with a nearest neighbor separation of 2.487 Å (the experimental bond distance in fcc Ni).[7] For this cluster, each Ni atom possesses only three nearest neighbors, rather than 12, as found for the bulk face-centered cubic lattice.

To replace the argon core of each Ni atom, the modified effective potential (MEP) of Sollenberger and Goddard[8] was used. This potential is based on the ab initio potential of Melius, Olafson, and Goddard,[9] but includes additional terms designed to account in an approximate way for correlation effects among the 3d orbitals and allow a proper energetic description of atomic states. Use of the MEP allows truncation of the basis set to include only valence Ni basis functions. Thus the (4s, 1p, 5d/2s, 1p, 2d) basis set adapted from Wachters[10] and listed in Appendix V.A was used on each Ni atom. Using this basis and MEP, all calculations on the Ni_8 cluster were carried out at the hartree-fock level.

III. Electronic Structure

In Table I, we show the results of hartree-fock calculations characterizing a number of states of the Ni_8 cluster. The lowest energy configuration has 72 electrons in essentially pure 3d-like orbitals (to be referred to hereafter as the 3d band) and 8 electrons in delocalized orbitals with 4s and 4p character on each Ni (to be referred to as the 4s band). A Mulliken population analysis for this state leads to an occupation on each Ni atom of $4s^{0.77}\ 4p^{0.32}\ 3d^{8.91}$. Thus, as in Ni_2, the lowest states of the cluster may be viewed as resulting from an aggregation of $4s^1\ 3d^9$ Ni atoms.

Some insight into the nature of the bonding may be obtained by examining separately the "4s" and "3d bands" of Ni_8. With a $3d^9$ shell on each center, the low-lying states of Ni_8 differ only in the orientation of the singly-occupied 3d orbitals on each Ni. The lowest states were

Table I: Excited States of Ni_8

Valence Occupation on each Ni Atom	Total Energy	Excitation Energy (eV)	Net Spin	4s occupation				3d occupation[a]							
				a_g	t_{2g}	t_{1u}	a_{2u}	a_g	e_g	t_{1g}	t_{2g}	a_{2u}	e_u	t_{1u}	t_{2u}
$4s^1\,3d^8$ (t_{2g} hole)	-322.6870	0.0	4	2	0	6	0	1	4	6	6	1	4	6	6
									4	6	6		4	6	6
											3			3	
$4s^1\,3d^8$ (t_{2g} hole)	-322.1991	13.3	8	1	3	1	3	1	4	6	6	1	4	6	6
									4	6	6		4	6	6
											3			3	
$4s^2\,3d^8$ (t_{2g} holes)	-321.8657	22.3	8	2	6	6	2	1	4	6	6	1	4	6	6
									3	4.5	4.5		3	4.5	4.5
											3			3	
$4s^2\,3d^8$ (e_g holes)	-321.8149	23.7	8	2	6	2	6	2	4	6	6	2	4	6	6
									2	3	6		2	6	3
											3			3	
$4s^0\,3d^{10}$ (filled 3d shell)	-321.5013	32.3	1	0	0	0	0	2	4	6	6	1	4	6	6
								1	4	6	6		4	6	6
											6			6	
$4s^0\,3d^{10}$ (filled 3d shell)	-321.4778	32.9	0	0	0	0	0	2	4	6	6	2	4	6	6
									4	6	6		4	6	6
											6			6	
$4s^{.25}\,3d^{9.75}$	-321.0490	44.6	0	2	0	0	0	2	4	6	6	2	4	6	6
											6			6	
											6			6	

[a]Numbers represent orbital occupation for orbitals of symmetry indicated by column headings.

found to possess a singly occupied $3d_\sigma$ orbital on each center pointing towards the center of the cube. These orbitals were highly localized and only weakly overlapping. As such they may be coupled to produce a variety of spin states, all close in energy. The lowest energy hartree-fock wavefunction however,

will be obtained by combining the eight electrons in these orbitals into an S = 4 (high spin) configuration. Expressed in terms of symmetry orbitals, this leads to the $1a_{1g}^1\ 3t_{1u}^3\ 1a_{2u}^1\ 3t_{2g}^3$ open shell occupation that may be found as part of the ground state configuration shown in Table I. For such highly localized orbitals, hartree-fock wavefunctions of intermediate spin ($0 \leq S < 4$) will possess a significant amount of ionic character, and will not be energetically competitive.

These observations are in contrast to what is found for the 4s orbitals of these "$4s^1\ 3d^9$" derived states. The 4s orbitals on each Ni atom are highly overlapping and dominate the bonding interaction. Here, the lowest energy configuration is one in which these eight electrons are singlet-coupled into four bonding orbitals, the $1a_{1g}^2\ 1t_{1u}^6$ configuration indicated for the ground state in Table I. Attempting to couple these diffuse orbitals into an S = 4 configuration produces a symmetry orbital occupation of $1a_{1g}^1\ 1t_{1u}^2\ 1a_{2u}^1\ 1t_{2g}^2$. This state, the second listed in Table I, is about 13.3 eV above the ground state. Unlike the singly occupied 3d orbitals, localization of the 4s orbitals onto individual centers through high-spin coupling is not energetically favorable.

It is also possible to consider states of Ni_8 that might arise through aggregation of eight $4s^2\ 3d^8$ Ni atoms. These states have

16 electrons in "4s band" orbitals and 64 electrons in localized "3d band" orbitals. Two such states are listed in Table I. The lowest of these has two singly occupied t_{2g}-like orbitals on each Ni while 1.4 eV higher in energy is a state with two singly-occupied e_g-like orbitals on each center. This 3d → 3d excitation however, requires far less energy than that which is required to reach either of these states from the ground state. Thus, forming the Ni_8 cluster from $4s^1 3d^9$ Ni atoms is almost 22 eV more favorable than by combining $4s^2 3d^8$ atoms.

The next two states in Table I result from the combination of $3d^{10}$-like atoms to create Ni_8. Such states are 40 eV above the ground state in the separated atom limit[11] and, as indicated in Table I, over 32 eV at the geometry used in these calculations.

IV. The $3d^9$ Averaged Potential

We note below a number of features common to both Ni_2 and Ni_8 that suggest a simplified approach to the study of clusters:

1) the 3d orbitals are highly localized and participate only weakly in the bonding;

2) changing 3d occupations produces only a minor perturbation on the 4s interactions;

3) the bonding is dominated by the 4s-4s interactions;

4) the lowest states of both Ni_2 and Ni_8 involve occupations on each Ni atom that are consistent with dissociation of the clusters to $4s' 3d^9$ Ni atoms.

The largely independent nature of the "4s" and "3d band" orbitals

suggests that it should be possible to study the properties of these bonds separately. For example, to study the 4s orbitals, it might be possible to freeze the 3d orbitals on each Ni in their atomic shapes.

To test this hypothesis, a state of the Ni atom was considered in which the $3d^9$ shell was spherically averaged, that is, each of the five 3d orbitals were allowed to have a occupation of 9/5 electrons. In this way, bias towards a specific spatial orientation of 3d orbitals could be avoided. Using this description of the atom, an effective potential was generated using the method of Melius, Olafson, and Goddard[9] to replace the $3d^9$ shell. The use of this potential (listed in Appendix V.A) allows reduction of the self-consistent problem for Ni to only a single 4s electron, thereby allowing an enormous increase in the size of clusters whose 4s band properties might be examined.

In Table II we show results of an application of this potential to the study of Ni_8. Here we compare the 4s properties of the two lowest states of Table I with the same properties obtained from calculations carried out using the new potential (hereafter referred to as the $3d^9$-averaged MEP). We find that the excitation energy and orbital energies of the two states are reproduced for the most part to well within 10%. Comparing Mulliken populations, we find that there is a slight shift from 4p to 3d in electron density. Since in using the $3d^9$ averaged MEP the 3d occupation and orbital shapes are essentially frozen at atomic values, there is essentially no freedom for the 3d orbitals on each Ni to polarize through mixing with 4p bass functions, and thus some shift is to be expected. The same 3d basis set was used in each calculation however, we find that the $3d^9$ averaged potential sufficiently reproduces

Table II: Comparison of 4s Orbital Properties for MEP and $3d^9$ Averaged MEP Calculations

Calculation (Method)	Excitation Energy (eV)	4s Occupation				4s Orbital Energies				Mulliken Populations		
		a_{1g}	t_{1u}	t_{2g}	a_{2u}	a_{1g}	t_{1u}	t_{2g}	a_{2u}	s	p	d
10 valence electrons on each Ni atom; MEP core potential on each atom	0.0	2	6	0	0	-0.477	-0.251	-	-	0.77	0.32	8.91
"	13.3	1	3	3	1	-0.682	-0.404	-0.236	-0.102	-	-	-
1 valence electron and $3d^9$ averaged MEP potential on each Ni atom	0.0	2	6	0	0	-0.448	-0.255	-	-	0.78	0.22	0.00
"	13.8	1	3	3	1	-0.636	-0.421	-0.235	-0.087	0.79	0.21	0.00

the 3d shell field such that no further d electron density is sought in that calculation. Almost no shift occurs in the 4s electron density on each Ni as a result of "freezing" the 3d electron fields.

V. Conclusions

We have presented calculations that suggest, in agreement with earlier Ni_2 results, that for large Ni clusters the effective atomic state of Ni may be taken to be the $4s^1\,3d^9$ configuration. Indeed a number of studies of Fe, Co, Ni, and Cu[12,13] have indicated that the $4s^1\,3d^n$ configuration is stabilized in metal-metal bonding. While experimental studies do not suggest that for Fe or Co the 3d orbitals are unimportant in bonding,[3] there are a number of indications that for Ni the 3d electrons are highly localized,[14,15] in agreement with our findings.

There are theoretical studies however that are in disagreement with our conclusion that the 3d electrons participate to only a minor extent in the bonding. Messmer et al.[6] have carried out X_α calculations on an identical Ni_8 cluster. In these calculations the lowest state of the cluster is found to be essentially $3d^{10}$-like on each Ni with only one doubly occupied "4s band" orbital. We have carried out calculations on this same state and find it to be extremely high-lying, almost 44 eV above the ground state. This state, the final entry in Table I, is poorly described from within the Hartree-Fock description, and should show significant ionic character in the X_α description as well. We must conclude that the preference exhibited for this state in the X_α results arises from the residual orbital self-energy term in the

X_α hamiltonian, a feature that has been discussed elsewhere.[16] Calculations on the Ni atom using an HF hamiltonian modified to reproduce the X_α exchange approximation results[17] in a ground state configuration of $4s^{0.6}\ 3d^{9.4}$. Thus a bias towards a $3d^{10}$ configuration is introduced at the atomic level and may propagate the Ni_8 treatment.

References and Notes

1. T. H. Upton and W. A. Goddard III, J. Am. Chem. Soc., 100, 5659 (1978); see also Part II.A of this thesis.
2. D. E. Eastman, J. Appl. Phys., 40, 1387 (1969).
3. J. R. Cuthill, A. J. McAlister, M. L. Williams, R. E. Watson, Phys. Rev., 164, 1006 (1967).
4. J. Callaway and C. S. Wang, Phys. Rev., B7, 1096 (1973).
5. C. S. Wang and J. Callaway, Phys. Rev., B9, 4897 (1974).
6. R. Messmer, S. Knudson, K. Johnson, J. Diamond, and C. Yang, Phys. Rev., B13, 1396 (1976).
7. W. P. Pearson, "Handbook of Lattice Spacings and Structures of Metals and Alloys," (Pergamon, New York, 1958).
8. M. Sollenberger, M.S. Thesis, Calif. Inst. of Technol., 1977.
9. C. F. Melius, B. D. Olafson, and W. A. Goddard III, Chem. Phys. Lett., 28, 457 (1974).
10. A. J. H. Wachters, J. Chem. Phys., 42, 1293 (1965).
11. It should be noted that the MEP places the $3d^{10}$ state about 5.0 eV above the ground state, whereas the experimental splitting is 1.75 eV.
12. M. B. Stearns, Phys. Lett. A34, 146 (1971); Phys. Rev. B8, 4383 (1973); B9, 2311 (1974); B13, 1183 (1976); B13, 4180 (1976).
13. K. Duff and J. Das, Phys. Rev., B3, 192, 2294 (1971); S. Wakoh and J. Yamashita, J. Phys. Soc. Japan, 21, 1712 (1966).
14. M. B. Stearns, Physics Today, 31, 34 (1978).

References (continued)

15. L. C. Davis and L. A. Fedkam, Solid State Commun., 19, 413 (1976).

16. S. J. Niemczyk and C. F. Melius, Chem. Phys. Lett., 46, 236 (1977).

17. C. F. Melius, unpublished results.

C. The 4s or Conduction Band Properties of Nickel: Clusters from 13 to 87 Atoms

I. Introduction

The approaches of band theory have long been successful in describing many electronic properties of solids; similarly, the techniques of quantum chemistry have been applied with some success to aspects of solids involving localized electronic states.[1-4] Examples of the latter include surface states,[1] relaxation and reconstruction of surfaces,[2] vacancies and impurity states,[3] and molecules chemisorbed on surfaces.[4] Characteristic of the quantum chemical approaches is the use of a small, finite cluster of atoms to represent the infinite solid. Obviously, the usefulness of the model depends upon the extent to which the long-range effects that have been excluded might determine the properties of the localized states of interest. In this paper, we will examine specifically the adequacy of finite clusters for describing the properties of the bulk solid. Clusters ranging in size from 13 to 87 atoms will be discussed, with an emphasis on the behavior of the 4s or "conduction band" orbitals of these systems. Properties to be examined include: (1) the ionization potential (IP); (II) the electron affinity (EA); (iii) the bandwidth and character of the s-conduction band and the d bands; (iv) the ligand-field type splitting of the d orbitals; (v) the cohesive energy; (vi) the low-lying excited states of the conduction band; and (vii) the optimum Ni-Ni bond length.

II. Calculational Details

The ability to economically apply ab initio methods to clusters as large as Ni_{87} results from a fundamental simplifying approximation, as

described in the previous section.[5] The 4s orbital of Ni is almost $2\frac{1}{2}$ times the size of the 3d orbital, and as a result, the 3d shell tends to remain localized in molecular bonding situations and generally the $4s^1 3d^9$ state of the atom is stabilized. The energetic effect of the 3d orbitals upon bonding is not negligible; different occupations of the five d orbitals by the nine electrons leads to a range of bond energies of about 0.5 eV per Ni atom for NiH,[6] $NiCH_3$,[7] and Ni_2,[8] as compared with total bond energies of 2.5 to 3.0 eV. However, the major effects of one Ni atom upon another are well described by the potential curve obtained from averaging the five configurations arising from $(3d)^9$. In particular, we found that the lower electronic states of Ni_2 and Ni_8[5] have a localized $3d^9$ configuration on each Ni atom, with the remaining electrons in delocalized (conduction band) orbitals dominated by the 4s-like component on each Ni atom. The 3d band spectrum and orbital character are nearly independent of the conduction band occupation and, in fact, these orbitals are of only minor importance in the bonding. These findings suggest a simplification in which the conduction band is studied separately from the 3d bands. To avoid bias towards a particular $3d^9$ configuration on each atom, we averaged over the five possible $3d^9$ spatial configurations. To retain the effect of this $3d^9$ field without having to treat these orbitals explicitly, we replaced the $3d^9$ field with an effective potential.[5,9] This reduces the conduction band problem to one electron per Ni atom, allowing a significant truncation in the basis set required, and an enormous increase in the size of the clusters that can be economically considered. For Ni_2 the use of this d^9 potential on each Ni reduces the problem to a two-electron

problem and leads to R_e = 2.09 Å and D_e = 2.0 eV, in good agreement with the averaged values R_e = 2.04 Å and D_e = 2.2 eV estimated from full 20 valence electron GVB calculations. For a given Ni_n cluster in this description, all orbitals were solved for selfconsistently (Hartree-Fock) for a number of states of the neutral, positive ion, and negative ion systems. Since most states possessed open-shell orbitals, it was necessary to use the proper variational technique[10] to ensure that each state was a correct spin eigenfunction.

Two different systematic schemes were used to select clusters. Cubic clusters (O_h symmetry) were formed by selecting an atom of the face-centered-cubic (fcc) Ni structure (2.487 Å bond distance)[11] and taking the first six shells of atoms surrounding a central atom, numbering 13, 19, 43, 55, 79, and 87 atoms. Two clusters (Ni_{20} and Ni_{28}) of lower symmetry, D_{2h}, were obtained by selecting two adjacent atoms of the fcc structure and surrounding each of them simultaneously with shells of atoms in the same manner as above. The 19 and 28 atom clusters are illustrated in Figure 1.

To probe the effect of bulk coordination (12 nearest neighbors) or the properties of the localized 3d orbitals, calculations were carried out on the 13 atom cluster in which the shapes and energies of the 3d orbitals on the central atom were explicitly evaluated. This atom was surrounded by the remaining 12 atoms, each using the $3d^9$ averaged MEP. The 10 electrons on the central atom were given full variational freedom to interact and delocalize onto the surrounding Ni atoms. The validity of the $3d^9$ averaged potential concept could be tested in part by comparing the 4s or "conduction band" properties of this 22 electron

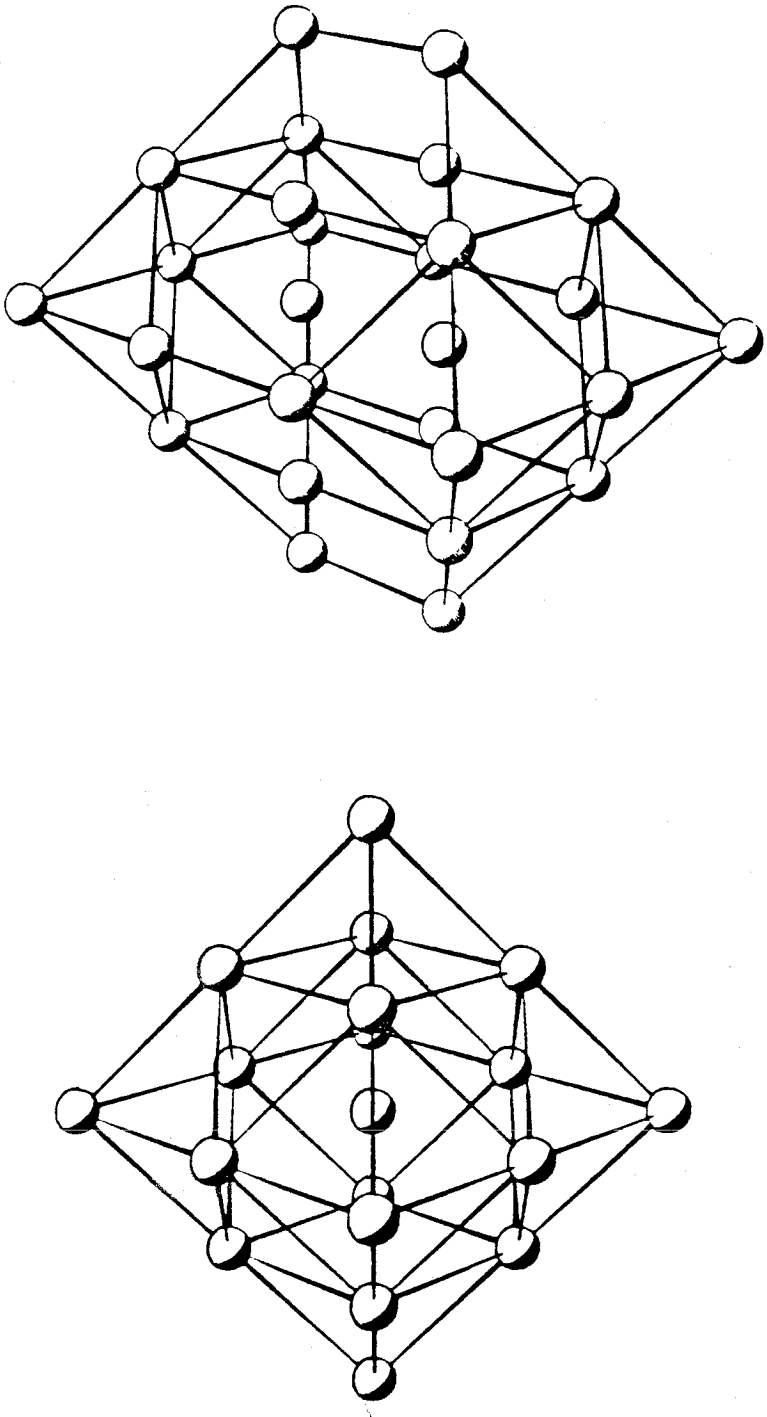

Figure 1: The 19 and 28 atom clusters.

cluster with these of an identical (13 atom) cluster in which the $3d^9$ averaged potential was used on all centers.

As in previous work, the 3d basis functions were those of Wachters,[12] while the 4s and 4p functions used were constructed from the most diffuse (valence) gaussians obtained for that same basis set. These are summarized, along with the effective potentials used, in Appendix V.A. This resulted in 65 and 77 function basis sets for the Ni_{13S} (13 electron) and Ni_{13d} (22 electron) calculations, respectively. The 4s-p basis was also used in calculations on the 19 and 20 electron clusters, to be labelled as Ni_{19S} and Ni_{20S}, respectively. To study trends in the conduction band properties of all of the clusters, the double zeta 4s gaussian set also used without 4p functions, resulting in calculations ranging in size from 26 basis functions for Ni_{13} to 174 functions for Ni_{87}. Hereafter the 4s-p basis will be denoted as Dz+p, and the smaller double zeta 4s basis as imply DZ.

III. The Thirteen Atom Clusters

A. Character of the wavefunctions

For the Ni_{13S} and Ni_{13d} clusters, extensive calculations were carried out to determine the character and separation of the low-lying states. All calculations on the Ni_{13d} cluster led to two distinct sets of orbitals, a set of five 3d-like orbitals localized near the central Ni and a set of 4s, 4p-like orbitals fully delocalized over the complex. For simplicity these orbitals will be referred to as the 3d- or 4s-band orbitals.

1. The 3d Configuration

In terms of O_h symmetry the d orbitals on the central Ni are of t_{2g} and e_g symmetry. Ignoring for the moment the 4s band, the two lowest states are of $(3d)^9$ character:

$$[t_{2g}] \equiv {}^2T_{2g} = (e_g)^4 (t_{2g})^5 \tag{1}$$

$$[e_g] \equiv {}^2E_g = (e_g)^3 (t_{2g})^6, \tag{2}$$

which we will denote as $[t_{2g}]$ and $[e_g]$, indicating the location of the hole in the d^9 configuration. Even though the d orbitals are rather localized on the central Ni atom there are interactions with the 4s band orbitals and the adjacent Ni cores, leading to a splitting of the t_{2g} and e_g orbitals. The states leading to this description are summarized in Table I. The first two states in the table result from solving for each $[e_g]$ configuration along with the lowest 4s band occupation. As the 4s-band occupation is one component of a state of t_{2g} symmetry the energy of the wavefunction is insensitive to choice of 3d e_g hole (or 4s t_{2g} hole) and the two states are degenerate. Placing the 3d hole in the $[t_{2g}]$ configuration alters this however. Now both 3d and 4s holes are of t_{2g} symmetry and degeneracy is lost, as illustrated by the third through fifth states of Table I. To remove the effects of this specific choice of 4s band occupation, we average over these three states (E(ave) = -44.4188) and find that the $[t_{2g}]$ configuration is favored by 0.37 eV. Carrying out a similar analysis of the Ni_{13}^+ and Ni_{13}^- states also listed in the table reveals that in each the $[t_{2g}]$ configuration remains favored, by 0.23 eV and 0.54 eV, respectively. Thus the occupation of the 3d orbitals is

Table I: Low-Lying Neutral and Ion States of Ni_{13d} (with $4s^1 3d^9$ Central Atom)

Cluster State	Total Energy	Excitation Energy (eV)	4s Occupation									3d Occupation				
				t_{1u}			t_{2g}			e_g		t_{2g}			e_g	
			a_{1g}	x	y	z	xy	xz	yz	z^2	x^2-y^2	yx	xz	yz	z^2	x^2-y^2
	-44.4053	0.56	2	2	2	2	2	2	1	0	0	2	2	2	2	1
	-44.4053	0.56	2	2	2	2	2	2	1	0	0	2	2	2	1	2
	-44.4045	0.58	2	2	2	2	2	2	1	0	0	2	2	1	2	2
Neutral	-44.4259	0.0	2	2	2	2	2	2	1	0	0	2	1	2	2	2
Ni_{13}	-44.4259	0.0	2	2	2	2	2	2	1	0	0	1	2	2	2	2
	-44.4018	0.66	2	2	2	2	1	1	1	1	1	1	2	2	2	2
	-44.3954	0.83	2	2	2	2	1	1	1	1	1	2	2	2	2	1
	-44.3993	0.72	2	2	2	2	1	1	1	1	1	2	2	2	1	2
	-44.2626	0.0	2	2	2	2	2	1	1	0	0	1	2	2	2	2
Positive Ion	-44.2394	0.63	2	2	2	2	1	1	2	0	0	1	2	2	2	2
	-44.2386	0.65	2	2	2	2	1	2	1	0	0	2	2	2	2	1
Ni_{13}^+	-44.2386	0.65	2	2	2	2	1	1	2	0	0	2	2	2	1	2
Negative Ion	-44.4620	0.0	2	2	2	2	2	2	2	0	0	1	2	2	2	2
Ni_{13}^-	-44.4421	0.54	2	2	2	2	2	2	2	0	0	2	2	2	2	1

sensitive to the 4s band configuration, with $[t_{2g}]$ being most favored when the t_{2g} field of the conduction orbitals is strongest. This bias towards t_{2g} symmetry in the conduction band orbitals may be eliminated by solving for a low-lying excited state of the 4s-band (vide infra) in which each t_{2g} and e_g orbital is singly occupied. These states, the final neutral entries in Table I, lead to a preference for $[t_{2g}]$ of only 0.12 eV.

By promoting an electron from the 3d shell on the central Ni to the 4s band it was possible to consider $3d^8$ states of this cluster. As shown in Table II, the lowest energy 4s configuration has filled t_{2g} orbitals, thus it is not surprising that the lowest 3d configuration is:

$$^3[t_{2g}, t'_{2g}] \equiv {}^3T_{2g} = (e_g)^4 (t_{2g})^4 \qquad (3)$$

lying at 1.03 eV above the $[t_{2g}]$ state. The highest triplet d^8 state is found to be

$$^3[e_g, e'_g] \equiv {}^3A_{2g} = (e_g)^2 (t_{2g})^6 \qquad (4)$$

lying 2.65 eV above $[t_{2g}]$. The positive ion states, also included in the table are incomplete, making a clear assessment of the trends difficult. Qualitatively however, the preference for $^3[t_{2g}, t'_{2g}]$ is seen to be preserved upon removal of an electron from the 4s t_{2g} orbital. An attempt was made to solve for states with a $3d^{10}$ occupation on the central atom, however, it was found that these solutions were numerically unstable with respect to collapsing into the lower $3d^9$ states of the cluster.

Table II: Low-Lying Neutral and Ion States of Ni_{13d} (with $4s^2 3d^8$ Central Atom)

Cluster State	Total Energy	Excitation Energy (eV)	4s Occupation									3d Occupation				
			a_{1g}	t_{1u}		t_{2g}			e_g			t_{2g}			e_g	
				x	y	z	xy	xz	yz	z^2	x^2-y^2	yx	xz	yz	z^2	x^2-y^2
Neutral	-44.3810	0.0	2	2	2	2	2	2	2	0	0	1	1	2	2	2
Ni_{13}	~-44.3610	~0.5	2	2	2	2	2	2	2	0	0	1	2	1	1	2
	-44.3216	1.62	2	2	2	2	2	2	2	0	0	2	2	2	1	1
Positive	-44.2107	0.0	2	2	2	2	2	2	1	0	0	1	1	2	2	2
Ion	-44.1444	1.80	2	2	2	2	1	2	2	0	0	1	2	2	1	2
Ni_{13}^+	-44.1383	1.97	2	2	2	2	1	2	2	0	0	2	2	2	1	1

2. The Conduction Band Configurations

The reducible representation consisting of the thirteen 4s orbitals in the Ni_{13} cluster may be broken down into two a_{1g} representations and one each of e_g, t_{1u}, t_{2u}, and t_{2g} symmetries. The low-lying 4s symmetry (molecular) orbitals may be classified according to these symmetry types and have shapes that may be understood by analyzing each in terms of its angular momentum (with respect to the central atom). Thus the orbitals are 1s-like ($1a_{1g}$), 2s-like ($2a_{1g}$), 2p (t_{1u}), 3d (t_{2g}, e_g) and 4f (t_{2u}). It is not surprising then that they may be ordered in energy as:

$$1a_g,\ t_{1u},\ t_{2g},\ e_g,\ 2a_g,\ t_{2u}$$

where only the $2a_g$ orbital appears in an unexpected position.

Focussing on those conduction band states that arise from a $3d^9$ occupation on the central atom, the ground state is seen to be (Table I):

$$^2[265000] = 1a_g^2\ t_{1u}^6\ t_{2g}^5\ e_g^0\ 2a_g^0\ t_{2u}^0$$

where we have used a simple occupation number scheme to define the state. The superscript 2 outside the brackets indicates the spin state (doublet). The only other state represented in Table I is:

$$^6[263200]$$

which, after averaging over the five possible $3d^9$ configurations, is found to be 0.36 eV above the ground state. In Table III, we show the

Table III: Conduction Band States of Ni_{13S}

Cluster State	Total Energy	Excitation Energy (eV)	Occupation						Orbital Energies[a]					
			$1a_{1g}$	t_{1u}	t_{2g}	e_g	$2a_{1g}$	t_{2u}	$1a_{ig}$	t_{1u}	t_{2g}	e_g	$2a_{1g}$	t_{2u}
	-4.3105	0.0	2	6	5	0	0	0	-.575	-.371	-.194	-	-	-
Neutral	-4.2997	0.29	2	6	3	2	0	0	-.571	-.366	-.216	-.177	-	-
Ni_{13}	-4.2980	0.34	2	6	4	1	0	0	-.575	-.369	-.202	-.172	-	-
	-3.9488	9.84	1	6	6	0	0	0	-.621	-.382	-.199	-	-	-
Positive	-4.1355	4.76	2	6	4	0	0	0	-.722	-.510	-.339	-	-	-
Ion	-4.1304	4.90	2	6	3	1	0	0	-.720	-.508	-.353	-.307	-	-
Ni_{13}^{+}	-3.7642	14.86	1	6	5	0	0	0	-.776	-.524	-.348	-	-	-
Negative Ion	-4.3576	-1.28	2	6	6	0	0	0	-.432	-.234	-.055	-	-	-
Ni_{13}^{-}	-4.3263	-0.43	2	6	3	2	1	0	-.435	-.229	-.093	-.052	-.038	-

[a]For fractionally occupied symmetries, orbital energies are an average of the individual occupied orbitals within that symmetry.

results of calculations on these same two states in which the $3d^9$ averaged potential was used on all atoms (the Ni_{13S} cluster). Here we see the splitting between these two states is 0.29 eV, in very good agreement with the self-consistent average value listed above. In addition, there is another low-lying state,

$$^4[264100]$$

at 0.34 eV above the ground state. The apparently anomalous ordering of the states (the lower state is doubly excited) arises from the increased exchange stabilization associated with the sextet ($S = \frac{5}{2}$) state.

The lowest ion states found in Table III are the positive ion:

$$^3[264000]$$

and negative ion:

$$^1[266000]$$

states obtained by adding or removing an electron from the t_{2g} shell. Although we defer detailed discussion of ionization processes to a later section, we note here that the positions of these ion states as calculated using the Ni_{13S} duster [4.76 eV for Ni_{13}^+; -1.28 eV for Ni_{13}^-] are in good agreement with average values extracted from the Ni_{13d} results in Table I [4.62 eV and -1.11 eV, respectively], lending further support to the concepts behind the $3d^9$ averaged potential.

3. Geometry Optimization

In previous work, we found that the optimum bond distance for the nickel dimer[8] was extremely short, at 2.04 Å. This contrasts sharply with the experimental bulk value for nearest neighbor separation of 2.487 Å.[11] Clearly, there must be a trend towards bond lengthening with increased coordination of the Ni atoms. Such a result would be expected for several reasons

a) with increasing coordination, the effective "bond order" of each Ni-Ni interaction should decrease;

b) increasing coordination should increase unshielded (short range) core-core or nuclear repulsions;

c) electron-electron repulsion and Pauli principle effects should increase with increasing coordination. The Pauli principle requires that bonding orbitals remain orthogonal, a difficult objective with high coordination.

These concepts are supported by experimental results for the alkali metals,[11,13] where dimer bond distances are significantly less than those of the metal.

To gain further insight into these phenomena bond distances were optimized in the Ni_{13S} cluster. As mentioned in Section II-A the $3d^9$ averaged potential reproduces the bond distance of the 20-electron dimer calculations, and thus the Ni_{13S} results should be reliable.

Calculations were carried out in which the fcc lattice parameter was varied for Ni_{13}, producing the results in Table IV. The calculated minimum leads to an optimum nearest neighbor separation of 2.406 Å,

Table IV: Lattice Parameter Variation: $Ni_{13}S$

Bond Distance (Å)	Lattice Parameter (Å)	Total Energy
2.01	2.84	-4.0254
2.28	3.22	-4.3190
2.38	3.37	-4.3433
2.49	3.52	-4.3344
2.59	3.66	-4.2994
	Optimum Values	
2.406	3.403	-4.3436

considerably longer than calculated for the dimer. It remains shorter than the experimental bulk value, a result that is in agreement with recent EXAFS results.[14]

IV. Larger Clusters: From Ni_{13} to Ni_{87}

A series of calculations examining conduction band properties was also carried out for clusters as large as 87 atoms using the double zeta 4s basis set. In the following discussion we will emphasize a description of trends in the macroscopic observable properties that arive from an analysis of the calculations. Thus reference to specific cluster states will be made only when necessary.

A. Work Function, Electron Affinity and Bandwidth

In Table V, we summarize these values for the conduction band as a function of cluster size. For the 13, 19, and 20-atom calculations were carried out using the more extensive 4s-4p basis set as described in previous sections. In all calculations the $3d^9$ averaged potential was used on each center.

The ionization potentials were calculated by two different methods. The simpler of the two is the Koopmans' Theorem method, in which ionization potentials are obtained as orbital energies from a Hartree-Fock calculation on the ground state of the neutral species. There are two major errors implicit in determining ionization potentials by this method:

TABLE V. Comparison of Calculated Cluster Properties. All energies are in eV.

	Number of Shells	Number of Atoms	Multiplicity of Ground State	Ionization Potential[b]		Bandwidth[a]		Electron Affinity	
				DZ[b] SCF (KT)	DZ + P[b] SCF (KT)	DZ[b] KT	DZ + P[b] KT	DZ[b] SCF	DZ + P[b] SCF
O_h	0	1	2	7.63 (7.63)	7.63 (7.63)	--	--	--	--
	1	13	2	6.18 (6.39)	4.76 (5.14)	12.6	10.5	2.62	1.28
	2	19	2	7.45 (7.67)	4.99 (5.36)	12.5	11.3	3.49	1.60
	3	43	4	5.10 (5.19)		15.4		2.07	
	4	55	6	5.52 (5.68)		16.5		2.91	
	5	79	4	5.92 (5.76)		16.1		3.16	
	6	87	2	4.86 (5.05)		16.3		2.75	
	∞	∞		5.2[c]	5.2[c]	--		5.2[c]	5.2[c]
D_{2h}	1	20	3	5.88 (5.77)	4.25 (4.68)	14.3	11.9	2.28	.81
	2	28	1	5.63 (5.74)		14.6		2.61	
	∞	∞		5.2[c]	5.2[c]	--		5.2[c]	5.2[c]

[a] Values in parentheses are from Koopman's Theorem. Values not in parentheses are from Hartree-Fock calculations on both neutral and ion states.

[b] DZ (double zeta) results are for basis sets with two s-like contracted functions per center; DZ+P results are for basis sets consisting of the DZ basis augmented with a single p-like gaussian in each direction on each center.

[c] Reference 15.

1) the orbital energies are obtained from a calculation on the neutral. Thus an IP obtained by this method is really measuring the energetic cost of removing an electron from an orbital whose shape is optimum for the neutral rather than the positive ion. This introduces a bias against the ion state (i.e., the implicit wavefunction for the ion is less optimum).

2) hartree-fock calculations do not account for electron correlation effects. As there are more electrons in the neutral than in the ion state there will be more electron-electron interactions in the neutral than in the ion for which correlation effects are important ($\frac{1}{2}N(N-1)$ for an N electron neutral vs. $\frac{1}{2}(N-1)(N-2)$ for the corresponding positive ion). Ignoring these interactions for both the neutral and the ion as is implicit in Koopmans' Theorem thus biases against the neutral.

Thus, there are errors with opposing directions, and in some cases cancellation occurs resulting in an accurate Koopmans' Theorem IP.

The second method involves calculating separate hartree-fock wavefunctions for both the neutral and ion states and subtracting total energies. By this method we avoid problem (1) above and the only error is due to (2). Typically, by biasing against the neutral, a low (too small) IP is obtained.

A cursory examination of Table V reveals two features:

1) the Koopmans' Theorem (KT) and self-consistent (SCF) IP values differ by only ~ 0.2 eV.

2) the trend is towards decreasing IP with increasing cluster size and fairly good agreement with the bulk value.

The fact that the KT and SCF values are quite close indicates that relaxation effects are small (~ 0.2 eV). The fact that both the KT and SCF values trend towards the bulk result further suggests that electron correlation effects also are small, perhaps a few tenths of an eV per electron. Thus a "free-electron" quality is evident in the conduction band states even for very small particles. The convergence in IP's towards the bulk value of 5.2 eV[15] is not monotonic, but for $N \geq 43$, it is within 0.5 eV of this value. The EA on the other hand, is still 2.5 eV smaller than the bulk value, even for N = 87! The reason for this may be seen by examining the energy expressions for the EA and IP of each system. For a neutral state with m singly-occupied orbitals in addition to a particular singly-occupied orbital o, the IP and EA differ by

$$IP - EP = J_{oo} + \sum_{n=1}^{m} K_{no} ,$$

where K_{no} are exchange integrals ($K_{no} \leq 0.01$ hartrees). In this sum, the dominant term is J_{oo}, the self-energy for orbital o. In Table VI, we see that J_{oo} is within 0.2 eV of the calculated (self-consistent) IP-EA for various clusters. For these Ni clusters, we find that $J_{oo}(eV) \approx 14.4/R(Å)$ for orbitals near the fermi energy. Thus, we expect convergence of IP-EA to be quite slow; in fact, for a cluster of 1146 atoms (R = 14.4 Å), the EA-IP should be ≈ 1 eV.

The significance of these results for chemisorption is as follows. For electronegative adsorbates (e.g., H, CH_3, OH) the charge transfer

TABLE VI. Convergence of IP-EA with Cluster Size.

Cluster	Neutral State	J_{oo}(eV)	IP-EA (eV)	$\frac{14.4}{R}$(eV)
Ni_{19}	$^2A_1$	3.96	3.71	4.09
Ni_{43}	$^2T_{2g}$	3.09	2.99	3.34
Ni_{55}	$^2T_{1g}$	2.92	2.75	2.90
Ni_{79}	-	-	2.64	2.58
Ni_{87}	-	-	2.35	2.36

is away from the cluster and hence it is the IP of the cluster that is relevant in determining bond energy. On the other hand, for electropositive adsorbates (such as Na, K, Li) the charge transfer should be towards the bulk and hence the EA is more relevant in determining bond energy. Since the cluster electron affinity is significantly less than that of the bulk, we would expect bond energies of electropositive species to be less on small aggregates than on the bulk surface. Electronegative species may well behave the same in both systems. Note that these results are <u>not</u> theoretical artifacts; the difference between IP and EA arises from the non-vanishing value of the self-energy and should be experimentally observable. It has been suggested[16] that electron tunnelling spectroscopy could provide a direct test of these predictions. Metal drops of ~ 50 Å would allow determination of the threshold for successive charge transfer to each drop.

As measured in a photoemission experiment, the width of the conduction band is the difference in IP between the highest MO and the lowest MO of the conduction band. For the Ni_{13S} cluster use of the Koopmans theorem leads to a 4s-bandwidth of 10.5 eV, whereas direct, self-consistent calculation of the corresponding ion states leads to a 4s-bandwidth of 10.10 eV. An alternative definition of the bandwidth is the excitation energy from the lowest band (using KT this is approximately equal to the previous definition). From direct self-consistent calculations we find for Ni_{13S} that this definition yields a bandwidth of 9.84 eV. Since all these definitions yield quite similar results, the use of the KT value (the usual approach) seems justified. These values are collected for each of the clusters in Table V. The conduction

bandwidth appears to be essentially converged to ~ 16 eV by N = 87. There are no established experimental values available for this property, but measurable energy state density has been found as much as 10-11 eV below the fermi level.[17]

B. Surface Electron Density

A property of interest both for understanding the surface properties of bulk metals and of clusters is the calculated surface electron density. In Fig. 2 we show electron populations as a function of shell radius for the largest cubic clusters, N = 55, 79, and 87 atoms. Two factors appear to control the surface density in these clusters:

(i) As the number of shells possessing full coordination (12 nearest neighbors for a bulk fcc atom) increases, the fluctuations in electron density as a function of radius are reduced.

(ii) Absolute cluster size does not fully determine surface density as indicated by the Ni_{79} and Ni_{87} results. The coordination number of the surface atoms is of considerable importance in determining the magnitude of the density of electrons at the surface.

The implications of these results for the infinite system are:

i) The surface atoms may be electron-deficient with the deficiency greater for less dense surfaces [i.e., $\rho_{(111)} > \rho_{(100)} > \rho_{(110)}$], which may relate directly to changes in work function and reactivity for different surfaces.

ii) The layers just below the surface may have electron densities greater than the bulk. Thus electronegative interstitials may be

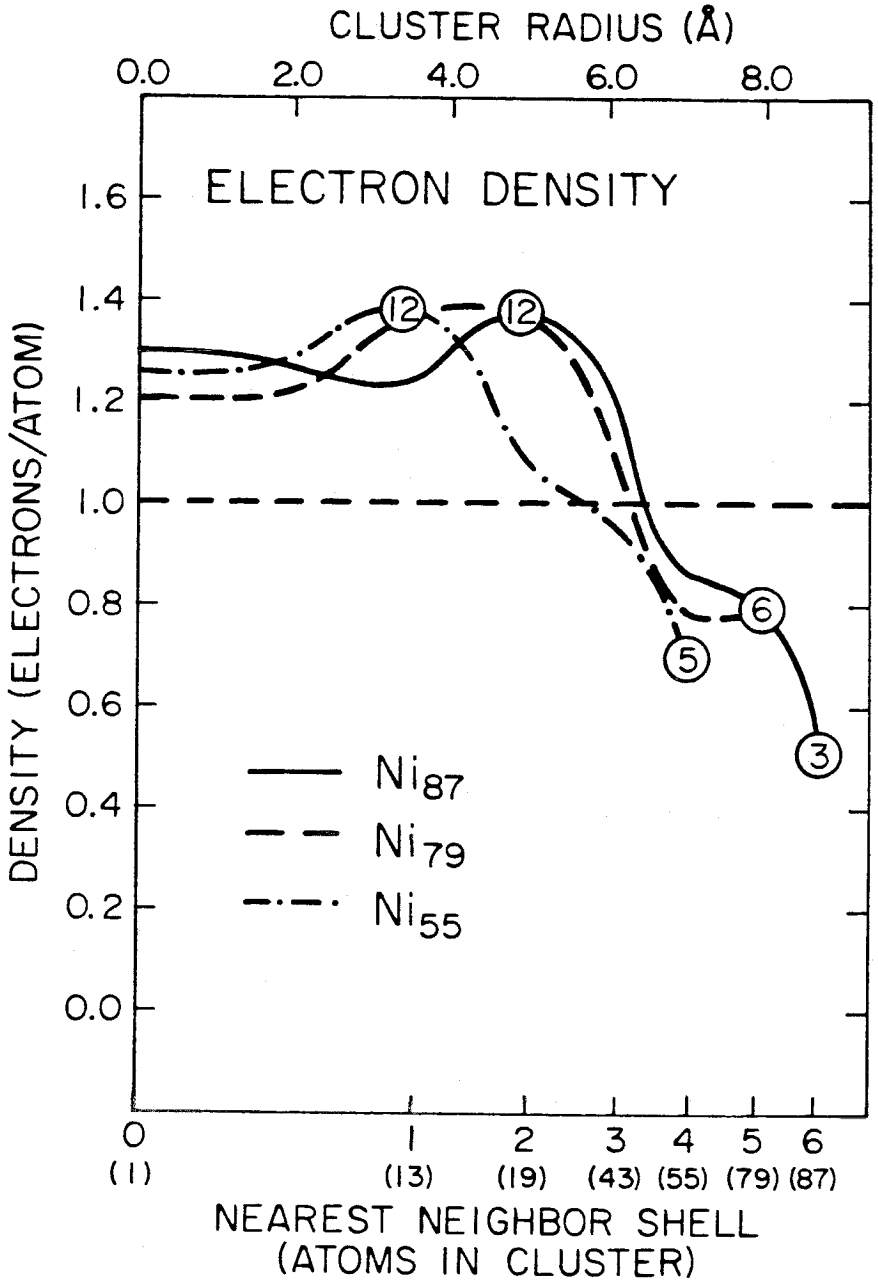

Figure 2: Electron density oer atom for largest clusters plotted as a function of nearest-neighbor shell. Dashed line indicates the average bulk density.

more localized in these near-surface regions, while electropositive interstitials may have a significant barrier to moving from the bulk to the surface layer.

iii) The structure near the surface may have a non-uniform behavior corresponding to the non-uniform density. For example, these results would suggest that a larger spacing should occur between the outermost layers, while some layers slightly below the surface may be closer together than the bulk spacing.

iv) Corner atoms at steps and kinks should be even more electron-deficient than the remaining surface atoms and hence more reactive towards nucleophiles, as has also been suggested by other investigators.[18]

v) To better mimic surface atoms, the outer atoms of the cluster should have coordination numbers approaching those of the actual surface. In this respect, the 79-atom cluster should be a more successful surface model than the 87-atom cluster.

vi) As an extension of (iv) above, the complexes with a low coordination number for the outer shell may be more appropriate as models for the reactivity of steps and kinks than the infinite surface.

C. Densities of States

In Fig. 3 we show the orbital energies obtained for the ground state of each of the six cubic clusters. As each level represents an approximate ionization potential (Koopmans' Theorem), the range of energies shown in each case represents an effective cluster density

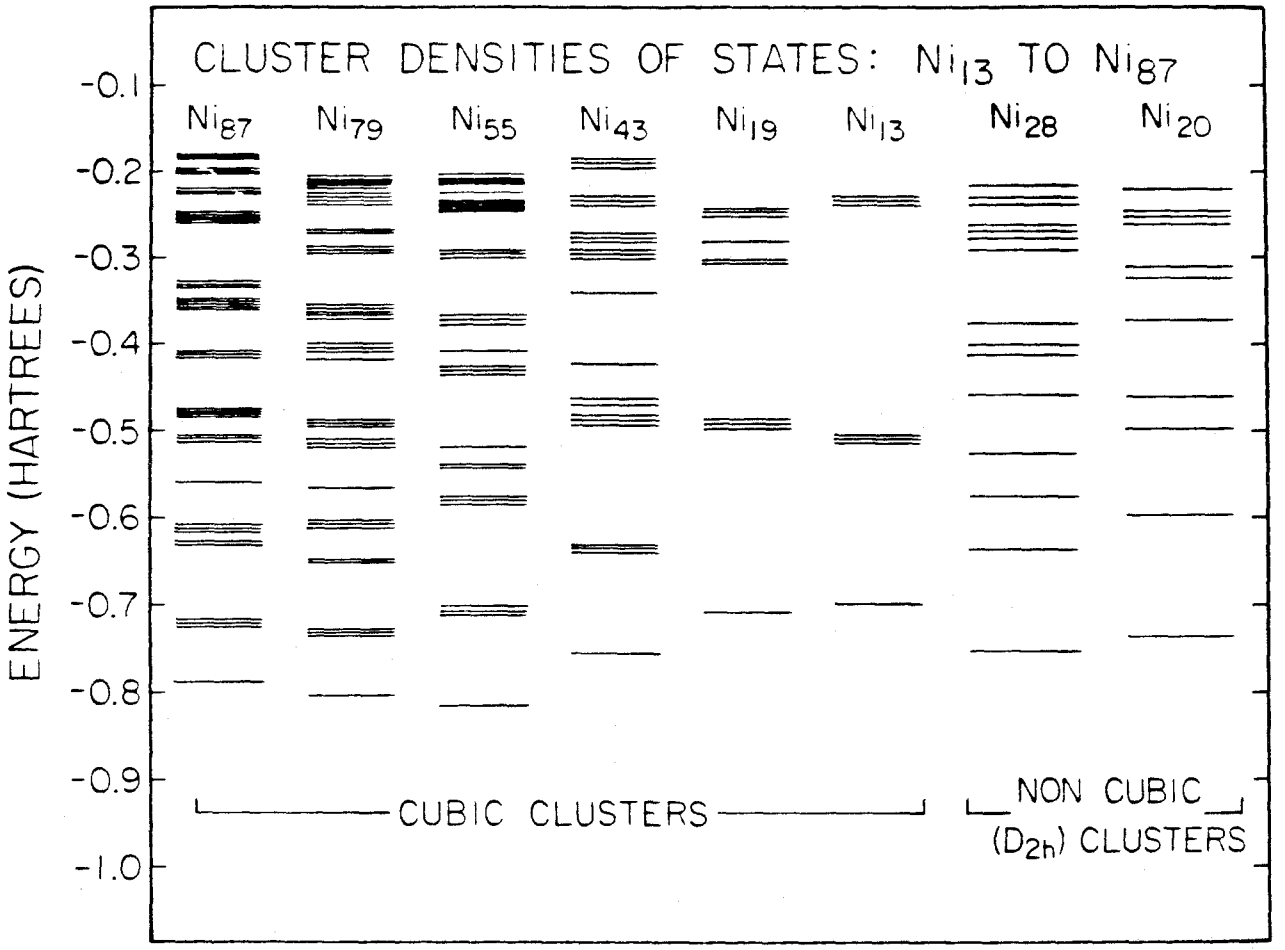

FIG.3. Approximate densities of states for both cubic and D_{2h} clusters. Levels are obtained as orbital energies from Hartree-Fock calculations. Degenerate levels have been plotted as multiplets to indicate actual state density. Only occupied states are shown.

of states (levels that are doubly or triply degenerate have been plotted as closely spaced groups of lines to indicate this degeneracy). The 13- and 19-atom clusters show a very discrete spectrum, and only the clusters larger than 43 atoms show a rather continuous density of states. For these clusters there is an increase in density near the fermi level, in agreement with the ideas of simple, nearly free-electron band theory.[19]

While the absolute positions of orbital energies are not of great importance in the formation of chemisorptive bonds, they are of importance in producing a reliable description of the photoemission properties of the bonding. As was discussed in a previous section, the Koopmans' Theorem IP values (orbital energies) are reliable for the clusters. Thus it would be of interest to determine how the cluster levels shift in position in response to adsorbate bonding.

It is clear, however, that the highly degenerate levels exhibited by the 13-atom cluster would be inadequate for this purpose. Such a discrete spectrum is in no way representative of the bulk conduction band ionization spectrum. Thus, to attempt to extract such information as chemisorption-induced adsorbate level width, adsorbate level position, or changes in bulk photoemission (attenuation or intensification) as a result of adsorption, from the smaller cubic clusters would not be effective. A good cluster for modelling chemisorption on the solid surface should exhibit a density of states that is as continuous as possible. Based on these considerations, the 13-, 19-, and 43-atom clusters are quite inadequate and even the 79- and 87-atom clusters are barely satisfactory. The non-degenerate D_{2h} clusters, Ni_{20} and Ni_{28}

show a much more continuous spectrum of orbital energies, as Fig. 3 indicates. For the ultimate purpose of modelling observable properties of chemisorbed species, we would expect clusters of this type to be more effective.

D. Cohesive Energies

The calculation of total energies for each of the clusters allows some comments to be made regarding trends in cohesive energies.

To define cohesive energies we must first develop some concept of "bond breaking" in a metallic system. The highly diffuse 4s bonding orbitals do not admit a simple concept of individual metal-metal bonds. Nevertheless, some accounting must be made for the different degrees of coordination represented by the surface atoms of various faces and atoms fully imbedded in the bulk. This consideration is of significant importance for small clusters where the (surface atoms)/(bulk atoms) ratio is quite high.

We define total cohesive energy as follows:

$$E_{BOND} = \sum_{i=1}^{\infty} \ell_i \frac{E_{BULK}}{12}$$

where ℓ_i is the ligancy of atom i in the bulk, and E_{BULK} is the bond energy contribution of a single fully-coordinated atom imbedded in the bulk. An fcc lattice is assumed here, where maximum coordination is 12.

Using this definition of cohesive energy we may consider two further quantities, the energy of vacancy formation:

$$\Delta H_{vac} = E_N + E_{N-1} = E_{BULK} + 12 \cdot \frac{E_{BULK}}{12} = 2E_{BULK} \quad (1)$$

and the vaporization energy:

$$\Delta H_{vap} = E_N - E_{N-1}(SURFACE) = \ell_i(SURF) * \frac{E_{BULK}}{12} + \ell_i(SURF) * \frac{1}{12} E_{BULK} =$$

$$= \frac{\ell_i}{6} E_{BULK} \cdot \quad (2)$$

In ΔH_{vac}, there is a contribution due to the atom being removed from the bulk as well as fractional contributions from each of its 12 neighbors. The quantity ΔH_{vap} differs only in that the coordination of the surface atom being removed will be less than 12. Experimentally, ΔH_{vap} is known to be 4.43 eV,[21] and assuming $\ell_i = 9$ (as for a (111) surface) produces $\Delta H_{vac} = 5.92$ eV and $E_{BULK} = 2.96$ eV.

For small clusters, it is of interest to determine how the quantity E_{BOND} will change as a function of cluster size. Assuming a simple cubic lattice with N atoms on each side gives:

$$E_{BOND} = N^3 E_{BULK} - 6N^2 \cdot \frac{1}{6} E_{BULK}$$

or

$$\frac{E_{BOND}}{n} = E_{BULK}(1 - n^{-0.33})$$

where in the first expression the first term assumes full coordination of all atoms, and the second term corrects for the incomplete coordination of the surface atoms. Setting $N^3 = n$ produces

the second simpler expression. This is, in face quite close to the expression obtained empirically by Freund and Bauer:[20]

$$\frac{E_{BOND}}{n} = E_{BULK}\,(1 - 0.91\,n^{-0.235})$$

through a best fit to theoretical and experimental sublimation data for a number of metal particles.

A similar analysis may be made for metal particles arranged in fcc lattice structures. For simplicity, the clusters will be assumed to be spherical with surfaces composed of (111) facets, an arrangement that most closely resembles the features of the clusters used here. Using the general form:

$$E_{BOND} = \text{BULK TERM} * E_{BULK} - \text{SURFACE CORRECTION} * E_{BULK}$$

and noting that for an fcc lattice:

$$\text{VOLUME/ATOM} = b^3/\sqrt{2} \qquad \text{AREA(111)/ATOM} = \sqrt{3}/2b^2$$

gives:

$$E_{BOND} = \frac{\frac{4}{3}\pi R^3}{b^3/\sqrt{2}} \cdot E_{BULK} - \frac{4\pi R^2}{\sqrt{\frac{3}{2}}\,b^2} \cdot \frac{4}{12}\,E_{BULK}$$

where R is the radius of the spherical cluster and b is the bond distance between metal atoms. Noting that

$$\frac{\frac{4}{3}\pi R^3}{b^3/\sqrt{2}} = n$$

results in the form:

$$\frac{E_{BOND}}{n} = E_{BULK}\left[1 - 1.1080\, n^{-\frac{1}{3}}\right].$$

A similar analysis carried out using (100) facets gives:

$$\frac{E_{BOND}}{n} = E_{BULK}\left[1 - 1.2792\, n^{-\frac{1}{3}}\right]$$

and for (110) facets:

$$\frac{E_{BOND}}{n} = E_{BULK}\left[1 - 1.1306\, n^{-\frac{1}{3}}\right]$$

and thus the final equation is not strongly sensitive to assumptions made about surface structure.

In Fig. 4 we have plotted the total bond energy per atom against $n^{-\frac{1}{3}}$ for each of the clusters from 13 to 87 atoms (using the double zeta basis). Calculating a least-squares fit to the data produces an equation of the form:

$$\frac{E_{BOND}(eV)}{n} = 1.95\left[1 - 1.3216\, n^{-\frac{1}{3}}\right].$$

Fitting a line to the Ni_{13S} and Ni_{19S} data gives a coefficient of a = 1.1137 and produces an E_{BULK} value of 2.65 eV. Finally, we note that taking the "experimental" value for E_{BULK} = 2.96 eV along with the same value of a produces the third line shown in the figure. The intercepts establish the n = ∞ limit of bond energy per atom, and

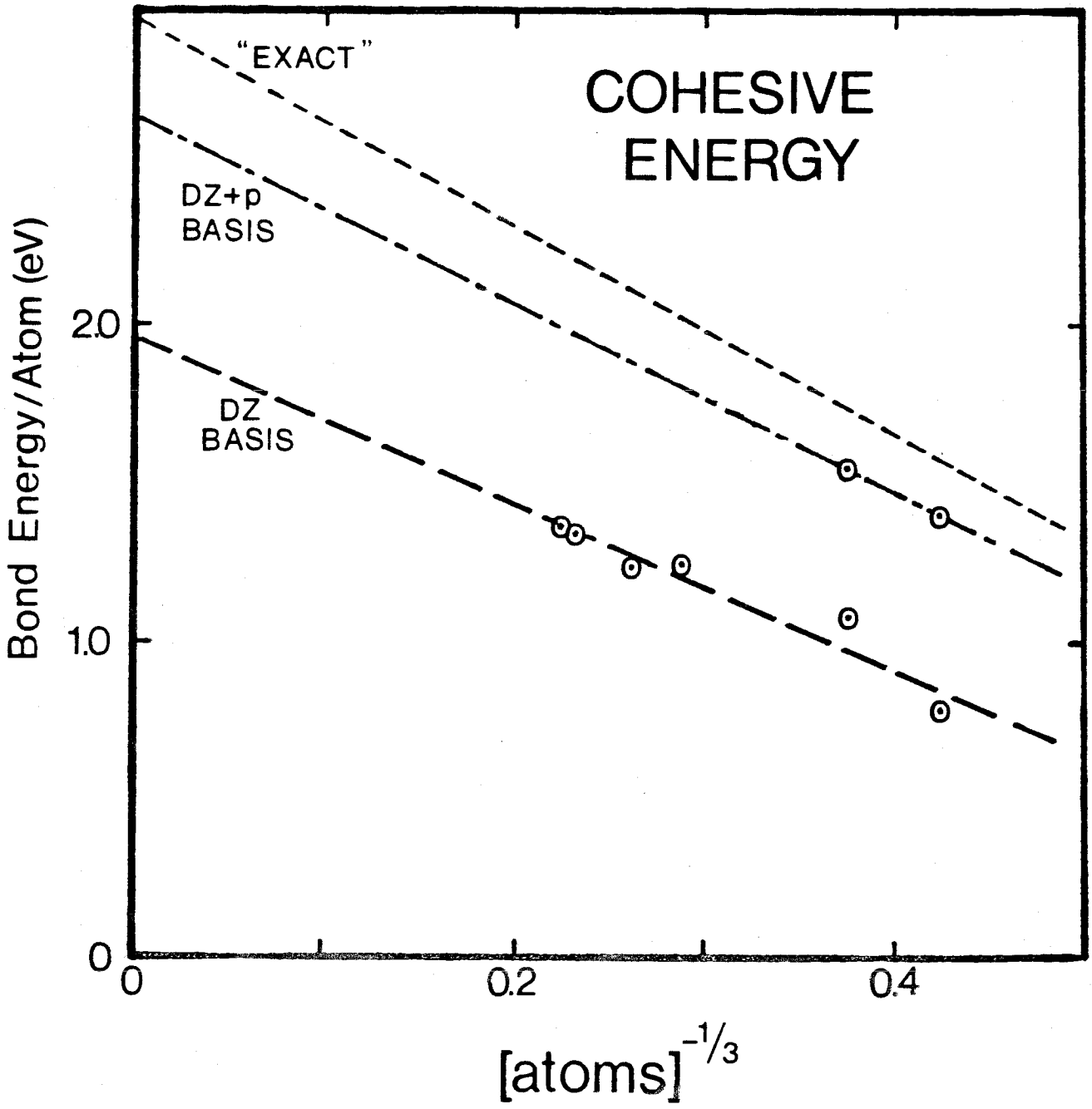

Figure 4: Cohesive energies of small particles as a function of cluster size. Data points are from calculations. "Exact" line uses the slope of the DZ+p line and the "exact intercept ($n = \infty$).

suggest that improvements in basis sets and wavefunctions for the clusters (i.e., inclusion of electron correlation) should only produce a change of about 0.2 eV per electron in the total bond energy. Typically, for small molecules the corresponding values is about 1.0 eV per electron. It would seem then that electron correlation effects are of less importance in metal-metal bonding and that in many cases a hartree-fock description of the cluster will be adequate.

The E_{BULK} value obtained from the double zeta data translates into a ΔH_{vap} of 2.93 eV (assuming $\ell_i = 9$) using the prescription of equation (2). It also provides a limiting value for ΔH_{vac} of 3.90 eV. To test the reliability of the concepts used in generating the ΔH_{vac} value, additional calculations were carried out on each of the cubic clusters in which the central atom was removed. Comparison of the total energies of the Ni_n and Ni_{n-1} clusters allows a direct evaluation of ΔH_{vac} as a function of cluster size. In this case, the binding energy of a specific atom is being monitored, as opposed to the average binding energy per atom that was used to construct Fig. 4. As a result, the data are more sensitive to the specific electron density distribution in the cluster as exhibited in Table VII. Although not monotonic, there does appear to be a trend in the data towards the independently evaluated "bulk" value of 3.90 eV.

E. Summary

From studies of the change in conduction band states of metallic clusters as a function of cluster size, we have obtained data on the convergence of electronic properties towards bulk values. We find

Table VII: Calculation of ΔH_{vac} Using DZ Basis

Number of Atoms	$E_{N-1}-E_N$ (eV)	Predicted[a] (eV)
13	0.75	1.71
19	0.83	1.97
43	3.24	2.43
55	1.96	2.54
79	2.30	2.70
87	3.03	2.74
∞	--	3.90

[a]Estimated using DZ fit in Fig. 4.

that although there is convergence of almost all properties, the rate at which these values change towards the bulk value varies widely. We have attempted to determine the nature of these variations in such a manner as to provide insight into how well the surface may be represented in a theoretical study of chemisorption. In addition, the implications of these results on the behavior of different infinite metal surfaces is considered. We find that small clusters have some properties differing from bulk surfaces, perhaps leading to changes in their chemisorptive and catalytic properties.

References and Notes

1. A. Redondo, W. A. Goddard III and T. C. McGill, Solid State Commun., submitted.
2. W. A. Goddard III and T. C. McGill, J. Vac. Sci. Technol., 16, 1308 (1979).
3. G. T. Surratt and W. A. Goddard III, Solid State Commun., 22, 413 (1977).
4. T. H. Upton and W. A. Goddard III, Phys. Rev. Lett., 42, 472 (1979).
5. Part II.B of this thesis.
6. M. Sollenberger, M.S. Thesis, Calif. Inst. of Technol., 1977.
7. A. K. Rappé and W. A. Goddard III, J. Am. Chem. Soc., 99, 3966 (1977).
8. T. H. Upton and W. A. Goddard III, J. Am. Chem. Soc., 100, 5659 (1978); see also Part II.A of this thesis.
9. C. F. Melius, T. H. Upton, and W. A. Goddard III, Solid State Commun., 28, 501 (1978).
10. W. J. Hunt, W. A. Goddard III, and T. H. Dunning Jr., Chem. Phys. Lett., 6, 147 (1970).
11. W. P. Pearson, "Handbook of Lattice Spacings and Structures of Metals and Alloys," (Pergamon, New York, 1958).
12. A. J. H. Wachters, J. Chem. Phys., 42, 1293 (1965).
13. G. Herzberg and K. P. Huber, "Constants of Diatomic Molecules," (Van Nostrand Reinhold, New York, 1979).
14. G. Apai, J. F. Hamilton, J. Stohr, and A. Thompson, Phys. Rev. Lett., 43, 165 (1979).

References (continued)

15. A. A. Holscher, Surf. Sci., 4, 89 (1966).

16. R. C. Jaclevie, Ford Motor Co. (private communication).

17. C. S. Fadley and D. A. Shirley, Phys. Rev. Lett., 21, 980 (1968).

18. G. A. Somerjai, J. Coll. Interfac. Sci., 58, 150 (1977).

19. See for example W. A. Harrison, "Solid State Theory," (McGraw-Hill, New York, 1970).

20. H. J. Freund and S. H. Bauer, J. Phys. Chem., 81, 994 (1977).

PART THREE:

Atomic Adsorption on Large Nickel Cluster Surfaces

I. INTRODUCTION

In the last few years considerable advances have been made in the characterization of adsorbed species, largely as a result of dramatic improvements in the application of experimental probes (for example HRELS,[1] XPS,[2] UPS,[3] LEED,[4] and TPDS.[5] While this has greatly increased the understanding of specific systems, it has not as yet led to the formation of a conceptual basis which might be used to make semi-quantitative predictions about the observable properties of new systems. Predictions of this type are critical in assessing the relative importance of possible reactive intermediates, species too short-lived for observation by conventional experimental methods. Without such data it will be difficult to draw unambiguous conclusions about mechanisms in heterogeneous catalysis.

As our initial contribution to the development of such a conceptual understanding we have begun a systematic study of a sequence of atomic adsorbates on nickel surfaces. In this paper, we have used an Ni_{20} cluster as a model for the bulk, and have considered in detail the bonding of H, Cl, Na, O, and S at four-coordinate, two-coordinate, and terminal sites representative of the corresponding sites on the bulk Ni(100) surface. Complementary data are also presented for hydrogen on binding at sites representative of the (111) face. From the trends that emerge, we may characterize more precisely the properties of not only the adsorbates, but the adsorption sites themselves. Thus we may use the distinctive behavior of the different adsorbates to develop such concepts as the pi and sigma basicity of each type of site, principles

that should be of importance in determining adsorbate site preference.

In this study all wavefunctions were generated at the Hartree-Fock or Generalized Valence Bond level (where electron correlation effects were included in the metal-adsorbate bonds). The calculational details are collected in Appendix V.A. The Ar core of Ni and the Ne core of Na, S, and Cl were replaced by effective potentials.[6] For the latter three, this allowed truncation of the basis set to include only a double zeta or split valence set of functions appropriate for the 3s, 3p shell.[6] In addition, for Ni the 3d electrons were required to retain the shape of atomic 3d orbitals appropriate for a $4s^1\,3d^9$ valence configuration[7] (spherically averaged to eliminate bias towards a particular $3d^9$ configuration). For most calculations this averaged $3d^9$ shell was incorporated into the Ar core potential (which included corrections for intra-atomic electron-correlation effects).[6] A double zeta basis was used to describe the remaining 4s orbital.[7]

In the next section we begin with a discussion of the relevant electronic properties of the Ni_{20} cluster. This will be followed by a detailed discussion of hydrogen chemisorption emphasizing the qualitative aspects of bonding at sites of importance on all of the low index faces of nickel [(100), (110), and (111)]. A comparison with similar results obtained using a 28 atom cluster[8] will be given in Appendix III.A. In Section III, a qualitative discussion of the bonding of all other atomic species will be presented in which the Ni(100) sites will be emphasized. In the final sections a more quantitative discussion of the bonding will be presented in light of their experimental implications.

II. HYDROGEN CHEMISORPTION

A. The Ni_{20} Cluster. The atom positions used in the 20 atom cluster were arranged to be consistent with the fcc lattice of bulk nickel, including the experimental 2.48 Å nearest neighbor separation.[9] The cluster consists of two adjacent atoms, each surrounded by their full complement of 12 nearest neighbors. As indicated in Fig. 1, the major facets of the cluster are (100) and (111) planes. Arrows indicate four-coordinate sites on the (100) plane (to be denoted hereafter as 4(100), as well as two-coordinate and one-coordinate or terminal sites [2(100) and 1(100), respectively]. Three-coordinate 3(111) sites are also shown. These sites correspond to sites of the same symmetry on the bulk surfaces and will be used to model chemisorption on these faces.

The orbitals of the Ni_{20} cluster occupied by the 4s electrons are delocalized, with "conduction-band" character. The orbitals of the ground state of the cluster are shown in Fig. 2, and the orbital energy spectrum produced is shown in Fig. 3.[10] They possess an approximate lattice periodicity with a lowest "$\underset{\sim}{k} = 0$" nodeless orbital and higher orbitals falling roughly into groups characterized by increasing periodicity along symmetry directions. The orbital energies define a "bandwidth" of 14.3 eV and indicate an ionization potential (I), or approximate "work function" of 5.9 eV. The ionization potential is considerably less than the experimental value of 7.6 eV for an isolated Ni atom[11] much closer to the bulk work function of 5.2 eV.[12] Thus, we might expect the cluster to behave in a manner analogous to the bulk

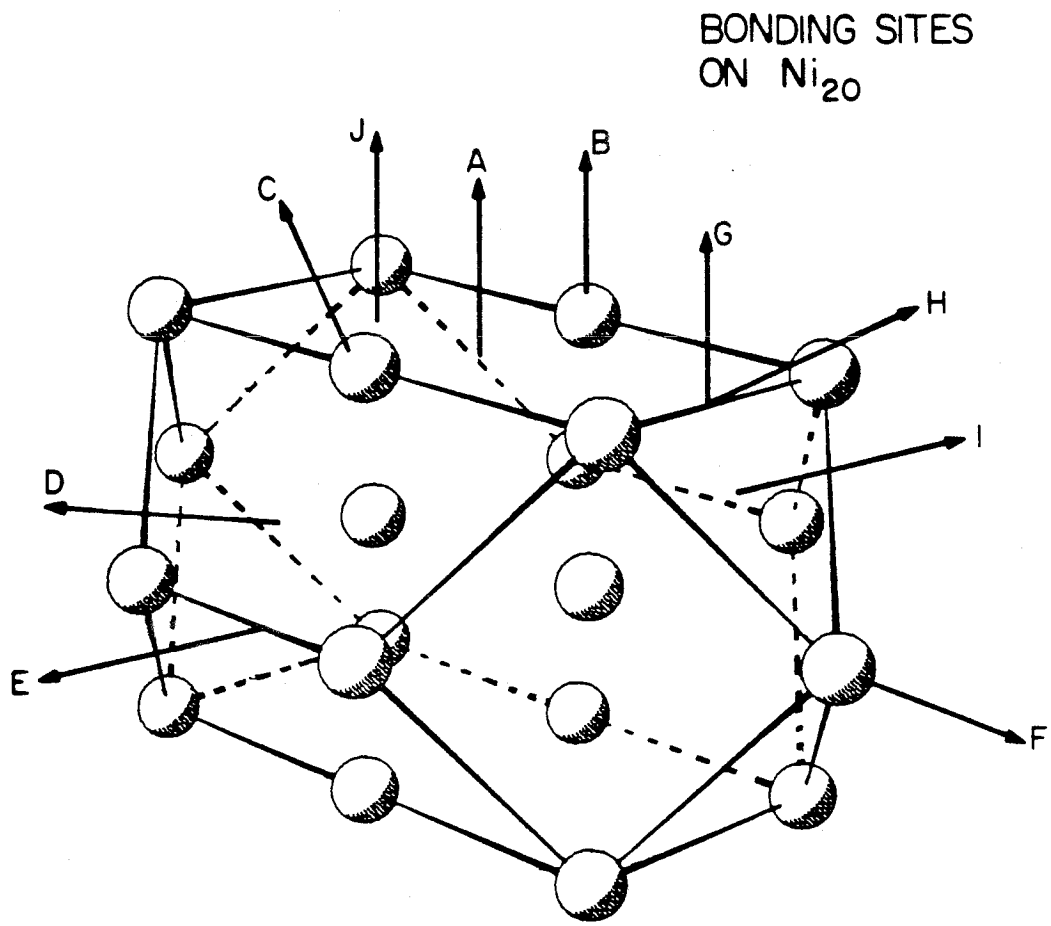

Figure 1: The Ni_{20} cluster with bonding sites indicated. Optimization of $R(\perp)$ was done along the surface normals shown at each site.

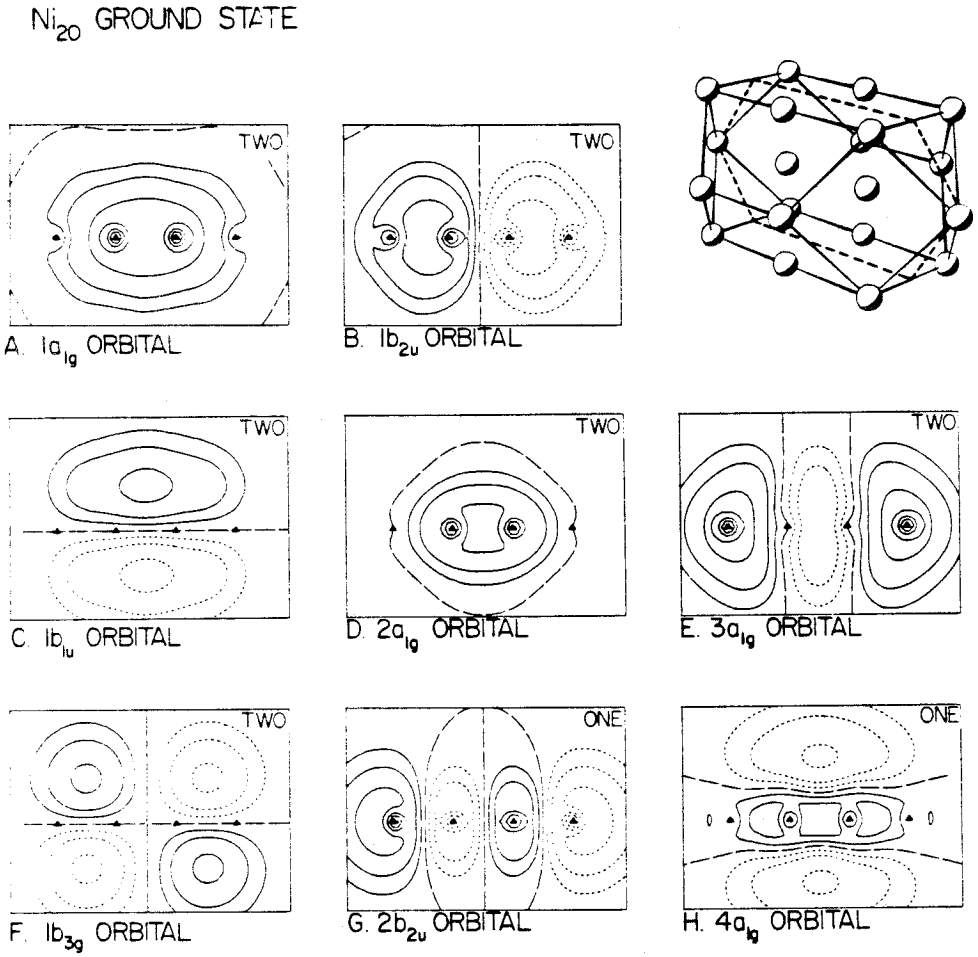

Figure 2: Bonding orbitals for Ni_{20}. Amplitudes are plotted in the (110) plane shown as a heavy dashed line in the cluster illustration at upper right.

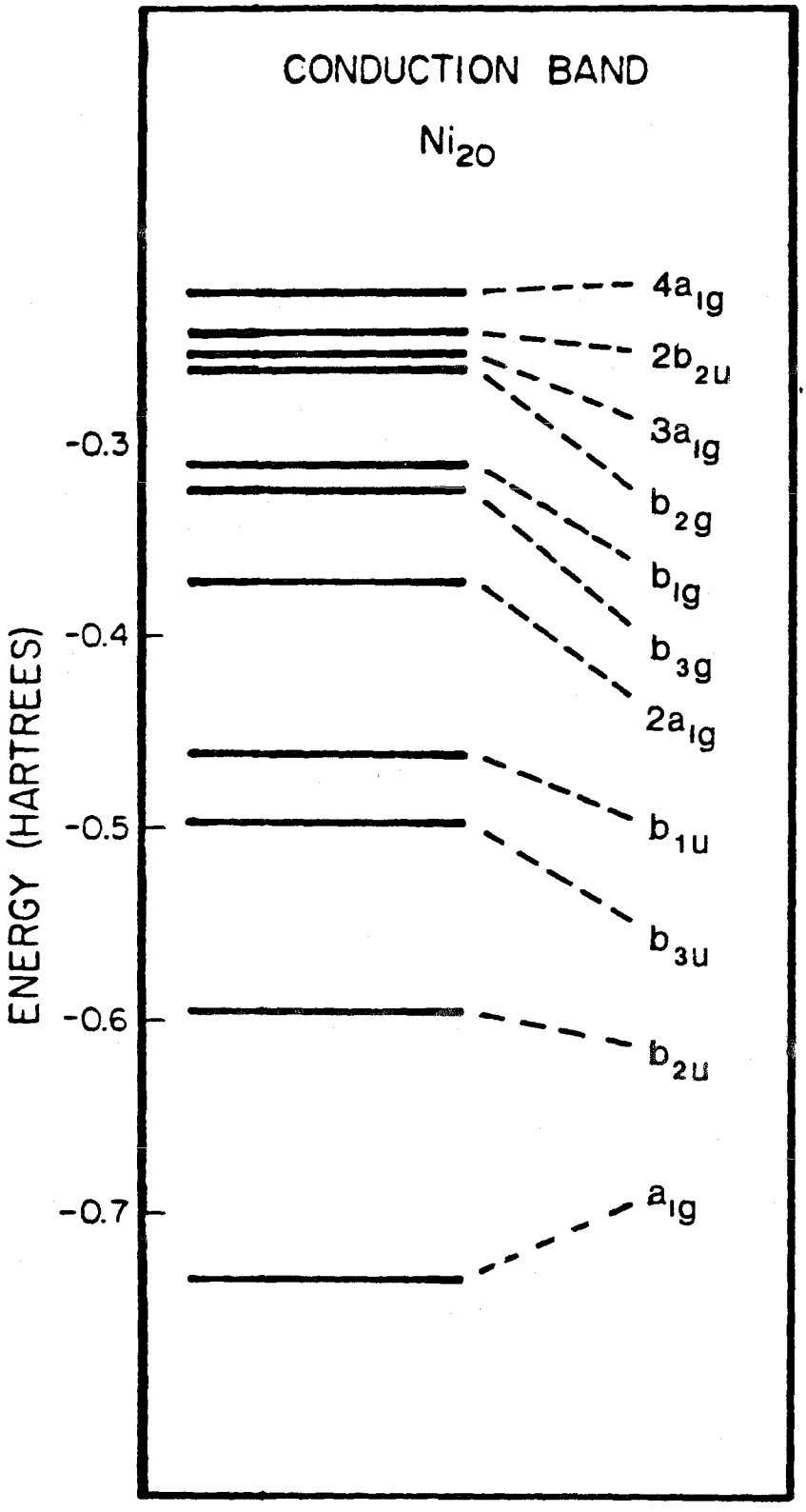

Figure 3: Orbital energy spectrum for Ni_{20}.

when bonded to electronegative species. On the other hand, the electron affinity (EA) of the cluster (obtained by calculating the total energy of its lowest anionic state) is only about 2.5 eV, well below the bulk value of 5.2 eV.[12] As discussed elsewhere[8,10] this finding is not a calculational artifact, and has important implications for chemisorption on small particles. Since the bonding of electropositive species, such as sodium should involve significant charge transfer to the surface, the small EA of Ni_{20} should lead to less charge transfer, and thus longer and weaker bonds than are observed in Na-bulk interactions.

As would be expected of a realistic bulk model, there are a number of low-lying electronic states for the 4s "conduction band". These are sampled in Table I. The ground state of the cluster is a triplet state, with the singly occupied orbitals of Fig. 2 being high-spin coupled. In addition to this, there are nine other triplet states within about 2 eV, all resulting from single or double excitations from the ground state. There are a number of low-lying singlet (and quintet) states as well, a few of which are also shown in the table. With such an array of readily accessible states, we would expect the conduction band electron density to be highly polarizable, thus behaving in a manner analogous to the bulk in bond formation and in response to molecular multipolar fields. As will be shown below, this polarizable charge density is important in determining adsorbate binding site preference, and is a feature that allows Ni_{20} to be more successful as a general bulk model than the smaller 2-5 atom clusters often used.

TABLE I: Low-Lying States of Ni_{20}

Species	Total Energy (h)	Excitation Energy (eV)	Term	Orbital Occupation							
				a_{1g}	b_{1g}	b_{3g}	b_{2g}	a_u	b_{1u}	b_{3u}	b_{2u}
Ni_{20}	-6.3620	0.0	$^3B_{3u}$	2221	2	2	2	0	20	20	21
	-6.3477	0.39	$^3B_{2g}$	2220	2	2	2	0	21	20	210
	-6.3215	1.10	$^3B_{3g}$	2221	2	2	1	0	20	20	220
	-6.3169	1.23	$^3B_{1u}$	2221	2	2	2	0	21	20	200
	-6.3153	1.27	$^3B_{3g}$	2220	2	2	2	1	20	20	210
	-6.3097	1.42	^3A_u	2222	2	2	1	0	20	20	210
	-6.3052	1.55	$^3B_{1g}$	2220	2	2	2	0	20	21	210
	-6.2970	1.77	$^3A_{1g}$	2220	2	2	2	0	20	20	211
	-6.2893	1.98	^3A_u	2221	2	2	2	1	20	20	200
	-6.2820	2.18	$^3B_{2u}$	2221	2	2	2	0	20	21	200
	-6.3523	0.26	$^1A_{1g}$	2220	2	2	2	0	20	20	220
	-6.3102	1.41	$^1A_{1g}$	2222	2	2	2	0	20	20	200
	-6.2972	1.76	$^1A_{1g}$	2220	2	2	2	0	22	20	200
Ni_{20}^+	-6.1450	5.90	$^2B_{3u}$	2220	2	2	2	0	20	20	210
	-6.1176	6.65	$^2A_{1g}$	2221	2	2	2	0	20	20	200
	-6.1083	6.90	$^2B_{1u}$	2220	2	2	2	0	21	20	200
Ni_{20}^-	-6.4544	-2.51	$^2A_{1g}$	2221	2	2	2	0	20	20	220
	-6.4393	-2.10	$^2B_{3g}$	2222	2	2	2	1	20	20	210
	-6.4321	-1.91	$^2B_{1u}$	2220	2	2	2	0	21	20	220
	-6.4128	-1.38	$^2B_{3u}$	2220	2	2	2	0	22	20	210

B. The Ni_{20} H Clusters. Upon bringing a hydrogen atom to the surface, the initial interaction would be expected to occur between the hydrogen 1s orbital and a cluster orbital having significant electron density at the binding site. In fact, we find that, in placing the hydrogen at 1(100), 2(001) or 4(001) sites, the bonding interaction is strongest with the highest occupied cluster orbital (orbital h in Fig. 2) having large amplitude along the (001) surface. The same is also true of bringing the H atom to one of the 3(111) sites, site I in Fig. 1. As discussed below, however, this cannot be said of 3(111) site D, a cluster effect that results in unreliable bonding parameters. In all cases, however, the remaining cluster orbital shapes are only weakly perturbed. The calculated bond parameters for each of the sites listed in Table II were quite different. Summarizing, we note that:

i) Bond energies tend to increase with the ligancy of the H atom (number of nearest neighbors to the hydrogen) with D_e = 1.6, 2.8, 3.2, and 3.0 eV for ligancies of 1, 2, 3, and 4.

ii) The Ni-H bond distance increases monotonically with ligancy of the H atom with R_e(NiH) = 1.50, 1.59, 1.63, and 1.778 Å for ligancies of 1, 2, 3, and 4. In comparison for diatomic NiH the bond length is 1.47 Å.[13]

iii) The vibrational frequency of the H atom relative to the surfaces changes markedly with H ligancy, with $\omega_e \approx$ 275, 170, 150, and 74 meV for ligancies of 1, 2, 3, and 4. By comparison, ω_e = 237 meV[13] for diatomic NiH.

To provide further characterization of the bonding, we also considered the modifications of the band spectrum resulting from chemi-

TABLE II. Bond parameters for H binding sites.

Site	Description		Bond Length (Å)	Vibrational Frequency	Chemisorption Energy
	Surface	Ligancy of H[a]	$R_{\perp}$[b]	meV	eV
B	⟨001⟩	1(7)	1.50	283	1.56
F	⟨110⟩	1(5)	1.49	280	1.43
C	⟨112⟩	1(7)	1.49	(231)	(1.00)
A	⟨001⟩	2(7)	0.99	177	2.73
G	⟨001⟩	2(5)	0.99	(173)	(2.17)
E	⟨110⟩	2(6)	0.93	(161)	(1.56)
H	⟨112⟩	2(5)	0.96	176	2.43
I	⟨111⟩	3(5,5)hcp	0.78	155	3.21
D	⟨111⟩	3(6,7)fcc	0.79	(131)	(2.12)
J	⟨001⟩	4(7,5)	0.30	73	3.04

[a]In parentheses is the number of nearest neighbors for the Ni atom(s) binding site. Where nonequivalent surface atoms are present, values are given for each type.

[b]Optimum distance from H to the plane representing the surface.

sorption of an H atom at different sites. Spectra for representative sites are shown in Fig. 4, illustrating the following general trends:[14]

i) For each chemisorption site, one of the cluster orbitals originally occupied in Ni_{20} is destabilized above the fermi energy (i.e., unoccupied). Analysis of orbital shapes show this orbital to be the highest Ni_{20} orbital having significant density at the bonding site.

ii) The group of sites used in Fig. 4 represents a series of adjacent sites on the surface of the Ni_{20} cluster. Thus moving from Fig. 4b to 4f represents a traversal around the surface of the cluster. By taking the overlap of the Ni_{20} H orbitals with the Ni_{20} orbitals (Figs. 4a or 4g), it was found that the band orbitals at different sites correlate quite well (in the figure, orbitals of similar character are connected by dashed lines).

iii) A new H-like level appears at 3 to 11 eV below the fermi level and is denoted as "H" in Fig. 4. In all cases, this level interacts most strongly with one of two Ni_{20} levels near 13.6 eV absolute ionization potential (the value for a free H atom).

iv) Levels excluded by symmetry from direct interaction with the H atom are shown as dashed levels. Of the levels allowed to interact by symmetry, certain ones interact strongly and are marked with thick lines in the figure. Comparing these levels with the free cluster levels from which they originate shows them to be pushed away in energy from the new "H-binding" level.

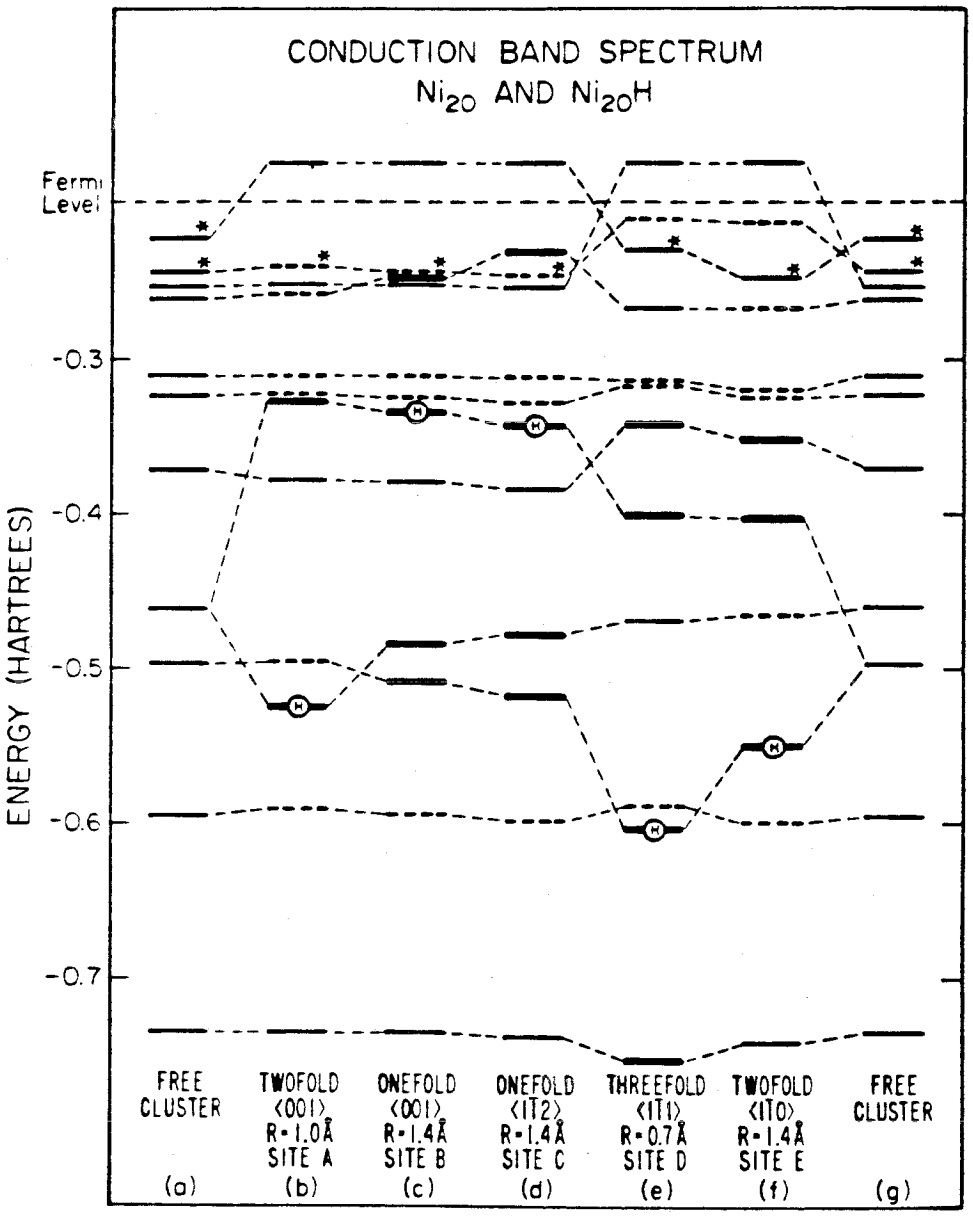

FIG. 4. Spectrum of states for Ni_{20} and $Ni_{20}H$ clusters. Levels connected by light dashed lines are of similar orbital character. Heavy lines indicate levels interacting significantly with the H atom. The H on a level indicates the orbital with maximum H character. Dashed levels are for orbitals unable to interact with the H atom by symmetry. Asterisks indicate singly-occupied orbital levels. The d levels are spatially localized and have been replaced by an effective potential. The position of the fermi level is approximate and is used primarily to distinguish between occupied and unoccupied levels.

v) The occupied band orbitals of $Ni_{20}H$ are linear combinations of the original Ni_{20} occupied orbitals, with less than 1 percent incorporation of empty Ni_{20} band orbitals in almost all cases.

Although these Koopmans' Theorem orbital energies contain information only about the ion states, they suggest the following qualitative model for the hydrogen chemisorptive bond. An electron is removed from a high-lying Ni_{20} orbital directed towards the H atom, allowing the H atom to adsorb effectively as an $H^{\delta-}$ species (i.e., with a small negative charge on the H). The orbital energies of the antisymmetric orbitals are insensitive to this change, indicating that the readjustments in electron density are too small to affect orbitals not directly involved in the bond.

To clarify this concept and gain some insight into the reasons for site selectivity we examine the bonding orbitals. In Fig. 5 we show orbitals obtained from calculations in which the hydrogen is bound at the 4(001) sites. In this case, the bonding orbitals are localized about the hydrogen, no longer showing the diffuse character of Fig. 2(h). The high degree of charge polarizability present in the "conduction band" makes this localization particularly facile when the hydrogen atom is only 0.3 Å above the fourfold site. However, even at a distance of 1. Å above the fourfold site, the binding energy is still about 1.5 eV, slightly more than when the hydrogen atom is placed the same distance above a linear site. This is illustrated in Fig. 6 where potential curves are plotted for each approach geometry. Apparently, when the hydrogen atom is above the fourfold site, the cluster is more capable of maintaining the high degree of overlap

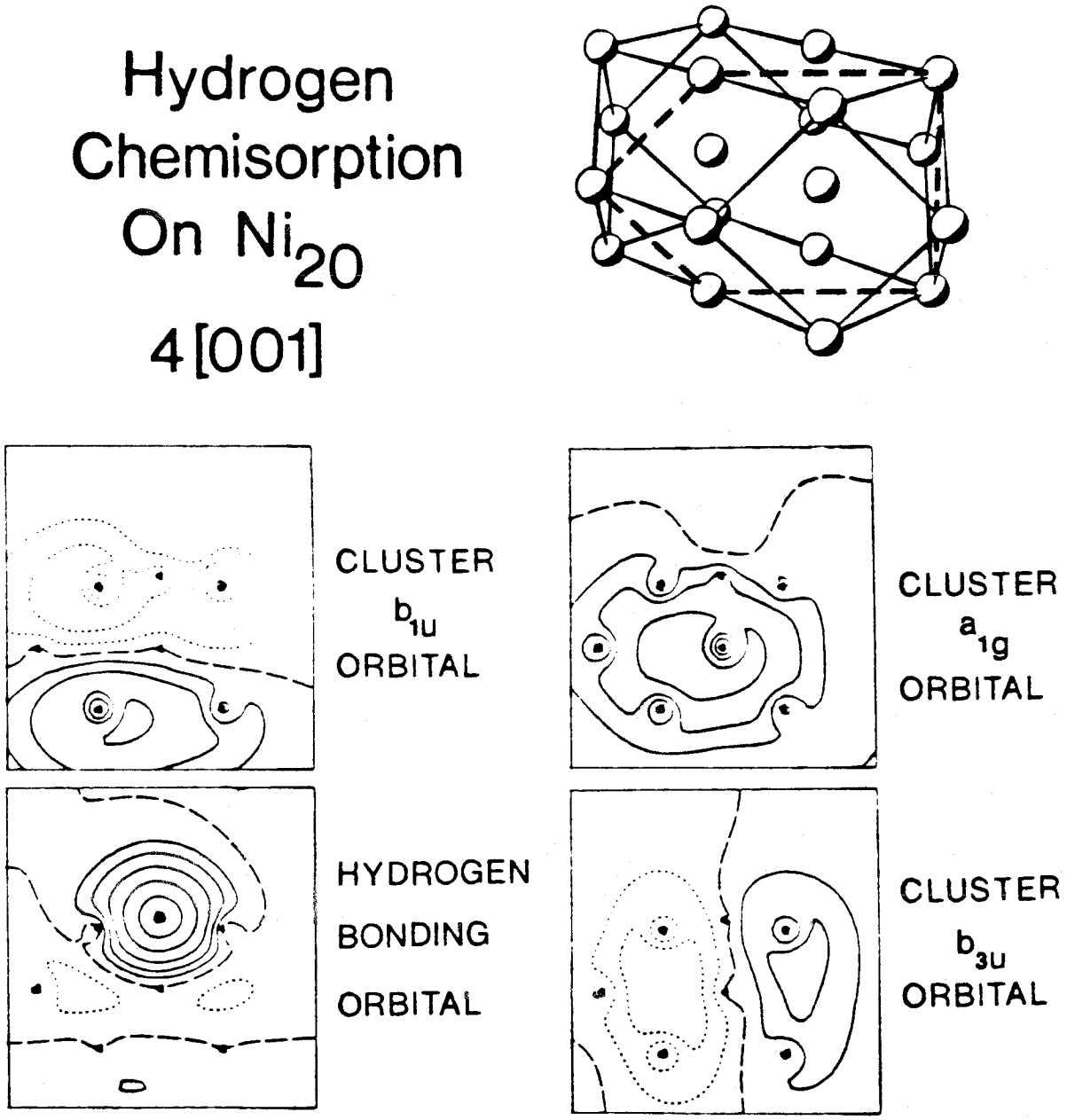

Figure 5: Bonding orbital for H at 4(001) site on Ni_{20}. Plotting plane in the ⟨100⟩ plane indicated by dashed line on cluster.

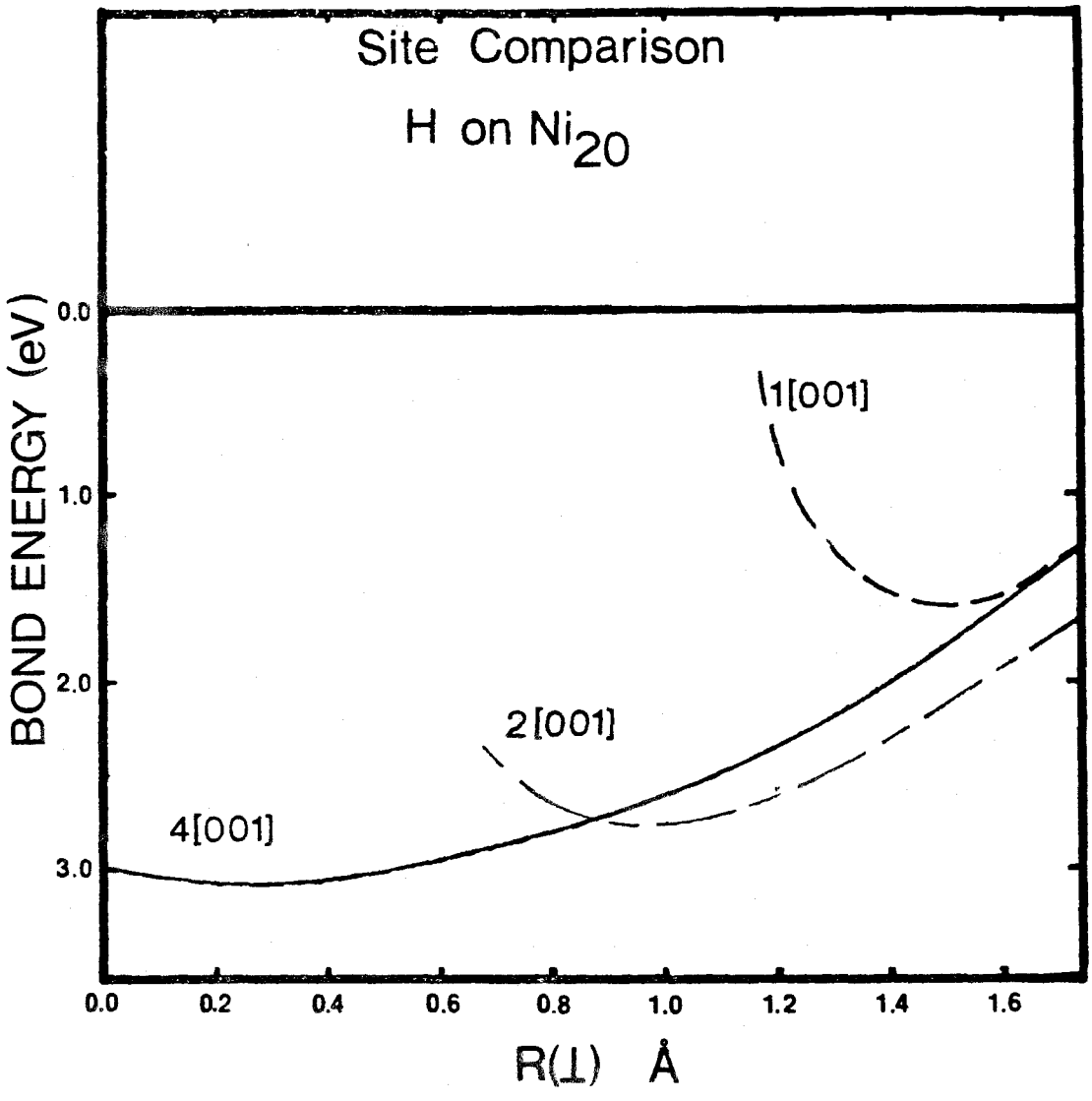

Figure 6. Potential curves along surface normal for an H atom at each type of (001) site.

necessary to form a strong covalent bond. From these results we may tentatively characterize the fourfold site as a stronger "sigma donor" than the twofold or onefold sites. Alternatively, we may say that the basicity of the 4(001) site is greater.

The variation in heats of adsorption noted in Table II may be addressed using the results of Fig. 4. Two sites, D and E in Table II, show binding energies that are significantly lower than the other values at similar sites. In Fig. 4 we see that for sites D and E it is the third highest Ni_{20} level that is "ionized" (Fig. 4e-f), while for the remaining sites in the figure it is the highest Ni_{20} orbital that is removed. The energy difference between these two orbitals is ~ 0.8 eV, the same magnitude as the discrepancy in the binding energies for sites D and E. Binding at all other sites considered leads to removal of an electron from the highest Ni_{20} orbital, resulting in internally consistent binding energies. Thus we conclude that a further condition for using clusters to obtain chemisorption energies, is that the cluster be such that the ground state wavefunction possesses a conduction band orbital near the fermi energy with large amplitude at the chemisorption site. If, in solving for the ground state of the Ni_nH complex, it is found that the ejected electron is from a deeper orbital, then we expect the bond energy to be low.

III. CHEMISORPTION ON Ni(001)

A. Monovalent Species. For direct comparison with hydrogen chemisorption two additional monovalent species, sodium and chlorine, were considered. Collectively, a wide range of electronegativities is

spanned allowing three very different probes of the surface electronic structure.

1. Chlorine. With its considerably larger electronegativity, charge transfer to the chlorine atom should be more pronounced than observed for hydrogen. In addition, bringing up the chlorine atom to any of these sites allows the possibility of forming either a "sigma" bond to the surface, through a singly-occupied 3p orbital along the surface normal, or a "pi" bond, through a 3p orbital parallel to the surface.

To begin, we note that trends established for hydrogen are unaltered in chlorine chemisorption. The results of Table III show increasing bond energy and bond distance with increasing site coordination, along with a less pronounced trend towards decreasing vibrational frequency. Comparison of Ni_{20} and Ni_{20} Cl orbitals shows that bonding occurs through interaction of the Cl atom with the same Ni_{20} orbital that was used in hydrogen chemisorption.

At each site, the bonding is dominated by the formation of a relatively polar "sigma" bond with the surface. Thus, the bond parameters for chlorine conform to the qualitative characteristics of the sites presented in the previous section: the strongest bond is formed with the site suggested to be the best sigma-donor. However, while the bond is polar it is incorrect to view the bonding as ionic. At each site, "pi" bonding occurs to a modest extent as well. The effect is most pronounced at the fourfold site. The net charge on the chlorine is reduced through back-donation to the Ni atoms surrounding

TABLE III. Bond Parameters for Cl on (001) Ni_{20}

Site	Ligancy of Cl	Bond Lengths (Å) R(⊥)	Bond Lengths (Å) R(NiCl)	Vibrational Freq. meV	Vibrational Freq. cm^{-1}	Bond Energy D_e (eV)
B	1	2.06	2.06	43.6	352	3.1
A	2	1.74	2.14	32.4	261	4.0
J	4	1.38	2.24	30.4	245	4.9

TABLE IV: Bond Parameters for Na on (001) Ni_{20}

Site	Ligancy of Cl	Bond Lengths (Å) R(⊥)	Bond Lengths (Å) R(NiCl)	Vibrational Freq. meV	Vibrational Freq. cm^{-1}	Bond Energy D_e (eV)
B	1	2.9	2.9	19.3	155	1.2
A	2	2.8	3.1	16.9	136	1.3
J	4	2.7	3.2	16.9	136	1.3

the fourfold site. This back-donation becomes progressively less important as site coordination is reduced,and thus the anionic character increases. Using Mulliken populations as a relative indicator (basis set effects preclude the use of Mulliken populations as an absolute indicator of charge; however relative trends are usually reliable) we find that the net "charge" on adsorbed Cl at the 4(001) site is about one-half that calculated for an H atom at the same site (Cl = -0.29; H= -0.64). Qualitatively then, those electronegativity characteristics which cause a surface atom to behave as a poor sigma-donor in one-fold bonding, allow it to behave as a "pi-acceptor" when participating in fourfold bonding. Thus, we would expect the "pi-acceptor" characteristics of surface sites to increase with increasing coordination.

2. Sodium. Upon cursory examination, atomic sodium might not be expected to exhibit bonding characteristics similar to either hydrogen or chlorine. With its far smaller electronegativity, the sigma donor characteristics of the surface sites do not appear relevant. Upon bringing the atom to the surface however, we find that at each site the bonding is ionic, with significant 3s electron density (Mulliken populations indicate a charge of ~ 0.65 on sodium) transferred to the surface. Qualitatively, the bonding may be described as the interaction between an anionic Ni_{20} cluster and an Na^+ core. To some extent, the proton affinity characteristics of the surface sites should dominate the bonding. Trends observed should thus parallel those of adsorbates controlled by the site basicity. In Table IV this is seen to be true for the geometric and vibrational parameters. Bond distances are very long however due

to core-core repulsions, and as a result thermodynamic differences between sites are largely washed out. Comparing $Ni_{20}H$ potential curves at $R(\perp) \approx 2.8$ Å in Fig. 6 shows a similar effect. At these distances, the surface appears almost homogeneous to the adsorbate.

Bonding orbitals for sodium bound near R_e are quite different from those of hydrogen. There is very little valence electron density present on the sodium atom, and the charge lost may be seen to be distributed in a delocalized manner over the cluster. There is only a very small localized component present in the bonding, as the Ni_{20} component of each $Ni_{20}Na$ orbital strongly resembles the corresponding isolated Ni_{20} orbital.

B. Divalent Species

1. Sulfur. The bonding of atomic sulfur was considered at both 2(001) and 4(001) sites on Ni_{20}. The more complicated chemisorptive bonding behavior possible for such a divalent species allows a probing of the surface site properties in greater detail.

In its ground state, the sulfur atom is capable of interacting with the 4(001) site in only two distinct ways. It is possible for the atom to approach the site with both $3p\pi$ orbitals parallel to the surface, and the doubly-occupied $3p_z$ orbital directed towards the center of the site. From previous discussions of site basicity however, such a state is not expected to be favorable. A strong sigma bond with the surface would only be possible if the 4(001) site were a better "sigma acceptor". In addition, the π bonds that might be formed with surface are not expected to be strong, as both the sulfur atom and the site are some-

what electron-withdrawing in π bond formation.

These same considerations would predict that more favorable results would be obtained by bringing the sulfur atom to the surface with a singly-occupied $3p_z$ orbital, and three electrons in the two π orbitals. In this way, a strong σ bond may be formed along with a π bond. The remaining doubly-occupied $3p_\pi$ orbital may delocalize slightly onto the cluster. The final description would be one in which the sulfur orbitals are very similar to those found previously for chlorine.

In carrying out the calculations, a final state is obtained that is very amenable to this qualitative discussion. In Fig. 7 we show the results of projecting the cluster component of the $Ni_{20}S$ orbitals onto the isolated Ni_{20} orbitals, as was done for $Ni_{20}H$. Sigma bond formation may be seen to be a result of an interaction between the sulfur $3p_z$ orbital and the high-lying cluster orbital (Fig. 2h) used in a σ bond formation with each of the other adsorbates. The projection reveals that to form the π bonds the cluster "bond" defined by the doubly-occupied b_{2g} orbital must be broken. One electron remains in an orbital similar in shape to the original b_{2g} orbital, while the remaining electron of this bond pair is coupled with the singly-occupied sulfur $3p_\pi$ orbital. The π orbitals are found to be equivalent in shape in the region near the bonding minimum, and each may be described as a combination of a sulfur $3p_\pi$ orbital with a cluster orbital consisting of a particular mixture of $1b_{1u}$ and $2b_{1u}$ character. Although the $2b_{1u}$ orbital is not occupied

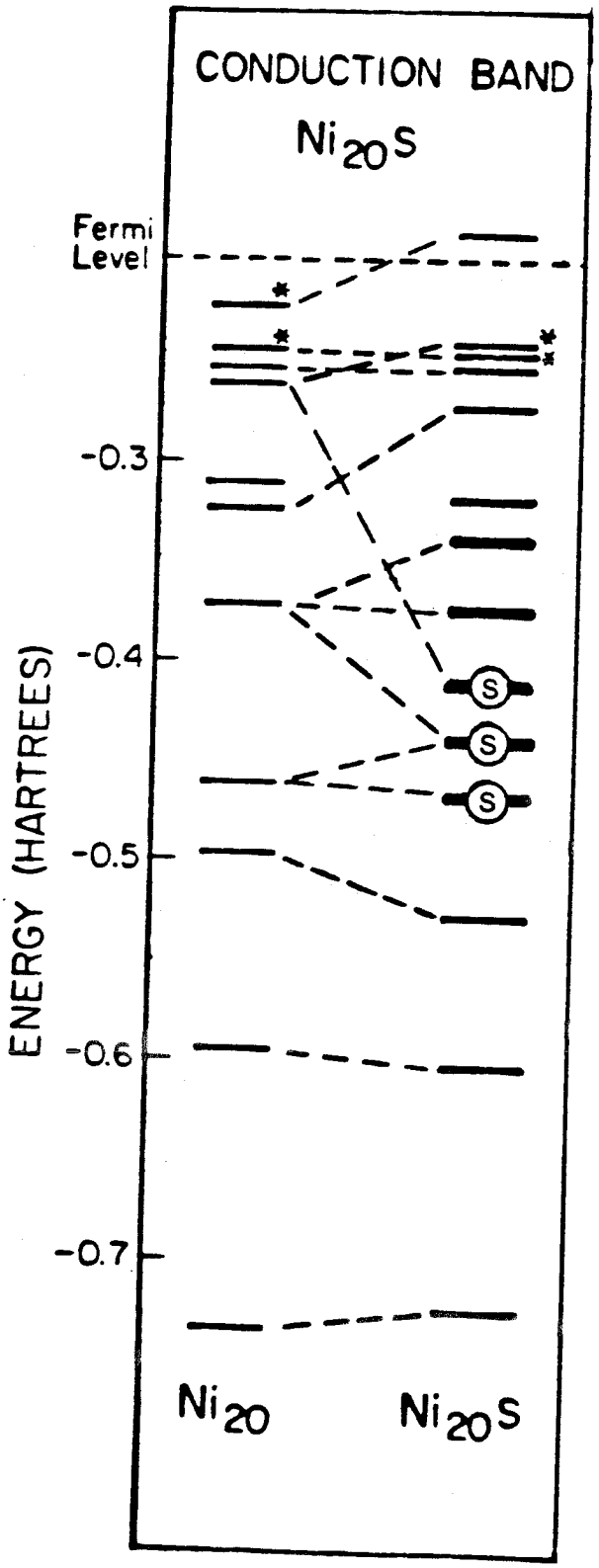

Figure 7: Changes in orbital position resulting from bonding of S at 4(001). Heavy lines are orbitals showing much sulfur character. Three orbitals best described as sulfur bonding orbitals are marked with S.

in the ground state, Table I reveals that there are low-lying neutral (at 0.4 and 1.2 eV) and anion states (at -1.4 eV) of Ni_{20} which involve occupation of this orbital. It is the high energetic accessibility of these states that allows covalent π-bond formation in $Ni_{20}S$ and π "backbonding" in $Ni_{20}Cl$. Bond orbitals for $Ni_{20}S$ are shown in Fig. 8.

The bond parameters for the system are listed in Table V. The optimum position for the sulfur atom is found to be about 1.3 Å above the surface, for which a bond energy of 4.3 eV is calculated. By comparison, the net bond energy of H_2S is about 7.6 eV or roughly 3.8 eV per sigma bond.[15] Similarly, calculations on diatomic NiS[16] yield a 3.3 eV bond energy (expt: 3.5 eV).[17] Tentatively, these values suggest that the π contribution is small (perhaps 1.0 eV) and that the bonding is dominated by the σ interaction.

Consideration of bonding at the 2(001) site is made slightly more complicated by the lower symmetry of the site. Assuming an orientation in which the $3p_z$ orbital is singly-occupied, the two possible configurations for the three π electrons are not equivalent. In each case, one $3p_\pi$ orbital is oriented parallel to the two fold site (denoted $3p_2$) while the remaining orbital is rotated to rest above the two adjacent 4(001) sites (denoted $3p_4$). The difficulty lies in determining the optimum occupations for these two orbitals.

In Fig. 9, portions of three potential curves are shown. Each corresponds to a different $3p_4$ occupation and coupling with the surface. In curve A orbital $3p_2$ is doubly-occupied, while singly-occupied orbital $3p_4$ is coupled with cluster orbital $2b_{2u}$ (Fig. 2g) into a singlet. In curve B, the occupations remain unchanged, however $3p_4$ and $2b_{2u}$ are triplet

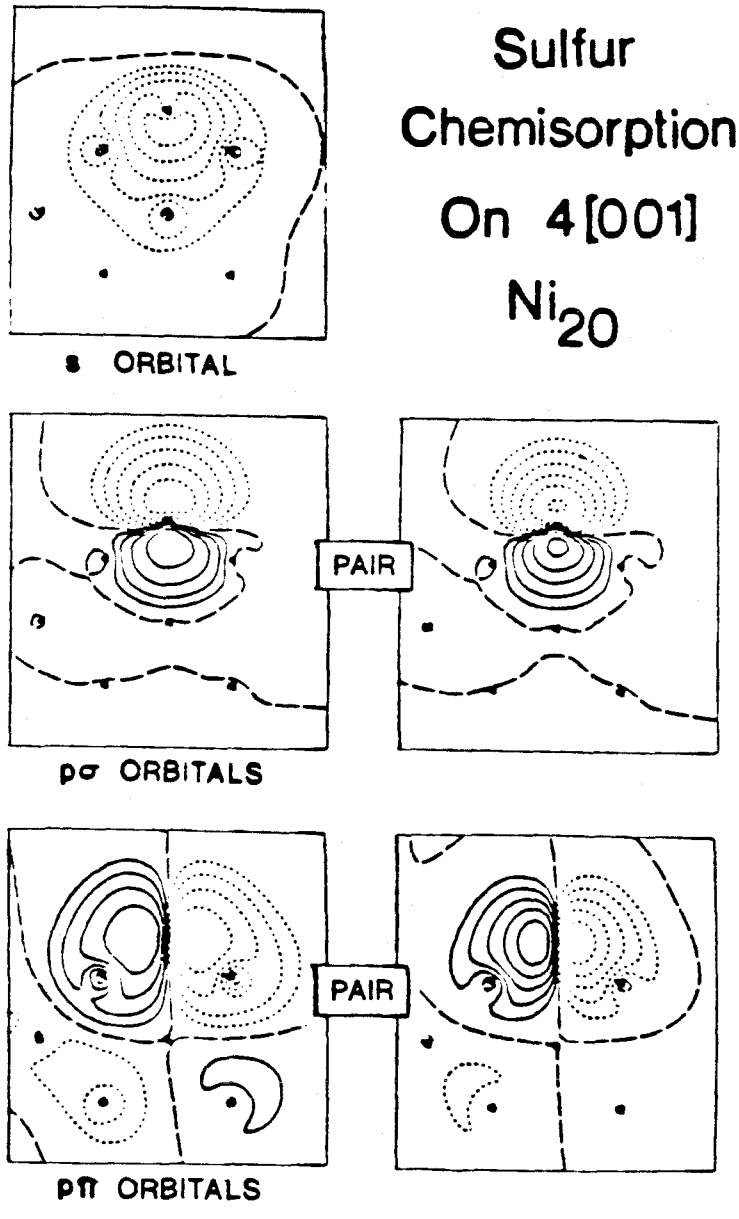

Figure 8: Bonding orbitals for $Ni_{20}S$. Plotting plane is the same used in Fig. 5. Note that the second π orbital pair has no amplitude in this plane.

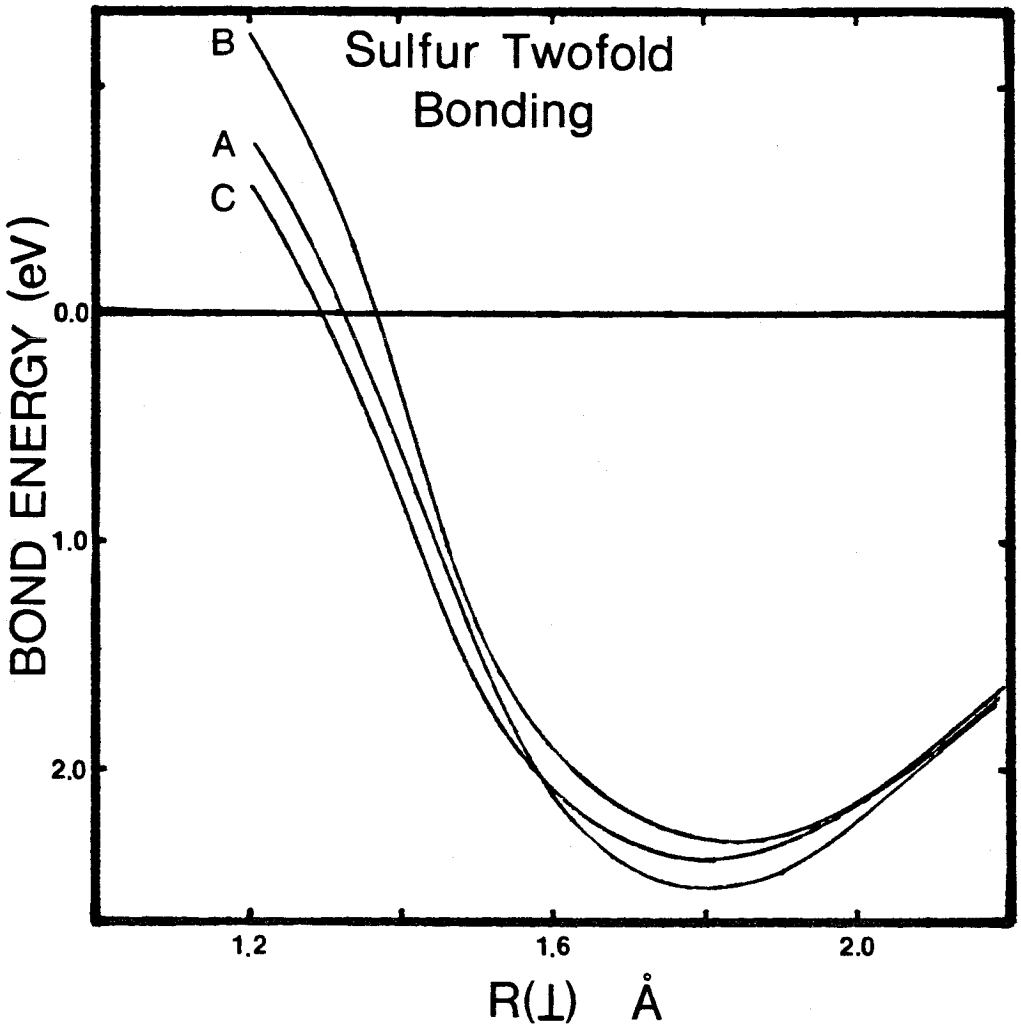

Figure 9: Comparison of three low-lying states of 2(001) $Ni_{20}S$ as a function of distance along the surface normal.

coupled. In the remaining curve (C), the $3p_4$ orbital is doubly occupied, and the $3p_2$ orbital is coupled with an electron originally occupying cluster orbital b_{2g}. There are a number of features here that relate strongly to bond formation at the 2(001) site.

1) Both curves A and C involve a "covalent" π bond in one direction, with repulsive interactions between a doubly occupied $3p_\pi$ orbital and the surface in the other direction. The repulsive interactions are more serious in curve A (between the $3p_2$ and $1b_{2g}$ doubly occupied orbitals) resulting in a longer bond length.
2) Comparing curves A and B reveals that the overlap between $3p_4$ and $2b_{2u}$ is sufficiently small that there is little energetic effect associated with altering the spin coupling. The separation between these curves suggests that the π bond strength in curve A cannot be much greater than 0.2 eV near the equilibrium position.
3) A weak π bond must also be present in curve C (since its total bond energy is not significantly different). To some extent this is due to the de-coupling of electrons in the b_{1g} orbital that was required prior to π bond formation. Effectively, the cluster must first be promoted to an excited state.

Since neither configuration ($3p_2^2\,3p_4^1$ or $3p_2^1\,3p_4^2$) is stabilized through formation of π bonds, it is tempting to attribute the presence of a $3p_2^2\,3p_4^1$ ground state to stabilization of the $3p_2^2$ orbital by the electron-withdrawing nature of the 2(001) site. Such a feature would be consistent with the results of 2(001) $Ni_{20}Cl$ calculations where the $3p_2^2$

orbital is found to be stabilized slightly relative to the $3p_4^2$ pair [IP$(3p_2^2) \approx 12.3$ eV and IP$(3p_4^2) \approx 12.1$ at $R(\perp) = 1.8$ Å]. Such a conclusion cannot be reliably drawn here however, since curve C (the $3p_4^2 3p_2^1$ state) will dissociate to an excited state limit (see point (3) above). While the effect of this anomaly may be small so near to R_e, it is a bias against the $3p_4^2 3p_2^1$ state that may mask out the importance of any $3p_2^2$ stabilization.

The bond parameters for 2(001) sulfur are collected in Table V for comparison with those of the 4(001) site. In spite of the difficulties associated with π bond formation, each of the parameters varies on going from 2(001) to 4(001) in precisely the same manner as observed for the monovalent systems. With the apparent weakness of the π-bonding interactions found for sulfur, such a result is not unexpected.

2. Oxygen. Comparison of the bonding properties of atomic oxygen and sulfur proves an opportunity to probe (isoelectronically) the response of the surface to variations in adsorbate size and electronegativity. Accordingly, we have considered the binding of oxygen at the same 2(001) and 4(001) sites that were discussed above.

In Fig. 10 we show orbitals for the ground state of the $Ni_{20}O$ system with the O atom positioned at the 4(001) site. These orbitals may be compared with the sulfur orbitals of Fig. 8.
There are few qualitative differences that may be observed. There is less delocalization of the $2p_\pi$ orbitals onto the cluster than is observed for sulfur, however these $2p_\pi$ orbitals are noticeably more diffuse than the $2p_\sigma$ orbital. A comparison of the

Table V: Bond Parameters S on (001) Ni_{20}.

Site	Ligancy of S	Bond Lengths (Å)		Vibrational Frequency		Bond Energy
		R (⊥)	R(NiH)	meV	cm^{-1}	D_e (eV)
A	2	1.81	2.20	48	387	2.5
J	4	1.24	2.15	37	298	4.3

Table VI: Low-Lying States of the Alkali Oxides. [a]

Molecule	Excitation Energy (cm^{-1})		Bond Energy, D_0^0, of Ground State (eV)
	$^2\Sigma^+$	$^2\Pi$	
LiO	2330	0	3.49
NaO	1500	0	2.60
KO	0	347	?
RbO	0	606	?
CsO	0	?	?

[a] From Ref. 17.

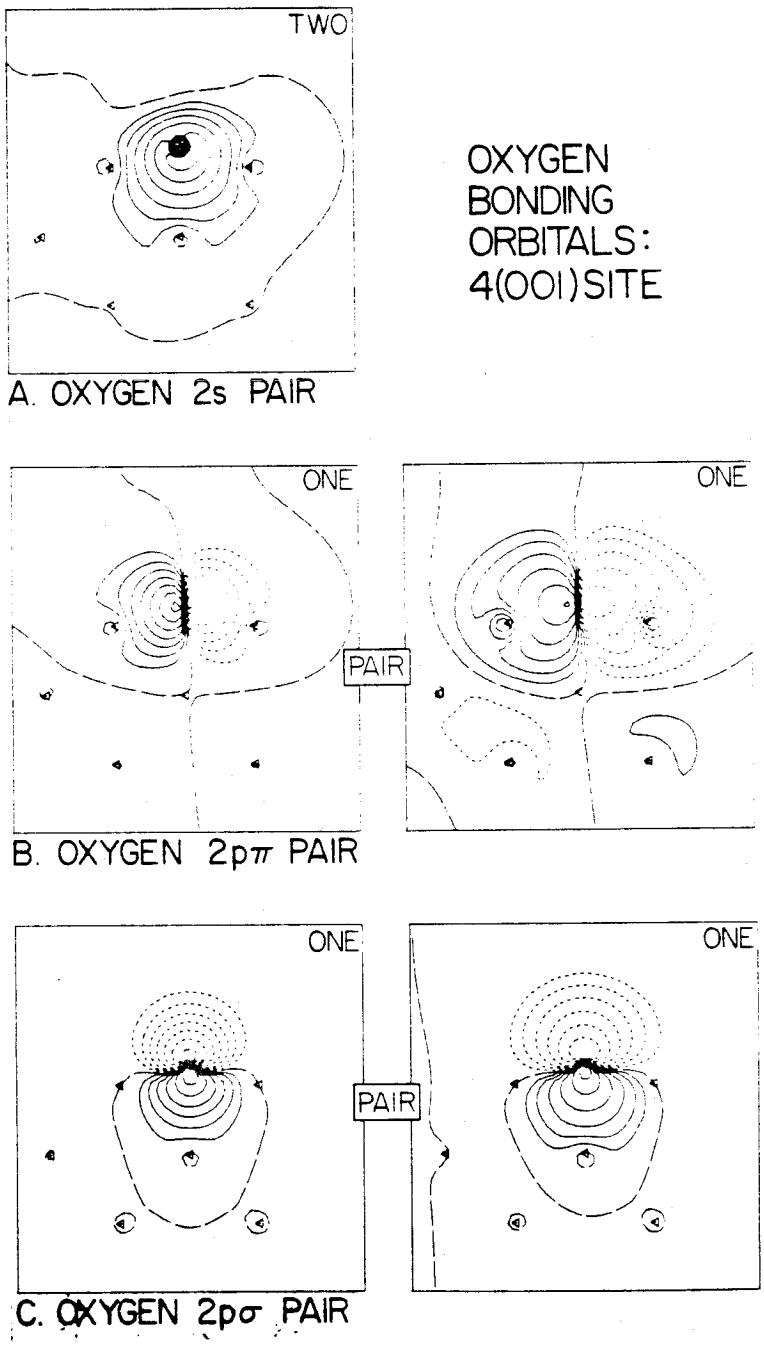

Figure 10: Bonding orbitals for the $Ni_{20}O$ 4(001) ground state. Plotting plane is that used in Fig. 5.

$Ni_{20}O$ and Ni_{20} orbitals reveals that here also, the σ bonding interaction is with the $4a_{1g}$ orbital of Ni_{20}, and that almost no $4a_{1g}$ character remains in $Ni_{20}O$. As for sulfur, the cluster π bonds are equivalent and less ionic than the sigma bond, producing the observed diffuse $2p_{\pi}$ orbitals. Mulliken populations suggest that the net result is a slightly larger "charge" on oxygen than was found for sulfur (-1.24 vs. -0.92).

The most interesting feature of the fourfold bonding results is that there is an additional state observed for oxygen chemisorption that lies only 0.3 eV above the ground state. No low-lying states were observed for sulfur. As indicated by the bonding orbitals of Fig. 11, this state exists in apparent defiance of the bonding concepts discussed previously. Both π orbitals are doubly occupied and equivalent as in the ground state; however,the $2p_{\sigma}$ orbital is singly occupied. Thus, whatever σ interaction that may be present is occurring through a one-electron bond.

To perhaps gain some insight into why such a state should be favorable, we present some equally unusual experimental data for the diatomic alkali oxides in Table VI. Two states are represented, and they may be illustrated schematically as:

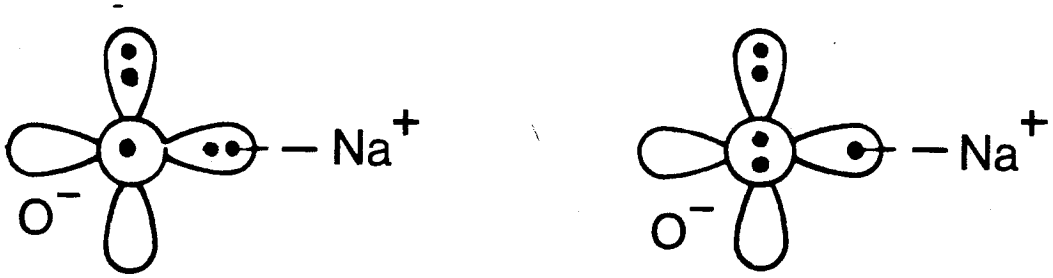

Radical Chemisorption

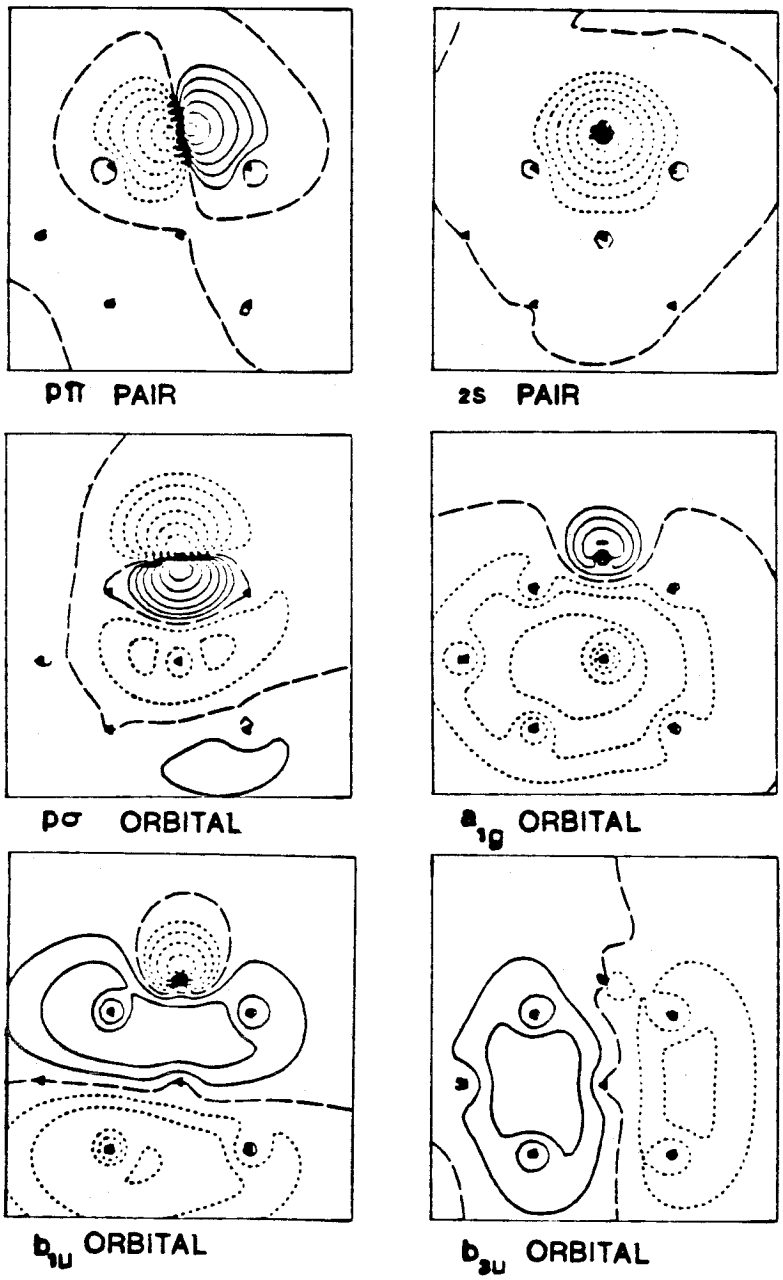

Figure 11: Bonding orbitals for the σ radical state of $Ni_{20}O$

where the states have been drawn as completely ionic for simplicity. Simple arguments would suggest that the $^2\Pi$ state should be the ground state, as it represents the simplest result of an interaction between isolated ground state atoms. Table VI indicates that this is true for LiO, but that the $^2\Sigma^+$ state becomes increasingly favorable as we move to heavier metal atoms. While the details of the bonding await more detailed study, it is apparent that the oxygen atom is capable of forming strong bonds in either arrangement to metal atoms whose electronegativity is similar to that of the nickel surface. The $^2\Sigma^+$ state represents an analogue to the state of Fig. 11, while the $^2\Pi$ state is similar to the $Ni_{20}O$ ground state prior to π bond formation. Assuming such a π bond to be weak, as was noted for sulfur, these two states of oxygen on the nickel surface might well be expected to be comparable in energy.

To further characterize the bonding in the ground state we may draw the same comparisons that were used previously for sulfur. Bond energies for H_2O are on the order of 4.8 eV,[15] while for diatomic NiO this is reduced to 3.8 eV.[17] The entries in Table VI for LiO [IP(Li) = 5.4][11] and NaO [IP(Na) = 5.1][11] are also relevant since the ionization potentials of these alkali atoms are similar to bulk Ni. Collectively, these results suggest that the π bonding in the ground state is minimal and it is likely that an upper limit of 1.0 eV is reliable as a measure of its contribution to the total bond energy.

In Fig. 12, four potential curves are shown for different states arising from bonding an O atom at a 2(001) site. Curves A-C are precisely analogous to the corresponding curves for sulfur chemi-

sorption shown in Fig. 9. The fourth curve represents a state that was found to involve a singly occupied $2p_\sigma$ orbital. Unlike 4(001) oxygen bonding, this configuration at the 2(001) site is not competitive with the ground state. It is equally unfavorable for 2(001) sulfur. The picture that arises for the other three curves is less ambiguous than it was for sulfur. Again, curves A and B are very close in energy suggesting that the π bond in curve A contributes almost no stabilization ($K_{y,2b_{2u}} = 0.00130$ at $R(\perp) = 1.4$ Å). Curve C has a different character for oxygen than found for sulfur. In this case, no bond is formed between the $2p_2$ orbital and the cluster b_{3u} orbital, but instead the $2p_2$ orbital remains singly occupied. Apparently, it is not energetically favorable for the b_{3u} pair to be uncoupled prior to forming a π bond. In this case, the $2p_2$ orbital is weakly triplet coupled to the cluster orbital ($K_{2p_2,b_{3u}} = 0.0001$ h). Thus for oxygen, curves A-C all involve a ground state cluster, a sigma bond, and essentially no covalent π bonding interaction (the Mulliken population for all three states is the same: -0.72 at $R(\perp) = 1.4$ Å). The energetic distinction between the states here is legitimately determined by the interactions between the doubly occupied $2p_2$ or $2p_4$ orbitals (in $2p_2^2 2p_4^1$ or $2p_2^1 2p_4^2$, respectively) and the surface. The π-acidity of the twofold site causes the $2p_2^2 2p_4^1$ configuration to be favored.

The bond parameters for the lowest state are listed in Table VII. Here again, since we may assume that the bonding is dominated by sigma interactions, trends in 2(001) and 4(001) sigma interactions are preserved.

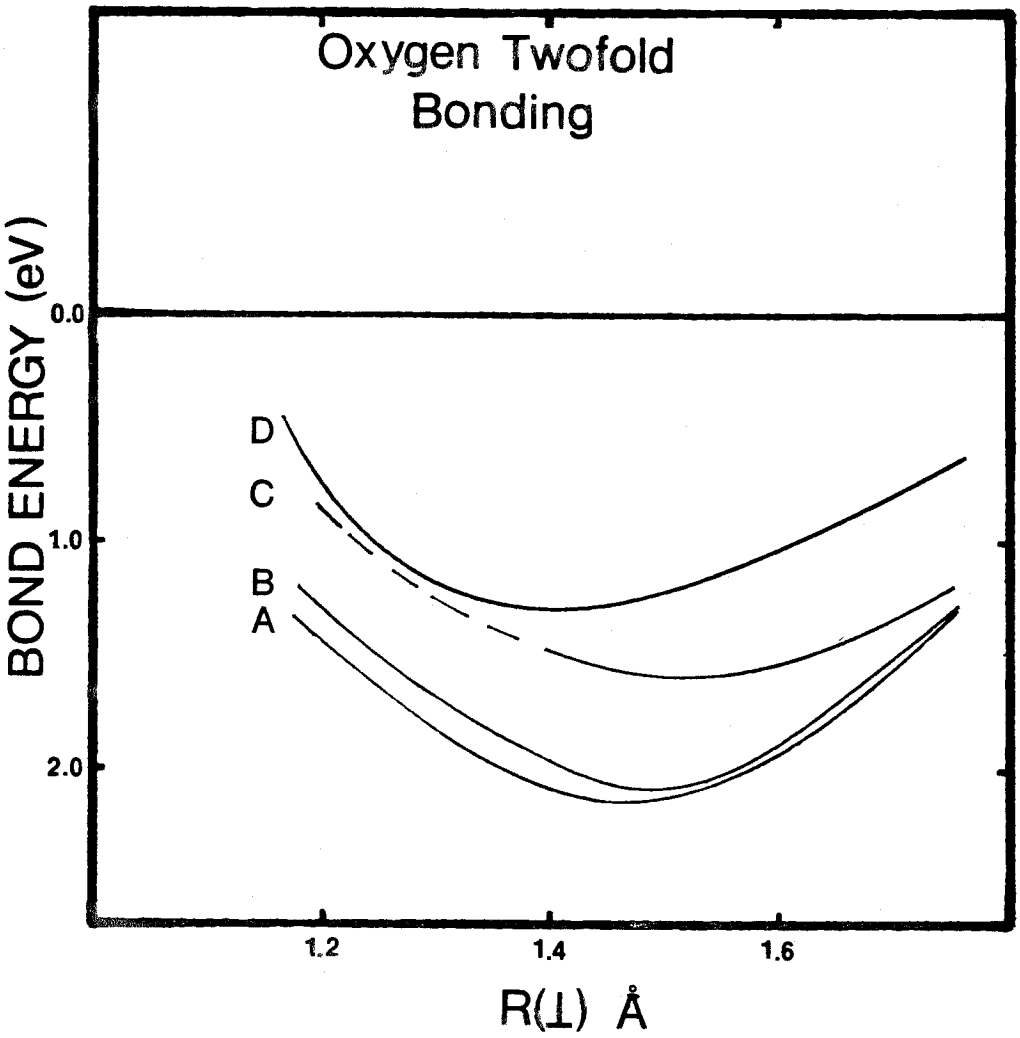

Figure 12: Comparison of four low-lying states of 2(001) $Ni_{20}O$ as a function of distance along the surface normal. Dotted line indicates region where curve is uncertain.

TABLE VII: Bond Parameters for O on (001) Ni_{20}

Site	Oxygen State	Ligancy of O	Bond Lengths (Å) R(⊥)	R(NiH)	Vibrational Freq. meV	cm^{-1}	Bond Energy D_e (eV)
A	σ radical	2	1.43	1.90	65	524	1.23
A	π_{p_4} radical	2	1.48	1.93	68	547	2.15
J	σ radical	4	0.88	1.97	46	371	3.29
J	closed shell	4	0.55	1.84	27	218	3.63

TABLE VIII: 3d Orbital Effects in Bonding H to Ni_{20}

Description of Cluster Atoms		Bond Energy		Vibrational Freq.		Bond Distance	
all ten[a] valence electrons	d^9 averaged potential	eV	kcal	cm^{-1}	meV	R(⊥)	R(NiH)
4	16	2.86	66	1507	187	1.03	1.61
0	20	2.73	63	1428	177	0.99	1.59

[a] 3d Orbitals allowed to readjust self-consistently.

IV. Quantitative Discussion

A. Hydrogen Chemisorption. In previous studies[10] we have found that replacing the spherically averaged $3d^9$ shell with an effective potential was adequate for description of the conduction band, but this did not imply that this potential would also be adequate for describing the bond of an H atom to the Ni. In order to test the use of d^9 averaged potential for Ni-H bonds, we examined $Ni_{20}H$ with H at a twofold site (site A in Fig. 1). In one calculation, referred to as $Ni_{16}Ni_4H$, all ten valence electrons were allowed full variational freedom[18] for the four Ni atoms closest to the H (a tetrahedron of Ni atoms consisting of the two-surface Ni bonding to the H and the two-center atoms of the cluster), and the d^9 averaged potential was used on the remaining 16 Ni atoms. In the second calculation, referred to as $Ni_{20}H$, the d^9 averaged potential was used for all 20 Ni atoms. As summarized in Table VIII, these calculations yield very similar results. The 3d orbitals remain localized and do not participate significantly in the NiH bond. Each of the bond parameters is affected by at most 5%, lending support to the concept that bonding properties in Ni are determined by the 4s electrons. Thus the use of the d^9 averaged potential appears adequate for describing the bonding of the H to Ni clusters, and in each of the calculations reported in Table II, all twenty Ni atoms were treated in this manner.

The results of these calculations allow some comparison with available experimental data for H atom chemisorption on low-index nickel surfaces:

1) HRELS data are available for H on (100) Ni in which a single loss peak at 75 meV is observed.[19] This compares very favorably with our calculated value of 73 meV for site J. Averaging similar values for threefold site I from Table II and additional sites from Ni_{28} (Appendix III.A) yields a frequency for motion along the surface normal of 150(±5) meV. Recently, electron loss experiments have been carried out for H on Ni(111), and a peak at 139 meV was found, in substantial agreement with our results. In that study, this was assigned to vibration of atoms adsorbed at 3(111) sites possessing no second layer Ni atom (fcc sites), while a second much weaker feature at 88 meV was attributed to atoms adsorbed at hcp-like 3(111) sites (second layer atom present). As indicated in Tables II and A-I, we find very little difference in vibrational frequency between these two sites, and thus cannot support this assignment. The lack of intensity in the loss peaks suggests that an impact scattering mechanism is operational, in which case the modes observed need not possess large normal dipole derivatives. Preliminary calculations have been carried out to characterize the asymmetric vibration (parallel to surface) of an atom at a threefold site. In these calculations, an fcc threefold site was used and surface atoms were held fixed in lattice positions. A loss at 140 meV is predicted, in poor agreement with the observed 88 meV loss. While the fixed lattice restriction should lead to a frequency larger than observable, it is unlikely that this restriction can

account for a discrepancy of the size found. It is worth noting here that the results of Ibach and Bruchmann[1] show no such 88 meV loss. Clearly, unambiguous assignment of this mode must await further study.

2) Heats of adsorption are accurately known on each of the low index faces from flash desorption studies. For the (100) and (111) surfaces, the most strongly bound states occur at 1.00 eV[20] and 0.98 eV[21,22] respectively (isosteric heats). Desorption follows second order kinetics, indicating that atomic adsorption is occurring with bond energies of 2.76 eV and 2.74 eV per atom, for the two types of sites. Incorporating zero-point energies into the bond energy values of Tables II and A-I yields the corresponding calculated D_0 values of 2.93 and 2.81 eV, respectively, in very good agreement with the experimental results.

3) Further thermodynamic characterization is provided by surface diffusion data. While it is clear that hydrogen atoms are able to move across the surface, it is not clear precisely <u>how</u> mobile they are. Gomer[23] has measured an activation energy of 0.3 eV for diffusion across a close-packed field emitter tip, a value which the author claims is relevant to the analogous process on a (111) surface. (It is perhaps relevant to note that a ΔH_{ads} of 2.0 eV was measured in this study). Lapujoulade, in thermal desorption studies, has measured pre-exponential factors, A, of 0.25[20] and 0.2[21] cm^2/atom-sec for the (100) and (111) surfaces from the

Arrhenius expression:

$$\frac{E}{RT_m^2} = \frac{2n_m A}{\beta} \exp\left(-\frac{E}{RT_m}\right)$$

where n_m is the surface population at T_m, the temperature of maximum desorption rate, and β is the heating rate. As pointed out there, completely mobile adsorption corresponds to $A \approx 0.004$ while completely immobile adsorption occurs when $A \approx 0.4$. In a similar study, Christmann et al.[22] obtain $A = 0.08$ cm^2/atom·sec for adsorption on Ni(111). These values all suggest that the H atoms are probably immobile at low temperatures, in agreement with the results of Gomer.[23] Christmann et al.[4] observe an order-disorder transition [from a (2×2) LEED pattern] that indicates mobility is possible at temperatures as low as 100 K. Assuming long-range mobility is not required for such a transition, a barrier height of ~ 0.2 eV would easily allow such a process (assuming jump rate $\approx \nu e^{-E/kT} \approx 7000$/sec when $\nu = 10^{13}$/sec, E = 0.2 eV, and T = 100 K). From our calculations, where fixed lattice positions were required, barriers of ~ 0.4 [for (100)] and 0.3 eV [for (111)] are predicted for short-range surface diffusion. It is expected that these barriers would be reduced by as much as half, were the effects of thermal motion of the Ni atoms properly incorporated.

4) Structural data are available both from LEED analysis of H on Ni(111)[4] and neutron diffraction studies[24] of a tetrahedral Ni

complex $H_3Ni_4(\eta^5\text{-}C_5H_5)_4$. In the finite complex, the H atoms are found to sit at the center of threefold faces (analogous to fcc 3(111) faces) at a distance of 1.69 Å from each Ni atom. This closely corresponds to our average calculated result of 1.64 Å. The LEED analysis represents an almost exhaustive study of possible overlayer geometries consistent with the observed (2×2) LEED pattern. By far the best fit was obtained for a structure in which the H atoms occupy 3(111) sites (both types) in a pattern of connected hexagons (resembling a graphitic structure), each H atom sitting 1.84 (± 0.06) Å from nearest neighbor Ni atoms [$R(\perp) = 1.15$ Å]. This represents an extremely long NiH interaction, much longer than from either our calculated geometry or the observed geometry of the Ni_4 complex. If correct, it would suggest that such small Ni complexes represent poor models for the bulk chemisorption system under higher coverage conditions. Increased adatom-adatom interactions, or the depletion of surface states (through bond formation as depicted in Fig. 5) might cause bond lengths to increase as coverage is increased. We must note however, that in the LEED study a relatively small muffin-tin potential was used to describe the H atom density (1.0 a.u. radius). Our calculations, as illustrated by Fig. 5, would suggest that a more "diffuse" potential might be more appropriate. As the LEED calculations exhibit some sensitivity to this parameter (see Fig. 6 in that study) there would seem to be a question as to whether the bond length discrepancy is as large as the results suggest.

5) In angle-averaged UPS spectra of H atoms adsorbed on Ni(111) a single broad level is observed about 6 eV below the fermi level.[25] Angle-resolved UPS studies of the clean Ni(111) surface revealed a surface state of sp character lying about 0.25 eV below ϵ_f, that is, attenuated upon hydrogen chemisorption.[26] In both studies, it was concluded that on nickel surfaces the predominant bonding interaction with adsorbed H atoms occurs through the 4s orbitals. Examination of Figs. 4 and A-3 (in Appendix III. A) allows some comparison to be made with these experimental details. The orbital energy spectra shown there contain some information concerning the position of ionization levels, as given by Koopmans' Theorem. A level due primarily to the H-cluster bonding orbital appears at 7-9 eV, and there is attenuation of density just below ϵ_f. Thus, the predicted ionization features are in qualitative agreement with the observed spectral details. The attenuation of the state density near ϵ_f suggests an increase in work function should occur, however the calculation is too crude to determine whether a value close to the observed $\Delta\phi = 0.12$ eV[22] would be predicted. The above discussion indicates that the use of 20 and 28 atom clusters is adequate for the purpose of providing not only a qualitative picture of hydrogen atom chemisorption, but quantitative data that are in substantial agreement with experiment.

B. Sodium. In previous studies of large Ni clusters, it was observed that the ionization potentials of the clusters steadily approached the bulk limit as their size increased.[8,10] Electron affinities on the other hand, showed little or no convergence towards this limit. As was pointed out there, the origin of this effect may be traced to the simple expression:

$$IP - EA = J_{kk}$$

where J_{kk} is the coulomb interaction between two electrons in the highest occupied orbital k. The size of this interaction is inversely proportional to the radius of the cluster, and thus exceedingly large clusters are required if a bulk-like electron affinity is desired.

As mentioned in Section II. A, the implications of this phenomenon on the interaction of sodium and Ni_{20} are major. The larger bulk electron affinity virtually guarantees a more ionic bond in the experimental chemisorption system, and as a result, rather different bonding parameters should be expected. A dynamic LEED analysis has been carried out for Na on Ni(100) and four-coordinate bonding was found,[27a] in agreement with our results in Table IV. The observed bond distance however, is ~ 2.3 Å, in poor agreement with the calculated result. Even more significant is the fact that flash desorption experiments yield a bond energy at this site of 2.8 eV,[27b] whereas all three types of sites on Ni_{20} show a much smaller ~ 1.2 eV interaction. Both discrepancies are manifestations of the reduced ionic character present in the Ni_{20}Na bond.

C. Sulfur. The same fundamental concerns that lead to poor agreement between $Ni_{20}Na$ and the corresponding bulk system should produce better agreement for this more electronegative adsorbate. Indeed, the results of dynamic LEED analysis suggest that on Ni(001) the 4(001) site is preferred at both p(2×2) and c(2×2) coverages, and that a bond distance of $R(\perp) = 1.3(\pm 0.1)$ occurs in each case.[28] Examination of Table V indicates that these observations are in excellent agreement with the $Ni_{20}S$ calculations.

The experimental information regarding adsorption is less clear cut. Windawi and Katzer[29] have considered the decompositions of H_2S on Ni foils and noting the equilibrium pressure ratio [$P_{H_2S}/P_{H_2} = 6 \times 10^{-7}$ at 550° C] required to produce a "monolayer" of adsorbed S they obtain a $\Delta G_{500°C}$ of -24 kcal/mole. The data of Table V allow a comparison with this value. We use standard values for $\Delta H_{773°K}$ (H_2S = -0.3 kcal) and $S_{773°K}$ (H_2S = 57.9 cal/deg; H_2 = 37.9 cal/deg) for the gas phase species,[15] and estimate:

$$Ni_{20} + S \rightarrow Ni_{20}S \qquad \Delta H_{f(0°K)} = -32.4 \text{ kcal}$$

or $\Delta H_{773}^{Ni_{20}S} = -27.8$ kcal. Using the expression:[30]

$$S_T^{Ni_{20}S} = k\left[\ell n\, q + T\,\frac{\partial \ell n q}{\partial T} - \ell n\,\theta - \frac{(1-\theta)}{\theta}\,\ell n(1-\theta)\right]$$

where q is the vibrational partition function at high temperature and θ is the coverage ($\theta \approx 0.5$) gives $S_{773}^{Ni_{20}S} \approx 10.9$ cal/deg. For bulk Ni, $S_{773} \approx 13$ kcal.[31] Collectively, these values yield $\Delta G_{773} = -11.1$ kcal/mole, in good agreement with the experimental result. McCarty et al.[32]

calculate an isosteric heat of adsorption of -38.2±5 kcal in a similar experiment on Ni(100) at 1080K. From this they extract a "heat of adsorption" (presumably a bond energy) of ~111 kcal, also in fair agreement with our bond energy of 99.1 kcal.

Although we are not aware of accurate surface diffusion data for sulfur on Ni(100) it is possible to speculate on the probability. The most likely route involves 4(001) → 2(001) → 4(001) jumps, and assuming a rate of 100/sec as indicative of experimentally observable surface hopping, the results of Table V suggest that a temperature of 750K would be required for thermal diffusion.

The photoemission spectrum of adsorbed S has been reported in a number of studies.[33] A single broad feature is observed, centered at 4.5 eV. Recently, it has been noted that extreme conditions of coverage or temperature cause this feature to split into two peaks at 4.5 and 5.75 eV.[34] There is evidence that the new feature may be associated with subsurface sulfur atoms. In Fig. 13 we show our calculated KT-CI[44] spectrum of sulfur induced changes in the density of states. A slight reduction in state density is predicted below ϵ_f, and two sulfur 3p levels are calculated to appear at 6 and 9 eV. While the exact position of these levels is not independent of the nearby cluster levels, it is worth noting that Koopmans' Theorem IP values for atomic sulfur typically place these levels about 1.4eV too deep in energy. It is apparently the case in the experimental spectrum either that one of these levels has a poor cross-section or that they are simply not resolvable into separate features. The latter argument is in tentative agreement with the observation cited above that under extreme conditions resolution into

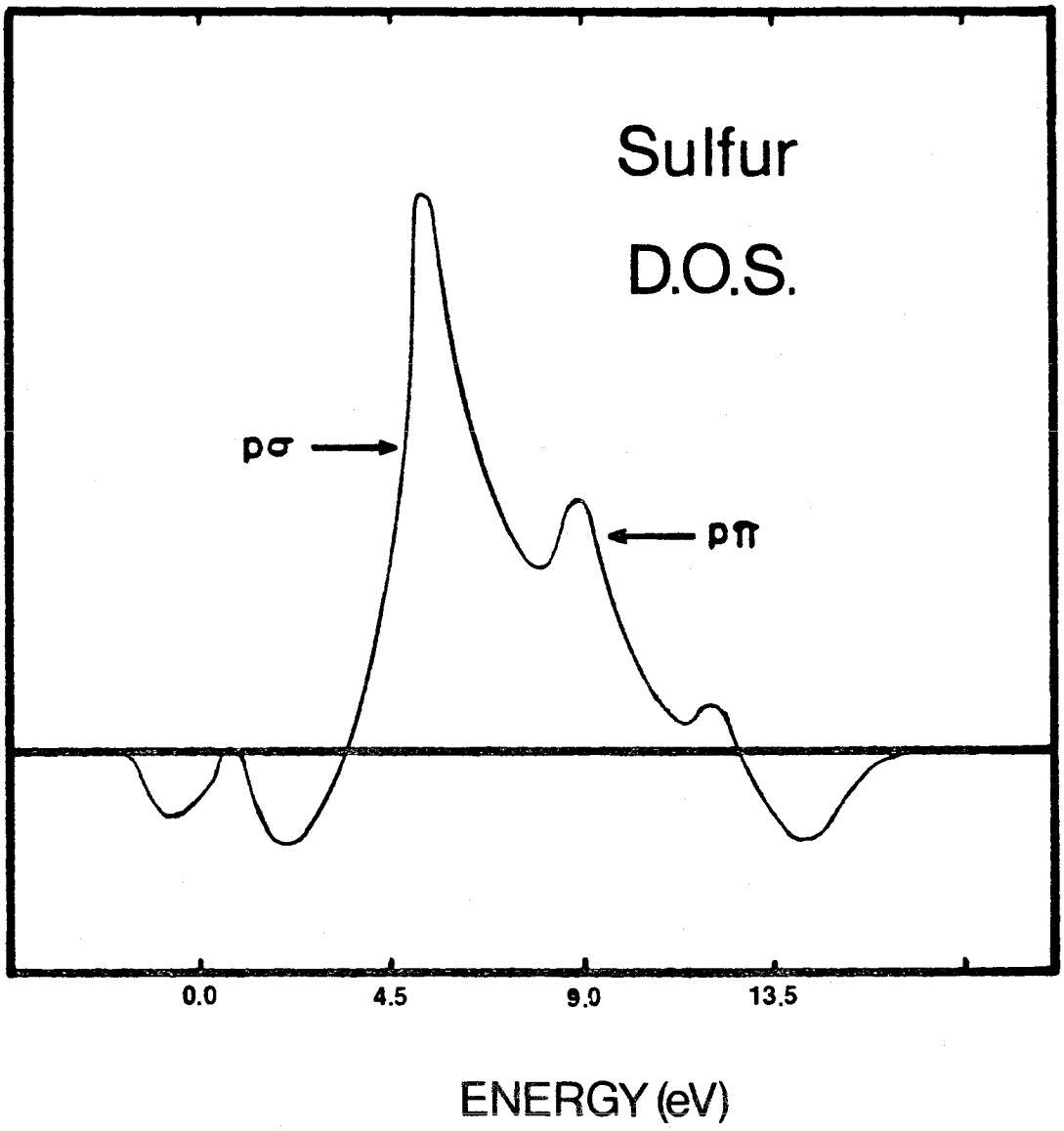

Figure 13: Change in density of states of Ni_{20} caused by the bonding of S at a 4(001) site, from KT-CI calculations.

two peaks is possible.

The rather benign quality of the bonding for sulfur suggests that there should be few pathological effects associated with increasing coverage up to $\theta \approx 0.5$. Little in the way of direct adatom interactions would be expected at p(2×2) coverages, but Fig. 8 suggests that the diffuse $3p_\pi$ orbitals might well begin to interact repulsively in a c(2×2) overlayer. The domination of the bonding by $3p_\sigma$ interactions, as discussed earlier, should make such coverage favorable in spite of the increase in electron pair repulsions. The results of HRELS studies appear to verify this comment: frequencies of 46 and 44 meV are observed for p(2×2)S and c(2×2)S structures[35] (to be compared with 37 meV in Table V), indicating a strong similarity between the two phases. Moving beyond $\theta = 0.5$ however, decreases nearest neighbor distances by ~40%. Interactions between $3p_\pi$ orbitals which are not yet severe in a c(2×2) structure, would undoubtedly become so at this level.

D. Oxygen. As was noted in section III.B.2, the adsorption of oxygen on Ni(100) is expected to show many similarities with sulfur chemisorption, yet there are some important differences. Two low-lying states of the oxygen atom were found on the Ni(100) surface, with an energy separation sufficiently small to warrant consideration of both of them as possible ground states in the bulk chemisorption system.

To probe the properties of these states in more detail, we present in Fig. 14 portions of potential curves resulting from varying $R(\perp)$ for each configuration. The closed shell ground state sits relatively close to the surface ($R_e(\perp) = 0.55$ Å) and in fact, there is only a ~15 kcal

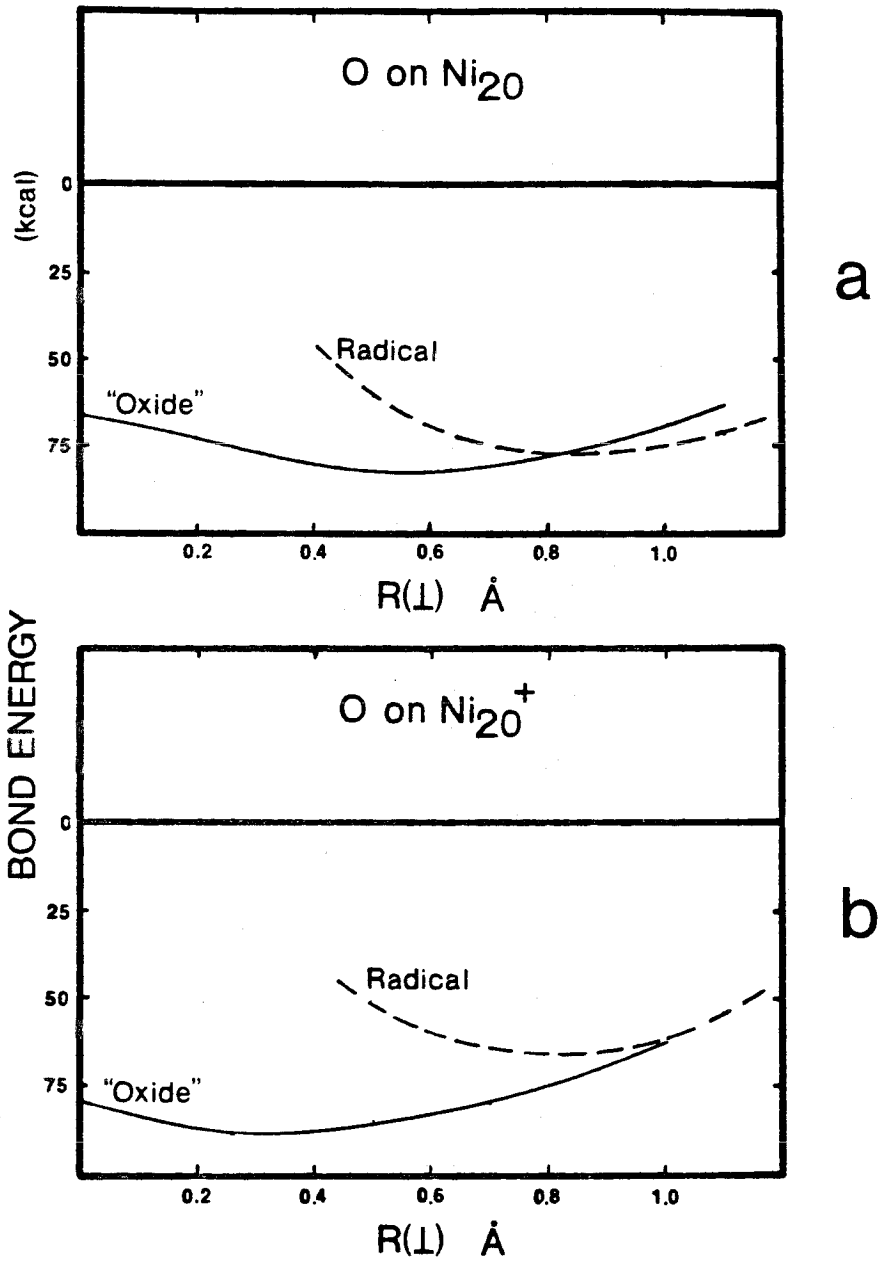

Figure 14: Potential curves for two low-lying states of oxygen on Ni_{20}: (a) for a neutral Ni_{20} substrate; (b) for Ni_{20} with the highest occupied orbital ionized.

barrier to bringing the atom down onto the surface ($R(\perp) = 0.0$ Å). Were Ni atom positions allowed to relax, it is likely that the barrier would be even smaller. On the other hand, the curvature of the radical surface is larger and it is unlikely that an O atom in this state would be able to enter the surface.

Since each of these states involved some ionic character in the bond, some charge depletion in the surface metal layers might be expected under coverage conditions leading to the observed $p(2\times 2)$ or $c(2\times 2)$ structures. To model such a condition, potential curves for both states were obtained where the cluster was in its lowest positive ion states, These curves are shown in Fig. 14b. There is little observable effect on the radical state; its bond distance decreases by only 0.05 Å. The closed shell state on the other hand, moves much closer to the surface and the barrier to bringing it down onto the surface is only ~ 7 kcal (again, where atom positions are forced to be fixed).

The picture that emerges then is one in which the two states might well be expected on thermodynamic grounds to coexist on the surface, but exhibit drastically different properties. Thus, the closed shell state appears to be an oxide precursor: its optimum geometry allows short Ni-O distances and its bonding configuration is precisely that to be expected of an oxygen interstitial. Based on these calculations, it would not be surprising to find little or no barrier to subsurface oxide formation on Ni(100), with any observed barrier being indicative of a transition from $R(\perp) \approx 0.0$ to $R(\perp) < 0.0$. The radical state, predicted to be almost equally favorable thermodynamically, appears insensitive to such charges. Since a transition between this state and the oxide state

is expected to involve at least a small barrier (due to spin recoupling), the existence of a pathway to surface oxide formation does not imply that all adsorbed oxygen atoms must proceed in that direction at lower temperature.

An obvious concern is whether there is experimental evidence to support such a scenario for oxygen chemisorption. Dynamic LEED analysis shows that O atoms sit $\sim 0.9(\pm 0.1)$ Å above 4(001) sites on Ni(001) in both p(2×2)[36] and c(2×2)[37] structures, in almost exact agreement with our results for the radical state. The LEED results cannot be taken as a contradiction of the discussion presented above: the effect of a weakly scattering coadsorbate in the selvedge region of the crystal surface is not expected to be large, nor was it considered in these LEED studies. There is ample evidence from LEED, auger, and work function data that dissolution of oxygen into the surface occurs even as domains of well-ordered overlayers (to LEED) remain.[38] Heating a c(2×2) overlayer to 400°C. or increasing the oxygen exposure at room temperature produces major changes in specular beam spectra and a sharpening of fractional order beams. Such changes are possibly indicative of increased order not only on the surface, but within the surface as well. Auger results show an increase in oxygen concentration when the exposure is increased, yet no increase in work function beyond the c(2×2) result is observed. The lineshapes of the oxygen auger signal, even for the lower coverage p(2×2) phase are highly reminiscent of a severely oxidized NiO surface.

Further support for two forms of oxygen on Ni(100) may be drawn from the results of Andersson's HRELS experiments.[35] At low coverage

[p(2×2) LEED structure], two losses are observed at energies of 32 and 53 meV. From Table III, our calculations would have predicted that under these conditions, when both states were occupied on the surface (i.e., $R(\perp) > 0.0$ Å), the closed shell state should produce a loss at ~27 meV while the radical state would have appeared at ~46 meV. Both numbers are lower than the actual observed frequencies, but are sufficiently close to support the hypothesis. Under higher coverage conditions (where considerations exemplified by Fig. 14b become important), it would be expected that losses due to the radical state would dominate the spectrum since much of the closed shell species would have moved into the surface. The calculations indicate that only a modest decrease in the energy of this loss (to ~44 meV) would result from surface charge depletion. In fact, at c(2×2) coverages a single loss at 39 meV is observed experimentally,[35] a result that is in qualitative agreement with the above but is also suggestive of more serious disruption of the substrate by the coincident dissolution process.

It should be noted that there is an alternate explanation for the HRELS observations. Ibach and Bruchmann[1] have recorded the HRELS spectrum of oxygen on Ni(111) and note a loss attributable to oxygen at 72 meV. There are additional weak features at 16.7 and 33 meV which the authors are able to assign as surface phonon modes. They note that since no $\underline{k}_{\parallel}$ is imparted to the surface in the ELS experiment, vibrations excited from a clean surface or from an adsorbate layer must correspond to modes at the $\underline{\Gamma}$ point in the respective surface brillouin zones (BZ).

However, the adsorbate BZ is in general smaller than the substrate BZ [for (n×m) ordered overlayers where n or m > 1] and in some cases the $\underline{\Gamma}$ point of an extended overlayer BZ may coincide with a point $\underline{k}'$ still within the first substrate zone. In these cases, motion of the substrate atoms with wavevector $\underline{k}'$ may couple with overlayer atom motion normal to the surface of $\underline{k}_{||} = 0$ producing a net dipole derivative. Thus, ELS activity is indirectly provided to surface phonons with $\underline{k}_{||} \neq 0$. The argument may also be applied to the more symmetric Ni(100) surface. In Fig. 15 we show the first surface BZ for the Ni(100) substrate and both p(2×2) and c(2×2) overlayers. In addition, adjacent BZ cells are shown for the overlayer structures from which it may be seen that the $\underline{\Gamma}$ point of the p(2×2) structure coincides with symmetry points $\underline{X}$ and $\underline{M}$ of the first substrate zone. The $\underline{\Gamma}$ point of the c(2×2) zone only coincides with point $\underline{M}$. In Fig. 16, we show both longitudinal and transverse modes with $\underline{k}_{||} = \underline{X}$ and $\underline{M}$ together with the (observed) fourfold lattice positions corresponding to p(2×2) and c(2×2) oxygen overlayers. As may be seen, a p(2×2) overlayer cannot (by symmetry) couple transverse motion to the transverse substrate mode $\underline{k} = \underline{X}$. A longitudinal substrate $\underline{k} = \underline{X}$ mode would force the p(2×2) atoms up and down in unison thus allowing ELS activity. At $\underline{k} = \underline{M}$ however, forces on the overlayer atoms would not lead to motion of p(2×2) or c(2×2) atoms along the surface normal for either transverse or longitudinal substrate motion. Thus, only for a p(2×2) overlayer would a surface phonon mode be observable and in fact, a single extra low energy peak is observed only in this spectrum.[35]

Certainly some of the ambiguity on this point could be removed

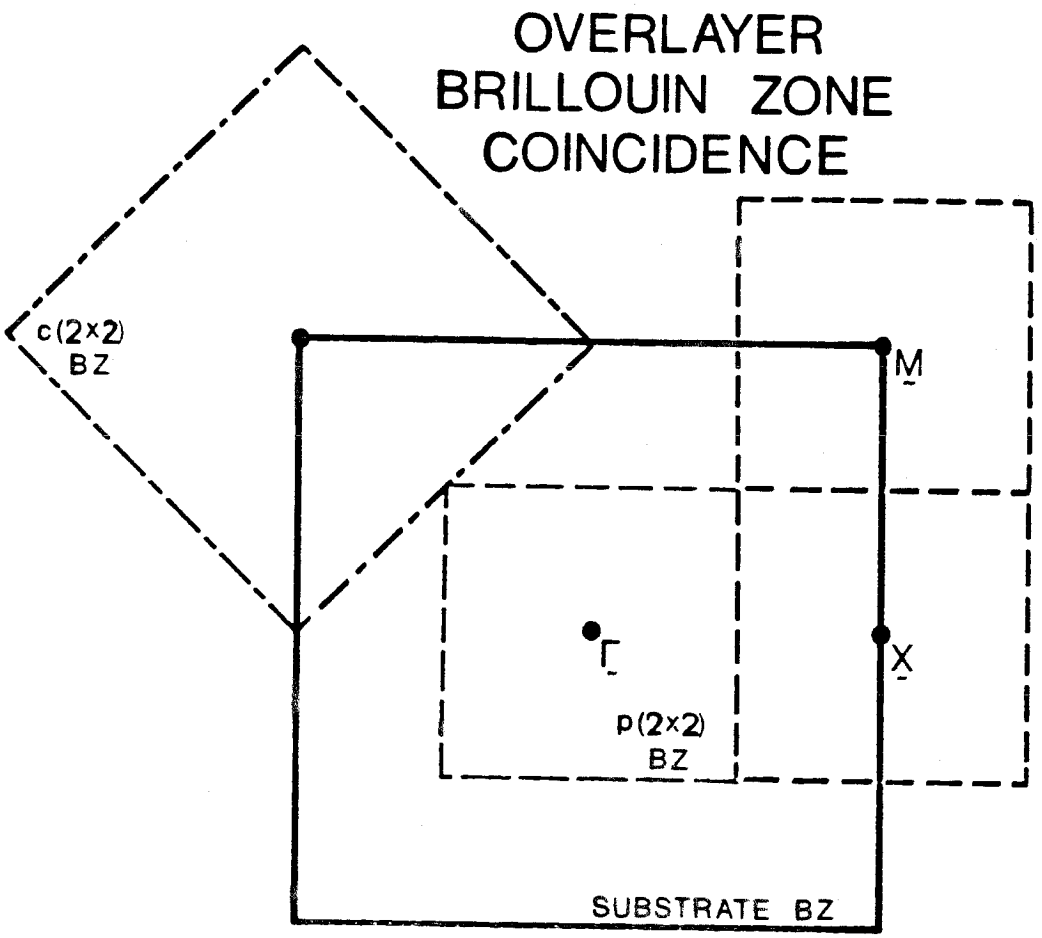

Figure 15: Coincidence of substrate BZ occurs with the p(2 × 2) BZ (— —) at X and M, but only at M with the c(2 × 2) BZ (– – –).

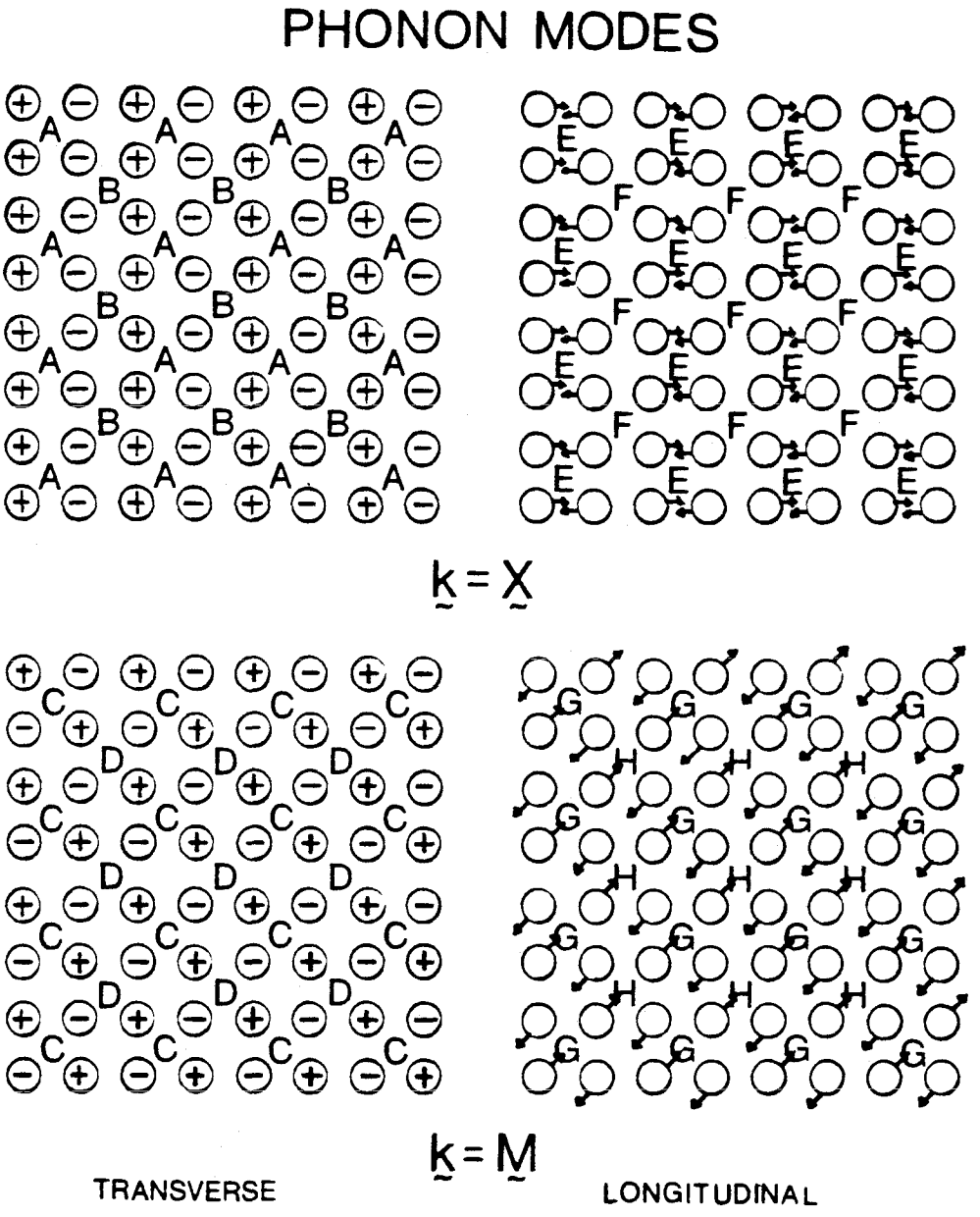

Figure 16: Atom motions corresponding to symmetry points in substrate BZ. Overlayer atom positions needed to form p(2 × 2) are shown as A, C, E, and G. Additional atoms needed to form c(2 × 2) are shown as B, D, F, and H.

through high-resolution analysis of other p(2×2) overlayer structures. No low energy loss is observed in the HRELS spectrum of p(2×2)S on Ni(100),[35] in agreement with our proposed interpretation, however the experimental resolution was such that its existence cannot be absolutely ruled out. Nevertheless, if the phonon coupling concept is correct, a ~32 meV loss should be observable in virtually any p(2×2) overlayer spectrum.

The high solubility of oxygen in nickel at elevated temperatures has made it difficult to measure accurate heats of adsorption. Values for polycrystalline data range from ~4.1-5.8 eV per atom,[39] which, if relevant for Ni(100), would indicate that our value is about 0.5 eV low.

Finally, we note that the Ni(100)-oxygen system has been subjected to both angle integrated[33,40] and angle resolved[33,41] UPS studies. The ARUPS data shows a peak at 8 eV below ϵ_f that is apparently of a_1 symmetry and is thus assigned to a $2p_z$ orbital. A larger peak at 6 eV is apparently due to the p_x and p_y orbitals. It should be pointed out however, that this assignment has recently been reinterpreted[42] in favor of a two-state model where the 6 eV is presumed to possess character due to a subsurface or imbedded oxygen species. Our KT-CI ionization spectra for the two states are plotted in Fig. 17. For an oxygen atom or anion KT errors are typically on the order of 2.0 to 3.0 eV, giving some indication of the inherent error here. Qualitatively, the orbitals of the closed shell state are more anionic and thus less bound, resulting in smaller IPs. From these results, a near coincidence of the radical $2p_\pi$ and closed shell peaks would be expected.

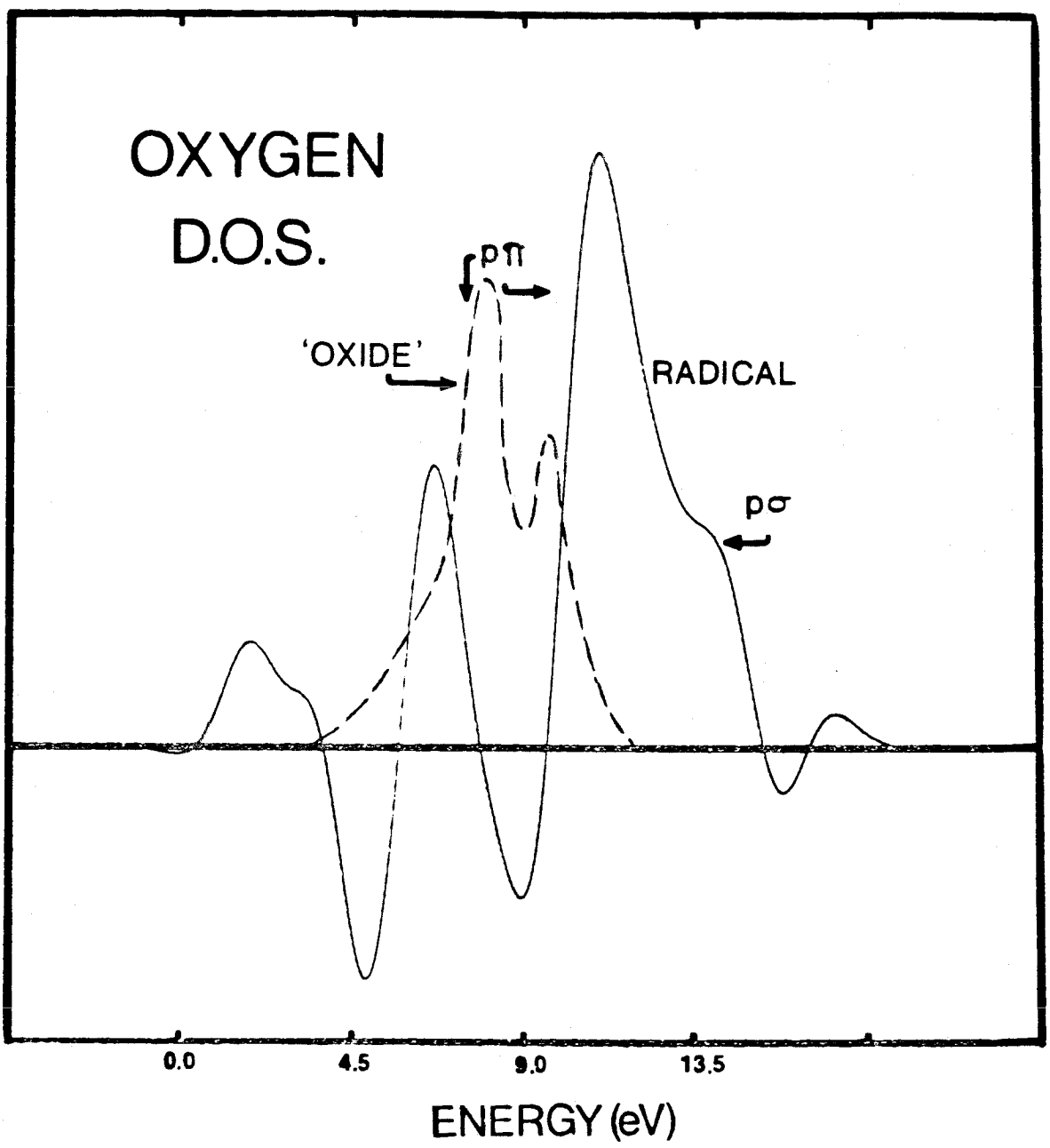

Figure 17: Change in Ni_{20} density of states arising from oxygen adsorption at 4(001) site, from KT-CI calculations.

REFERENCES AND NOTES

1. H. Ibach and D. Bruchmann, Phys. Rev. Lett. 44, 36 (1980).
2. C. D. Wagner, J. Vac. Sci. Technol. 15, 518 (1978).
3. T. Ngyyen, R. Cinti, and Y. Capiomont, Surf. Sci. 87, 613 (1979).
4. K. Christmann, R. J. Behm, G. Ertl, M. van Hove, and W. Weinberg, J. Chem. Phys. 70, 4168 (1979).
5. J. McCarty and R. J. Madix, J. Catal. 38, 402 (1975).
6. T. Smedley, A. K. Rappé, and W. A. Goddard III, unpublished results; for Ni: M. Sollenberger, M. S. Thesis, California Institute of Technology (1977); see Appendix V. A.
7. A. J. H. Wachters, J. Chem. Phys. 52, 1033 (1970).
8. T. H. Upton, W. A. Goddard III, and C. F. Melius, J. Vac. Sci. Technol. 16, 531 (1979).
9. W. P. Pearson, Handbook of Lattice Spacings and Structures of Metals and Alloys (Pergamon Press, New York, 1958).
10. C. F. Melius, T. H. Upton, and W. A. Goddard III, Solid State Commun. 28, 501 (1978).
11. C. E. Moore, NSRDS-NBS 35, Vol. II, 1971.
12. A. A. Holscher, Surf. Sci. 4, 89 (1966).
13. A. G. Gaydon, Dissociation Energies and Spectra of Diatomic Molecules (Chapman and Hall, London, 1969).
14. T. H. Upton and W. A. Goddard III, Phys. Rev. Lett. 42, 472 (1979).
15. S. Benson, Thermochemical Kinetics (Wiley, New York, 1976).
16. S. P. Walch and W. A. Goddard III, Surf. Sci. 72, 645 (1978).

17. K. P. Huber and G. Herzberg, Constants of Diatomic Molecules (Van Nostrand-Reinhold, New York, 1979).

18. See Appendix V. A for details of basis sets and effective potentials.

19. S. Andersson, Chem. Phys. Lett. 55, 185 (1978).

20. J. Lapujoulade and K. S. Neil, Surf. Sci. 35, 288 (1973).

21. J. Lapujoulade and K. S. Neil, J. Chem. Phys. 57, 3535 (1972).

22. K. Christmann, O. Schober, G. Ertl, and H. Neuman, J. Chem. Phys. 60, 4528 (1974).

23. R. Gomer, J. Chem. Phys. 27, 1099 (1957).

24. B. T. Huie, C. B. Knobler, and H. D. Kaesz, J. Chem. Soc. Chem. Commun. 684 (1975).

25. J. E. Demuth, Surf. Sci. 65, 365 (1977).

26. F. Himpsel and D. E. Eastman, Phys. Rev. Lett. 41, 507 (1978).

27. (a) J. E. Demuth, J. Phys. C: Solid State Phys. 8, L25-30;
(b) R. L. Gerlach and T. N. Rhodin, Surf. Sci. 19, 403 (1970).

28. J. E. Demuth, D. W. Jepsen, and P. M. Marcus, Phys. Rev. Lett. 31, 540 (1973).

29. H. Windawi and J. R. Katzer, J. Vac. Sci. Technol. 16, 497 (1979).

30. A. Clark, Theory of Adsorption and Catalysis (Academic Press, New York, 1970).

31. D. D. Wagman, National Bureau of Standards (U. S.) Technical Note No. 270-4.

32. J. McCarty, H. Wise, and B. J. Wood, J. Vac. Sci. Technol. 16, 566 (1979).

33. (a) H. Hagstrum and G. E. Becker, J. Vac. Sci. Technol. 14

369 (1977); (b) S. Weeks and E. Plummer, Solid State Commun. 21, 695 (1977); (c) G. B. Fisher, Surf. Sci. 62, 31 (1977); (d) E. McRae, D. Aberdam, R. Baudoing, and Y. Gauthier, Surf. Sci. 78, 518 (1978).

34. S. Weeks and E. Plummer, Chem. Phys. Lett, in press.

35. S. Andersson, Surf. Sci. 79, 385 (1979).

36. (a) P. Marcus, J. Demuth, and D. Jepsen, Surf. Sci. 53, 501 (1975); (b) M. van Hove and S. Tong, J. Vac. Sci. Technol. 12, 230 (1975).

37. J. Demuth, D. Jepsen, and P. Marcus, Phys. Rev. Lett. 31, 540 (1973); Solid State Commun. 13, 1311 (1973); J. Phys. C 6, L307 (1973).

38. J. Demuth and T. N. Rhodin, Surf. Sci. 45, 249 (1974).

39. I. Toyoshima and G. A. Somorjai, unpublished results.

40. (a) D. Eastman and J. Cashion, Phys. Rev. Lett. 27, 1520 (1971); (b) J. Kuppers and G. Ertl, Surf. Sci. 77, L647 (1978); (c) J. Miller, D. Ling, I. Lindau, D. Collins, and W. Spicer, ibid. 77, L651 (1978).

41. (a) F. Himpsel and D. Eastman, Phys. Rev. Lett. 41, 507 (1978); (b) K. Jacobi, M. Scheffler, K. Kambe, and F. Forstmann, Solid State Commun. 22, 17 (1977).

42. A. Bradshaw, private communication regarding Ref. 41b.

43. Small CI calculations (denoted KT-CI) were carried out to allow mixing of ion states much as occurs in a Koopmans' Theorem level IP. Each of the levels (doublets and quartets) was given a gaussian half-width of 2 eV, and the difference between Ni_{20} and $Ni_{20}X$ D. O. S. was plotted.

Appendix III.A: Cluster Size Effects in the Bonding of H on Ni_{28}

I. Introduction

A fundamenetal criterion for the success of a chemisorption study using cluster models for the bulk is that the results obtained be independent of cluster size. Certainly, results for a particular cluster that compare favorably with the analogous bulk results can be judged as no better than coincidental if the agreement deteriorates substantially upon altering the cluster.

In previous studies of clusters ranging in size from 4-10 atoms it was found that calculated geometries and force constants varied only slightly as cluster size was changed, but bond energies exhibited wide swings. Hydrogen atom bond energies ranged from 0.0 eV for an Ni_4 cluster to 4.5 eV for an Ni_7 cluster. A reliable cluster model of this size could not be found.

One faces a choice: very small clusters may be examined in great detail (including self-consistent treatment of 3d electrons) risking a possible loss of relevance to the bulk system or much larger clusters may be employed with a concomitant reduction in detail.

In the previous section, results were outlined for atomic chemisorption in which an Ni_{20} cluster was used as a bulk model. Features that led to its success included: 1) high density of states or equivalently 2) highly polarizable charge density and 3) bulk-like work function. Each of these properties is closely related to cluster size, and it was of great interest to determine whether these requirements were met sufficiently well by Ni_{20}, such that further increases in size would not produce changes in bond parameters. Accordingly, we have considered

the bonding of H on an Ni_{28} cluster. The Ni_{28} cluster is constructed by adding all new second nearest neighbors to the two adjacent "bulk" atoms of the Ni_{20} cluster. As such it has many sites in common with the Ni_{20} cluster, and direct comparisons are possible. The cluster and its bonding sites are illustrated in Fig. 1.

II. Discussion

The orbital energy spectrum for Ni_{28} is shown in Fig. 2. As was found for Ni_{20}, there is an even distribution of levels up to the "fermi energy". As a result, we would expect not only a good description of ion states (assuming adsorbate ion states are also well described by Koopmans' Theorem). but a large collection of low-lying virtual states just above ϵ_f. This latter feature should allow a sufficiently number of energetically accessible excited states to produce the polarizable electron density in the conduction band, found to be so important for Ni_{20}.

The 28 atom cluster is composed entirely of (111) facets as is evident from Fig. 1. As a result, the bond parameters collected in Table A-I include primarily 2(111) and 3(111) sites. The exceptions are 2(001) and 2(110) sites, representing edge or step sites on the cluster. The results in the Table may be compared directly with those in Table II of the previous section. For the twofold sites, the 2(110) site is unfavorable, as it was for Ni_{20}. Similarly, there are 3(111) sites that show deviant properties. The difficulties for each of the sites may be traced to the fact (vide infra) that at these sites the H atom must bond to a cluster excited state. Thus, here as in Table II, the bond parameters are noted in parentheses. For the remainder of

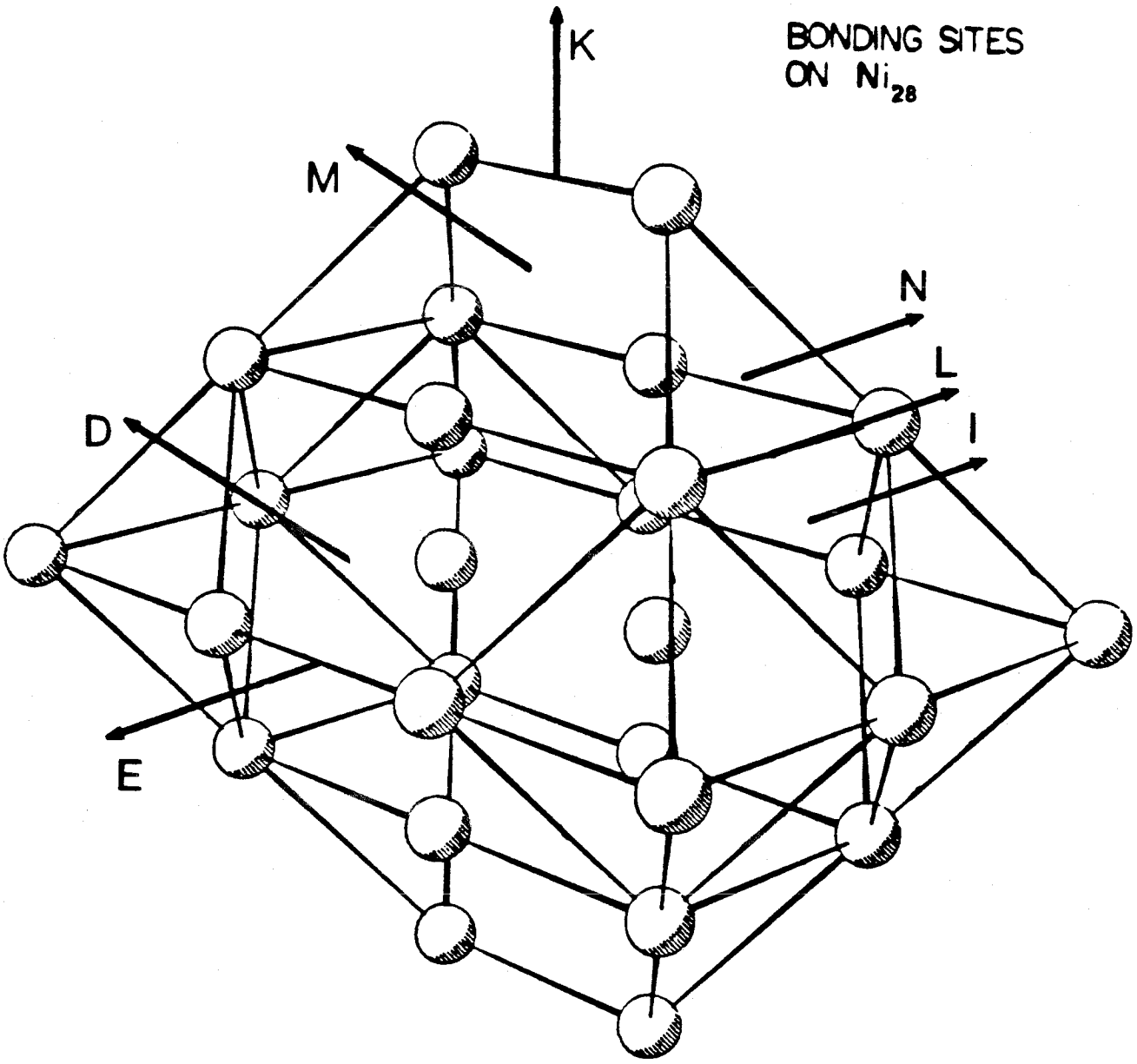

Figure 1: Bonding sites on Ni_{28}

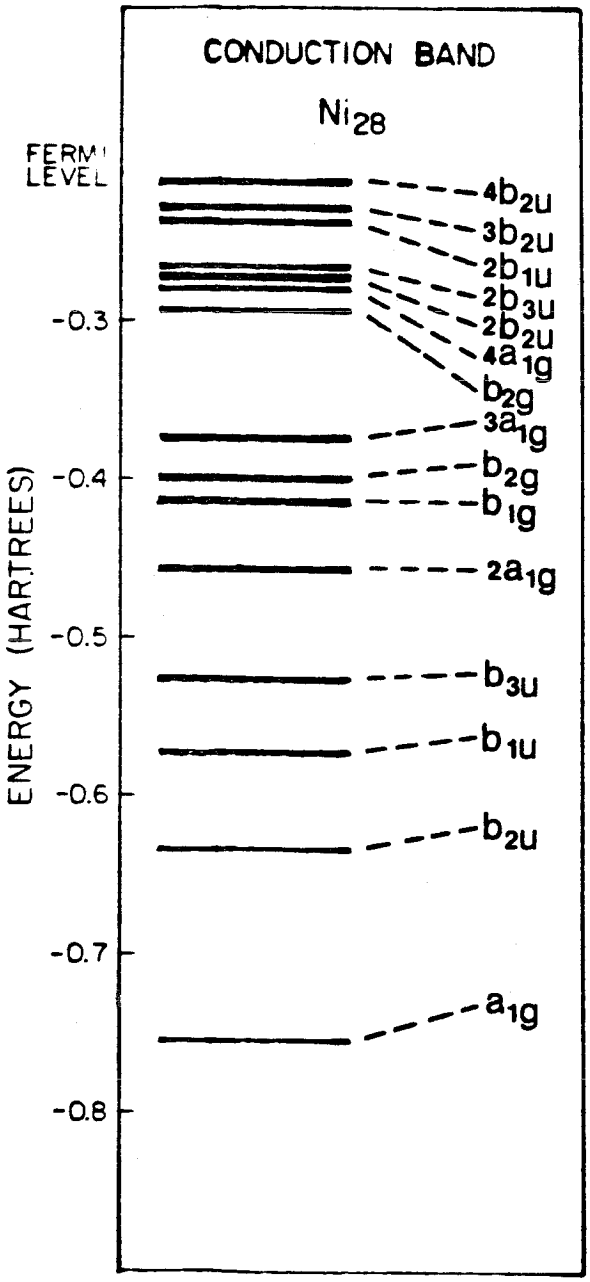

Figure 2: Orbital energies for Ni_{28}

the sites, the calculated bond parameters do not deviate appreciably from the Ni_{20} results.

In Fig. 3, a spectrum of orbital energies is shown that results when the H atom is bound at each of four different sites on the 28 atom cluster. Examination of Fig. 1 shows these sites to represent a traversal of the cluster in a ⟨110⟩ symmetry plane. The dotted lines connecting the different sets of levels trace the position of each cluster orbital from site to site. These correlations were obtained by projecting the cluster component of the $Ni_{28}H$ orbitals onto the original Ni_{28} set. In each case, it was found the $Ni_{28}H$ orbitals are described to about 99% as linear combinations of the original cluster orbitals.

Two very important modifications are noticable in the figure. At each site, a new level appears near -0.5 h and a high-lying cluster level is pushed above the fermi level (i.e., unoccupied). The new level is found to have predominantly H character ($> 50\%$), while the destabilized level is always the highest level with large density in the bonding region.

That the cluster does not fully mimic the bulk is indicated by the behavior of levels near the fermi energy. In Fig. 3, it is the second highest Ni_{28} levels that are destabilized at sites N and L. For both sites K and I, a deeper doubly-occupied orbital is forced to give up an electron. For site K, this produces a quartet state, while at site I, two of these singly-occupied orbitals collapse to form a net doublet. Thus, cluster "bonds" must be broken to accommodate the H at these sites. This occurrence is reflected in part by the smaller binding energy at sites K and I than at nearly equivalent sites L and N.

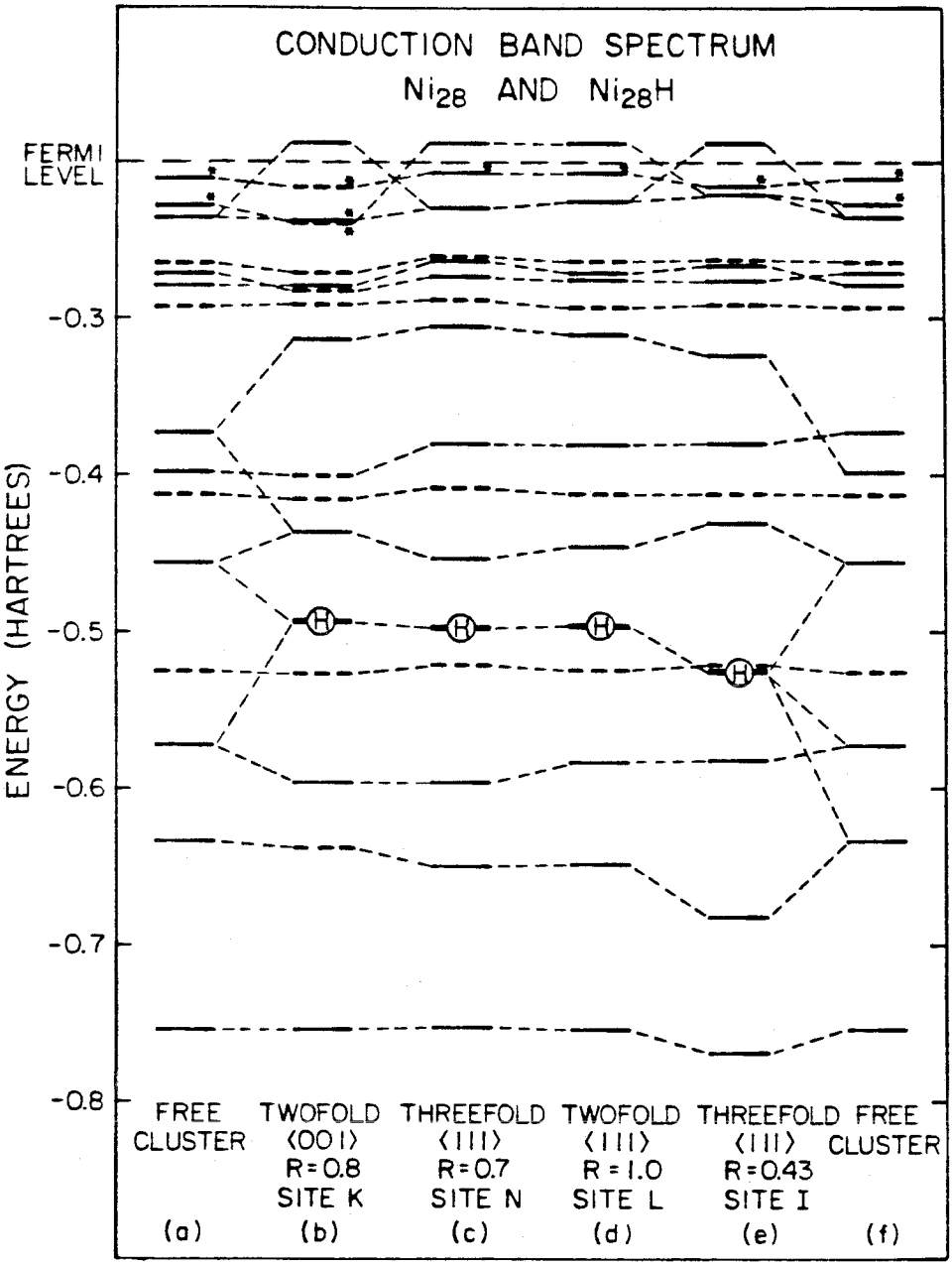

Figure 3 Spectrum of states for Ni_{28} and $Ni_{28}H$ clusters. Levels connected by light dashed lines are of similar orbital character. The H on a level indicates the orbital with maximum H character. Dashed levels are for orbitals unable to interact with the H atom by symmetry. The location of the "fermi level" is arbitrary and is used only to differentiate between occupied and unoccupied orbitals. Asterisks indicate singly-occupied orbital levels.

Similar, but more drastic, excitations lead to weaker binding energies at the other Ni_{28} threefold sites. For sites E, M, and D, the effect is severe enough to make the results questionable. Presumably, such juggling of states occurs in the bulk system, but the continuous density of states causes the energetic cost to be negligible.

III. Conclusion

The results in this Appendix may be summarized as follows:

1) A general analysis of the bonding parameters for H chemisorption indicates that the effects of changing cluster size do become small when clusters of this size (20-30 atoms) are considered. The results lend support to the concept that such systems may serve as models for bulk systems.

ii) There are cluster electronic effects that are present for both Ni_{20} and Ni_{28} that can affect the calculated bond parameters seriously. As these effects are closely tied to the density of states, it is unlikely that they will fully dissipate until very large cluster sizes are reached. Problem sites may be easily identified however, which lessens the impact of this difficulty.

Table A-I: Bond Parameters for H Binding Sites on Ni_{28}

Site	Description			Bondg Length (Å)	Vibrational Frequency	Chemisorption Energy
	Surface	Ligancy of H	Ligancy of Surface Ni Atoms[a]	$R_{\perp}$[b]	meV	eV
K	⟨001⟩	2	5,5	0.94	165	2.23
L	⟨111⟩	2	7,7	0.93	176	2.47
E	⟨110⟩	2	7,7	0.95	(158)	(1.31)
M	⟨111⟩	3	5,5,9 hcp	0.72	(147)	(2.25)
D	⟨111⟩	3	9,7,7 fcc	0.69	(157)	(2.11)
N	⟨111⟩	3	5,7,7 fcc	0.79	151	3.14
I	⟨111⟩	3	7,7,7 hcp	0.73	145	2.75

[a]Number of nearest neighbor atoms for the Ni atom(s) at the binding site. Where non-equivalent surface atoms are present, values are given for each type.

[b]Optimum distance from H to the plane representing the surface.

Appendix III.B: The Dissociation of H_2 on Ni(100); An Ab-Initio Parameterized LEPS Study

1. Introduction

The interaction between hydrogen and transition metal surfaces represents an appropriate system with which to begin study of dissociative chemisorption. While the experimental details of hydrogen chemisorption on many metals are complex, it is an attractive problem from a theoretical point of view because of the simplicity of the bond that must be broken.

A number of studies have considered dissociative chemisorption using techniques such as generalized valence bond (GVB) [1], extended Hückel [2, 3], CNDO [4], and a variety of more qualitative approaches [5]. Recently, we reported Hartree-Fock (HF) results for the atomic adsorption of hydrogen on large nickel clusters [6] that agreed well with available experimental data for the low index Ni surfaces [7]. As a first step towards examining the dissociative reaction, we report here the results of HF, GVB, and semi-empirical London-Eyring-Polanyi-Sato (LEPS) [8] calculations on possible reaction pathways by which the chemisorption reaction might occur. Of primary importance is the acquisition of a more thorough understanding of the competition between physically adsorbed (molecularly adsorbed) and chemisorbed states, and the degree to which transitions between the two are responsible for the observed lack of an activation energy for dissociative hydrogen adsorption on nickel. While primarily of qualitative interest, the calculations should delineate the dominant interactions and provide a focus for more detailed study.

2. Qualitative Considerations

It is well known that hydrogen chemisorbs dissociatively on nickel without an activation energy [7a, c]. A simple qualitative model put forth by Lennard-Jones [9] to explain such phenomena is shown schematically in fig. 1. In this model, the potential surface due to a weakly bound physically adsorbed state is crossed below the zero of energy by another surface due to more strongly chemisorbed atoms. Assuming that the energy required to recouple the electrons at the crossing point is small, bond scission will occur without activation.

An adequate theoretical treatment of this problem must be able to consider both types of bonding situations. Since there is limited detailed experimental information concerning the atomic binding limit, and almost none concerning possible physically adsorbed states, it is difficult to parameterize semi-empirical methods accurately. In addition, it is not practical to attempt an investigation of ab initio quality capable of considering the vast number of geometries required to construct a potential surface.

Accordingly, we have chosen an intermediate approach. HF calculations have been carried out previously to characterize the final chemisorbed state [6], and additional HF and GVB calculations are reported here that consider the limit in which the molecular bond is still intact. From these results, we have extracted the information necessary to obtain parameters for the LEPS method, and have generated full potential surfaces for several possible approach geometries on the Ni(001) surface.

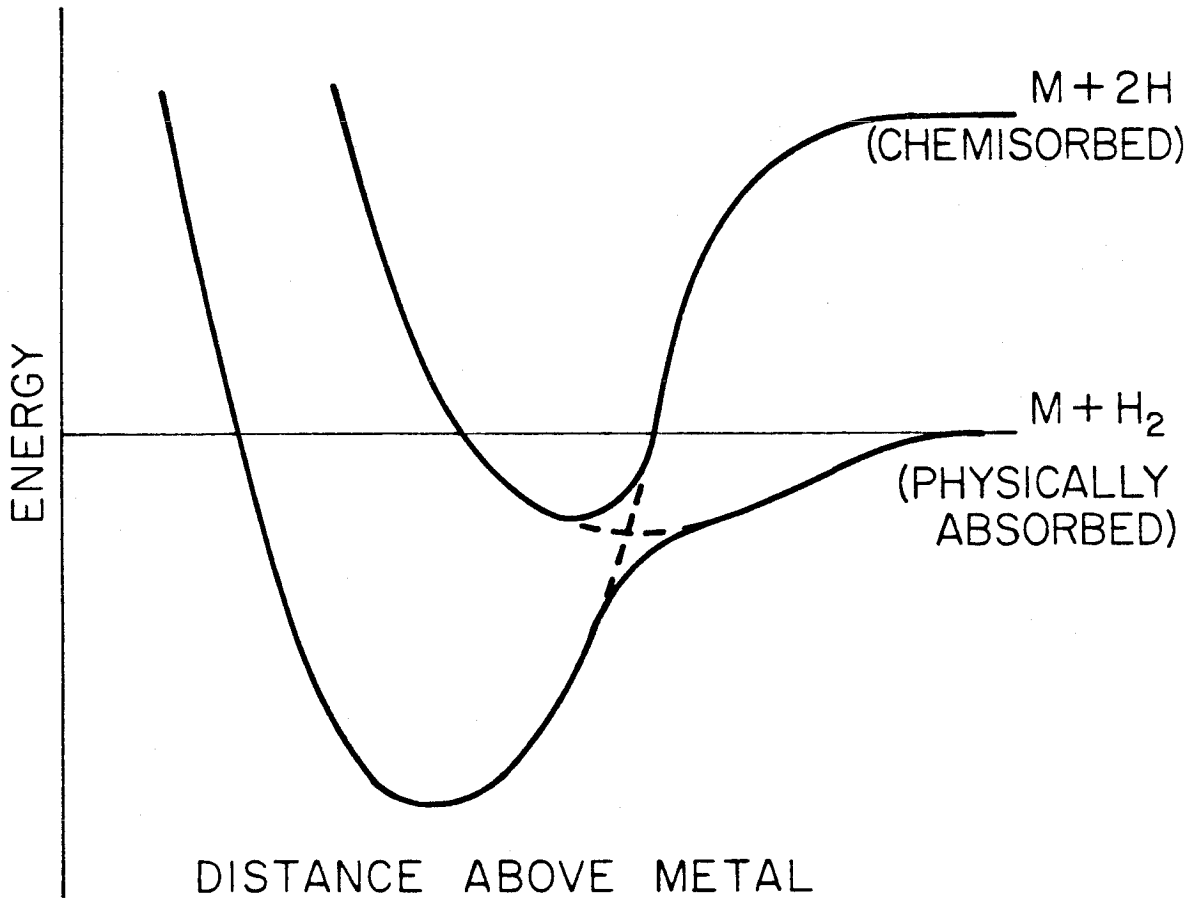

Fig. 1. Qualitative model due to Lennard-Jones, in which unactivated dissociation results from crossing of the physically adsorbed and chemisorbed potential curves.

3. First Principles Calculations

3.1 Calculational Details

For the physically adsorbed state, the interaction between the adsorbate and the surface is weak, and hence a relatively simple cluster may suffice to model the surface. Thus, a small eight-atom cluster was selected that emphasizes twofold and fourfold sites (sites calculated previously [6] to be of greatest importance on the Ni(001) surface). This cluster is shown in fig. 2a. An effective potential was used to replace the Ar core and the $3d^9$ shell on each Ni atom, reducing the variational problem to a single valence electron (primarily 4s in character) per metal atom. This procedure has been shown previously to be adequate both for studies of the chemisorption of hydrogen [6] and the electronic states of the cluster [10]. The effective potential was obtained using the method of Melius et al. [11a] and modified [11b] to ensure the correct ordering of the Ni atomic states. In the calculations, the basis set for the Ni atoms consisted of atomic 4s functions [from the $(4s)(3d)^9$ state] [12a], and an unscaled 1s basis was used for the hydrogens [12b]. All calculations on the cluster itself were at the HF level, while calculations on the physically adsorbed state included correlation effects (GVB [12c]) in the H_2 bond.

3.2 Results and Discussion

The ground state of the Ni_8 cluster was found to be closed-shell, $^1A_1$, with an electronic configuration of $1a_1^2 2a_1^2 1b_1^2 1b_2^2$. The orbital energy spectrum of this cluster is shown in fig. 3a. If an H_2 molecule approaches the cluster in the geometry shown in fig. 2b with the H-H distance constrained to be that of free H_2, we find that there is a local

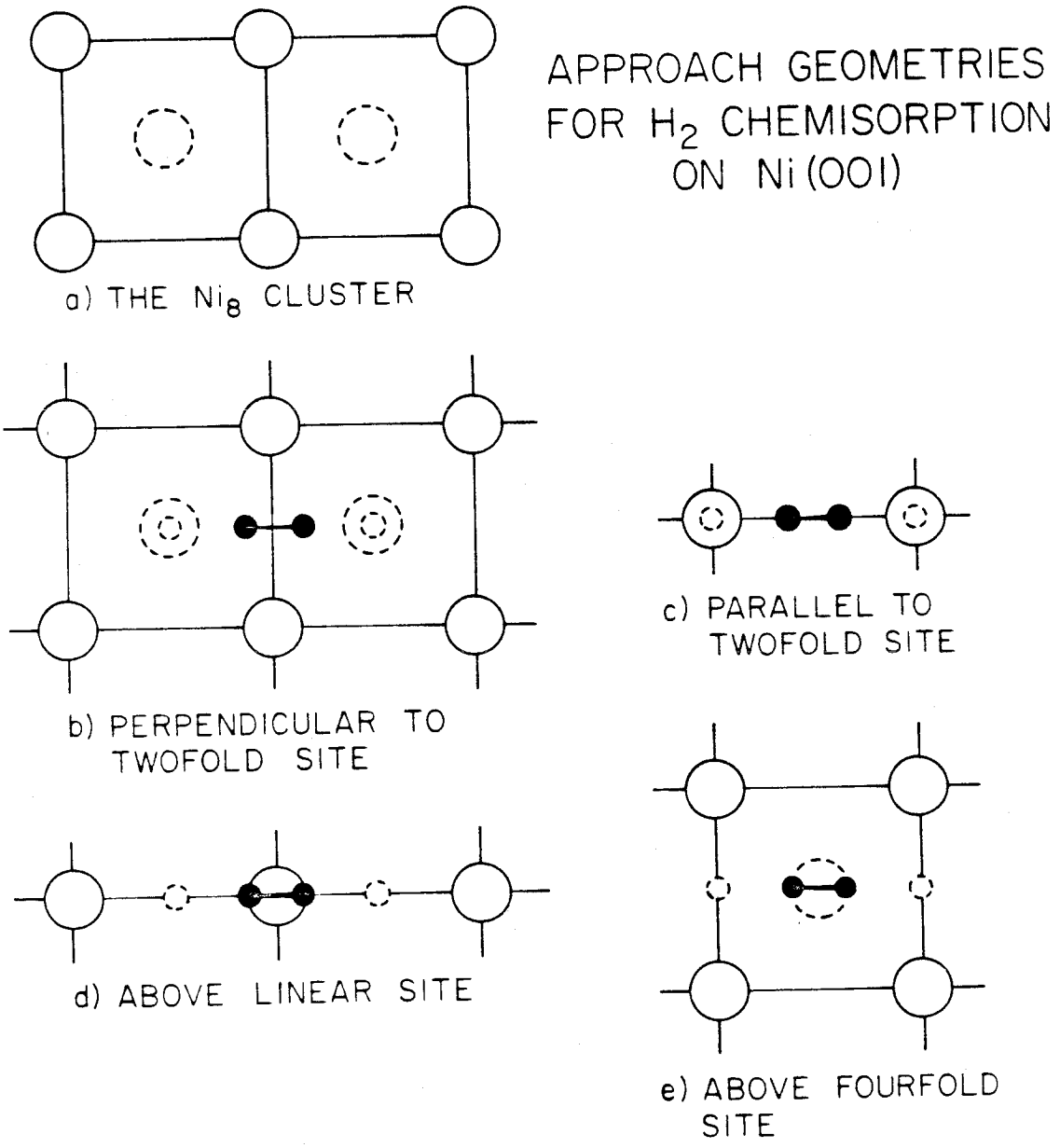

Fig. 2. The Ni_8 cluster and configurations for the H_2/Ni(001) system studied. The small dashed circles are the H atoms for limiting atomic adsorption. The H-H distance is parallel to y, and the middle point of this bond is above. (a) The Ni_8 cluster. (b) Dissociation across a twofold site (x = 0, y = a/2). (c) Dissociation parallel to twofold axis (x = 0, y = a/2). (d) Dissociation above Ni atom (x = 0, y = 0). (e) Dissociation above fourfold site (x = a/2, y = a/2).

minimum at a distance of 2.2 a.u. above the surface (the smallest Ni-H distance is 3.29 a.u.). The orbitals of the system retain their separated "molecular" character and thus this state represents a physically adsorbed hydrogen molecule. This is reflected in the Ni_8H_2 orbital energy spectrum, shown in fig. 3b, in which only the H_2 orbital changes position significantly. While the bond energy of 14 kcal identifies this as a physically adsorbed state, it is not clear that it would be stable with respect to H-H bond elongation. Our aim in this calculation was to obtain parameters for describing physically adsorbed states, and calculations involving H-H stretching were not undertaken.

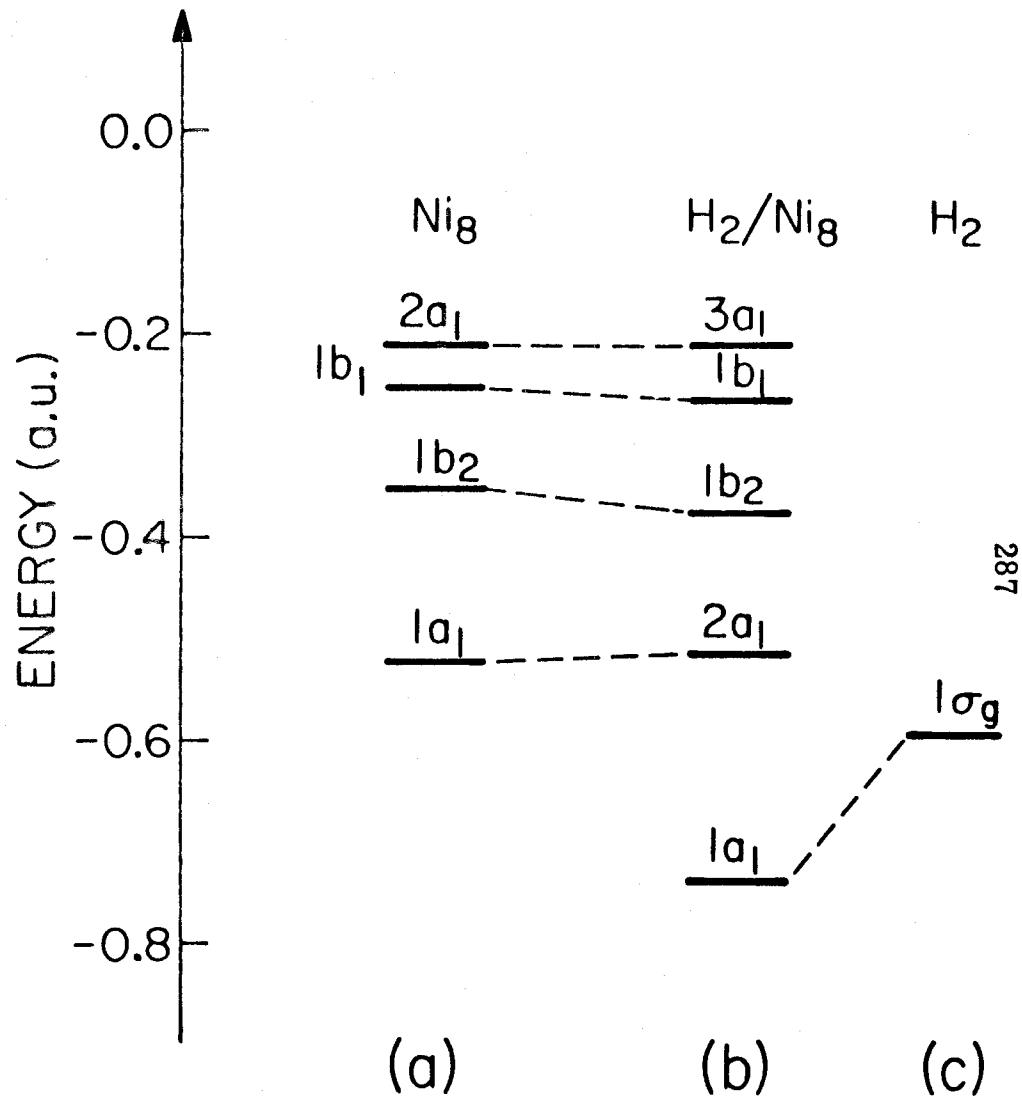

Fig. 3. Correlation diagram for the Ni_8-H_2 interaction. (a) Separate Ni_8 orbital energies. (b) The Ni_8 H_2 orbital energies. (c) Separate H_2 orbital energy.

4. Semi-Empirical Calculations

4.1 Calculational Details

The LEPS approximation has been used extensively to model gas phase dynamics [13] and more recently has been applied to the study of hydrogen chemisorption on tungsten [14] and copper [15]. Results have shown that the method provides a reasonable description of adsorption phenomena, and it is attractive in its simplicity. Following McCreery and Wolken [14], one assumes that for the interaction between the metal and hydrogen molecule, a simple four-electron valence bond treatment is applicable. The individual pairwise interactions included in such a treatment are indicated by the lines in fig. 4a. This is simplified further to include only the dominant interactions (H_1-H_2, H_1-M_1, H_2-M_2) as in fig. 4b. The corresponding energy expression is [14]

$$E(R) = J_{H_1H_2} + J_{H_1M_1} + J_{H_2M_2} - \{K^2_{H_1H_2} + (K_{H_1M_1} + K_{H_2M_2}) \times (K_{H_1M_1} + K_{H_2M_2} - K_{H_1H_2})\}^{\frac{1}{2}}, \quad (1)$$

where J_{ij} is a coulomb interaction and K_{ij} is an exchange interaction between centers i and j. These quantities are assumed to be related to bonding (Morse) and antibonding (anti-Morse) functions through the formulae,

$$E^b_{ij} \approx (J_{ij} - K_{ij})/(1 + \Delta_{ij}) \approx D_{ij} \exp[-\alpha_{ij}(r - r_e)] \{\exp[-\alpha_{ij}(r - r_e)] - 2\} \quad (2)$$

$$E^a_{ij} \approx (J_{ij} + K_{ij})/(1 - \Delta_{ij}) \approx D_{ij} \exp[-\alpha_{ij}(r - r_e)] \{\exp[-\alpha_{ij}(r - r_e)] + 2\}, \quad (3)$$

where Δ_{ij} is an adjustable parameter [8], and the remaining parameters are those of the Morse function:

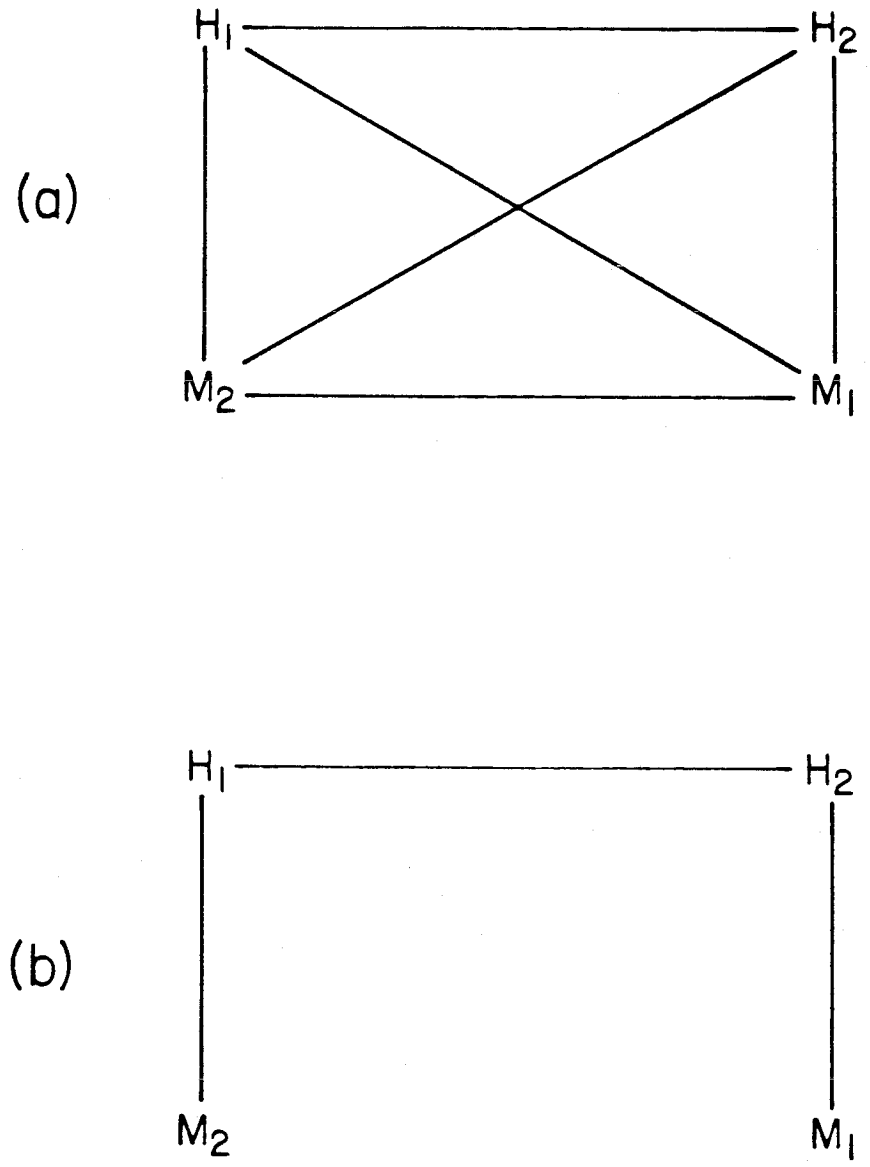

Fig. 4. Valence bond diagram for H_2-M interaction. (a) Full four-electron diagram. (b) Modified to include only dominant interactions.

D_{ij} - dissociation energy

r_0 - equilibrium separation

a_{ij} = $k(\mu/0)^{\frac{1}{2}}\omega$

μ - reduced mass

ω - vibrational frequency.

Thus, it remains only to determine empirical forms for E^b_{ij} and E^a_{ij} and to substitute them into eq. (1) to obtain the potential energy surface.

The Morse parameters of the H-H bond are well known [16], and are shown in table 1. For the H_i-M_i Morse function, the parameters are assumed to be dependent on surface site, as [14]

$$E^b_{HM} = D \exp[-\alpha_{HM}(z - z_e)]\{\exp[-\alpha_{HM}(z - z_e) - 2\}, \tag{4}$$

where the dissociation energy D, the equilibrium distance z_e, and the vibrational frequency ω are functions of x and y (in the surface plane),

$$D = D_0[1 + d_1 S(x, y) + d_2 P(x, y)] \tag{5}$$

$$z_e = z_0[1 + z_1 S(x, y) + z_2 P(x, y)] \tag{6}$$

$$\omega = \omega_0[1 + \nu_1 S(x, y) + \nu_2 P(x, y)] \ . \tag{7}$$

The functions S and P are determined by the structure of the surface,

$$S(x, y) = \cos(2\pi_x/\ell_1) + \cos(2\pi_y/\ell_2) \tag{8}$$

$$P(x, y) = 1 + \cos(2\pi_x/\ell_1)\cos(2\pi_y/\ell_2) \ , \tag{9}$$

where for Ni(001), $\ell_1 = \ell_2 = 4.7$ a.u.

With values obtained earlier [6] from ab initio studies of bonding a hydrogen atom at onefold, twofold, and fourfold sites on Ni(001), sufficient information is available to fit each of the three parameters for D,

Table 1

Bond values and Morse parameters for H-H and H-Ni interactions

Bond Values Calculated for Atomic Adsorption[a]			
Site	z_e (a.u.)	D (eV)	ω (cm^{-1})
Linear	2.83	1.56	2286
Twofold	1.87	2.73	1428
Fourfold	0.57	3.04	592
Calculated H-Ni Morse Parameters			
i	z_i (a.u.)	d_i (eV)	ω_i (cm^{-1})
0	1.87	2.73	1428
1	0.30303	-0.13553	0.29657
2	-0.04545	-0.07875	0.00385
Morse Parameters for H-H[b]			
	r_0	D_0 (eV)	ω (cm^{-1})
	0.7416	4.476	4395

[a] Upton and Goddard, ref. 6.

[b] Herzberg, ref. 16.

z_e, and ω. The bond values used in the fitting, and the resulting parameters are collected in table 1.

All that remains is to obtain values for the Δ_{ij}. This parameter is highly sensitive to the form of the potential surface being considered. Following McCreery and Wolken, we have used the same Δ parameter for each Morse curve. This was obtained by adjusting Δ in such a way as to cause the total energy function E(R) in eq. (1) to reproduce as closely as possible the potential curve for the molecule-solid interaction described in the previous section. The resulting fit is shown in fig. 5, where the E(R) function is compared with GVB results for physically adsorbed H_2 on the Ni_8 cluster.

By parameterizing the LEPS equations in this manner, information is included that allows discrimination between different possible bonding schemes on the Ni(001) surface. Given the large differences in calculated binding energies for different sites (see table 1), it is unlikely that experimental studies could provide sufficient information to define such a parameterization.

4.2 Results and Discussion

For simplicity, only approach geometries with the H_2 axis parallel to the surface were considered. They are shown schematically in fig. 2b-e, where initial positions of the hydrogen molecule are indicated by small dark circles, and final atomic positions by small dashed circles.

For an approach with the H-H axis above and parallel to a twofold site, as in fig. 2c, the potential surface shown in fig. 6 is obtained. In this figure, the H-H separation plotted along the ordinate (R) and the height of the molecule above the surface is indicated along the abscissa

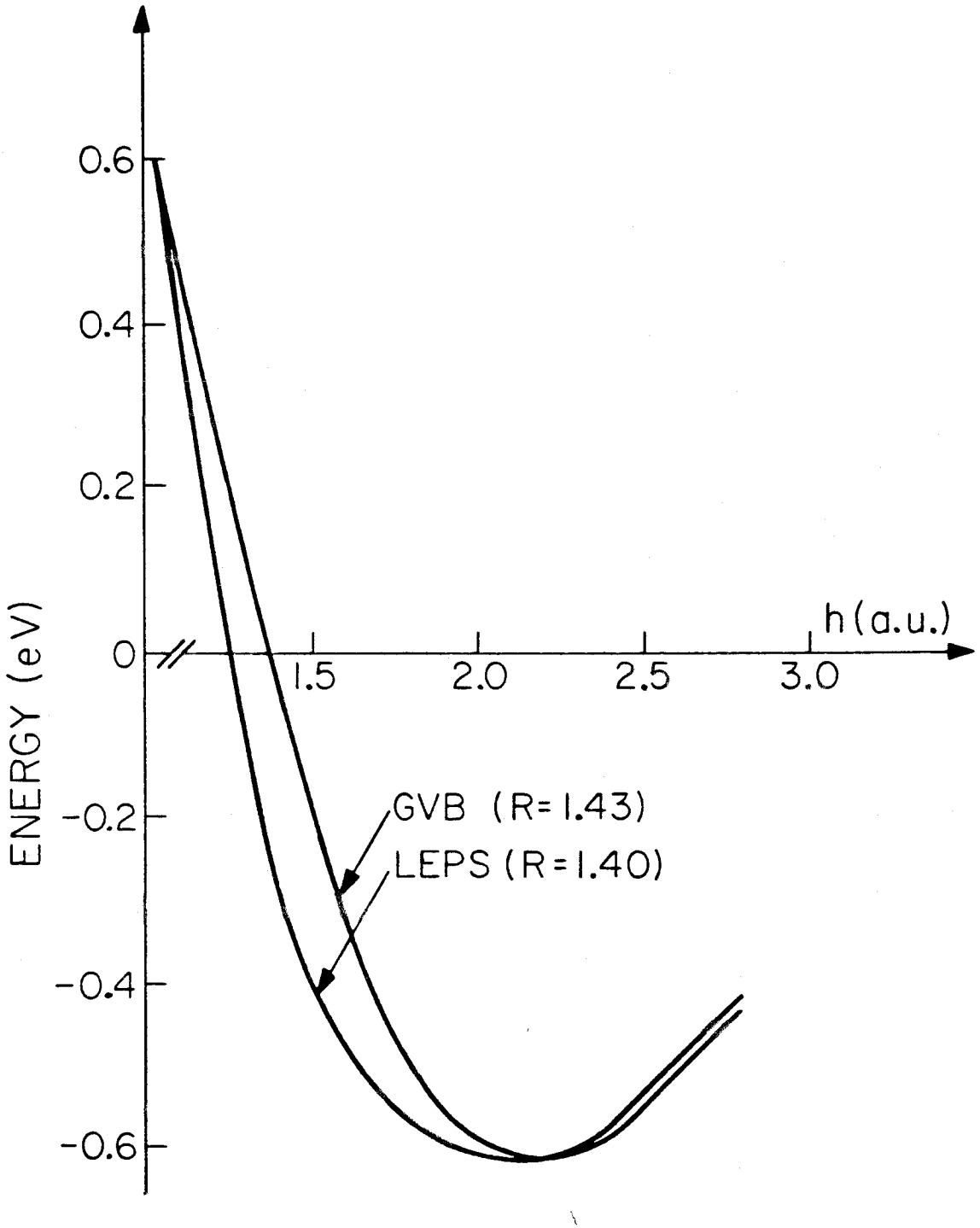

Fig. 5. Comparison of calculated GVB results for Ni_2H_2 and LEPS potential curve [eq. (1)]. Sato parameter is 0.2.

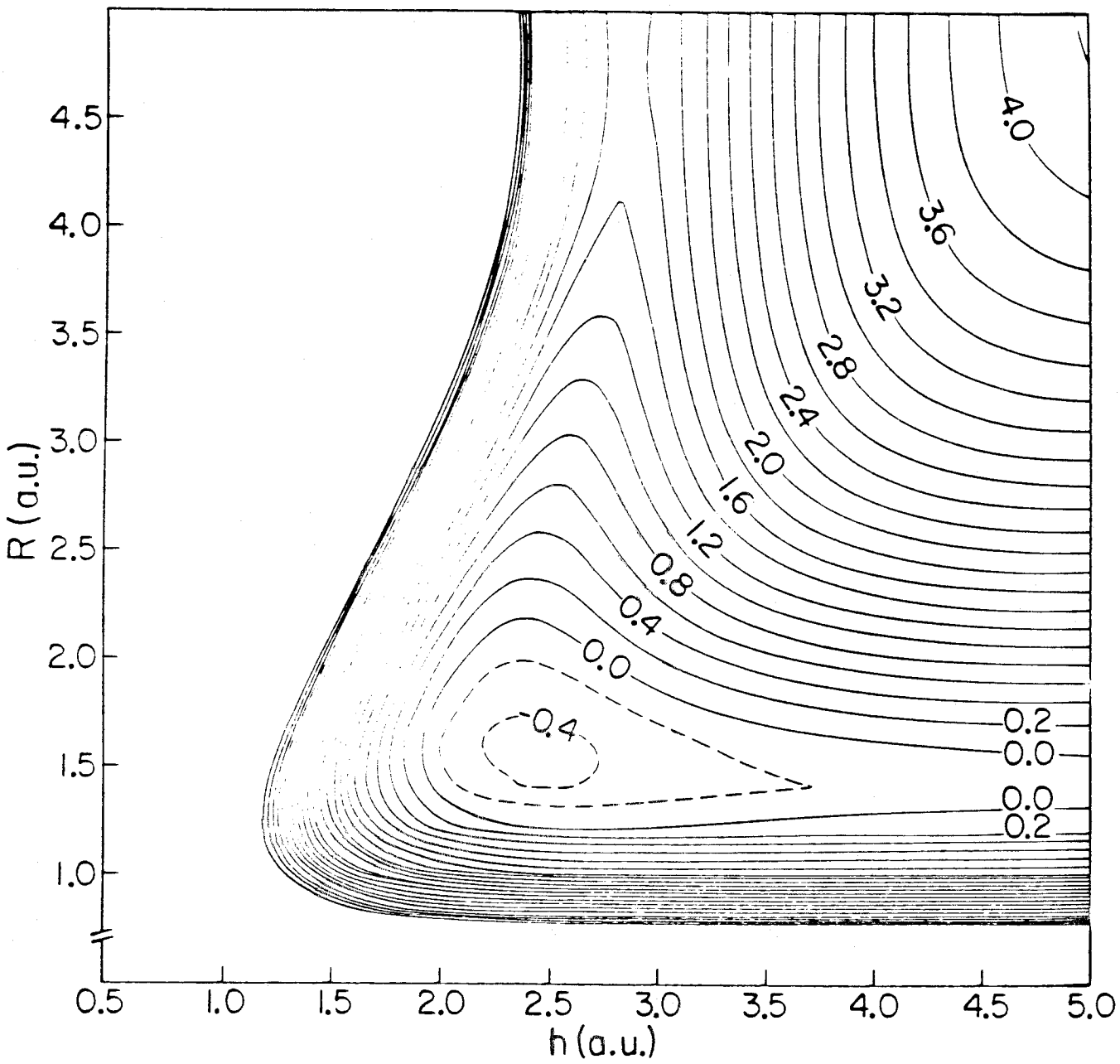

Fig. 6. Potential energy contours in R, h coordinates for interaction of H_2 with Ni(001). The starting energy point is taken as zero at $h \rightarrow \infty$, and the interval between contours is 0.2 eV. For all potential surfaces, the Sato parameter was $\Delta = 0.2$. The dashed lines represent negative values of energy. The H_2 is adsorbed above and parallel to a twofold site (see fig. 2c).

(h). As may be seen, dissociation to linearly adsorbed atoms will not occur, as there is a minimum in the surface that retains the H-H bond.

It is unlikely, however, that the minimum indicated here represents a stable, molecularly adsorbed state. A similar approach geometry, shown in fig. 2b, allows the hydrogen molecule to approach the surface above the twofold site. In this case the H-H axis is above and perpendicular to the site axis, and the final state is one in which both atoms are adsorbed at fourfold sites. The potential surface for this configuration in fig. 7 indicates that there is no barrier to dissociative adsorption at fourfold sites.

A related geometry is the one shown in fig. 2d. Here the H_2 molecule dissociates across the linear site, with the atoms assuming positions at adjacent twofold sites. The potential surface for this approach in fig. 8 shows a local minimum at small H-H separation and a barrier with respect to dissociation.

Finally, we consider an approach of the H_2 molecule directly over a single fourfold site (fig. 2e). A local minimum appears in the potential surface, shown in fig. 9, for an elongated bond distance of about $R = 1.9$ a.u. and a height above the surface of $h = 1.2$ a.u. Since the LEPS method does not adequately assess the effects of spin recoupling [17] in bond formation, it is difficult to determine whether such a state represents an elongated molecularly adsorbed state, or atoms adsorbed at the same fourfold site. More exact calculations would be required to resolve this question. In any case, such a state is not stable with respect to migration of one atom to an adjacent fourfold site, as comparison with fig. 7 will show.

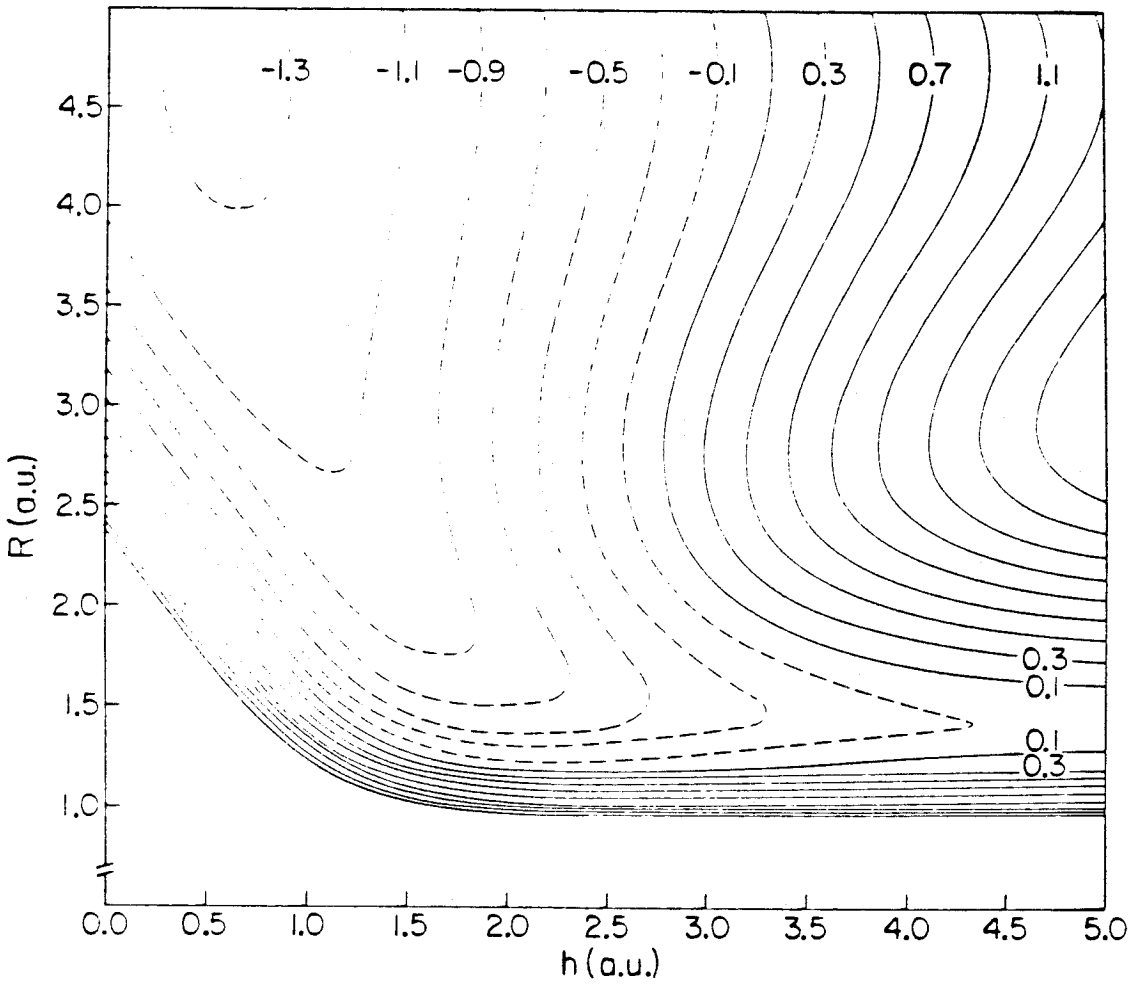

Fig. 7. As in fig. 6 except the approach of the H_2 is to a short-bridged site to form atomic adsorption on a fourfold site (see fig. 2b).

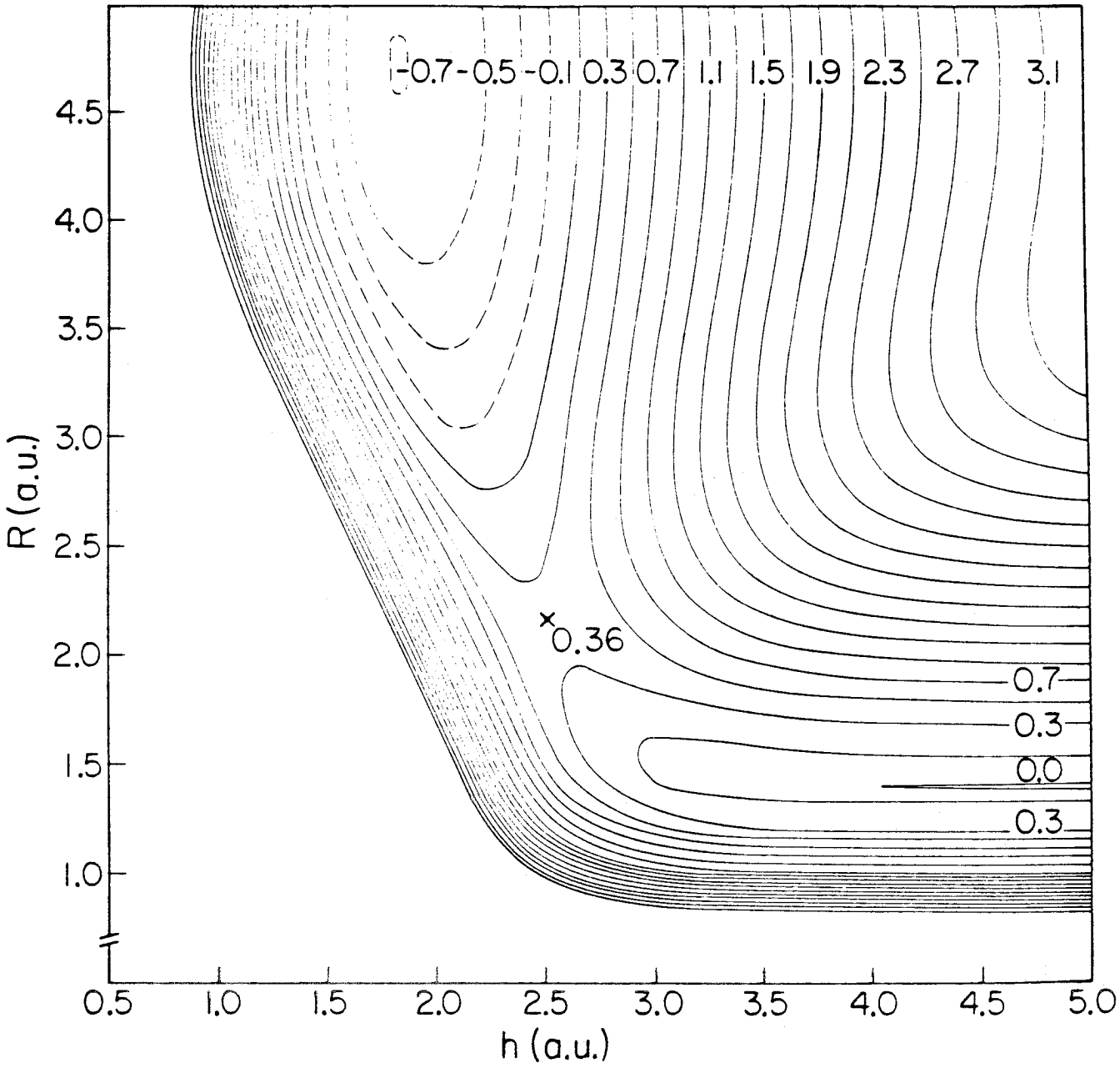

Fig. 8. As in fig. 6 except the H_2 is adsorbed on a linear site (see fig. 2d).

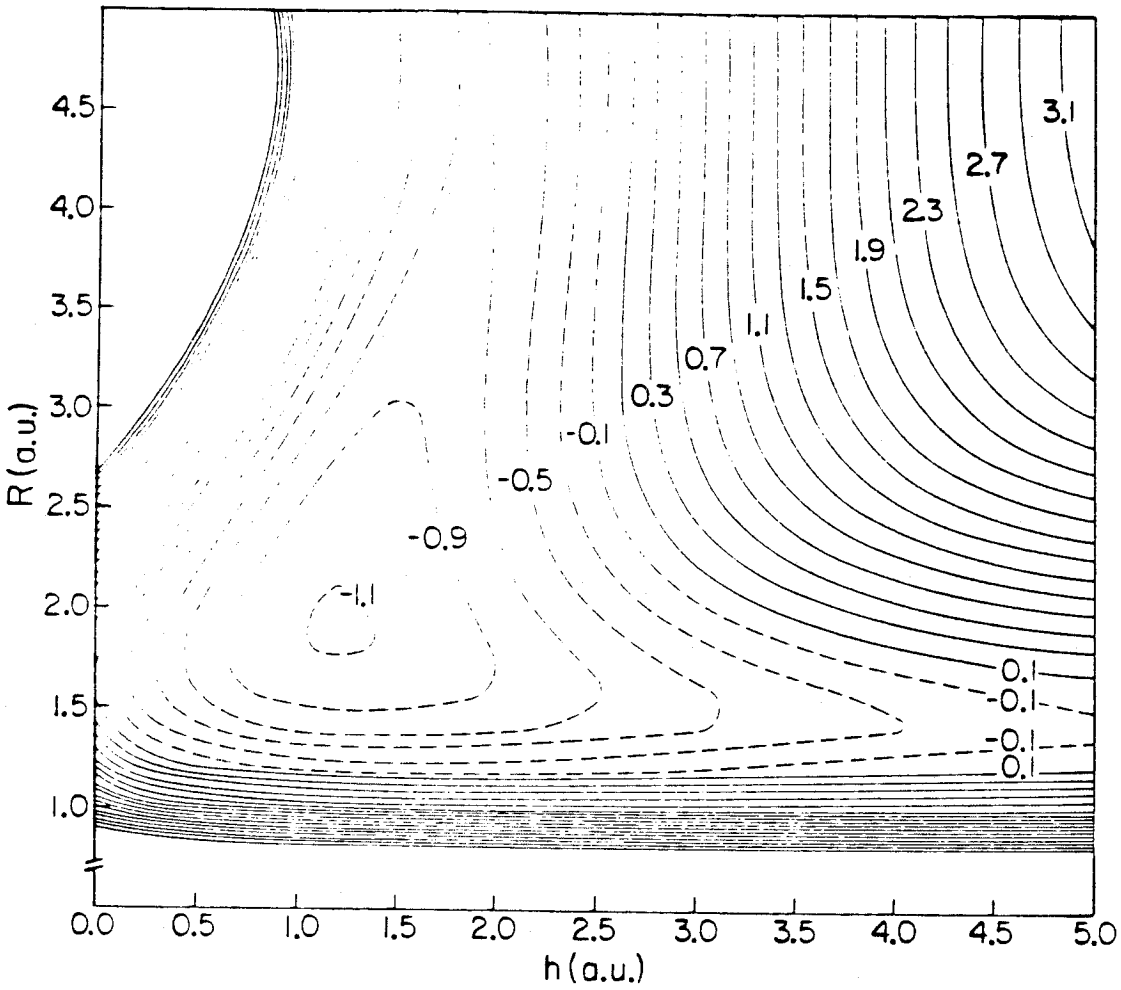

Fig. 9. As in fig. 6 except the H_2 is adsorbed at a fourfold site (see fig. 2e).

V. Conclusions

From the potential surfaces described above, it is possible to extract qualitative information about the competition between physically adsorbed and dissociatively adsorbed hydrogen. Comparing figs. 6, 7, and 9 (in each case fixing the H-H bond distance at 1.43 a.u.), we find that each leads to binding, as was suggested by the GVB calculations in section 3. These states are only transitional; in each case there is a subsequent pathway to fourfold atomic binding states without an additional barrier. Thus, at low coverage, we would expect the model discussed in section 2 to be qualitatively correct: activation-free dissociation results from a crossing between physically adsorbed and chemisorbed state potential surfaces. However, at higher coverages we might expect the situation to be altered. Local minima exhibited in figs 6 and 9 will become absolute minima in situations where adjacent fourfold sites are filled.

This interpretation appears to be consistent with the experimental details. A number of investigators have observed two binding states on single crystal [Ni(001) and Ni(111)] [7c] and polycrystalline samples [7e]. The so-called β_2-state is more strongly bound and obeys second-order desorption kinetics, indicating atomic adsorption. The β_1-state is slightly less strongly bound and appears only after complete filling of β_2. Experiments with polycrystalline surfaces indicate that this state may also follow second-order desorption kinetics, and an analysis of flash desorption lineshapes suggests the presence of repulsive interactions between adsorbed atoms. We would identify this state with the minimum shown in fig. 9, and note that the experimental details lend support to the

interpretation of this state as involving adjacent atom adsorption.

Finally, we note that the results obtained here predict behavior different from that based on extended Hückel calculations [3]. However, extended Hückel calculations predict that the bonding of an H atom is strongest to single Ni atoms and weakest to highly coordinated sites, whereas our previous HF results [6] and recent experimental evidence [7f-h] find the opposite. Thus the EH prediction that an approach geometry, such as that shown in fig. 6 is very favorable, may be associated with the EH finding that the linear site is most favorable for atomic hydrogen binding on Ni(001) [2].

References

[1] C. F. Melius, J. W. Moskowitz, A. P. Mortola, M. B. Baillie and M. A. Ratner, Surface Sci. 59 (1976) 279.

[2] (a) A. van der Avoird, S. P. Liebman and D. J. M. Fassaert, Phys. Rev. B 10 (1974) 1230.

(b) H. Deus and A. van der Avoird, Phys. Rev. B 8 (1973) 2441.

[3] D. J. M. Fassaert and A. van der Avoird, Surface Sci. 55 (1976) 291, 313.

[4] G. Blyholder, J. Chem. Phys. 62 (1975) 3193.

[5] (a) S. C. Ying, J. R. Smith and W. Kohn, Phys. Rev. B 11 (1975) 1483.

(b) S. W. Wang and W. H. Weinberg, Surface Sci. 77 (1978) 14.

(c) B. I. Lundqvist, J. K. Norskov and H. Hjelmberg, Surface Sci. 80 (1979) 441.

[6] (a) T. H. Upton and W. A. Goddard III, Phys. Rev. Lett. 42 (1979) 427.

(b) T. H. Upton, W. A. Goddard III and C. F. Melius, J. Vac. Sci. Technol. 16 (1979) 531.

[7] (a) K. Christmann, O. Schober, G. Ertl and M. Neumann, J. Chem. Phys. 60 (1974) 4528; Surface Sci. 40 (1973) 61, and references cited therein.

(b) T. N. Taylor and P. J. Estrup, J. Vac. Sci. Technol. 11 (1974) 244.

(c) J. Lapujoulade and K. S. Neil, Surface Sci. 35 (1973) 288; J. Chim. Phys. 70 (1973) 797.

(d) J. Küppers, Surface Sci. 36 (1973) 53.

(e) K. Y. Yu, D. T. Ling and W. E. Spicer, J. Catal. 44 (1976) 373.

(f) M. A. Van Hove, G. Ertl, K. Christmann, R. J. Behm and W. H. Weinberg, Solid State Commun. 28 (1978) 373.

(g) K. Christmann, R. J. Behm, G. Ertl, M. A. Van Hove and W. H. Weinberg, J. Chem. Phys. 70 (1979) 4168.

(h) S. Andersson, Chem. Phys. Lett. 55 (1978) 185.

[8] S. Sato, J. Chem. Phys. 23 (1955) 592, 2465.

[9] See, for example, A. J. B. Robertson, Catalysis of Gas Reactions by Metals (Springer-Verlag, New York, 1970).

[10] C. F. Melius, T. H. Upton and W. A. Goddard III, Solid State Commun. 28 (1978) 501.

[11] (a) C. F. Melius, B. D. Olafson and W. A. Goddard III, Chem. Phys. Lett. 28 (1974) 457.

(b) M. J. Sollenberger, M. S. thesis, California Institute of Technology (1975).

[12] (a) S. P. Walch and W. A. Goddard III, J. Am. Chem. Soc. 100 (1978) 1338.

(b) S. Huzinaga, J. Chem. Phys. 42 (1965) 1293.

(c) W. A. Goddard III, T. H. Dunning, Jr., W. J. Hunt and P. J. Hay, Accts. Chem. Res. 6 (1973) 368.

[13] J. T. Muckerman, J. Chem. Phys. 54 (1971) 1155; ibid. 56 (1972) 2997.

[14] J. H. McCreery and G. Wolken, J. Chem. Phys. 63 (1975) 2340.

[15] A. Gelb and M. J. Cardillo, Surface Sci. 59 (1976) 128; ibid. 64 (1977) 197; ibid. 75 (1978) 199.

[16] G. Herzberg, Spectra of Diatomic Molecules (Van Nostrand-Reinhold, New York, 1950).

[17] While the LEPS method does include the mixing of the two linearly independent four-electron singlet spin functions, the mixing is determined by the four-center geometry via eqn. (4). While such a treatment is qualitatively acceptable, it is inadequate to address detailed questions of spin coupling.

Part Four

Ab Initio Hartree-Fock Calculations on Crystalline Systems Using Full Symmetry Analysis of Basis Set Expansions

I. Introduction

In recent years it has become increasingly apparent that existing theoretical techniques are inadequate for the detailed study of electronic states at solid surfaces and defect sites. Semi-empirical band calculation methods allow treatment of long-range periodicity,[1] but do not permit the evaluation of total energies and hence cannot differentiate unambiguously between possible surface or defect structures. Ab initio methods do not suffer from this limitation and have been successful in the study of localized chemisorptive bonding states on metal[2] and semiconductor[3] surfaces. However, these calculations have required that the surface be modelled using a finite cluster of atoms. This restriction leaves these methods incapable of considering a host of phenomena whose characteristics are intimately related to the two-dimensional symmetry of the surface.

We feel that the solution to this dilemma lies in the development of an ab initio variational technique that includes full two-dimensional periodicity. Ultimately it will be necessary to allow systematic examination of electron correlation (many-body) effects; however, as a first step in this program we have considered a simpler problem: exact Hartree-Fock (HF) calculations on three-dimensional periodic systems. In this paper we generalize the ab initio techniques used previously in cluster studies[4] to take full account of periodicity. The resulting energy expressions retain the numerical simplicity of basis set expansion techniques[5] and may be cast in a rapidly convergent form. To illustrate its application, we report the results of calculations on some simple systems: face-centered cubic arrays of hydrogen, lithium, and sodium.

While the development presented here is specific to systems of three-dimensional periodicity, extension to systems of lesser periodicity is straightforward, and we conclude with a brief discussion of methods by which this may be done.

II. Hartree-Fock Formalism

A. Wavefunctions and Hamiltonian

The construction of general one-electron wavefunctions is begun by defining a basis of Bloch orbitals for each wave vector $\underset{\sim}{k}$ as

$$\varphi^a_{\underset{\sim}{k}}(\underset{\sim}{r}) = \sum_{\mu}^{N} e^{i\underset{\sim}{k}\cdot\underset{\sim}{R}_\mu}\phi^a(\underset{\sim}{r} - \underset{\sim}{R}_\mu) , \tag{1}$$

where (for simplicity) we have assumed a single atom per unit cell, and the sum runs over all N atoms (cells) of the semi-infinite lattice. Here the $\phi^a(\underset{\sim}{r})$ are basis functions centered on the atoms and located by the vector $\underset{\sim}{R}_\mu$. We will take them to be linear combinations of cartesian gaussians,

$$\phi^a(\underset{\sim}{r}) = x^\ell y^p z^q e^{-\alpha r^2}/\sqrt{N_a} , \tag{2}$$

where ℓ, p, and q are integers, α is a variable scale factor, and N_a is the normalization constant. The $\varphi^a_{\underset{\sim}{k}}$ are normalized but not orthogonal (for a given value of $\underset{\sim}{k}$). The one-electron functions (Hartree-Fock orbitals) are obtained from the basis functions as

$$\psi_{\underset{\sim}{k}n}(\underset{\sim}{r}) = \eta^{-\frac{1}{2}}_{\underset{\sim}{k}n} \sum_{a}^{m} C^a_{\underset{\sim}{k}n}\varphi^a_{\underset{\sim}{k}}(\underset{\sim}{r}) , \tag{3}$$

where the normalization factor is

$$\eta_{\underset{\sim}{k}n} = \sum_{a,b}^{m}\sum_{\mu,\nu}^{N} C^{*a}_{\underset{\sim}{k}n}C^b_{\underset{\sim}{k}n}e^{i\underset{\sim}{k}\cdot(\underset{\sim}{R}_\mu - \underset{\sim}{R}_\nu)}\langle\phi^a(\underset{\sim}{r} - \underset{\sim}{R}_\nu)|\phi^b(\underset{\sim}{r} - \underset{\sim}{R}_\mu)\rangle$$

$$= N\sum_{a,b}^{m}\sum_{\sigma}^{N} C^{*a}_{\underset{\sim}{k}n}C^b_{\underset{\sim}{k}n}e^{i\underset{\sim}{k}\cdot\underset{\sim}{R}_\sigma}\langle\phi^a(\underset{\sim}{r})|\phi^b(\underset{\sim}{r} - \underset{\sim}{R}_\sigma)\rangle . \tag{4}$$

In (3) the sum is over the m (non-orthogonal) basis functions for each $\underset{\sim}{k}$, and the subscript n identifies the band (i.e., root of the hamiltonian

matrix for a given $\underset{\sim}{k}$). The coefficients $C^{a}_{\underset{\sim}{k}n}$ are obtained variationally (solutions of the matrix HF equations). These one-electron wavefunctions (3) may be combined to form the single Slater determinant wavefunctions relevant to this study,

$$\Psi_{CS} = \mathcal{A}\{\psi_{\underset{\sim}{k}n_1}(\underset{\sim}{r}_1)\psi_{\underset{\sim}{k}n_1}(\underset{\sim}{r}_2)\ldots\psi_{\underset{\sim}{k}n_f}(\underset{\sim}{r}_{Np-1})\psi_{\underset{\sim}{k}n_f}(\underset{\sim}{r}_{Np})\chi_{CS}\} \quad (5)$$

$$\Psi_{HS} = \mathcal{A}\{\psi_{\underset{\sim}{k}n_1}(\underset{\sim}{r}_1)\psi_{\underset{\sim}{k}n_2}(\underset{\sim}{r}_2)\ldots\psi_{\underset{\sim}{k}n_{f-1}}(\underset{\sim}{r}_{Np-1})\psi_{\underset{\sim}{k}n_f}(\underset{\sim}{r}_{Np})\chi_{HS}\}. \quad (6)$$

Here Ψ_{CS} and Ψ_{HS} are wavefunctions for closed-shell (S = 0) and high-spin (S = Np/2) states for an array of N atoms, each with p valence electrons, and the χ_{CS} and χ_{HS} are the appropriate spin functions.[6]

The total electronic hamiltonian is

$$\mathcal{H} = \sum_{i}^{Np} h_i + \sum_{j>k}^{Np} \frac{1}{|\underset{\sim}{r}_j - \underset{\sim}{r}_k|} ,$$

where h_i is the one-electron operator,

$$h_i = -\tfrac{1}{2}\nabla_i^2 - \sum_{\mu}^{N}\left[\frac{Z_\mu}{|\underset{\sim}{R}_\mu - \underset{\sim}{r}_i|} - V_\mu^{core}\right] , \quad (7)$$

and V_μ^{core} is the potential for the core electrons on center μ. The total energies of Ψ_{CS} and Ψ_{HS} are

$$E = \sum_{\underset{\sim}{k}n}^{Np/f} f\, h_{\underset{\sim}{k}n,\underset{\sim}{k}n} + \sum_{\underset{\sim}{k}n,\underset{\sim}{k}'n'}^{Np/f}(AJ_{\underset{\sim}{k}n,\underset{\sim}{k}'n'} - BK_{\underset{\sim}{k}n,\underset{\sim}{k}'n'}) + \sum_{\mu>\nu}^{N}\frac{Z_\mu Z_\nu}{|\underset{\sim}{R}_\mu - \underset{\sim}{R}_\nu|} , \quad (8)$$

and the orbital eigenvalues are

$$\epsilon_{\underset{\sim}{k}n} = h_{\underset{\sim}{k}n,\underset{\sim}{k}n} + \frac{2}{f}\sum_{\underset{\sim}{k}'n'}^{Np/f}(AJ_{\underset{\sim}{k}n,\underset{\sim}{k}'n'} - BK_{\underset{\sim}{k}n,\underset{\sim}{k}'n'}). \quad (9)$$

Expressions (8) and (9) permit a very general class of wavefunctions[7] of which two special cases are considered here,

$$f = 2\,, \quad A = 2\,, \quad B = 1\,, \quad \text{for } \Psi_{CS}\,;$$
$$f = 1\,, \quad A = \tfrac{1}{2}\,, \quad B = \tfrac{1}{2}\,, \quad \text{for } \Psi_{HS}\,.$$

The $\underset{\sim}{kn}$ sums are over all occupied orbitals. The first term in (8) is a sum of one-electron energies,

$$\sum_{\underset{\sim}{kn}}^{Np/f} f h_{\underset{\sim}{kn},\underset{\sim}{kn}} = \sum_{\underset{\sim}{kn}}^{Np/f} f\, \eta_{\underset{\sim}{kn}}^{-1} \sum_{a,b}^{m} C_{\underset{\sim}{kn}}^{*a} C_{\underset{\sim}{kn}}^{b} \langle \varphi_{\underset{\sim}{k}}^{a}(\underset{\sim}{r}) | h | \varphi_{\underset{\sim}{k}}^{b}(\underset{\sim}{r}) \rangle$$

$$= fN \sum_{\underset{\sim}{kn}}^{Np/f} \eta_{\underset{\sim}{kn}}^{-1} \sum_{a,b}^{m} \sum_{\sigma}^{N} C_{\underset{\sim}{kn}}^{*a} C_{\underset{\sim}{kn}}^{b} e^{i\underset{\sim}{k}\cdot\underset{\sim}{R}_\sigma} \langle \phi^a(\underset{\sim}{r}) | h | \phi^b(\underset{\sim}{r} - \underset{\sim}{R}_\sigma) \rangle$$

$$= f\,N \sum_{a,b}^{m} \sum_{\sigma}^{N} D_{1\sigma}^{ab} h_{1\sigma}^{ab}\,, \tag{10}$$

where

$$D_{\mu\nu}^{ab} = \sum_{\underset{\sim}{kn}}^{Np/f} \eta_{\underset{\sim}{kn}}^{-1} C_{\underset{\sim}{kn}}^{*a} C_{\underset{\sim}{kn}}^{b} e^{i\underset{\sim}{k}\cdot(\underset{\sim}{R}_\nu - \underset{\sim}{R}_\mu)}$$

$$h_{\mu\nu}^{ab} = \langle \phi^a(\underset{\sim}{r} - \underset{\sim}{R}_\mu) | h | \phi^b(\underset{\sim}{r} - \underset{\sim}{R}_\nu) \rangle \tag{11}$$

and $\sigma = 1$ refers to the atom chosen as the origin. The quantities $D_{\mu\nu}^{ab}$ may be identified as elements of the one-particle density matrix upon noting that

$$\rho(\underset{\sim}{r}) = f \sum_{\underset{\sim}{kn}}^{Np/f} \psi_{\underset{\sim}{kn}}^{*}(\underset{\sim}{r}) \psi_{\underset{\sim}{kn}}(\underset{\sim}{r})$$

...

$$= f \sum_{a,b}^{m} \sum_{\mu,\nu}^{N} \sum_{\underset{\sim}{kn}}^{Np/f} \eta_{\underset{\sim}{kn}}^{-1} C_{\underset{\sim}{kn}}^{*a} C_{\underset{\sim}{kn}}^{b} e^{i\underset{\sim}{k}\cdot(\underset{\sim}{R}_\nu - \underset{\sim}{R}_\mu)} \phi^a(\underset{\sim}{r} - \underset{\sim}{R}_\mu)\phi^b(\underset{\sim}{r} - \underset{\sim}{R}_\nu)$$

$$= f \sum_{a,b}^{m} \sum_{\mu,\nu}^{N} D_{\mu\nu}^{ab} \phi^a(\underset{\sim}{r} - \underset{\sim}{R}_\mu)\phi^b(\underset{\sim}{r} - \underset{\sim}{R}_\nu) .$$

In addition, we have

$$\rho(\underset{\sim}{r}) = \sum_{\nu}^{N} \rho_\nu(\underset{\sim}{r}) ,$$

where

$$\rho_\nu(\underset{\sim}{r}) = f \sum_{a,b}^{m} \sum_{\mu}^{N} D_{\mu\nu}^{ab} \phi^a(\underset{\sim}{r} - \underset{\sim}{R}_\mu)\phi^b(\underset{\sim}{r} - \underset{\sim}{R}_\nu) .$$

Integrating over all space leads to

$$p = \int d^3\underset{\sim}{r}\, \rho_\nu(\underset{\sim}{r}) = f \sum_{a,b}^{m} \sum_{\mu}^{N} D_{\mu\nu}^{ab} S_{\mu\nu}^{ab} .$$

Thus, $\rho_\nu(\underset{\sim}{r})$ is the density function for the p electrons near atom ν.

Applying (11) to the two-electron coulomb, $J_{\underset{\sim}{kn},\underset{\sim}{k}'n'}$, and exchange, $K_{\underset{\sim}{kn},\underset{\sim}{k}'n'}$, sums in (8) leads to

$$\sum_{\underset{\sim}{kn},\underset{\sim}{k}'n'}^{Np/f} (AJ_{\underset{\sim}{kn},\underset{\sim}{k}'n'} - BK_{\underset{\sim}{kn},\underset{\sim}{k}'n'})$$

$$= N \sum_{a,b}^{m} \sum_{\sigma}^{N} D_{1\sigma}^{ab} \sum_{c,d}^{m} \sum_{\mu,\nu}^{N} D_{\mu\nu}^{cd} \{A(a^1b^\sigma|c^\mu d^\nu) - B(a^1c^\mu|b^\sigma d^\nu)\} \quad (12)$$

using the notation

$$(a^\sigma b^\gamma|c^\mu d^\nu) \equiv \int \phi^a(\underset{\sim}{r}_1 - \underset{\sim}{R}_\sigma)\phi^b(\underset{\sim}{r}_1 - \underset{\sim}{R}_\gamma) d^3\underset{\sim}{r}_1 \int \frac{1}{|\underset{\sim}{r}_1 - \underset{\sim}{r}_2|} \times \phi^c(\underset{\sim}{r}_2 - \underset{\sim}{R}_\mu)\phi^d(\underset{\sim}{r}_2 - \underset{\sim}{R}_\nu) d^3\underset{\sim}{r}_2 .$$

Combining the above equations leads to

$$E = N \sum_{a,b}^{m} \sum_{\sigma}^{N} D_{1\sigma}^{ab} \left[f\, h_{1\sigma}^{ab} + \sum_{c,d}^{m} \sum_{\mu,\nu}^{N} D_{\mu\nu}^{cd} \{ A(a^1 b^\sigma | c^\mu d^\nu) - B(a^1 c^\mu | b^\sigma d^\nu) \} \right] + \sum_{\mu > \nu}^{N} \frac{Z_\mu Z_\nu}{|\underset{\sim}{R}_\mu - \underset{\sim}{R}_\nu|} \tag{13}$$

and

$$\epsilon_{\underset{\sim}{k}n} = N \eta_{\underset{\sim}{k}n}^{-1} \sum_{\sigma}^{N} \sum_{a,b}^{m} C_{\underset{\sim}{k}n}^{*a} C_{\underset{\sim}{k}n}^{b} e^{i\underset{\sim}{k} \cdot \underset{\sim}{R}_\sigma} \left[h_{1\sigma}^{ab} + \frac{2}{f} \sum_{c,d}^{m} \sum_{\mu,\nu}^{N} D_{\mu\nu}^{cd} \times \{ A(a^1 b^\sigma | c^\mu d^\nu) - B(a^1 c^\mu | b^\sigma d^\nu) \} \right]. \tag{14}$$

For systems with inversion symmetry,

$$\phi_{\underset{\sim}{k}n} = \phi^*_{-\underset{\sim}{k}n}$$

and

$$\epsilon_{\underset{\sim}{k}n} = \epsilon_{-\underset{\sim}{k}n} .$$

As a result, we may avoid dealing with complex quantities by redefining (14) as

$$\tfrac{1}{2}(\epsilon_{\underset{\sim}{k}n} + \epsilon_{-\underset{\sim}{k}n}) = N(\eta_{\underset{\sim}{k}n} + \eta_{-\underset{\sim}{k}n})^{-1} \sum_{\sigma}^{N} \sum_{a,b}^{m} \mathrm{Re} \left\{ C_{\underset{\sim}{k}n}^{*a} C_{\underset{\sim}{k}n}^{b} e^{i\underset{\sim}{k} \cdot \underset{\sim}{R}_\sigma} \right\} \times \left[h_{1\sigma}^{ab} + \frac{2}{f} \sum_{c,d}^{m} \sum_{\mu,\nu}^{N} D_{\mu\nu}^{cd} \{ A(a^1 b^\sigma | c^\mu d^\nu) - B(a^1 c^\mu | b^\sigma d^\nu) \} \right].$$

B. The Density Matrix

The form of (11) for the density matrix elements, while general, is not particularly useful, as it defines $N^2 m^2$ distinct elements. It is immediately apparent that this value is too large since $D_{\mu\nu}^{ab}$ depends

only on $\underset{\sim}{R}_\nu - \underset{\sim}{R}_\mu$. Thus, there are at most the Nm^2 distinct values, $D^{ab}_{1\sigma}$.

Consideration of point group symmetry allows this set to be reduced still further. The atoms surrounding atom 1 may be broken into λ "shells", where each atom in a shell has the same value for $|\underset{\sim}{R}_\sigma|$ and is related to the others by an operation of the lattice point group. Thus, Eq. (11) may be rewritten

$$D^{ab}_{1\sigma} = \sum_{s}^{\text{unique}} \left(\sum_{j}^{t_s} \eta^{-1}_{nk_{\underset{\sim}{}}js} C^{*a}_{nk_{\underset{\sim}{}}js} C^{b}_{nk_{\underset{\sim}{}}js} e^{i\underset{\sim}{k}_{js} \cdot \underset{\sim}{R}_\sigma} \right),$$

where the sum over $\underset{\sim}{k}n$ has been broken into an outer sum over stars of vectors s, and an inner sum j over the t_s members of each of these stars (and occupied bands). But, from the definition of a star, this is equivalent to

$$D^{ab}_{1\sigma} = \sum_{s}^{\text{unique}} \frac{1}{g_s} \sum_{j}^{\mathcal{G}} \eta^{-1}_{nK_{\underset{\sim}{}}j} C^{*a}_{nK_{\underset{\sim}{}}j} C^{b}_{nK_{\underset{\sim}{}}j} e^{i(\underset{\sim}{K}_j \cdot \underset{\sim}{R}_\sigma)}, \qquad (15a)$$

where, for simplicity,

$$\underset{\sim}{K}_j = \mathcal{P}_j(\underset{\sim}{k}_s)$$

and the inner sum is over the operations $\mathcal{P}_j$ of the lattice point group $\mathcal{G}$. Using the reciprocal relationship between $\underset{\sim}{k}$ and $\underset{\sim}{r}$ this becomes

$$D^{ab}_{1\sigma} = \sum_{s}^{\text{unique}} \frac{1}{g_\sigma} \sum_{j}^{\mathcal{G}} \eta^{-1}_{nk_{\underset{\sim}{}}s} C^{*A_j}_{nk_{\underset{\sim}{}}s} C^{B_j}_{nk_{\underset{\sim}{}}s} e^{i\underset{\sim}{k}_s \cdot \mathcal{P}_j^{-1}(\underset{\sim}{R}_\sigma)}, \qquad (15b)$$

where, for example,

$$A_j = \mathcal{P}_j^{-1}(a).$$

The leading factors g_s and g_σ in (15a) and (15b) are degeneracy factors from the application of the $\mathcal{P}_j$ to vectors in $\underset{\sim}{k}$ and $\underset{\sim}{r}$ space, respectively.

From (15b) we have, for a particular atom $\sigma' = \mathcal{P}_z(\sigma)$,

$$D_{1\sigma'}^{a'b'} = D_{1\mathcal{P}_z(\sigma)}^{A_zB_z} = \sum_s^{\mathcal{G}} \frac{1}{g_\sigma} \sum_j \eta_{nk_s}^{-1} C_{nk_s}^{*\mathcal{P}_zA_j} C_{nk_s}^{\mathcal{P}_zB_j} \exp[ik_s \cdot \mathcal{P}_z \mathcal{P}_j^{-1}(R_\sigma)]$$

$$= D_{1\sigma}^{ab} \quad .$$

Thus, only a single atom in any particular shell need be considered, reducing the number of necessary elements to λm^2 (where λ is the number of shells). Once again, for systems with inversion symmetry, it is convenient to redefine (15b) as

$$D_{1\sigma}^{ab} = 2 \sum_s \frac{1}{g_\sigma} \sum_j^{\mathcal{G}/i} \eta_{nk_s}^{-1} \mathrm{Re}\{C_{nk_s}^{*A_j} C_{nk_s}^{B_j} e^{ik_s \cdot \mathcal{P}_j^{-1}(R_\sigma)}\} \ ,$$

where $\mathcal{G}/i$ is the pure rotation subgroup of $\mathcal{G}$, and the inversion symmetry has been explicitly included in obtaining the real function. For these cases,

$$D_{1\sigma}^{ab} = D_{1\sigma}^{ba}$$

and only $\frac{1}{2}\lambda m(m+1)$ elements are unique among the density matrix elements.

C. Matrix Elements

An additional difficulty arising from the use of Eqs. (13) and (14) is that they appear to require an exorbitant number of one- and two-electron matrix elements. The problem of defining a unique set of one-electron matrix elements has been dealt with in detail by Slater and Koster,[8a] and others.[8b] Defining a set of unique two-electron integrals is greatly facilitated by the results of the previous section. Since in (13)

and (14) the two-electron integrals are multiplied by factors depending only on $\underset{\sim}{R}_\nu - \underset{\sim}{R}_\mu$, a minimum set will consist only of those integrals $(ab|cd)$ that possess unique spatial orientations of ab and cd, without regard to the absolute position of $(ab|cd)$. Thus, an integral involving four centers may be used four times (excluding consideration of point group symmetry) by translating the indices of the integral such that the centers other than 1 may be taken to coincide with the origin.

This is seen more clearly by noting that a given integral

$$\left(\varphi^a(\underset{\sim}{r})\varphi^b(\underset{\sim}{r} - \underset{\sim}{R}_\sigma)\,|\,\varphi^c(\underset{\sim}{r} - \underset{\sim}{R}_\mu)\varphi^d(\underset{\sim}{r} - \underset{\sim}{R}_\nu)\right)$$

may be expressed equivalently as

$$\left(\varphi^a(\underset{\sim}{r})\varphi^b(\underset{\sim}{r} - \underset{\sim}{R}_\sigma)\,|\,\{\underset{\sim}{E}\,|\,-\underset{\sim}{R}_\mu\}\{\varphi^c(\underset{\sim}{r})\varphi^d(\underset{\sim}{r} - \underset{\sim}{R}_\omega)\}\right), \tag{16}$$

where $\underset{\sim}{R}_\omega = \underset{\sim}{R}_\nu - \underset{\sim}{R}_\mu$. With cubic symmetry, there will be $\sim \frac{1}{2}N^2/48$ distinct combinations of $\underset{\sim}{R}_\sigma$ and $\underset{\sim}{R}_\omega$. This defines all unique angular orientations of $\underset{\sim}{R}_\omega$ with respect to $\underset{\sim}{R}_\sigma$. The translation $\{\underset{\sim}{E}\,|\,\underset{\sim}{R}_\mu\}$ provides radial separation of $\underset{\sim}{R}_\omega$ and $\underset{\sim}{R}_\sigma$. Since each four-center integral may be used four times due to translational symmetry, there will be $\sim N/4$ unique operations $\{\underset{\sim}{E}\,|\,\underset{\sim}{R}_\mu\}$ for each choice of $\underset{\sim}{R}_\sigma$ and $\underset{\sim}{R}_\omega$. As a result, the number of matrix elements requiring explicit evaluation is reduced from $\sim \frac{1}{2}m^4N^3$, as suggested by Eqs. (13) and (14), to only $\sim \frac{1}{392}m^4N^3$, a savings of over two orders of magnitude.

III. Evaluation of Energy Expressions

A. Repeating Unit

Equations (13) and (14) represent general expressions for total energies and eigenvalues, but involve semi-infinite sums over atoms. Practical considerations dictate truncation of these sums and care is required to achieve a balance between one- and two-electron quantities such that rapid convergence may be attained. This situation is very similar to that in the classical Madelung problem, suggesting that rearrangement of the terms in the sums might be beneficial.

We begin by combining nuclear and electronic terms in Eq. (13) to obtain

$$E = N \sum_{\sigma}^{N} \left\{ \frac{Z_\sigma Z_1 (1 - \delta_{1\sigma})}{2|\underset{\sim}{R}_\sigma|} + \sum_{a,b}^{m} D_{1\sigma}^{ab} \left[f\, h_{1\sigma}^{ab} + \sum_{\mu,\nu}^{N} \sum_{c,d}^{m} D_{\mu\nu}^{cd} \times \{A(a^1 b^\sigma | c^\mu d^\nu) - B(a^1 c^\mu | b^\sigma d^\nu)\} \right] \right\}.$$

Noting that

$$\sum_{\sigma}^{N} \sum_{\mu}^{N'} \langle \varphi^a(\underset{\sim}{r} - \underset{\sim}{R}_\sigma) \left| \frac{Z}{|\underset{\sim}{r} - \underset{\sim}{R}_\mu|} \right| \varphi^b(\underset{\sim}{r}) \rangle$$

$$= \sum_{\omega}^{N} \sum_{\mu}^{\prime} \langle \varphi^a(\underset{\sim}{r} - \underset{\sim}{R}_\omega) \left| \frac{Z}{|\underset{\sim}{r}|} \right| \varphi^b(\underset{\sim}{r} + \underset{\sim}{R}_\mu) \rangle ,$$

where the prime indicates $\mu \neq 1$ in the sum and $\underset{\sim}{R}_\omega = \underset{\sim}{R}_\sigma - \underset{\sim}{R}_\mu$, the sum may be partitioned as follows,

$$E/N = \sum_{a,b}^{m} \sum_{\sigma}^{N} D_{1\sigma}^{ab} \left\{ f \langle a^1 \left| -\tfrac{1}{2}\nabla^2 - \frac{Z}{|r|} \right| b^\sigma \rangle \right.$$

$$+ \sum_{c,d}^{m} \sum_{\nu}^{N} D_{1\nu}^{cd} \left[A(a^1 b^\sigma | c^1 d^\nu) - \frac{B}{2}(a^1 c^1 | b^\sigma d^\nu) - \frac{B}{2}(a^1 d^\nu | b^\sigma c^1) \right] \Bigg\} \quad (17a)$$

$$+ \sum_{a,b}^{m} \sum_{\sigma}^{N} \left\{ \frac{f}{2} D_{1\sigma}^{ab} \langle a^1 | \sum_{\mu}^{N}{}' \frac{-Z}{|\underset{\sim}{r} - \underset{\sim}{R}_\mu|} | b^\sigma \rangle + \frac{Z^2(1 - \delta_{\sigma 1})}{|\underset{\sim}{R}_\sigma|} \right\} \quad (17b)$$

$$+ \sum_{c,d}^{m} \sum_{\mu}^{N} \sum_{\nu}^{N}{}' D_{\mu\nu}^{cd} \left\{ \frac{f}{2} \langle c^\mu | \frac{-Z}{\underset{\sim}{r}} | d^\nu \rangle \right.$$

$$\left. + \sum_{\sigma}^{N} \sum_{a,b}^{m} D_{1\sigma}^{ab} \left[A(a^1 b^\sigma | c^\mu d^\nu) - \frac{B}{2}(a^1 c^\mu | b^\sigma d^\nu) - \frac{B}{2}(a^1 d^\nu | b^\sigma c^\mu) \right] \right\}. \quad (17c)$$

The reasons for this choice of partitioning become apparent upon consideration of the properties of the $D_{\mu\nu}^{ab}$ defined in Sec. II. B. From the definition of $\rho_\nu(\underset{\sim}{r})$ we see that (17a) includes all coulomb and exchange quantities resulting from the interaction of the local density at the origin with itself. In addition, there are terms describing the interaction of this local density with the nuclear charge at the origin. Thus, (17a) represents the self energy of a neutral charge unit consisting of the local electron density and the associated nucleus. Equation (17b) is the total energy of interaction between this unit and all other nuclei of the lattice, while (17c) represents the interaction between this unit and all other local electron densities. Collectively then, Eqs. (17) express the total energy as a sum of pairwise interactions between such neutral charge units centered at each site in the lattice.

In Fig. 1, we have plotted the density function $\rho_1(r)$ along symmetry directions for a face-centered cubic lattice of H atoms [lattice constant a = 2.44 Å and $\phi(r)$ is a 1s basis function]. The $D_{1\sigma}^{aa}$ values

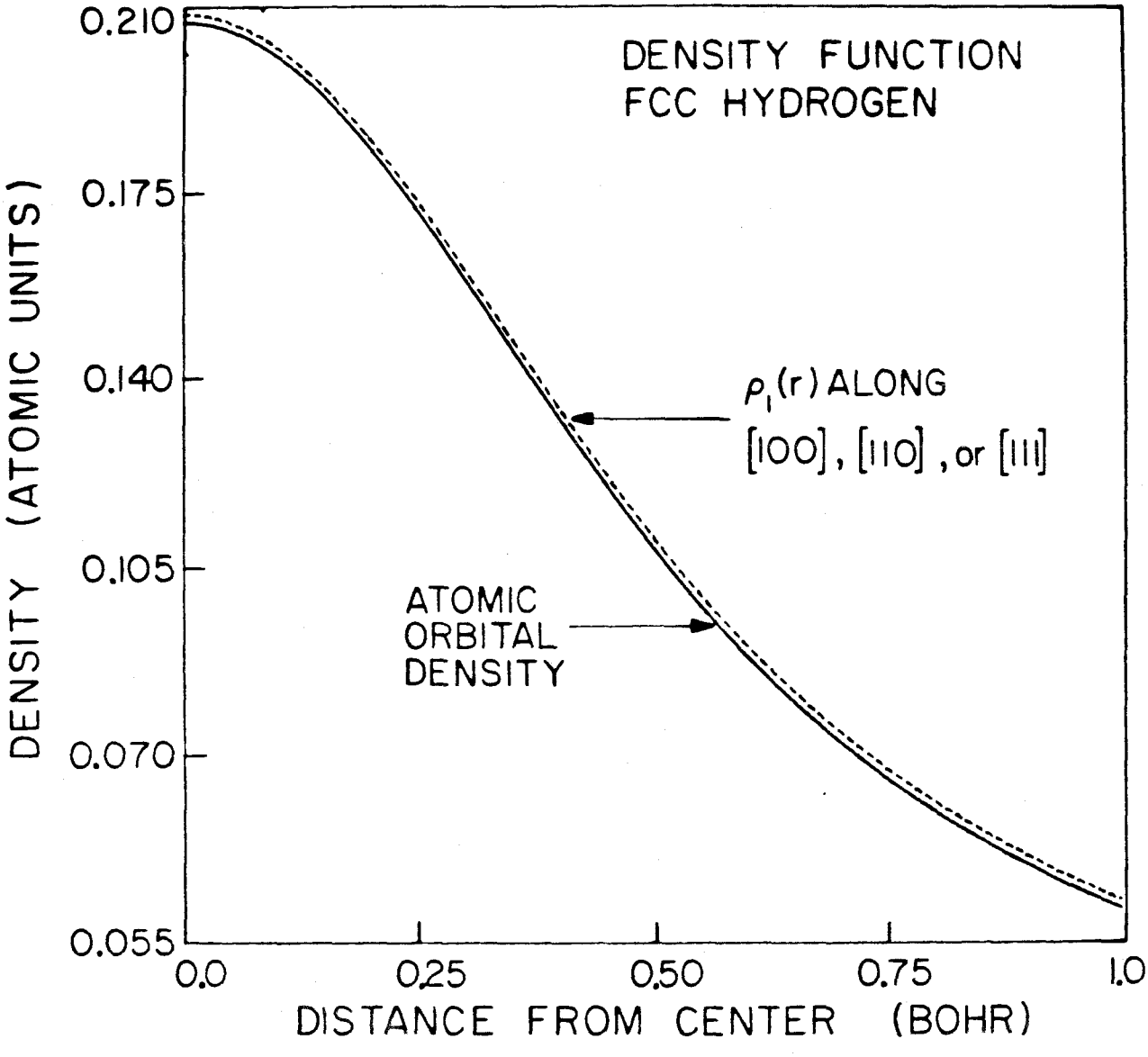

FIG. 1. Orbital density function $\phi(\underset{\sim}{r})\phi(\underset{\sim}{r})$ and local density function $\rho_1(\underset{\sim}{r})$ for a face-centered cubic lattice of hydrogen atoms. In this calculation, $\underset{\sim}{a}$ = 2.44 Å and $\phi(\underset{\sim}{r})$ is a 1s basis function (with a nearest neighbor overlap of 0.30). The calculation included 381 charge units. The relative shift of the two curves is real $\rho_1(\underset{\sim}{r})$ becomes slightly negative at large distances, ensuring normalization.

are highly peaked about the nucleus, producing a density function $\rho_1(r)$ that extends with only small amplitude beyond the boundary of the Wigner-Seitz cell.

The partitioning of energy quantities in this fashion, while not unique, does clearly indicate the difficulties that might arise with straightforward truncation of (13). In using such a spherical cluster approach, two-electron integrals that retain all four indices within a radius R_λ of the origin are summed into the total energy. All nuclei within this radius are used in the computation of electron-nuclear (EN) attraction and nuclear-nuclear (NN) repulsion terms. As $R_\lambda \to \infty$, the correct limit is reached, but, in general, the convergence is very slow.[9] The reasons for this can be seen in Fig. 2a. Here we show a particular atom μ within a radius R_λ of the origin. A radius r' about μ is indicated for which $\rho_\mu(r)$ should be significant. For this atom, the EN and NN interactions with the charge unit at 1 will be fully counted, but only a portion of the interaction between $\rho_\mu(r)$ and this unit will be included. Coulomb (and corresponding exchange) integrals of the form $(a^\sigma b^1 | c^\mu d^\nu)$ for $|\underset{\sim}{R}_\nu| > R_\lambda$ are arbitrarily excluded, and thus the shaded portion of $\rho_\mu(\underset{\sim}{r})$ shown in the figure is omitted from the sum. Consequently, truncating the sum in this manner would be expected to produce an imbalance between one- and two-electron quantities. Indeed, Euwema et al.[10] employed such a method in a study of the diamond lattice and found it necessary to include monopole and dipole corrections to the potential in order to obtain adequate results.

The analysis leading to Eqs. (17) suggests an alternate bispherical approach. Here, a sphere of radius R_λ is defined about each center μ

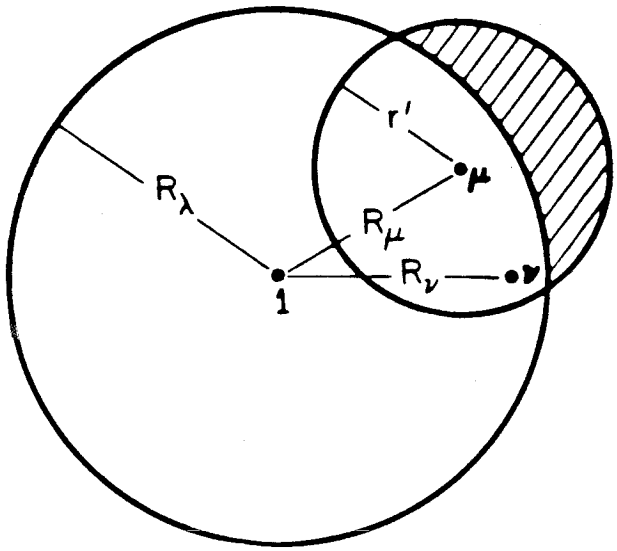

(a)

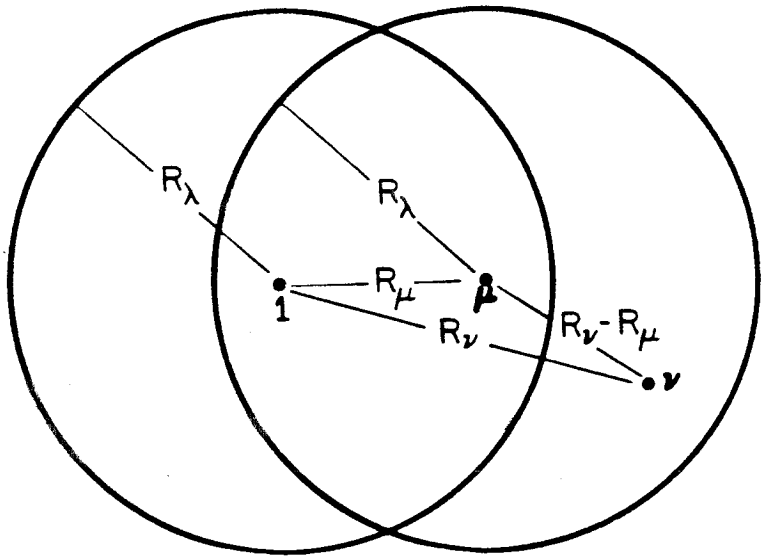

(b)

FIG. 2. (a) Schematic illustration of the spherical cluster approach. Integrals $(a^{\sigma}b^{1}|c^{\mu}d^{\nu})$ are excluded when ν is in the shaded region. (b) In the bispherical cluster approach, electrons one and two are treated equivalently by including all centers σ and ν such that $|\underset{\sim}{R}_{\sigma}| < R_{\lambda}$ and $|\underset{\sim}{R}_{\nu} - \underset{\sim}{R}_{\mu}| < R_{\lambda}$.

that is within R_λ of the origin. As before, all EN and NN interactions between the atoms μ and the charge unit at the origin are included; however, to define repulsions between the $\rho_\mu(\underset{\sim}{r})$ and $\rho_1(\underset{\sim}{r})$, all two-electron integrals $(a^\sigma b^1 | c^\mu d^\nu)$ satisfying

$$|\underset{\sim}{R}_\sigma| < R_\lambda \ , \quad |\underset{\sim}{R}_\mu| < R_\lambda \ , \text{ and } |\underset{\sim}{R}_\mu - \underset{\sim}{R}_\nu| < R_\lambda$$

are included. This arrangement of "bispherical" clusters is shown for a particular atom μ in Fig. 2b. Not only does this approach avoid charge imbalance, but it is also apparent that the sum need not be taken beyond the point where

$$\rho_1(\underset{\sim}{R}_{\mu'}/2) = \rho_{\mu'}(\underset{\sim}{R}_{\mu'}/2) \ll 1 \ ,$$

since the charge unit at the origin is effectively shielded from all charge units farther away from the origin than $|\underset{\sim}{R}_{\mu'}|$.[11]

B. Balancing Calculated Quantities

Truncating the energy sums in any manner necessitates some modification of the concepts discussed in Sec. II. Partitioning the sums in the manner described above makes further discussion of the density matrix and two-electron integrals particularly appropriate.

The discussion of charge units unambiguously defines the necessary two-electron contributions to coulomb sums, but it is less clear concerning the unbiased evaluation of the exchange sums. The Hartree-Fock hamiltonian provides a simple criterion for balancing coulomb and exchange contributions since we must guarantee that

$$J_{\underset{\sim}{kn},\underset{\sim}{kn}} - K_{\underset{\sim}{kn},\underset{\sim}{kn}} = 0. \qquad (18)$$

This cancellation of self-coulomb and exchange terms is assumed to occur in deriving Eq. (8). Deviations from this condition are inherent in methods utilizing exchange approximations, and the resultant residual coulomb repulsions can seriously affect orbital shapes and total energies.[12] To examine this cancellation for ab initio methods, we first expand the expression (19) (leaving implicit the sums over a, b, c, and d),

$$0 = J_{\underset{\sim}{kn},\underset{\sim}{kn}} - K_{\underset{\sim}{kn},\underset{\sim}{kn}} = \sum_{\sigma}^{N'} e^{i\underset{\sim}{k}\cdot\underset{\sim}{R}_\sigma} \sum_{\mu,\nu}^{N'} e^{i\underset{\sim}{k}\cdot(\underset{\sim}{R}_\nu - \underset{\sim}{R}_\mu)} \times \mathbb{C}\{(a^1b^\sigma|c^\mu d^\nu) - (a^1c^\mu|b^\sigma d^\nu)\} ,$$

where $\mathbb{C} = C^{*a}C^{b}C^{*c}C^{d}$. This may be broken into six terms,

$$\sum_{\nu}^{N'} \mathbb{C}\, e^{i\underset{\sim}{k}\cdot\underset{\sim}{R}_\nu}\{(a^1b^1|c^1d^\nu) - (a^1c^1|b^1d^\nu)\} , \qquad \sigma = 1 \quad \mu = 1 \tag{19a}$$

$$+ \sum_{\mu}^{N'}{}' \mathbb{C}\, e^{-i\underset{\sim}{k}\cdot\underset{\sim}{R}_\mu}\{(a^1b^1|c^\mu d^1) - (a^1c^\mu|b^1d^1)\} , \quad \sigma = 1 \quad \begin{matrix}\mu \neq 1\\ \nu = 1\end{matrix} \tag{19b}$$

$$+ \sum_{\mu,\nu}^{N'}{}'' \mathbb{C}\, e^{i\underset{\sim}{k}\cdot(\underset{\sim}{R}_\nu - \underset{\sim}{R}_\mu)}\{(a^1b^1|c^\mu d^\nu) - (a^1c^\mu|b^1d^\nu)\} , \sigma = 1 \quad \begin{matrix}\mu \neq 1\\ \nu \neq 1\end{matrix} \tag{19c}$$

$$+ \sum_{\sigma}^{N'}{}' e^{i\underset{\sim}{k}\cdot\underset{\sim}{R}_\sigma} \sum_{\nu}^{N'} e^{i\underset{\sim}{k}\cdot\underset{\sim}{R}_\nu} \mathbb{C}\{(a^1b^\sigma|c^1d^\nu) - (a^1c^1|b^\sigma d^\nu)\}, \sigma \neq 1 \quad \mu = 1 \tag{19d}$$

$$+ \sum_{\sigma}^{N'}{}' e^{i\underset{\sim}{k}\cdot\underset{\sim}{R}_\sigma} \sum_{\mu}^{N'}{}' e^{-i\underset{\sim}{k}\cdot\underset{\sim}{R}_\mu} \mathbb{C}\{(a^1b^\sigma|c^\mu d^1) - (a^1c^\mu|b^\sigma d^1)\}, \sigma \neq 1 \quad \begin{matrix}\mu \neq 1\\ \nu = 1\end{matrix} \tag{19e}$$

$$+ \sum_{\sigma}^{N'}{}' e^{i\underset{\sim}{k}\cdot\underset{\sim}{R}_\sigma} \sum_{\mu,\nu}^{N'}{}'' e^{i\underset{\sim}{k}\cdot(\underset{\sim}{R}_\nu - \underset{\sim}{R}_\mu)} \mathbb{C}\{(a^1b^\sigma|c^\mu d^\nu) - (a^1c^\mu|b^\sigma d^\nu)\} , \tag{19f}$$

$$\sigma \neq 1 \quad \begin{matrix}\mu \neq 1\\ \nu \neq 1\end{matrix} .$$

The sum restrictions over atoms used in each expression are shown at right. Of the six, (19a), (19b), and (19e) always cancel on a term-by-term basis. The same is true of (19f) if each integral included in the coulomb (first) sum is also included in the appropriate position in the exchange (second) sum of that expression. Similarly, under these conditions, the coulomb and exchange sums in (19c) will cancel exchange and coulomb sums, respectively, of (19d) on a term-by-term basis. Thus, Eq. (18) will be satisfied exactly if each integral generated for summation into the coulomb field of Eq. (13) is also entered into the correct position in the exchange sums. This is precisely the condition suggested by the partitioning of terms shown in Eqs. (17).

IV. Face-Centered Cubic Hydrogen

In this section we present an application of the concepts discussed in the previous sections to a face-centered cubic lattice of hydrogen atoms. Calculations were carried out using an expansion of 1s gaussians

$$\phi^a(r, \zeta) = \sum_{i=1}^{P} C_i e^{-\alpha_i r^2} / \sqrt{N}$$

on each center, where the coefficients C_i and α_i are determined by fitting to a Slater orbital $e^{-\zeta r}$ of scale parameter ζ, and the number of functions (P) in the expansion was allowed to be 1, 2, and 3. Both lattice constant a and scaling parameter ζ were optimized, and we present a detailed discussion of the convergence and magnitude of the energy quantities involved in the $\epsilon_{\hat{kn}}$ and E/N sums.

A. Calculational Details

Both one- and two-electron matrix elements were generated using a program developed to incorporate all rotational and translational symmetries. The one-electron portion of Eq. (14) may be simplified to[8a]:

$$\epsilon_{\hat{kn}}^{one} = N \eta_{\hat{kn}}^{-1} \sum_{a,b}^{m} \sum_{\lambda} h_{1\sigma(\lambda)}^{ab} C_{\hat{kn}}^{*a} C_{\hat{kn}}^{b} \sum_{\sigma}^{n_\lambda} e^{i\hat{k} \cdot \hat{R}_\sigma} ,$$

where $\sigma(\lambda)$ is an atom in shell λ and the inner sum is over the n_λ atoms in shell λ. For this case, only λ integrals $h_{1\sigma(\lambda)}^{aa}$ are required. The symmetry properties of the density matrix allow processing of the two-electron integral list prior to evaluation of the hamiltonian matrix in a manner that greatly facilitates manipulation of these integrals. We will illustrate this by using (16) to rewrite (12) as

$$N \sum_{a,b}^{m} \sum_{\sigma}^{N} D_{1\sigma}^{ab} \sum_{c,d}^{m} \sum_{\omega}^{N} D_{1\omega}^{cd} \sum_{\mu}^{N} \Big\{ A(a^1 b^\sigma | \{\underset{\sim}{E}|-\underset{\sim}{R}_\mu\}\{c^1 d^\omega\}) - B(a^1\{\underset{\sim}{E}|-\underset{\sim}{R}_\mu\}\{c^1\}|b^\sigma\{\underset{\sim}{E}|-\underset{\sim}{R}_\mu\}\{d^\omega\}) \Big\}$$

$$= N \sum_{a,b}^{m} \sum_{\lambda} n_\lambda D_{1\sigma(\lambda)}^{ab} \sum_{c,d}^{m} \sum_{\lambda'} D_{1\omega(\lambda')}^{cd} \frac{1}{g_\sigma} \sum_{j}^{\mathcal{G}} \sum_{\mu}^{N} \Big\{ A(a^1 b^{\sigma(\lambda)} | \{\underset{\sim}{P}_j|-\underset{\sim}{R}_\mu\} \times \{c^1 d^{\omega(\lambda')}\}) - B(a^1\{\underset{\sim}{P}_j|-\underset{\sim}{R}_\mu\}\{c^1\}|b^{\sigma(\lambda)}\{\underset{\sim}{P}_j|-\underset{\sim}{R}_\mu\}\{d^{\omega(\lambda')}\}) \Big\}$$

$$= N \sum_{a,b}^{m} \sum_{\lambda} n_\lambda D_{1\sigma(\lambda)}^{ab} \sum_{c,d}^{m} \sum_{\lambda'} D_{1\omega(\lambda')}^{cd} \{AJ_{1\sigma(\lambda),1\omega(\lambda')}^{abcd} - BK_{11,\sigma(\lambda)\omega(\lambda')}^{acbd}\}, \quad (20)$$

where $\underset{\sim}{R}_\omega = \underset{\sim}{R}_\nu - \underset{\sim}{R}_\mu$. Here again $\mathcal{G}$ is the lattice point group and g_σ is the appropriate degeneracy factor. The quantities $J_{1\sigma 1\omega}^{abcd}$ and $K_{11\sigma\omega}^{acbd}$ are independent of changes in the wavefunction, depending only on the choice of basis. For the largest case considered here ($\lambda = 18$, $N = 381$), truncating these sums in accordance with the definition of bispherical clusters produced an integrals list consisting of 324 values of $J_{1\sigma 1\omega}^{aaaa}$ and 5184 values for the $K_{11\sigma\omega}^{aaaa}$.

A variety of sophisticated schemes have been developed for carrying out the sums over occupied states necessary to evaluate the density matrix elements.[13] Such schemes are necessary because evaluating the $C_{\underset{\sim}{k}n}^{a}$ values requires diagonalization of an $m \times m$ matrix at each $\underset{\sim}{k}$ point to be considered. In these calculations $m = 1$, and no diagonalization is necessary. It is a relatively straightforward task in this case to carry out the sum by dividing the Brillouin zone into a fine grid of weighted

volume elements, using an average value of $\underset{\sim}{k}$ for each element. The position of the Fermi surface was determined by noting the variation in $\epsilon_{\underset{\sim}{k}}$ in all directions radiating outward from the zone origin. The weights of elements intersected by the surface were made proportional to the volume enclosed. The actual summation (integration) was carried out using a simple Romberg procedure.[14] Some experimentation with grid size indicated that errors of $O(10^{-4}\,h)$ could be obtained with a grid of ~ 600 points within the $1/48^{th}$ of the total occupied portion of the zone.

In these calculations (m = 1), the only task to be performed on an iterative basis is to achieve self-consistency in constructing the Fermi surface. Iterative changes in E/N and grid weights were monitored, and convergence to 10^{-7} h and 10^{-3}%, respectively, could be obtained in a few (≤ 5) iterations starting from a spherical Fermi surface.

B. Results

To obtain a readily verifiable test of the stability and accuracy of the procedures used in this study, calculations were first carried out using a high-spin wavefunction (6) in the separated-atom limit (a = 40.0 Bohr = 21.16 Å). Such a test is useful because in this limit $\eta_{\underset{\sim}{kn}} = N$ for all $\underset{\sim}{kn}$ and, since all states in the first Brillouin zone are filled,

$$D_{\mu\nu} = \sum_{\underset{\sim}{kn}}^{N} \eta_{\underset{\sim}{kn}}^{-1} e^{i\underset{\sim}{k}\cdot(\underset{\sim}{R}_\nu - \underset{\sim}{R}_\mu)} = \delta_{\mu\nu} \ .$$

This condition provides an exacting test of the integration procedure over the zone. In addition, we would expect to obtain

$$\underset{\sim}{\epsilon}_{kn} = E/N = E_{atom}$$

for a high-spin wavefunction in the Ewald limit, where E_{atom} is the energy of an isolated hydrogen atom. This test was carried out using the two-function gaussian 1s basis of Huzinaga[15] contracted for $\zeta = 1.0$ (the free atom value). Eight shells of repeating units were considered (N = 135), resulting in only eight unique non-zero two-electron integrals.[16] A grid of 1140 points was used in the Brillouin zone integration. The calculated density matrix elements, listed in Table I, are within 10^{-4} of the theoretical values. These errors propagate as shown in Table II, producing a total energy per atom and band spectrum deviating by no more than 0.00005 h from the theoretical value of -0.48581.

The optimum lattice parameter for the closed-shell (singlet) wavefunction was obtained from a series of HF calculations at different lattice spacings. As discussed below, 14 shells of charge units (N = 249) were adequate for this purpose, leading to E/N values within < 0.001 h of the largest systems considered. The two-function Huzinaga basis[15] was used on each atom, and the scaling parameter ζ was optimized for each value of a considered. The results of these calculations in terms of E/N and the virial ratio are shown for nine combinations of a and ζ in Table III. The optimum energy per atom of -0.4638 h is unbound with respect to isolated H atoms (E = -0.4858 h) by about 0.6 eV. This result is consistent (by the virial theorem) with an optimum exponent that is more diffuse ($\zeta = 0.96$) than for an isolated H atom.

The behavior of energy quantities as a function of increasing N was examined in some detail. In Table IV are shown a variety of quan-

TABLE I. Density Matrix Values for a High-Spin Wavefunction in the Separated Atom Limit.[a] (N = 135)

	λ (shell number)							
	1	2	3	4	5	6	7	8
$D^{aa}_{1\sigma(\lambda)}$	1.00000	1×10^{-5}	2×10^{-5}	2×10^{-5}	1×10^{-5}	-2×10^{-5}	-1×10^{-4}	4×10^{-5}

[a] Using the two-gaussian basis from Ref. 15 with $\zeta = 1.0$ and a = 40.0 bohr.

TABLE II. Total Energy and Band Spectrum for a High-Spin Wavefunction in the Separated Atom Limit. ($a = 40\ a_0$ and $N = 135$)

Total Energies		Eigenvalues at Symmetry Points				
E/N	E_{atom} [a]	Γ	X	W	L	K
-0.48581	-0.48581	-0.48584	-0.48578	-0.48581	-0.48582	-0.48581

[a] Using the two-gaussian basis from Ref. 15, with $\xi = 1.0$.

TABLE III. Optimization of Lattice Constant and Scale Factor for Face-Centered Cubic Hydrogen.[a]

Lattice Constant (Å)	Scale Factor ζ	Total Energies E/N (h)	Virial Ratio
2.2376	0.90	-0.45973	1.0560
2.2376	1.00	-0.46100	1.0818
2.2376	1.10	-0.45703	1.1274
2.4614	0.90	-0.46340	0.97564
2.4614	1.00	-0.46307	1.0117
2.4614	1.10	-0.45642	1.0718
2.6851	0.90	-0.46055	0.92531
2.6851	1.00	-0.45860	0.97302
2.6851	1.10	-0.44925	1.0497
Optimum Calculated Values			
2.4388	0.958	-0.46384	0.99999

[a] Using a two-gaussian expansion with N = 249.

TABLE IV. Total Energies and Band Spectra for Face-Centered Cubic Hydrogen as a Function of Cluster Size.[a]

Shell Number λ	No. of Charge Units $\sigma(\lambda)$	Total Energy (h)[b]		Eigenvalues (h)		Virial Ratio
		Spherical Surface	Converged Surface	$\lvert\underset{\sim}{k}\rvert = 0$	$\lvert\underset{\sim}{k}\rvert = k_f$	
2	13	-0.5379	-0.5267	-0.7379	-0.5162	0.83900
4	43	-0.4561	-0.4613	-0.8761	-0.0146	1.00831
6	79	-0.4572	-0.4596	-0.9110	-0.0675	1.00926
8	135	-0.46209	-0.46347	-0.92774	-0.06895	1.00050
11	177	-0.46231	-0.46394	-0.93328	-0.06547	0.99984
12	201	-0.46221	-0.46381	-0.93444	-0.06348	1.00001
14	249	-0.46226	-0.46384	-0.93384	-0.06330	0.99999
16	321	-0.46257	-0.46421	-0.93022	-0.06356	0.99961
18	381	-0.46262	-0.46427	-0.92757	-0.06183	0.99958

[a] Using a two-gaussian expansion with $\zeta = 0.958$ and lattice constant $\underline{a} = 2.44$ Å.

[b] Isolated atom energy is -0.4858 h.

tities obtained using optimum a and ζ for values of N between 13 and 381. In the first column, E/N values are given where in each case the Fermi surface was assumed to be completely spherical. The convergence, while not completely monotonic, is very rapid with the last three "clusters" differing in energy by less than 0.0004 h. Self-consistent energy values obtained after converging the Fermi surface are shown in the second column. It was expected initially that the iterative process might magnify errors inherent in the larger clusters; however, comparison of the two columns shows that this was not the case. Thus, it appears unlikely that addition of further shells would produce a change in this value by as much as 0.001 h.

More detailed information about convergence may be obtained by examining the individual terms in the energy sums. The terms listed in Tables V and VI are defined by recasting (14) in the simplified form,

$$\epsilon_{\underset{\sim}{kn}} = N\eta^{-1}_{\underset{\sim}{kn}} \sum_{\lambda} H^{aa}_{1\sigma(\lambda)} \sum_{\sigma}^{n_\lambda} e^{i\underset{\sim}{k}\cdot\underset{\sim}{R}_\sigma}$$

$$= N\eta^{-1}_{\underset{\sim}{kn}} \sum_{\lambda} \left\{ h^{aa}_{1\sigma(\lambda)} + \frac{2}{f}\left[AJ^{aa}_{1\sigma(\lambda)} - BK^{aa}_{1\sigma(\lambda)}\right] \right\} \sum_{\sigma}^{n_\lambda} e^{i\underset{\sim}{k}\cdot\underset{\sim}{R}_\sigma} ,$$

in which the innermost sum is over the n_λ atoms in a particular shell λ, and $J^{aa}_{1\sigma}$ and $K^{aa}_{1\sigma}$ include interactions with all other local density functions included in the calculation. A similar expression is possible for the total energy E in (13). The total hamiltonian elements appear in Table V for selected values of λ from 2 to 18 (N = 13 to 381). A comparison of the matrix elements common to the N = 225 and N = 381 cases reveals that for all 13 matrix elements the discrepancies are no greater than

TABLE V. Total Hamiltonian Matrix Elements $H_{1\sigma(\lambda)}$ for Face-Centered Cubic Hydrogen.[a]

Shell No. σ	Magnitude	Charge Units in Calculation				
		43	135	225	321	381
1	10^{-1}	-4.6071	-4.6173	-4.6190	-4.6191	-4.6192
2	10^{-1}	-2.5683	-2.5806	-2.5811	-2.5812	-2.5812
3	10^{-1}	-1.1138	-1.1262	-1.1217	-1.1217	-1.1212
4	10^{-2}	-4.6785	-4.8401	-4.8480	-4.8476	-4.8490
5	10^{-2}	0.0	-2.0438	-2.0560	-2.0564	-2.0582
6	10^{-3}	0.0	-7.9322	-7.8527	-7.8572	-7.8461
7	10^{-3}	0.0	-3.3410	-3.3597	-3.3612	-3.3458
8	10^{-3}	0.0	-2.0588	-2.0359	-2.0303	-2.0319
9	10^{-3}	0.0	0.0	-1.5705	-1.5381	-1.5370
10	10^{-4}	0.0	0.0	-8.3562	-8.3783	-8.1912
11	10^{-4}	0.0	0.0	-8.9267	-8.9491	-9.0147
12	10^{-4}	0.0	0.0	-3.4751	-3.7483	-3.7957
13	10^{-5}	0.0	0.0	-2.1242	-3.6317	-2.9707
14	10^{-4}	0.0	0.0	0.0	1.4807	1.3651
15	10^{-4}	0.0	0.0	0.0	3.3233	3.2874
16	10^{-4}	0.0	0.0	0.0	3.1503	3.1738
17	10^{-4}	0.0	0.0	0.0	0.0	3.1900
18	10^{-4}	0.0	0.0	0.0	0.0	1.6276

[a] Using a two-gaussian expansion with $\zeta = 0.958$ and lattice constant $\underline{a} = 2.44$ Å.

TABLE VI. Hamiltonian Components for Face-Centered Cubic Hydrogen.[a]

Shell No. σ	Total Coulomb $h^{aa}_{1\sigma(\lambda)} + (2/f) J^{aa}_{1\sigma(\lambda)}$						Total Exchange $K^{aa}_{1\sigma(\lambda)}$					
	Magnitude	Charge Units					Magnitude	Charge Units				
		43	135	225	321	381		43	135	225	321	381
1	10^{-2}	7.0405	5.9309	5.9104	5.9105	5.9062	10^{-1}	5.3111	5.2104	5.2100	5.2101	5.2098
2	10^{-2}	-5.6655	-5.9749	-5.9808	-5.9808	-5.9821	10^{-1}	2.0018	1.9831	1.9831	1.9831	1.9830
3	10^{-2}	-3.6024	-3.7045	-3.7065	-3.7065	-3.7070	10^{-2}	7.5352	7.5576	7.5103	7.5108	7.5046
4	10^{-2}	-1.9367	-1.9756	-1.9762	-1.9762	-1.9764	10^{-2}	2.7418	2.8644	2.8717	2.8714	2.8726
5	10^{-2}	0.0	-9.7403	-9.7418	-9.7417	-9.7423	10^{-2}	0.0	1.0697	1.0818	1.0822	1.0840
6	10^{-3}	0.0	-4.3849	-4.3849	-4.3849	-4.3851	10^{-3}	0.0	3.5474	3.4678	3.4723	3.4611
7	10^{-3}	0.0	-1.9421	-1.9421	-1.9421	-1.9422	10^{-3}	0.0	1.3989	1.4176	1.4191	1.4037
8	10^{-4}	0.0	-8.5856	-8.5849	-8.5844	-8.5847	10^{-3}	0.0	1.2002	1.1774	1.1718	1.1735
9	10^{-4}	0.0	0.0	-3.7313	-3.7310	-3.7309	10^{-3}	0.0	0.0	1.1974	1.1650	1.1640
10	10^{-4}	0.0	0.0	-1.5580	-1.5577	-1.5577	10^{-4}	0.0	0.0	6.7982	6.8206	6.8336
11	10^{-4}	0.0	0.0	-1.5580	-1.5577	-1.5577	10^{-4}	0.0	0.0	7.3687	7.3914	7.4570
12	10^{-5}	0.0	0.0	-6.4636	-6.4618	-6.4615	10^{-4}	0.0	0.0	2.8287	3.1021	3.1495
13	10^{-5}	0.0	0.0	-2.6881	-2.6873	-2.6873	10^{-5}	0.0	0.0	-5.6389	9.4435	2.8339
14	10^{-5}	0.0	0.0	0.0	-1.1114	-1.1115	10^{-4}	0.0	0.0	0.0	-1.5919	-1.4762
15	10^{-6}	0.0	0.0	0.0	-4.5120	-4.5206	10^{-4}	0.0	0.0	0.0	-3.3685	-3.3326
16	10^{-6}	0.0	0.0	0.0	-4.5122	-4.5208	10^{-4}	0.0	0.0	0.0	-3.1954	-3.2190
17	10^{-7}	0.0	0.0	0.0	0.0	-7.6948	10^{-4}	0.0	0.0	0.0	0.0	-3.1977
18	10^{-7}	0.0	0.0	0.0	0.0	-3.0129	10^{-4}	0.0	0.0	0.0	0.0	-1.6306

[a] Using a two-gaussian expansion with $\zeta = 0.958$ and lattice constant $\underline{a} = 2.44$ Å.

0.0005 h. Much of the difference between N = 225 and N = 381 total energies must be attributed simply to the additional terms in the N = 381 expansion.

The individual coulomb and exchange matrix elements are grouped in Table VI. The coulomb matrix elements for a given "cluster" tend towards zero with increasing $\sigma(\lambda)$ at a rate proportional to the overlap terms $S_{1\sigma(\lambda)}$. The degree to which a given element deviates from zero in the converged limit is a measure of the non-point charge character of the local density functions. It is an indication of the penetration of the charge units surrounding the origin into the unit at that point. The fact that these matrix elements approach a limiting value is an indication that this unit is fully shielded from all further additions.

The exchange matrix elements are larger in magnitude and tend towards zero more slowly than the corresponding coulomb elements. An examination of Eqs. (13) and (14) shows that there are integrals of the form $(1^a 1^a | \sigma^a \sigma^a)$ that contribute to the matrix element $K_{1\sigma(\lambda)}$ whose values dissipate as $|\underset{\sim}{R}_\sigma|^{-1}$. These are not, however, the predominant contributions to $K_{1\sigma(\lambda)}$ and the elements for large $\sigma(\lambda)$ are negligibly small.

Finally, in Fig. 3 we show the calculated band spectrum and E/N for a calculation with N = 381 at the optimum lattice spacing. The P = 3 basis[15] was used with ζ = 0.958 (the optimum value from the P = 2 basis). Comparison with the separated atom energy of -0.4970 h indicates that at this level of calculation, the system is unbound by 0.9 eV.

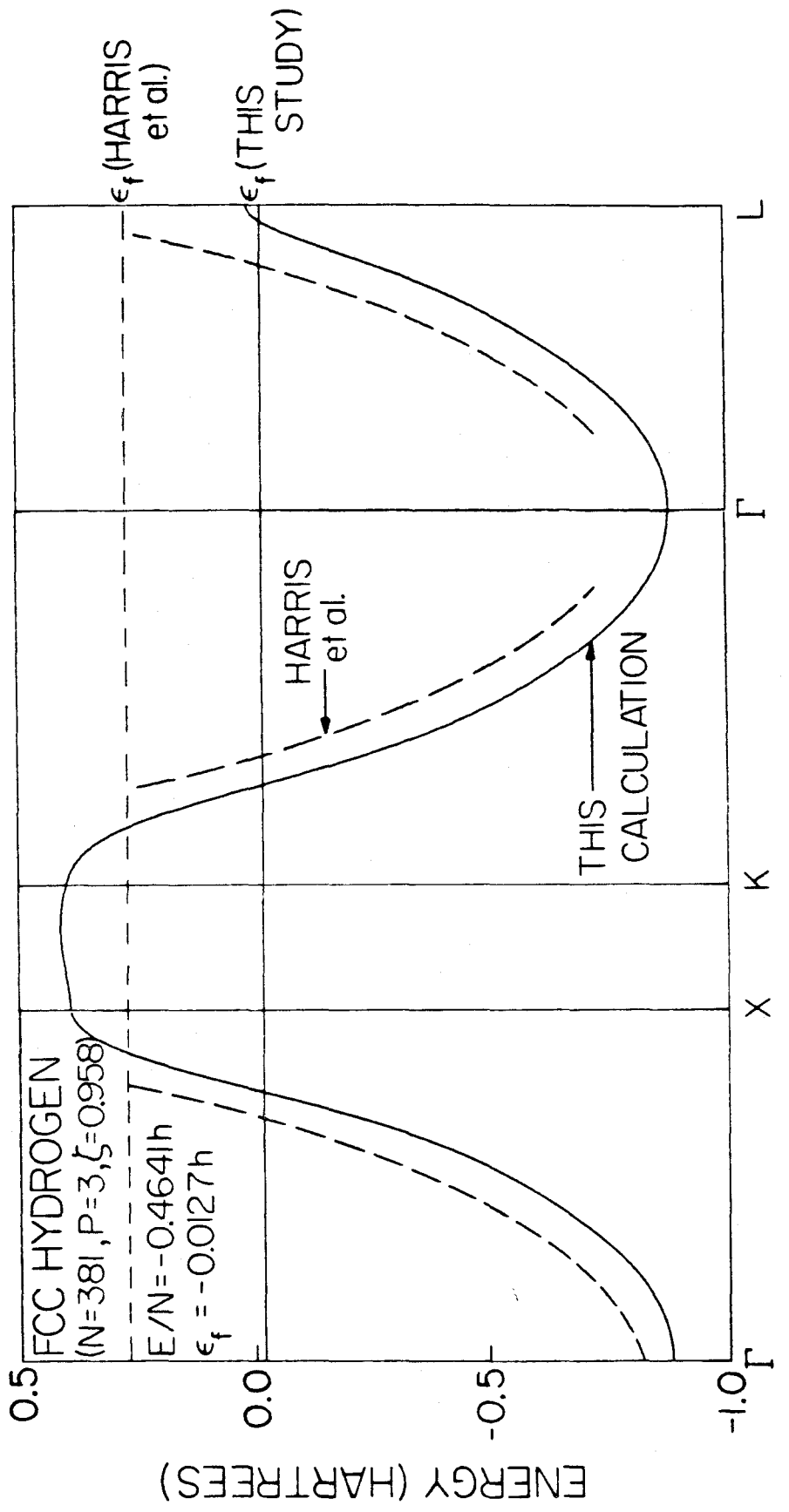

FIG. 3. Band spectrum along symmetry directions for face-centered cubic hydrogen using N = 381 and a three-gaussian expansion (Ref. 15) for the 1s orbital.

V. Sodium and Lithium Conduction Bands

The application of real space basis set expansion techniques has been limited for the most part to ionic[17] or insulating systems[10] possessing very localized orbitals. The highly diffuse basis sets necessary to describe nearly free electron metal systems would be expected to produce poor convergence in conventional spherical cluster expansions. The definition of local electron density functions in the bispherical cluster approach provides a means by which this limitation might be eliminated. Accordingly, we have carried out additional calculations for the conduction band states of face-centered cubic (f. c. c.) sodium and lithium crystals, using the atomic orbital basis. This basis is too restricted to provide quantitative information about these conduction bands, but should illustrate the convergence properties of this technique.

In these calculations, the core electrons were removed from the problem through the application of standard ab initio effective potential techniques.[18] Here, the one-particle equation for the valence orbital of the atom is written as

$$[-\tfrac{1}{2}\nabla^2 - \frac{Z}{|r|} + V^{core}]\phi_v = \epsilon_v \phi_v \ ,$$

where

$$V^{core} = \sum_{\ell, m=0}^{\infty} V_\ell(r) |\ell_m\rangle\langle\ell_m|$$

and each $V_\ell(r)$ is a local potential describing the coulomb and exchange interactions between the valence orbital ϕ_v and the core orbitals. The functions $V_\ell(r)$ are obtained from ab initio calculations on the atom, and

the resultant orbital ϕ_v correctly mimics the character of a valence orbital obtained with all core electrons explicitly included in the calculation.

A. Calculational Details

Under standard conditions, both sodium and lithium exist in body-centered cubic lattices.[19] Both metals undergo a martensitic transition at low temperature, which for lithium produces a partial conversion to a f.c.c. structure. The f.c.c. structure is thought to be favorable for sodium at low temperature,[20] although it has not been observed.

The f.c.c. lithium structure has been characterized with $\underline{a}$ = 4.370 Å, representing a 1.88% expansion of the nearest neighbor distance relative to the b.c.c. phase.[19] This distance was used in calculations on the f.c.c. lithium structure, while for sodium, bond distances for the b.c.c. lattice were scaled outward by 1.88% to obtain $\underline{a}$ = 5.343 Å. The effective potentials and basis sets used were those of Melius and Goddard.[18] For both sodium and lithium, the valence orbital consisted of four gaussian expansions in which the three most contracted functions used coefficients found optimum for the atom. The coefficient for the most diffuse gaussian was optimized in the band calculations involving 135 charge units.[18] The optimum basis sets were then used in calculations of up to 249 charge units to assess the convergence of energetic quantities. In addition, the lattice parameter $\underline{a}$ was optimized for each metal in calculations with N = 135.

B. Results and Discussion

Energy quantities for the four largest clusters considered (N = 177 to 249) are collected in Tables VII and VIII for sodium and lithium, respectively. Comparison with trends in Table IV suggests that E/N values are converged to within 0.001 h, while fermi energies and bandwidths are only slightly less reliable. Overlap values $S^{aa}_{1\mu}$ are collected in Table IX, together with those of the two-gaussian hydrogen basis, and indicate the insensitivity of the bispherical method to the diffuse character of the metal basis sets.

The reasons for this insensitivity may be seen by examining Fig. 4. Here we show the $\rho_\nu(\underset{\sim}{r})$ function for lithium along several symmetry directions, together with the corresponding atomic orbital density function $\phi(\underset{\sim}{r})\phi(\underset{\sim}{r})$. While the overlap values of Table IX suggest that the $\rho_\nu(\underset{\sim}{r})$ function might extend to very long range, the figure indicates that it is very similar in shape to the atomic orbital density. It is the oscillating nature of the $D^{aa}_{1\nu}$ values that results in the highly localized nature of $\rho_\nu(\underset{\sim}{r})$.

As indicated by Fig. 5 and Table X, the calculated band spectra for these systems deviate only slightly from a totally spherical distribution, in agreement with experimental information.[21] Work function values for lithium and sodium may be estimated from fermi energies ϵ_f, listed in Tables VII and VIII (using $\lambda = 14$), and correcting for the potential shift due to the metal surface.[22] Values calculated in this manner (0.2 eV and 1.2 eV) are smaller than the observed values for b.c.c. lithium and sodium (2.49 eV[23a] and 2.26 eV[23b]). To some extent, the error is a result of simple basis set deficiencies, particularly in the

TABLE VII. Total Energies and Band Spectra for Face-Centered Cubic Lithium as a Function of Cluster Size.[a]

Shell Number λ	No. of Charge Units $\sigma(\lambda)$	Total Energy (h)[b]		Eigenvalues (h)	
		Spherical Surface	Converged Surface	$\lvert\underset{\sim}{k}\rvert = 0$	$\lvert\underset{\sim}{k}\rvert = k_f$
11	177	-0.17849	-0.17995	-0.30552	0.03534
12	201	-0.17817	-0.17955	-0.30324	0.04625
13	225	-0.17791	-0.17929	-0.30112	0.05175
14	249	-0.17771	-0.17913	-0.29952	0.05449

[a] Using the atomic orbital from Ref. 18 and a lattice constant of $\underline{a}$ = 4.370 Å.

[b] Isolated atom energy with effective potential is -0.1964 h.

TABLE VIII. Total Energies and Band Spectra for Face-Centered Cubic Sodium as a Function of Cluster Size.[a]

Shell Number λ	No. of Charge Units $\sigma(\lambda)$	Total Energy (h)[b]		Eigenvalues (h)	
		Spherical Surface	Converged Surface	$\lvert\underset{\sim}{k}\rvert = 0$	$\lvert\underset{\sim}{k}\rvert = k_f$
11	177	-0.16597	-0.16688	-0.28001	-0.01440
12	201	-0.16589	-0.16675	-0.28012	-0.01199
13	225	-0.16585	-0.16672	-0.27987	-0.01123
14	249	-0.16585	-0.16671	-0.27957	-0.01097

[a] Using the atomic orbital from Ref. 18 and a lattice constant of $\underline{a}$ = 5.343 Å.

[b] Isolated atom energy with effective potential is -0.1819 h.

TABLE IX. Overlap Values Using Optimum Basis Sets.

Shell Number λ	2	4	6	8	10	12
Shell Coordinates (in lattice units)	(110)	(211)	(310)	(321)	(330)	(420)
Sodium[a]	0.35968	0.06008	0.01321	0.00332	0.00090	0.00048
Lithium[b]	0.44454	0.10453	0.02945	0.00915	0.00301	0.00176
Hydrogen[c]	0.29843	0.03703	0.00504	0.00070	0.00010	0.00004

[a] Lattice constant = 5.343 Å.

[b] Lattice constant = 4.370 Å.

[c] Lattice constant = 2.439 Å (two-Gaussian expansion with ξ = 0.958).

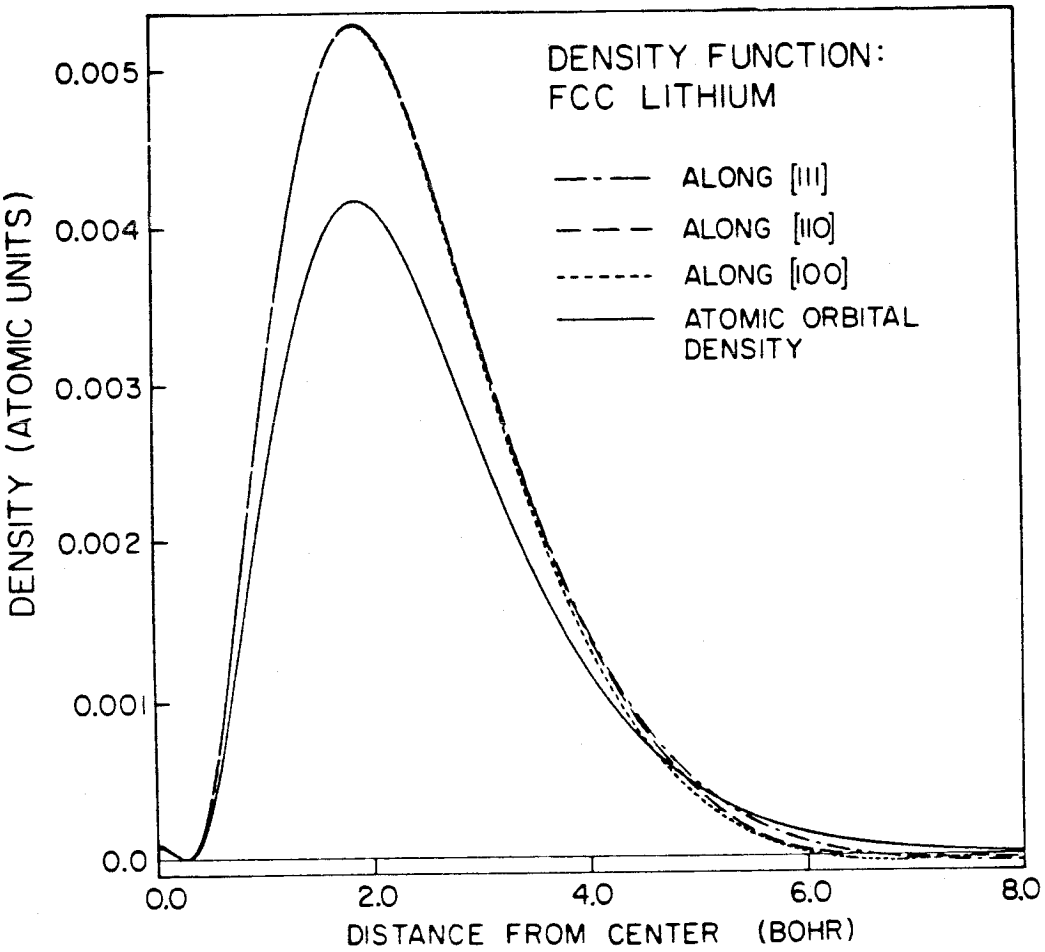

FIG. 4. Orbital density function and local density function for a face-centered cubic array of lithium atoms. The experimental lattice parameter of $\underline{a}$ = 4.370 Å was used in a calculation with N = 249.

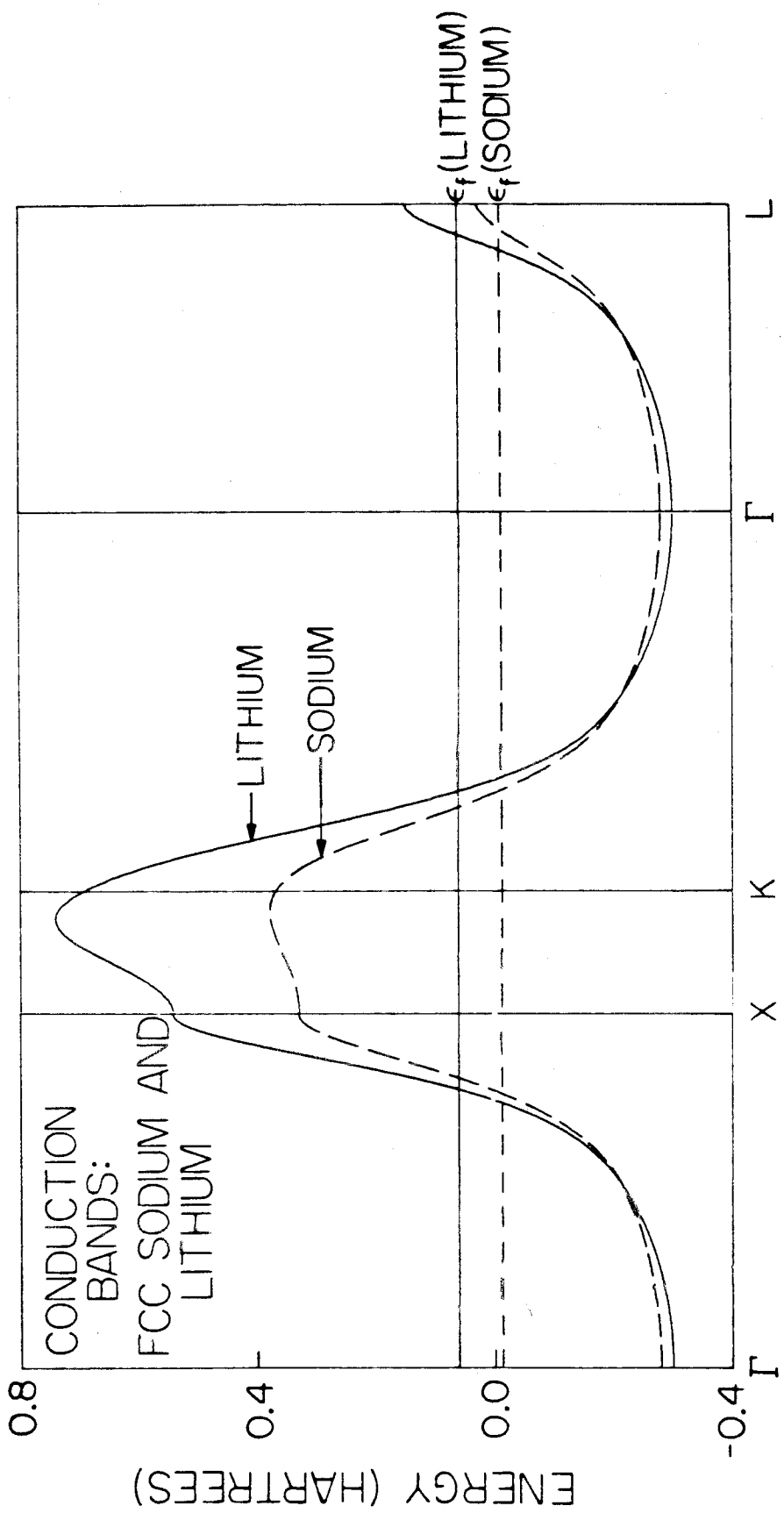

FIG. 5. Conduction band spectra for sodium and lithium along symmetry directions. Both calculations involved 249 charge units at the experimental face-centered cubic lattice separation and both were carried out using the optimized basis sets.

TABEL X. Comparison of k_f Values Between Calculated and Spherical (Free-Electron) Fermi Surfaces

System	k_f Values at Symmetry Points		
	K	X	L
Hydrogen[a]	0.77759	0.76915	0.82585
Lithium[b]	0.78277	0.78457	0.77659
Sodium[c]	0.77621	0.78142	0.79670
Free Electron	0.78159	0.78159	0.78159

[a] Using P = 3 basis set and $\underline{a}$ = 2.44 Å.

[b] Using optimum four-gaussian basis and $\underline{a}$ = 4.370 Å.

[c] Using optimum four-gaussian basis and $\underline{a}$ = 5.343 Å.

region near the Fermi surface.

The result of lattice optimizations are shown in Table XI where the optimum lattice constant for lithium is found to be 5.17 Å, 17% larger than the experimental value, and the system is unbound by 0.2 eV per atom. The calculated bulk modulus of 8.37×10^{10} dynes/cm^2 is comparable to the experimental b.c.c. value[24] (11.6×10^{10} dynes/cm^2) and is quite weak, indicating that large changes in bond distances will be accompanied by relatively small energy changes. Thus we might expect significant improvements in the calculated value of $\underline{a}$ with modest improvement of wavefunction quality. Similar considerations apply to the sodium lattice. Here, the calculated lattice constant is expanded by 11% relative to the estimated f.c.c. value, and the lattice is unstable by 0.3 eV.

TABLE XI. Lattice Constant Optimization for Sodium and Lithium (N = 135).

Metal	Lattice Constant (Å)	Energy (h)	Eigenvalues (h)		Bulk Modulus (10^{10} dynes/cm^2)
			$\lvert\underset{\sim}{k}\rvert = 0$	$\lvert\underset{\sim}{k}\rvert = k_f$	
Sodium	5.244	-0.16377	-0.2966	-0.0073	7.67
	5.774	-0.16905	-0.3025	-0.0383	
	6.303	-0.16776	-0.2875	-0.0497	
	Optimum Values				
	5.934	-0.17136	-0.28532	-0.0455	
Lithium	4.688	-0.18539	-0.3193	-0.0022	8.37
	5.005	-0.18768	-0.3261	-0.0245	
	5.323	-0.18772	-0.3289	-0.0453	
	Optimum Values				
	5.169	-0.18811	-0.3320	-0.0394	

VI. Discussion

A. Comparison with Other Methods

The high symmetry and infinite periodicity of a three-dimensional lattice allow the crystalline HF problem to be considered from within a variety of different representations. Of those investigators who have formulated the problem in real space, Calais and Sperber[25] have described a method that bears the closest resemblance to our own. They arrived at the same choice of repeating density unit through consideration of the properties of the density matrix;[25c] however, their evaluation of the total energy was quite different. Whereas we have chosen to integrate the field experienced by a single unit cell over all space, Calais and Sperber integrate the field due to all atoms in the lattice over a single Wigner-Seitz cell. While elegant, the resulting integrations are difficult and make self-consistent evaluation of coefficients and the fermi surface less practical.

Euwema et al.[10] have carried out calculations on the diamond lattice using the spherical cluster method. Some consideration is given in that paper to the definition of a minimum set of two-electron integrals within the constraints of the method. As mentioned earlier, they approach the problem of charge imbalance inherent in the spherical cluster method through the application of monopole and dipole corrections to the potential. The calculations so defined are carried out self-consistently, producing optimum orbital coefficients and zone point weights for the integration in $\underline{k}$ space.

Several methods utilize a fourier representation. Mauger and Lannoo[26] utilize the fourier transform of an LCAO (Bloch) wavefunction.

Brener and Fry[27] expand the coulomb potential in a fourier series and the exchange operator as a double fourier integral. To overcome slowly converging sums, the overlapping atomic potential approximation is invoked to obtain the core contributions to the sums.

The method of Harris et al.[28] is most directly comparable to the one described here, as it is formulated with the intention of providing results in the Ewald limit, and has been applied to both the hydrogen and lithium problems discussed here. They have chosen a formalism in which the coulomb potential is expressed as a fourier transform, producing energetic quantities in terms of weighted lattice sums of orbital products. The method involves considerable numerical complexity and is limited to systems involving a single occupied band.[29a] As current fourier representation methods do not permit the use of ab initio effective potential techniques, a zero differential overlap approximation is invoked in the treatment of core states.[28, 30a]

Unlike the real space techniques, the method of Harris et al. is able to economically utilize Slater-type orbitals, and this is done in the studies of hydrogen[29] and lithium.[30] In Fig. 3 we show the calculated band spectrum for hydrogen obtained by this method for comparison with our own. While the shapes are quite similar, there is clearly a discrepancy in the absolute position of the band spectrum. Although Harris et al. do not report energies near the Γ point, total energies are quoted and the system is found to be unbound by a measure (0.9 eV) identical to that obtained here. Since total electronic energies of a restricted HF wavefunction may be expressed as

$$E = \sum_{\underset{\sim}{kn}}^{Np/f} f(\epsilon_{\underset{\sim}{kn}} + h_{\underset{\sim}{kn},\underset{\sim}{kn}})/2 \ ,$$

the similarity in total energies and disparity in band spectra are surprising. Our calculated lattice constant of 2.44 Å is somewhat longer than the 2.24 Å obtained in the Harris et al. study, and the optimum scale parameters of 0.96 and ~1.25, respectively, are quite different. Based on the virial theorem, one would expect an unbound system to yield a ζ smaller than the free atom, and it is difficult to understand why their value is larger. These differences could arise from the somewhat different form of Bloch wavefunctions employed by Harris et al.[28]

Because of the use of a single (contracted) s function on each atom, our / lithium results are of limited quantitative value; however, some comparisons with the results of Kumar et al.[30] are valuable. In that study, numerical instabilities in the normal procedures required fitting results to a free-electron, logarithmic exchange term in order to obtain ϵ_k. Thus, full band spectra were not reported; however, the limiting values, ϵ_f and ϵ_0, were quoted. Their band spectrum is shifted upwards by about 0.1 h relative to our comparable results at the optimum lattice spacing shown in Table XI. The calculated bandwidth in that study of 0.265 h is also somewhat different from our own (0.293 h). While these differences may be due to choice of basis set, it is relevant to note that the optimum lattice parameter obtained in that study is 5.45 Å, considerably larger than that obtained here. A similar discrepancy is observed in comparing the b.c.c. results of Calais and Sperber[25a] (a = 7.0 a.u.) with those of Kumar et al.[30] (a = 8.2 a.u.). This comparison is particularly relevant

in that both methods employ Slater-type atomic orbitals, differing only in the treatment of core orbitals and the form of Bloch expansion used. While Kumar et al.[30] attribute the discrepancy to the differences in Bloch expansions, the extremely small change in energy obtained with variation of a raises some concern about the validity of the core approximation used by Kumar et al.[30]

B. On Generalization to Lesser Periodicity

As mentioned at the outset, the development of this HF procedure was conceived as a first step in producing more general methods capable of dealing with lesser periodicity. Emphasis has been placed on numerical simplicity and stability and maximizing the use of existing, mathematically straightforward techniques of theoretical chemistry. There are a variety of ways in which this formalism might be generalized to two-dimensional systems:

1. Two-dimensional Bloch basis functions of the form

$$\varphi^a_{\underset{\sim}{k}_\parallel}(\ell, \underset{\sim}{r}) = \sum_\mu e^{i\underset{\sim}{k}_\parallel \cdot \underset{\sim}{R}_\mu} \phi^a(\underset{\sim}{r} - \underset{\sim}{R}_\mu - \underset{\sim}{R}_\ell)$$

may be used, where $\underset{\sim}{R}_\ell$ determines the origin of a particular layer in the slab, $\underset{\sim}{R}_\mu$ is measured from that origin within the layer, and $\underset{\sim}{k}_\parallel$ is a two-dimensional wave vector. One-electron wavefunctions are

$$\psi_{\underset{\sim}{k}n_\parallel, qn_\perp}(\underset{\sim}{r}) = \eta^{-\frac{1}{2}}_{\underset{\sim}{k}n_\parallel, qn_\perp} \sum_a^m C^a_{\underset{\sim}{k}n_\parallel} \sum_\ell C^a_{qn_\perp}(\ell) \varphi^a_{\underset{\sim}{k}_\parallel}(\ell, \underset{\sim}{r}) ,$$

where a separate coefficient $C^a_{qn_\perp}$ is needed to define oscillations in the direction perpendicular to the surface (there will be ℓ values

of q for each bound n). Within the formalism defined here, such functions would lead to the definition of a two-dimensional local density function and manipulation would be much the same as discussed above. For slabs of a sufficient number of layers, the local density functions at one face could be constrained to be those of a bulk calculation, thereby eliminating the artificial "thickness" phenomena characteristic of a slab calculation.

2. For systems in which localized bonding or pair correlation effects are important, it would be more effective to define a basis for a compound unit cell extending through the thickness of the slab,

$$\varphi^{a}_{q_\perp}(\omega, \underset{\sim}{r}) = \sum_{\mu} C^{a}_{q_\perp} \phi^{a}(\underset{\sim}{r} - \underset{\sim}{R}_{\omega} - \underset{\sim}{R}_{\mu}) ,$$

where $\underset{\sim}{R}_{\omega}$ locates the compound cell origin and the $\underset{\sim}{R}_{\mu}$ locate atoms within the cell from that origin. There will be as many values of $q_\perp$ as there are atoms in the cell possessing a particular $\phi^{a}(\underset{\sim}{r})$. The coefficients $C^{a}_{q_\perp}$ are fixed, and are chosen so as to make the $\varphi^{a}_{q_\perp}(\omega, \underset{\sim}{r})$ orthogonal for a given choice of $\underline{a}$ and ω. One-electron functions become

$$\psi_{\underset{\sim}{k}n_\parallel, qn_\perp}(\underset{\sim}{r}) = \eta^{-\frac{1}{2}}_{\underset{\sim}{k}n_\parallel, qn_\perp} \sum_{\omega} e^{i\underset{\sim}{k}_\parallel \cdot \underset{\sim}{R}_{\omega}} \sum_{a} C^{a}_{\underset{\sim}{k}n_\parallel} \sum_{q_\perp} C^{a}_{qn_\perp} \varphi^{a}_{q_\perp}(\omega, \underset{\sim}{r}) \quad .$$

In this way, all the information relevant to a single compound cell may be isolated by the terms in brackets. Linear combinations of such orbitals could be used effectively in describing correlation effects in a generalized valence bond wavefunction.[7]

3. Noting that the matrix elements $H^{aa}_{1\sigma(\lambda)}$, discussed in Sec. IV. B,

contain all of the hamiltonian information relevant to a pair of atoms separated by $|\underset{\sim}{R}_1 - \underset{\sim}{R}_{\sigma(\lambda)}|$, one may design a finite cluster method in which the atoms are "unaware" that they are set in a finite lattice. Using these elements to define a zero-order hamiltonian matrix between atoms, the finite cluster would experience the field of an infinite surrounding array (when corrected for the neighboring atoms included explicitly). Thus interstitial migration or vacancy formation could be treated rigorously as a correction to this hamiltonian.

Loss of periodicity in the direction perpendicular to the surface necessarily leads to the generation of more non-unique two-electron matrix elements in methods (1) and (2). From the results of both semi-empirical[1] slab calculations and ab initio cluster calculations[2a] it appears unlikely that sufficient layers will be required for this to be of serious consequence.

Acknowledgment: This research was carried out with partial support from the U. S. Department of Energy Grant No. EX-76-G-03-1305. However, any opinions, findings, conclusions, or recommendations expressed herein are those of the authors and do not necessarily reflect the views of the DOE. Caltech Chemistry Contribution No. 6140.

References

1. See, for example, (a) F. J. Arlinghaus, J. G. Gay, and J. R. Smith, Theory of Chemisorption, J. R. Smith, Ed. (Springer-Verlag), in press; (b) J. Ferrante and J. R. Smith, Phys. Rev. B 19, 3911 (1979).
2. (a) T. H. Upton, W. A. Goddard III, and C. F. Melius, J. Vac. Sci. Technol. 16, 531 (1979); (b) G. T. Surratt and A. B. Kunz, Phys. Rev. Lett. 40, 347 (1978).
3. W. A. Goddard III, J. J. Barton, A. Redondo, and T. C. McGill, J. Vac. Sci. Technol. 15, 1274 (1978).
4. C. F. Melius, T. H. Upton, and W. A. Goddard III, Solid State Commun. 28, 504 (1978).
5. C. C. J. Roothaan and P. S. Bagus, Methods in Computational Physics, 2, 47 (1963).
6. For the wavefunctions indicated,

$$\chi_{HS} = \alpha\alpha\alpha\alpha\ldots\alpha$$

$$\chi_{CS} = \alpha\beta\alpha\beta\alpha\beta\alpha\beta\ldots.$$

7. F. W. Bobrowicz and W. A. Goddard III, Modern Theoretical Chemistry: Methods of Electronic Structure Theory, H. F. Schaefer III, Ed. (Plenum Press, New York, 1977), Vol. 3, pp. 79-127.
8. (a) J. C. Slater and G. F. Koster, Phys. Rev. 94, 1498 (1954); (b) M. Miasek, Bull. Acad. Pol. Sci. Cl. III, 4, 805 (1956).
9. T. H. Upton and W. A. Goddard III, unpublished results.
10. R. N. Euwema, D. L. Wilhite, and G. T. Surratt, Phys. Rev. B 7, 818 (1973).

11. It is appropriate to consider the limiting behavior of the energy sums. This question has been considered in some detail for ionic lattices. It has been shown [F. E. Harris, Ref. 28; R. N. Euwema and G. T. Surratt, J. Phys. Chem. Solids 36, 67 (1975); A. Redlack and J. Grindlay, ibid. 36, 73 (1975)] that the conditionally convergent sums approach the Ewald or infinite crystal limit if the repeating unit has net zero dipole moment and second moment trace. For non-ionic systems with continuous charge distribution, as are treated here, a moment expansion [F. W. De Wette and B. R. A. Nijboer, Physica 24, 1105 (1958)] reveals that the neutral charge unit need only have vanishing dipole and quadrupole moments to converge absolutely.

12. S. J. Niemczyk and C. F. Melius, Chem. Phys. Lett. 46, 236 (1977).

13. (a) H. J. Monkhorst and J. D. Pack, Phys. Rev. B 13, 5188 (1976); (b) D. J. Chadi and M. L. Cohen, ibid. 8, 5747 (1973).

14. See, for example, C. F. Gerald, Applied Numerical Analysis (Addison-Wesley, Reading, MA, 1978), pp. 212-214.

15. S. Huzinaga, J. Chem. Phys. 42, 1293 (1965).

16. For large interatomic separation, only those integrals $(a^1 b^1 | c^\mu d^\mu)$ that scale as $|\underset{\sim}{R}_\mu|^{-1}$ are nonzero. For eight shells of repeating units, there will be eight such unique integrals.

17. A. B. Kunz and N. O. Lipari, Phys. Rev. B 4, 1374 (1971).

18. C. F. Melius and W. A. Goddard III, Phys. Rev. A 10, 1528 (1974). The coefficients used with the most diffuse (fourth) gaussians were $C_4(\mathrm{Na}) = 0.26480$ and $C_4(\mathrm{Li}) = 0.32840$.

19. W. P. Pearson, A Handbook of Lattice Spacings and Structure of Metals and Alloys (Pergamon Press, New York, 1958).

20. C. S. Barrett, Amer. Min. 33, 749 (1948); J. Inst. Met. 84, 43 (1955).

21. D. L. Randles and M. Springford, J. Phys. F 3, L185 (1973).

22. N. D. Lang and W. Kohn, Phys. Rev. B 3, 1215 (1971).

23. (a) P. A. Anderson, Phys. Rev. 75, 1205 (1949); (b) E. Patai, Z. Physik 59, 697 (1930).

24. K. A. Gschneider, Jr., Solid State Phys. 16, 276 (1964).

25. (a) J. L. Calais and G. Sperber, Int. J. Quant. Chem. 7, 501 (1973); (b) G. Sperber and J. L. Calais, ibid. 7, 521 (1973); (c) G. Sperber, ibid. 7, 537 (1973).

26. A. Mauger and M. Lannoo, Phys. Rev. B 15, 2324 (1977).

27. N. E. Brener and J. L. Bry, Phys. Rev. B 17, 506 (1978).

28. F. E. Harris, Theor. Chem.: Adv. Perspect. 1, 147 (1975). "Modulated plane wave" Bloch functions of the form

$$\psi^{j}_{\underset{\sim}{k}}(\underset{\sim}{r}) = e^{2\pi i \underset{\sim}{k}\cdot\underset{\sim}{r}/a} \sum_{\underset{\sim}{\mu}} \phi_j(\underset{\sim}{r} - a\,\underset{\sim}{\mu})$$

are used in this paper and in Refs. 29-30.

29. (a) F. E. Harris, L. Kumar, and H. J. Monkhorst, Phys. Rev. B 7, 2850 (1973); (b) D. E. Ramaker, L. Kumar, and F. E. Harris, Phys. Rev. Lett. 34, 812 (1975).

30. (a) L. Kumar, H. J. Monkhorst, and F. E. Harris, Phys. Rev. B 9, 4084 (1974); (b) L. Kumar and H. J. Monkhorst, J. Phys. F 4, 1135 (1974).

Part V

Appendices

Appendix V.A

Calculational Details: Nickel

Basis Sets and Effective Potentials

I. Introduction

To avoid unnecessary duplication, some remarks concerning nickel basis sets, effective potentials have been excluded from the body of the thesis. Most of the basis sets and potentials for the other atoms may be found in the literature, and citations have been given where appropriate. This is not true of the basis sets and effective potentials used for nickel atoms, and these will be described in more detail here.

II. Basis Sets and Effective Potentials

Implicit in all of the calculations reported here is the understanding that the argon core does not interact significantly with the valence electrons of the nickel atom and is not important in its chemistry. In previous calculations on Ni_2 and Ni_8 clusters, we have found it useful to avoid explicit treatment of these core orbitals by replacing them with an effective potential that properly described their coulomb and exchange fields. This potential was obtained by the method of Melius, Olafson, and Goddard[1] through a fit to an ab initio description of the Ni atom, with subsequent modification by Sollenberger[2] to incorporate intra-atomic correlation effects in an appropriate sense. In this manner self-consistent calculations could be carried out that explicitly optimized orbitals for only the ten valence electrons, each properly moving within the field of a forzen argon core. The resulting modified effective potential (MEP) is summarized in Table Ia.

As was described in Part II.B, low-lying metal cluster states generally involved a localized $3d^9$ configuration on each Ni atom, with the remaining electrons in delocalized orbitals of predominantly 4s

character. The localized 3d orbitals were found to be of secondary importance in the bonding, both to other Ni atoms and the adspecies considered (see Part III). This information served as justification for the generation of the 3d-averaged MEP, a potential in which the 3d electrons were incorporated into the potential leaving only the 4s orbital to be obtained variationally.

The procedure for generation of this potential was as follows:

1. A state of the Ni atom was solved for in which the five spatial $3d^9$ configurations were averaged, resulting in orbitals each with $\frac{9}{5}$ electron occupation. In this way bias towards a particular $3d^9$ configuration was avoided.

2. Similar states were obtained having the averaged 3d shell, but with net $4p^1\,3d^9$ and $4d^1\,3d^9$ occupations.

3. Terms were added to the MEP that would allow these states to be well-described without explicit treatment of the 3d electrons. The new potential (denoted 3d-MEP) thus described the field seen by a single electron outside the $3d^9$ shell. The method of Melius, Olafson and Goddard[1] was used in fitting the new MEP terms, listed in Table Ib.

Several different basis sets were used with this potential, and these are summarized in Tables II, III and IV. The 4s basis sets in Table II were obtained from Wachters, and contracted variously as triple zeta, double zeta (DZ), and minimum basis (MBS). For the MBS contraction, atomic ^3D coefficients were used. Two different 4p basis sets were used (Table III). The 4 gaussian set was obtained by Sollenberger.[2] Almost all calculations were insensitive to the 4p basis, and for most calcula-

tions the single gaussian was used. The 3d basis in Table IV is from Wachters,[3] and was contracted both DZ and MBS, where [3]D coefficients were used here too for the MBS contraction.

These sets were used in various combinations as summarized in Table V. The notation is as follows: (4s, 4p, 5d) → (3s, 2p, 2d) implies a combination of the (4s|3s), (4p|2p), and (5d|2d) sets from Tables II-IV.

References and Notes

1. C. Melius, B. Olafson, and W. Goddard, Chem. Phys. Lett., 28, 457 (1974).

2. M. Sollenberger, Masters Thesis, Calif. Inst. of Technology, 1977.

3. A. Wachters, J. Chem. Phys., 52, 1033 (1970).

Table I: Nickel Effective Potentials

Potential	n+2	Exponent	Coefficient
	1	21.66000	-9.827000
	1	0.65900	-1.247000
V(D)	2	5.02000	-12.840000
	0	0.50000	0.850000
	2	2.00000	-6.800000
	0	0.46500	4.807000
	2	5.62000	23.610000
V(P-D)	0	0.03750	0.500000
	2	0.15000	-0.300000
(a)	0	0.50000	-0.850000
	2	2.00000	6.800000
	0	0.95900	7.465000
	2	0.50400	0.848000
	2	8.87000	-28.670000
V(S-D)	0	0.03750	1.500000
	2	0.15000	-0.900000
	0	0.50000	-0.850000
	2	2.00000	6.800000
V(D)	1	0.41409	1.085750
(b)			
V(P-D	2	0.27339	0.485057
	0	0.21425	-3.631800
V(S-D)	2	3.94705	0.923367
	0	0.34183	-3.735220

Table II: Nickel 4s Basis Sets

Contraction	COMPONENT	TYPE	EXPONENT	COEFFICIENT
(4s|1s)	1	S	2.3941700	-0.0128600
	2	S	0.9181690	-0.1518800
	3	S	0.1301760	0.4106200
	4	S	0.0463920	0.6858800
(4s|2s)	1	S	2.3941700	-0.0128510
	2	S	0.9181690	-0.1517810
	3	S	0.1301760	0.4101900
	1	S	0.0463920	1.0000000
(4s|3s)	1	S	2.3941700	0.0106000
	2	S	0.9181690	0.1251900
	1	S	0.1301760	1.0000000
	1	S	0.0463920	1.0000000

Table III: Nickel 4p Basis Sets

Contraction	COMPONENT	TYPE	EXPONENT	COEFFICIENT
(4p|2p)	1	X	2.0350400	-0.0259000
	2	X	0.7804440	0.0385000
	3	X	0.1106500	0.6211000
	1	X	0.0394330	1.0000000
(1p|1p)	1	X	0.1000000	1.0000000

Table IV: Nickel 3d Basis Sets

Contraction	COMPONENT	TYPE	EXPONENT	COEFFICIENT
(5d|1d)	1	XX	48.9403000	0.0256380
	2	XX	13.7169000	0.1383090
	3	XX	4.6395100	0.3450430
	4	XX	1.5743300	0.4399780
	5	XX	0.4864090	0.3931200
(5d|2d)	1	XX	48.9403000	0.0270600
	2	XX	13.7169000	0.1459800
	3	XX	4.6395100	0.3641800
	4	XX	1.5743300	0.4643800
	1	XX	0.4864090	1.0000000

Table V: Utilization of Nickel Basis Sets and Effective Potentials

Basis Set	Effective Potential	System	Thesis Section
(4s, 4p, 5d) → (3s, 2p, 2d)	MEP	Ni_2	Part II.A
(4s, 2p, 5d) → (3s, 1p, 2d)	"	NiC_2H_2	Part I.A, I.C
" "	"	$Ni_2C_2H_2$ d-π, di-σ	Appendix I.A
(4s, 1p, 5d) → (2s, 1p, 1d)	"	NiC_2H_4, $Ni_2C_2H_4$	Part I.B, I.C
(4s, 1p, 5d) → (2s, 1p, 2d)	"	Ni_8	Part II.B
"		$Ni_{13}d$, $Ni_{19}d$	Part II.C
(4s, 1p) → (2s, 1p)	3d-MEP	$Ni_{13}S$, $Ni_{19}S$	"
(4s | 2s)	"	Ni_{13}-Ni_{87}	"
"	"	$Ni_{20}X$, $Ni_{28}X$	Part III
(4s | 1s)	"	Ni_{13}-Ni_{55}	Part II.C

Appendix V.B.

Constructing a Unique Matrix Element List for Ab Initio Calculations: A Procedure for Transforming Integrals Over an Abelian Point Group Symmetry Orbital Basis Set.

I. Introduction

In a typical ab initio calculation in which an atomic orbital (AO) basis is used, the generation of hamiltonian matrices requires the prior evaluation of up to $\sim\frac{1}{8}N^4$ (N = number of AO functions) two-electron matrix elements. When point group symmetry is present in the molecule, many of these matrix elements will have identical values, differing only in the spatial orientation of the integrands. While a computational savings may be registered by evaluating only one out of each set of duplicate elements, the most general treatment of SCF procedures requires that a value be carried for each of the duplicates. Thus, point group symmetry permits no savings in the amount of data that must be handled in constructing the hamiltonian matrices when an AO basis is employed.

It has long been recognized that this wasteful situation may be simply improved by constructing a symmetry orbital (SO) basis from the original AO set. This is done by applying projection operators to the AO basis, producing a set of functions that transform according to the irreducible representation of the molecular point group. The use of such a basis in evaluating one- and two-electron integrals renders far more powerful the usual symmetry constraint on their values: for a non-zero value, the integrand must contain a part which transforms according to the totally symmetric representation.[1]

As a simple illustration, consider a system of N AO functions which transform under C_{2v} symmetry, an Abelian group of order 4. Applying projection operators to such a basis will produce N SO

functions, with roughly N/4 of these transforming according to each of the four irreducible representations. As the one-electron hamiltonian is totally symmetric, the values of the one-electron matrix elements will be determined by:

$$\langle \varphi_{\Gamma_1} | H | \varphi_{\Gamma_2} \rangle = V \delta_{\Gamma_1 \Gamma_2}$$

where Γ_1 and Γ_2 are the irreducible representations of the two functions. As a result only $\sim \frac{1}{8} N^2$ of these integrals will be non-zero, a savings of a factor of 4 over the $\sim \frac{1}{2} N^2$ non-zero integrals of the AO basis. In general, for systems of abelian symmetry the number of both one- and two-electron matrix elements will be reduced by a factor equal to the order of the molecular point group.

This situation is altered for systems of non-abelian symmetry. The reduction factor is no longer given by the order of the point group and, since degeneracies are now present, there is an additional question of uniqueness. This may be illustrated by a more specific example. In Fig. 1, a tetrahedral array of atoms is shown, with each atom shown to be at a particular corner of a cube for illustrative purposes. Assuming each atom to have an AO basis set consisting of a single S, X, Y, and Z function produces a 16-dimensional reducible representation of T_d. We can also consider these functions to constitute a reducible representation of the subgroups D_2 and C_{2v}. Reducing this representation for both D_2 and C_{2v} produces the SO bases listed in Table I. Concentrating first on the S representation, we see that it spans the irreducible representation (I.Rs) of D_2 (i.e.,

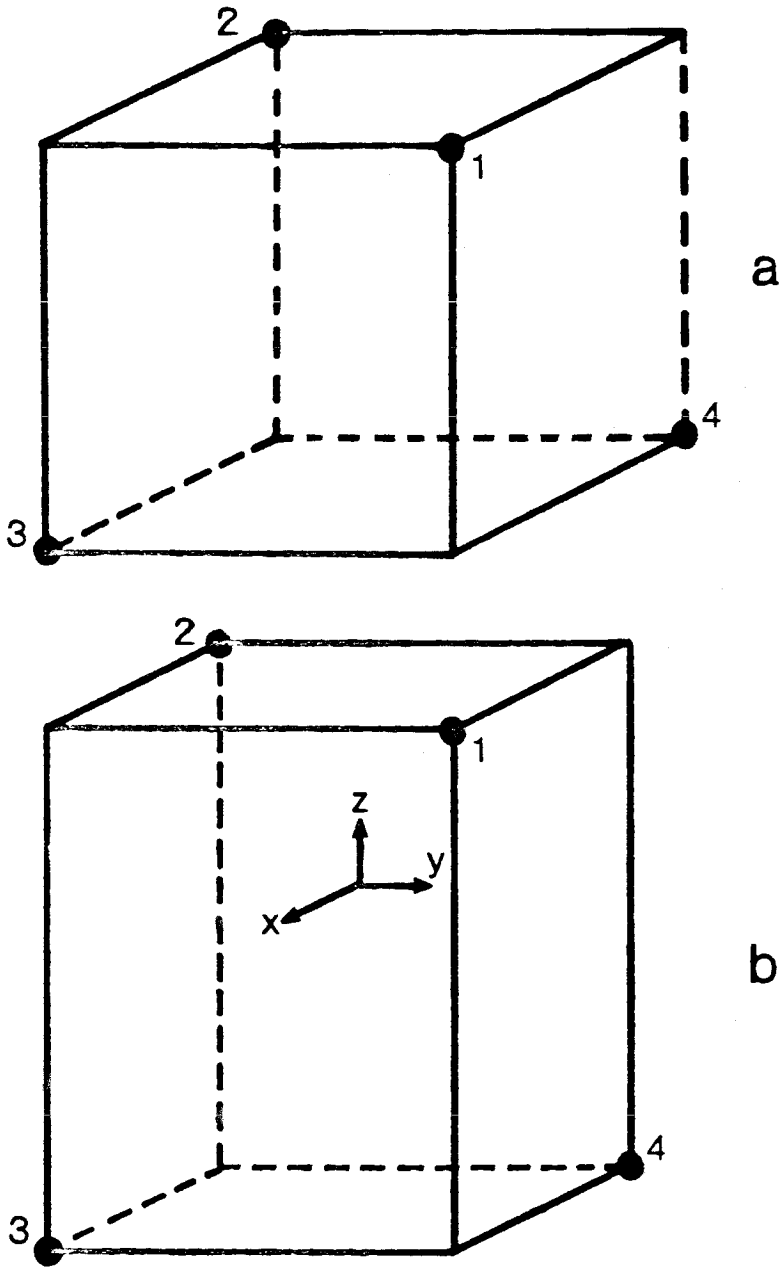

Figure 1: Arrays of atoms drawn with cubes to illustrate symmetry: a) T_d symmetry; b) D_2 symmetry.

Table I: Reduction of AO Basis to SO Basis for Tetrehedral Array of Atoms in Figure 1.

Point Group	SO Function	Irreducible Representation	AO Function Combinations
C_{2v}	1	A_1	$S_1 + S_2$
	2	B_1	$S_1 - S_2$
	3	A_1	$S_3 + S_4$
	4	B_2	$S_3 - S_4$
	5	B_1	$X_1 + Y_1 + X_2 + Y_2$
	6	A_1	$X_1 + Y_1 - X_2 - Y_2$
	7	B_2	$X_1 - Y_1 + X_2 - Y_2$
	8	A_2	$X_1 - Y_1 - X_2 + Y_2$
	9	A_1	$Z_1 + Z_2$
	10	B_1	$Z_1 - Z_2$
	11	B_1	$X_3 + Y_3 + X_4 + Y_4$
	12	A_2	$X_3 + Y_3 + X_4 - Y_4$
	13	B_2	$X_3 - Y_3 + X_4 - Y_4$
	14	A_1	$X_3 - Y_3 - X_4 + Y_4$
	15	A_1	$Z_3 + Z_4$
	16	B_2	$Z_3 - Z_4$

Table I: (Continued)

Point Group	SO Function	Irreducible Representation	AO Function Combinations
D_2	1	A_1	$S_1 + S_2 + S_3 + S_4$
	2	B_1	$S_1 + S_2 - S_3 - S_4$
	3	B_3	$S_1 - S_2 + S_3 - S_4$
	4	B_2	$S_1 - S_2 - S_3 + S_4$
	5	B_3	$X_1 + X_2 + X_3 + X_4$
	6	B_2	$X_1 + X_2 - X_3 - X_4$
	7	A_1	$X_1 - X_2 - X_3 - X_4$
	8	B_1	$X_1 - X_2 - X_3 + X_4$
	9	B_2	$Y_1 + Y_2 + Y_3 + Y_4$
	10	B_3	$Y_1 + Y_2 - Y_3 - Y_4$
	11	B_1	$Y_1 - Y_2 + Y_3 - Y_4$
	12	A_1	$Y_1 - Y_2 - Y_3 + Y_4$
	13	B_1	$Z_1 + Z_2 + Z_3 + Z_4$
	14	A_1	$Z_1 + Z_2 - Z_3 - Z_4$
	15	B_2	$Z_1 - Z_2 + Z_3 - Z_4$
	16	B_3	$Z_1 - Z_3 - Z_3 + Z_4$

there is one function transforming as each I.R.) but not those of C_{2v} (i.e., there is no A_2 function). The immediate implication of this is that there will be more non-zero one-electron $\langle S|S\rangle$ matrix elements if the AO basis is reduced to a C_{2v} basis than if it were reduced to a D_2 basis (by inspection: 5 vs. 4). This arises from the fact that under D_2, the operations of the group connect each member of the AO S basis, whereas in C_{2v} the operations only connect pairs of equivalent functions.

Considering the actual point group symmetry of the system (T_d), it is tempting to suggest that reduction in the number of non-zero elements by a factor of 24 is to be expected. To indicate the reasons why this is not true, we first write down the SO functions of this system under T_d (Table II). We also note that:

$$D_2 \times C_3 \times \sigma_v = T_d$$

and

$$C_{2v} \times C_3 \times \sigma_v = T_d.$$

If the basis used to represent the operations of D_2 will also represent the operations C_3 and σ_v, then the D_2 basis may be used to represent all the operations of T_d. Similar comments may be made for C_{2v} and C_3. When constrained to use a cartesian AO basis, as we are here, this will always be true. Thus, we rewrite the T_d SO functions in Table III as combinations of the D_2 basis functions. Written in this way, it is apparent that the effect of increasing the symmetry is small. We note that the 4 dimensional representation consisting of A, functions

Table II: Reduction of AO Basis to T_d Symmetry

SO Function	Irreducible Representation	AO Function Combinations
1	A_1	$S_1 + S_2 + S_3 + S_4$
2	T_{2z}	$S_1 + S_2 - S_3 - S_4$
3	T_{2x}	$S_1 - S_2 + S_3 - S_4$
4	T_{2y}	$S_1 - S_2 - S_3 + S_4$
5	A_1	$X_1 + Y_1 + Z_1 - X_2 - Y_2 + Z_2 + X_3 - Y_3 - Z_3 - X_4 + Y_4 - Z_4$
6	T_{2z}	$X_1 + Y_1 + Z_1 - X_2 - Y_2 + Z_2 - X_3 + Y_3 + Z_3 + X_4 - Y_4 + Z_4$
7	T_{2y}	$X_1 + Y_1 + Z_1 + X_2 + Y_2 - Z_2 - X_3 + Y_3 + Z_3 - X_4 - Y_4 - Z_4$
8	T_{2x}	$X_1 + Y_2 + Z_1 + X_2 + Y_2 - Z_2 + X_3 - Y_3 - Z_3 + X_4 - Y_4 + Z_4$
9	T_{1z}	$X_1 - Y_1 - X_2 + Y_2 - X_3 - Y_3 + X_4 + Y_4$
10	T_{1y}	$X_1 - Z_1 + X_2 + Z_2 - X_3 - Z_3 - X_4 + Z_4$
11	T_{1x}	$Y_1 - Z_1 + Y_2 + Z_2 - Y_3 + Z_3 - Y_4 - Z_4$
12	T_{2z}	$X_1 + Y_1 - 2Z_1 - X_2 - Y_2 - 2Z_2 - X_3 - Y_3 - 2Z_3 + X_4 - Y_4 - 2Z_4$
13	T_{2y}	$X_1 + 2Y_1 - Z_1 + X_2 + 2Y_2 + Z_2 + X_3 - 2Y_3 + Z_3 + X_4 - 2Y_4 - Z_4$
14	T_{2x}	$2X_1 + Y_1 - Z_1 + 2X_2 + Y_2 + Z_2 - 2X_3 + Y_3 - Z_3 - 2X_4 + Y_4 + Z_4$
15	E_{Z^2}	$X_1 + Y_1 - 2Z_1 - X_2 - Y_2 - 2Z_2 + X_3 - Y_3 + 2Z_3 - X_4 + Y_4 + 2Z_4$
16	$E_{X^2-y^2}$	$X_1 - Y_1 - X_2 - Y_2 + X_3 + Y_3 - X_4 - Y_4$

Table III: Reduction of D_2 SO Basis to T_d

SO Function[a]	Irreducible Representation	SO Functions to be Combined[b]
1	A_1	$A_1(1)$
2	T_{2z}	$B_1(2)$
3	T_{2y}	$B_2(4)$
4	T_{2x}	$B_3(3)$
5	A_1	$A_1(7) + A_1(12) + A_1(14)$
15	E_{z^2}	$A_1(7) + A_1(12) - 2A_1(14)$
16	$E_{x^2-y^2}$	$A_1(7) - A_1(12)$
6	T_{2z}	$B_1(8) + B_1(11) + B_1(13)$
9	T_{1z}	$B_1(8) - B_1(11)$
12	T_{2z}	$B_1(8) + B_1(11) - 2B_1(13)$
7	T_{2y}	$B_2(6) + B_2(9) + B_2(15)$
10	T_{1y}	$B_2(6) - B_2(15)$
13	T_{2y}	$B_2(6) - B_2(15) - 2B_2(9)$
8	T_{2x}	$B_3(5) + B_3(10) + B_3(16)$
11	T_{1x}	$B_3(10) - B_3(16)$
14	T_{2x}	$B_3(10) + B_3(16) - 2B_3(5)$

[a]Numbers refer to SO FUNCTION numbers of Table II.

[b]Numbers in parentheses refer to SO FUNCTION numbers of Table I.

(under D_2) is reduced to $2A_1 + E$ functions under T_d. Precisely the same set of functions would result if this 4-dimensional representation were reduced under C_3 point group symmetry. In the same manner, examination of the B_1, B_2, and B_3 representation (9-dimensional) shows that the reduction process under T_d yields the same result as if the B_1, B_2, and B_3 representations were each reduced separately under C_3.

The point of all this is to illustrate that, although there are six times as many operations in T_d as in D_2 (or C_{2v}), these new operations do not connect all the members of the D_2 or C_{2v} basis. As was shown above (in comparing C_{2v} and D_2 matrix elements), this is directly related to the number of non-zero matrix elements that will result . Since the actual reduction of the basis beyond D_2 is comparable to forming C_3 representations, an additional factor of 3 savings beyond D_2 is the most that can be expected. In this case, the reduction is from 136 matrix elements using an AO basis, to 40 and 26 for D_2 and T_d, respectively.

If one focuses on uniqueness, there is no savings associated with choosing T_d over D_2. Under D_2, the eleven unique non-zero one-electron matrix elements are:

$$\langle 1A_1|1A_1\rangle\langle 2A_1|2A_1\rangle\langle 2A_1|1A_1\rangle\langle 3A_1|2A_1\rangle\langle 1B_1|1B_1\rangle\langle 2B_1|2B_1\rangle$$

$$\langle 2B_1|1B_1\rangle\langle 3B_1|2B_1\rangle\langle 3B_1|3B_1\rangle\langle 4B_1|3B_1\rangle\langle 3B_1|1B_1\rangle$$

and under T_d:

$$\langle 1A_1|1A_1\rangle\langle 2A_1|2A_1\rangle\langle 2A_1|1A_1\rangle\langle 1E_X|1E_X\rangle\langle 1T_{2X}|1T_{2X}\rangle\langle 2T_{2X}|2T_{2X}\rangle$$

$$\langle 2T_{2X}|1T_{2X}\rangle\langle 3T_{2X}|2T_{2X}\rangle\langle 3T_{2X}|3T_{2X}\rangle\langle 1T_{1Z}|1T_{1Z}\rangle\langle 3T_{2X}|1T_{2X}\rangle.$$

Thus, regardless of symmetry treatment, duplicate integrals cannot be fully avoided when degeneracies are present. Lifting the degeneracy by stretching the cube in Fig. 1a to create Fig. 1b produces a system whose highest order group is now D_2. The basis of Table I is still appropriate. In this case none of the functions are symmetry related, and each of the 4s non-zero matrix elements will have a unique value. This is a general result: when the highest order point group symmetry is Abelian, each of the non-zero SO matrix elements will have a unique value.

II. Practical Consideration

Many of the problems that arise in attempting to make use of non-Abelian point groups may be eliminated if a "shell-averaged" basis is employed. This approach has been explored thoroughly by Pitzer.[2] The basic principle here is that individual components of a degenerate representation need not be explicitly considered. For example, rather than evaluating the individual integrals $\langle 1E_X|1E_X\rangle$ and $\langle 1E_y|1E_y\rangle$ as discussed in the previous section, only the integral:

$$\langle E|E\rangle = \tfrac{1}{2}\langle 1E_X|1E_y\rangle + \tfrac{1}{2}\langle 1E_y|1E_y\rangle$$

is evaluated. By forming this combination, a totally symmetric integrand is generated, and the resulting integral is particularly easy

to evaluate. Obviously, with such a formalism an enormous savings will be realized for the non-Abelian groups. The difficulty here is that it becomes impossible to differentiate between E_x and E_y. As a result occupations such as $E_x^2 E_y^1$ are inaccessible in self-consistent calculations, rather the averaged configuration E^3 is obtained. While this limitation is not critical for single configuration wavefunctions, wavefunctions such as those of O_2:[3]

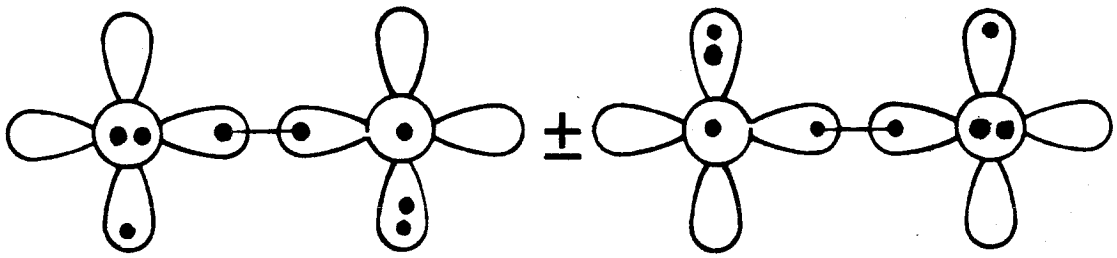

cannot be treated at all.

If such an averaged method is inappropriate, the simple projection operator appraoch defined in the previous section is dictated. Extreme care is required, however. Choosing to evaluate the integral $\langle T_{1ux} | T_{1ux} \rangle$ (D_h symmetry) by brute force may be done as:

$$\langle T_{1ux} | T_{1ux} \rangle = \frac{1}{g^2} \sum_{R,S,\epsilon\mathcal{G}} D_{ji}^{T_{1u}}(R^{-1}) D_{ji}^{T_{1u}}(S^{-1}) \langle R\varphi_{AO} | S\varphi_{AO} \rangle$$

a process that could require as many as 2304 one-electron integrals over AO functions. Clearly, nothing is gained if, to generate a short list of integrals over SOs, one must first generate an enormous number (including duplicates) of integrals over AO functions. Davidson[4] has demonstrated a general approach in which the AO → SO transformation is carried out by beginning with a list of unique AO integrals. In this way the intermediate data to be manipulated never

requires more storage than the final list generated. The theory is not intuitive however, and would be extremely difficult to cast in a readily programmable form.

III. A Simple Transformation Scheme

The essential points to be conveyed in Section I are that there is a considerable advantage in employing an SO basis set in ab initio calculations, and that the highest order abelian point group is adequate for most applications. The additional effort involved in carrying the transformation to higher order groups is not in general rewarded with a corresponding reduction in data. In what follows, a scheme is presented in which the simple properties of the IRs of abelian point groups (notably unit characters) may be advantageously used to perform an AO $\rightarrow$ SO transformation with minimal effort. The approach is formally similar to that of Davidson,[4] but will be developed in such a way as to simplify computational implementation.

A. Matrix Elements of Symmetric One-Electron Operators

Defining a one-dimensional projection operator as:[1]

$$P^{\mu} = \frac{1}{g} \sum_{R \in \mathcal{G}} \chi^{\mu}(R^{-1})\, R$$

where μ is the (one-dimensional) irreducible representation (IR), χ^{μ} is the character of the operation R in the IR μ, and g is the order of the group, allows:

$$I^{\mu\nu}_{aAbB} = \langle P^{\mu}\varphi_{aA}|O|P^{\nu}\varphi_{bB}\rangle$$

$$= \langle \varphi_{aA}|O|P^{\mu}\varphi_{bB}\rangle \delta_{\mu\nu} .$$

This is the standard result, which makes use only of projection operator orthogonality (φ_{aA} is the a^{th} basis function on center A). For some cases, this is not the simplest expression that may be obtained. There is no guarantee that the AO integrals $\langle \varphi_{aA}|O|R\varphi_{bB}\rangle$ will all be unique. To examine this more closely, the last expression must be expanded:

$$I^{\mu\nu}_{aAbB} = \delta_{\mu\nu} \frac{1}{g} \sum_{R} \chi^{\nu}(R^{-1})\langle \varphi_{aA}|O|R\varphi_{bB}\rangle$$

Now, there are subgroups of $\mathcal{G}$, also abelian, which contain sets of operations which produce unique results when applied to φ_{bB}. There will be m_B such operations in a given subgroup, denoted $\mathcal{M}_B$ ($\frac{g}{m_B}$ = an integer). We have made the tacit assumption that the $R\varphi_{bB}$ are able to represent the IR ν and thus the above expression becomes:

$$I^{\mu\nu}_{aAbB} = \delta_{\mu\nu} \frac{1}{m_B} \sum_{R'\epsilon\mathcal{M}B} \chi^{\nu}(R'^{-1})\langle \varphi_{aA}|O|R'\varphi_{bB}\rangle .$$

A more subtle observation is the fact that there will be a subgroup of each $\mathcal{M}_B$, to be denoted $\mathcal{M}_{B(A)}$, whose operations leave φ_{aA} invariant. As will become apparent, it is important to choose the $\mathcal{M}_B$ with the largest such subgroup $\mathcal{M}_{B(A)}$. Making use of the properties of an abelian group:[1]

1) all elements commute;

2) as a consequence, all subgroups $\mathcal{M}$ of $\mathcal{G}$ are invariant,

we note that:

$$\mathcal{M}_B = \mathcal{M}_{B(A)} \times \mathcal{M}_{B(B)}$$

in other words, there must exist a direct factor group $\mathcal{M}_{B(B)}$ (in addition to $\mathcal{M}_{B(A)}$) of the subgroup $\mathcal{M}_B$. The importance of this is as follows:

$$I^{\mu\nu}_{aAbB} = \delta_{\mu\nu} \frac{1}{m_B} \sum_{R' \in \mathcal{M}_B} \chi^{\nu}(R'^{-1}) \langle \varphi_{aA} | O | R' \varphi_{bB} \rangle$$

$$= \delta_{\mu\nu} \frac{1}{m_B} \left\{ \sum_{S \in \mathcal{M}_{B(A)}} \chi^{\nu}(S^{-1}) \langle S \varphi_{aA} | O | S \varphi_{bB} \rangle \right.$$

$$\left. + \sum_{P \in C_{B(A)}} \chi^{\nu}(P^{-1}) \langle \varphi_{aA} | O | P \varphi_{bB} \rangle \right\}$$

where $C_{B(A)}$ is the subset of operations defined by:

$$P \in \mathcal{M}_B \quad \text{but} \quad P \notin \mathcal{M}_{B(A)}.$$

This is a clumsy way to partition the sum, because the same thing may be done in a more compact manner using $\mathcal{M}_{B(B)}$. First, the sum is written as:

$$I^{\mu\nu}_{aAbB} = \delta_{\mu\nu} \frac{1}{m_B} \sum_{S \in \mathcal{M}_{B(A)}} \sum'_{R \in \mathcal{M}_{B(B)}} \chi^{\nu}(S^{-1} P^{-1}) \langle \varphi_{aA} | O | SP \varphi_{bB} \rangle$$

where we have used

$$R = SP \quad \text{with} \quad S \in \mathcal{M}_{B(A)} \quad \text{and} \quad P \in \mathcal{M}_{B(B)}$$

from the definition of a direct factor.[1] Since φ_{aA} is invariant under the S, the characters $\chi^{\nu}(S^{-1})$ must always be unity. This allows:

$$I^{\mu\nu}_{aAbB} = \delta_{\mu\nu} \frac{1}{m_B} \sum_{S}^{\mathscr{M}B(A)} \sum_{P}^{\mathscr{M}B(B)} \chi^{\nu}(S^{-1})\, \chi^{\nu}(S^{-1})\, \chi^{\nu}(P^{-1}) \langle S\varphi_{aA} | O | SP\varphi_{bB} \rangle$$

$$= \delta_{\mu\nu} \frac{m_{B(A)}}{m_B} \sum_{P}^{\mathscr{M}B(B)} \chi^{\nu}(P^{-1}) \langle \varphi_{aA} | O | P\varphi_{bB} \rangle \qquad (1)$$

The last expression is obtained by factoring S from the matrix element, and applying the orthogonality theorem. The importance of choosing $\mathscr{M}$ carefully is made apparent here. The larger the intersection of $\mathscr{M}_{B(A)}$ and $\mathscr{M}_{B}$, the more operations S that may ultimately be eliminated. The only question remaining is how to extract $\mathscr{M}_{B(B)}$ from $\mathscr{M}_{B}$ when $\mathscr{M}_{B(A)}$ is known. To do this, we use the subset $C_{B(A)}$ defined earlier. By definition, the intersection of $\mathscr{M}_{B(A)}$ and $\mathscr{M}_{B(B)}$ is E. Thus the other members (besides E) of $\mathscr{M}_{B(B)}$ must be in $C_{B(A)}$. To find which members of $C_{B(A)}$ are needed to fill out $\mathscr{M}_{B(B)}$, form all right cosets:

$$H_P = \mathscr{M}_{B(A)} \times P \quad \text{where} \quad P \in C_{B(A)}.$$

there can be at most $(\frac{g}{m_{B(A)}} - 1)$ distinct cosets H_p.[1] None of the elements of these H_p are in $\mathscr{M}_{B(A)}$, and they don't include the identity, of course. But in forming the unique H_p we have isolated a set of $(g/m_{B(A)} - 1)$ operations (other than the identity) that when multiplied by $\mathscr{M}_{B(A)}$, collectively yield all members of $C_{B(A)}$. The group $\mathscr{M}_{B(B)}$ is defined by taking one element (arbitrarily; the

$\mathcal{M}_{B(B)}$ are not unique) from each distinct H_p and combining this set with E.

This lengthy discussion serves to fully define the symmetry conditions leading to an AO → SO one-electron transformation involving only unique AO matrix elements. It is similar in form to that derived by Davidson.[4] It is not intended however to define a practical computational scheme. The determination of the subgroups $\mathcal{M}_{B(B)}$ can be seen to involve significant effort, and must be done for each set of functions aA.

An examination of the final expression (1) for $I^{\mu\nu}_{aAbB}$ indicates that all that is really required is:

1) knowledge of the order of the groups $\mathcal{M}_{B(A)}$ and $\mathcal{M}_{B}$, both easily obtained;

2) a list of the unique matrix elements (and corresponding characters) arising from applying all $R \in \mathcal{G}$ to φ_{bB}. Thus, there is no need to be concerned with the details of defining $\mathcal{M}_{B(B)}$.

Modification of the standard POLYATOM procedures (or equivalent) needed to produce the above are minor.

B. Matrix Elements of Symmetric Two-Electron Operators

Most of the considerations derived above are applicable to coulombic two-electron matrix elements. The SO integral is defined as:

$$I^{\mu\nu\delta\lambda}_{ABCD} = (P^{\mu}\varphi_A\, P^{\nu}\varphi_B | P^{\delta}\varphi_C\, P^{\lambda}\varphi_D)$$

where the designations aA have been combined as A for simplicity.

The standard "curved bracket" notation is used. Expanding this gives:

$$I^{\mu\nu\delta\lambda}_{ABCD} = \frac{1}{g^4} \sum_P^{\mathscr{G}} \sum_Q^{\mathscr{G}} \sum_R^{\mathscr{G}} \sum_S^{\mathscr{G}} \chi^{\mu}(P^{-1}) \chi^{\nu}(Q^{-1}) \chi^{\delta}(R^{-1}) \chi^{\lambda}(S^{-1}) \times$$

$$(P\varphi_A \, Q\varphi_B | R\varphi_C \, S\varphi_D).$$

Factoring the operations P out of each sum:

$$I^{\mu\nu\delta\lambda}_{ABCD} = \frac{1}{g^4} \sum_P^{\mathscr{G}} \sum_T^{\mathscr{G}} \sum_U^{\mathscr{G}} \sum_V^{\mathscr{G}} \chi^{\mu}(P^{-1}) \chi^{\nu}(P^{-1}T^{-1}) \chi^{\delta}(P^{-1}U^{-1}) \chi^{\lambda}(P^{-1}V^{-1}) \times$$

$$(P\varphi_A \, PT\varphi_B | PU\varphi_C \, PV\varphi_D)$$

$$= \frac{1}{g^4} \sum_P^{\mathscr{G}} \chi^{\mu}(P^{-1}) \chi^{\nu}(P^{-1}) \chi^{\delta}(P^{-1}) \chi^{\lambda}(P^{-1}) P \{ \sum_T^{\mathscr{G}} \sum_U^{\mathscr{G}} \sum_V^{\mathscr{G}} \chi^{\nu}(T^{-1}) \chi^{\delta}(U^{-1}) \chi^{\lambda}(V^{-1})$$

$$\times (\varphi_A T\varphi_B | U\varphi_C V\varphi_D) \}$$

$$= \frac{1}{g^3} \delta_{\mu,\nu\delta\lambda} \sum_T^{\mathscr{G}} \sum_U^{\mathscr{G}} \sum_V^{\mathscr{G}} \chi^{\nu}(T^{-1}) \chi^{\delta}(U^{-1}) \chi^{\lambda}(V^{-1}) \times \qquad (2)$$

$$(\varphi_A T\varphi_B | U\varphi_C V\varphi_D)$$

This final result represents the equivalent of having applied projection operator orthogonality relations to the one-electron matrix elements, as discussed earlier. As in that case, further reduction is possible. It is tempting to try to eliminate another of the operator sums (i.e., another projection operator). This leads to:

$$= \frac{1}{g^3}\,\delta_{\mu,\nu\delta\lambda} \sum_{T}^{\mathcal{G}} \chi^{\nu}(T^{-1})\,\chi^{\delta}(T^{-1})\,\chi^{\lambda}(T^{-1})\,T\Big\{\sum_{X}^{\mathcal{G}}\sum_{Y}^{\mathcal{G}} \chi^{\delta}(X^{-1})\,\chi^{\lambda}(Y^{-1}) \times$$

$$(T^{-1}\varphi_A\varphi_B|X\varphi_C Y\varphi_D)\Big\}\ ,$$

which is valuable only if $T^{-1}\varphi_A = \varphi_A$ for all φ_A. A more general approach follows along the lines of the previous section. We first determine the subgroup $\mathcal{N}_A$ of $\mathcal{G}$ whose operations leave the φ_A invariant. Next, for one set of functions, e.g., φ_B, subgroups that uniquely connect all members of φ_B are noted and the one having the most elements in common with $\mathcal{N}_A$ is selected. This allows (2) to be rewritten as:

$$I^{\mu\nu\delta\lambda}_{ABCD} = \frac{1}{g^2 m_B}\,\delta_{\mu,\nu\delta\lambda} \sum_{S}^{\mathcal{N}_A}\sum_{P}^{\mathcal{M}_{B(B)}} \sum_{U}\sum_{V} \chi^{\mu}(S^{-1})\,\chi^{\nu}(S^{-1}P^{-1})\,\chi^{\delta}(U^{-1})\,\chi^{\lambda}(V^{-1}) \times$$

$$(S\varphi_A SP\varphi_B|U\varphi_C V\varphi_D)$$

where

$$\mathcal{M}_B = \mathcal{N}_A \times \mathcal{M}_{B(B)}$$

and all operations are exactly analogous to those in the previous section. Factoring gives:

$$I^{\mu\nu\delta\lambda}_{ABCD} = \frac{1}{g^2 m_B}\,\delta_{\mu,\nu\delta\lambda} \sum_{S}^{\mathcal{N}_A}\sum_{P}^{\mathcal{M}_{B(B)}} \sum_{X}^{\mathcal{G}}\sum_{Y}^{\mathcal{G}} \chi^{\mu}(S^{-1})\,\chi^{\nu}(S^{-1})\,\chi^{\delta}(S^{-1})\,\chi^{\lambda}(S^{-1}) \times$$

$$\chi^{\nu}(P^{-1})\,\chi^{\delta}(X^{-1})\,\chi^{\lambda}(Y^{-1})(S\varphi_A SP\varphi_B|SX\varphi_C SY\varphi_D)$$

$$= \frac{n_A}{g^2 m_B} \delta_{\mu,\nu\delta\lambda} \sum_{P}^{\mathcal{M}_{B(B)}} \sum_{X}^{\mathcal{G}} \sum_{Y}^{\mathcal{G}} \chi^{\nu}(P^{-1}) \chi^{\delta}(X^{-1}) \chi^{\lambda}(Y^{-1}) \times$$

$$(\varphi_A P \varphi_B | X \varphi_C Y \varphi_D).$$

And finally, after factoring out the S, the sets of operations X and Y may be reduced to include only unique contributions:

$$I^{\mu\nu\delta\lambda}_{ABCD} = \frac{\bar{n}_A}{m_B m_C m_D} \delta_{\mu,\nu\delta\lambda} \sum_{P}^{\mathcal{M}_{B(B)}} \sum_{X'}^{\mathcal{M}_C} \sum_{Y'}^{\mathcal{M}_D} \chi^{\nu}(P^{-1}) \chi^{\delta}(X'^{-1}) \chi^{\lambda}(Y'^{-1}) \times$$

$$(\varphi_A P \varphi_B | X' \varphi_C Y' \varphi_D) \qquad (3)$$

C. Programming Consideration

The generation of two-electron integrals using this prescription is straightforward. All unique AO integrals defined within the sets A, B, C and D contribute equally (within a sign) to the SO integral, and are each multiplied by the easily determined factor $n_A/m_B m_C m_D$.

There are special cases, however, that require more detailed treatment. Application of the above procedures to the five classes of integrals:

1. $(\varphi_A \varphi_A | \varphi_C \varphi_D)$
2. $(\varphi_A \varphi_A | \varphi_B \varphi_B)$
3. $(\varphi_A \varphi_B | \varphi_C \varphi_C)$
4. $(\varphi_A \varphi_C | \varphi_A \varphi_C)$
5. $(\varphi_A \varphi_A | \varphi_A \varphi_A)$

will in some cases lead to the generation of redundant AO integrals as

contributions to the SO integral. In each of these cases there is the possibility that two of the subgroups $\mathcal{M}_{B(B)}$, $\mathcal{M}_C$, or $\mathcal{M}_D$ from Eq. (3) will be equivalent. The result of this, using case (3) as an example, is that applying all combinations of operations X and Y in $\mathcal{M}_C$ and $\mathcal{M}_D$ (where $\mathcal{M}_C = \mathcal{M}_D$ here) produces some identical integrals. If values are retained for each of these, then Eq. (3) may be used without alteration. This defeats the purpose, however, of the whole exercise: defining a unique AO → unique SO integral transformation.

The computational solution to this problem is a simple one; however, it requires that each of the five cases listed above be identified and treated explicitly. The process may be outlined using case (3) again as an example. As in the case where all four sets of AOs are different, the unique integrals may be found by applying all the operations of $\mathcal{G}$ to each of φ_B, φ_C, and φ_D. If all four sets were different, $\frac{g^3}{m_B m_C m_D}$ duplicates would be found for each unique AO integral, as prescribed by Eq. (3). In other words, the set of g^3 possible AO integrals may be partitioned into sets, each containing an equal number of duplicate integrals. The contribution of each unique AO to $I^{\mu\nu\delta\lambda}$ will be the same in magnitude, but will differ in size according to the product of the chracters in Eq. (3). For case (3) however, not all of these sets will always be distinct. Thus, the number of duplicates of each unique AO integral will be a multiple ℓ of $\frac{g^3}{m_B m_C m_D}$. The magnitude of the contribution of each unique AO in this case will be altered by this multiple, but the sign of the contribution is more difficult to determine. For case (3), this is done by noting whether the sign of the contribution changes upon

interchanging k and ℓ in the unique AO indice (ij/kℓ). This is equivalent to comparing the characters of the redundant integrals $(\varphi_A P \varphi_B | Q' \varphi_C R' \varphi_C)$ and $(\varphi_A P \varphi_B | R' \varphi_C Q' \varphi_C)$ where R' and Q' are operations in $\mathcal{M}_C$. If the sign changes, it indicates that the two sets of duplicates which were combined to create this "degenerate" set would normally contribute to this SO integral with opposite signs and thus the total contribution is zero. If the sign does not change upon exchanging φ_C and φ_D, the AO integral is added to the SO sum with a multiplier of this sign. This sequence of operations is straightforward to perform, and is entered as a flow chart in Fig. 2 . Similar flow charts are constructed for each of the other four special cases.

It would seem as though performing the above operations would lead to significant CPU times in performing the transformation. It should be noted however, that the majority (>75%) of SO integrals in a normal ab initio calculation will involve AO integrals that span four different sets of functions A, B, C and D. Thus Eq. (3) may be used without alteration. Each SO integral will have at most g^3 distinct contributions and there will be $\sim \frac{1}{g} \times \frac{N^4}{8}$ non-zero SO integrals. The work required to carry out the transform is no more than $\sim \frac{N^4 g^2}{8}$, significantly less than the N^5 or N^6 dependence required of more general transformation methods. In addition most steps involve integer arithmetic, and thus may be executed very rapidly. Experience has shown that the computational effort involved in the transformation is often less than that required to expand a list of unique AO integrals to full canonical length. Thus the transformation is effectively transparent to the user.

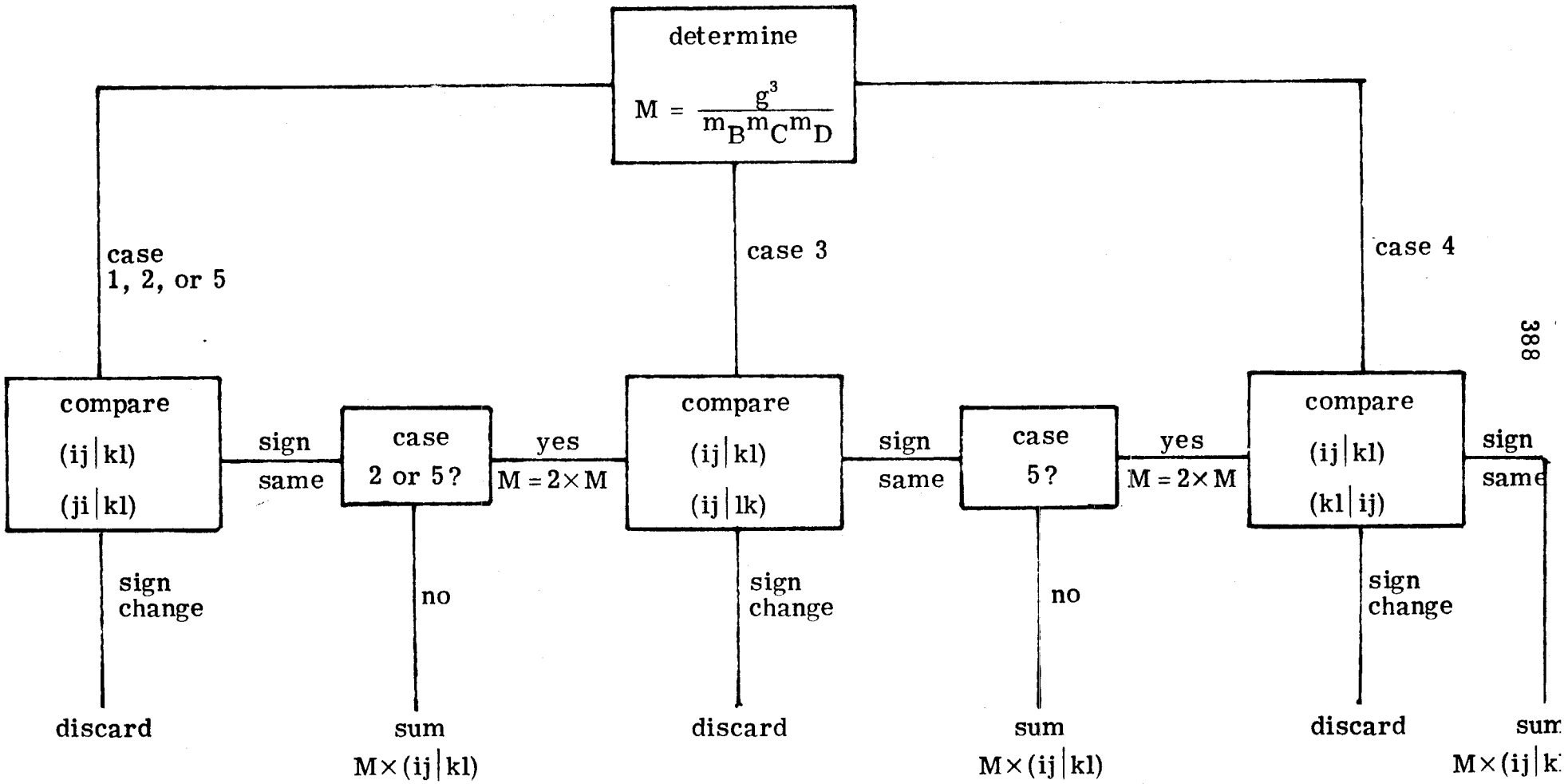
determine
$M = \frac{g^3}{m_B m_C m_D}$
case 1, 2, or 5
case 3
case 4
compare
(ij|kl)
(ji|kl)
sign change
discard
sign
same
case
2 or 5?
yes
M = 2×M
no
sum
M×(ij|kl)
compare
(ij|kl)
(ij|lk)
sign change
discard
sign
same
case
5?
yes
M = 2×M
no
sum
M×(ij|kl)
compare
(ij|kl)
(kl|ij)
sign change
discard
sign
same
sum
M×(ij|kl)

Figure 2.

A second concern arising in most two-electron transformation schemes is the excessive amount of storage required to hold the transformed result. For the special form of transformation discussed here, this need not be a problem. As evidenced by Fig.(3), the N to N transformation may be broken down into a series of transformations each involving at most g^3 integrals, once the sets of functions A, B, C and D have been identified. Generation of SO integrals is done most effectively by looping canonically over sets of functions. For n sets this allows the transformation to be broken down into $\sim n^4/8$ separate AO integral generation and transformation steps.

References and Notes

1. a) M. Tinkham, "Group Theory and Quantum Mechanics" (McGraw-Hill, New York, 1964); b) M. Hamermesh, "Group Theory," (Addison, Wesley, London, 1962).

2. R. M. Pitzer, J. Chem. Phys., 59, 3308 (1973).

3. B. Moss, F. Bobrowitz, and W. Goddard III, J. Chem. Phys., 63, 4632 (1975).

4. E. R. Davidson, J. Chem. Phys., 62, 400 (1975).